CRANFIELD UNIVERSITY

N TOULAS

SAFETY FACTORS AND RISK IN FATIGUE SUBSTANTIATION OF HELICOPTER COMPONENTS

SCHOOL OF INDUSTRIAL AND MANUFACTURING SCIENCE

PhD THESIS

CRANFIELD UNIVERSITY

SCHOOL OF INDUSTRIAL AND MANUFACTURING SCIENCE

PhD THESIS

N TOULAS

Safety factors and risk in fatigue substantiation of helicopter components

Supervisor: Prof. P.E. Irving

January 2005

This thesis is submitted in fulfilment of the requirements
for the degree of Doctor of Philosophy

Στους Γονεις μου...

To my family and friends

Freedom, love and dedication lead to gnosis.
Ignorance leads to Lethe.

ABSTRACT

Helicopter dynamic components are substantiated against fatigue using the safe life methodology. The advance of usage monitoring systems suggest the extension of the safe life according to measured usage, leading to maintenance credits. The question is whether the extended life is associated with a different probability of failure due to elevation of safety factors embedded within the safe life methodology.

The fatigue substantiation process was studied and its conservatisms were identified. Both S-N curve behaviour and service loading have been investigated. Three components were studied. One was a location on the lift frame, the others were a main rotor blade linkage and a rotor pitch change link. The variation in manoeuvre loads and usage during normal operation of a UK military helicopter was statistically estimated. Service loads were measured using strain gauged components and a data recording system. Usage was monitored by manual identification and recording of manoeuvres throughout the helicopter flight.

It was found that usage variability is very great, with coefficients of variation in excess of 100% for the majority of manoeuvres. It was found that usage measured in service was significantly more benign for all types of mission, than that assumed in design. Mechanical test results showed significant errors in damage accumulation and mean stress models for life prediction. Monte Carlo simulations demonstrate that calculated probability of failure is dominated by material and modelling errors; usage and manoeuvre load variability playing a minor role.

ACKNOWLEDGEMENTS

The author is grateful to: Prof. Phil Irving for patient, paternal supervision, UK Royal Air Force for funding, Westland Helicopters for information and Mr. Bob Hudson for assistance.

CONTENTS

NOMENCLATURE

Symbol /Abbreviation	Description	Unit
A	Coefficient in Weibull S-N equation	
B	Coefficient in Weibull S-N equation	
C	Coefficient in Weibull S-N equation	
CoV	Coefficient of Variation	
D	Cumulative fatigue damage index	
HUMS	Health, usage monitoring system	
K_t	Theoretical stress concentration factor	
K_f	Fatigue stress concentration factor	
LF	Life factor applied to S-N curve	
MDRE	Manual data recording exercise	
m	Parameter for mean stress correction equation	
N	Number of cycles to failure	
N	Number of component lives (Monte Carlo simulation)	
n	Number of cycles	
P_a	Load amplitude	kN
P_m	Load mean	kN
q	Notch sensitivity factor	
R	Stress ratio	
S	Stress	MPa
S_a	Alternating stress amplitude	MPa
S_m	Stress mean	MPa
S_{max}	Stress maximum	MPa
S_{min}	Stress minimum	MPa
S_μ	Stress range	MPa
S_G	Estimated stress amplitude at R -1	MPa
SF	Strength factor applied to S-N curve	
S_{inf}	Fatigue endurance limit	MPa
S_y	Yield strength	
UTS	Ultimate tensile strength	MPa
VNE	Velocity never exceed	knots
ζ	Logarithmic standard deviation	
μ	Population mean	

1. Introduction

1.1 Background

Safety factors and design safe lives for UK military (and civilian) helicopters have been derived 20-30 years ago and are still in use today despite modern developments in fatigue life assessment, and the advent of Fatigue Usage Monitoring Systems (FUMS). In addition, airworthiness certification in MOD aircraft is moving towards a more quantitative probabilistic approach.

The reliability of the safe-life approach being used in helicopters started to be questioned shortly after the results of a round robin in 1980 concerning a hypothetical problem [1] in which participants (various helicopter manufacturers) were asked to determine the retirement life of a helicopter pitch link. The results showed variations in predictions from 9 to 2,594 hours. Even though all the analyses used conservative assumptions on loads, strength etc, none of them could quantify the overall risk associated with a component's fatigue life.

Usage monitoring systems in helicopters offer the great benefit of maintenance credits on safe life parts. Maintenance credits are the possibility of cost savings via service life extension past the original safe life, if previous usage has been sufficiently benign. Practical implementation of usage monitoring has a number of difficulties. Many of these are associated with issues of what the original safe life represents in terms of probability of failure. How can it be ensured that a life extension indicated by a usage monitoring system, will not at the end of the extension have an unacceptable probability of failure- in effect, an airworthiness hazard?

Extensions in life predicted via a fatigue analysis alone, will not adequately represent changes in probability of failure arising from increased time in service. The level of life extension where this effect will have a significant influence on probability of failure is unknown.

Further issues are associated with variability and uncertainty of fatigue damage arising from individual manoeuvres. This arises partly through variability in service loads, partly through uncertainties in knowledge of the material or component S-N curve, and errors in the fatigue analysis process itself. Examples of the latter include errors in Miner's rule, and errors in the rule (usually Goodman) for mean stress corrections. Errors and uncertainty are overcome in deterministic fatigue analyses by applying factors of safety. However the uncertainties remain and can become an issue in usage monitoring wherever real values of loads, rather than conservatively assumed values of damage are measured. Without knowledge of the cause and extent of uncertainty in fatigue damage, it is difficult to ensure that any life extension will not result in unacceptable increases in probability of component failure.

In view of these factors it is timely to develop a fatigue substantiation approach based on the statistics of real service load data and of component fatigue properties. Such an approach will allow interpretation of load and material factors in probabilistic terms, and will allow full advantage to be taken of the benefits in life extension offered by FUMS without adverse changes in probabilities of component failure.

1.2 Research project objectives

(1) To identify the various stages of the helicopter fatigue substantiation process, and to quantify using both analysis and experiments, the uncertainties and conservatisms involved in each stage.

(2) Using modern methods of probabilistic fatigue life assessment (Monte Carlo simulations), to determine the contribution of each stage identified in (1) to the overall probability of failure of selected components

(3) To quantify the increase in failure probability with service life of selected components and to establish the benefits to component failure risk of fatigue usage monitoring, (FUMS)

(4) To use results of 1,2 & 3 above to determine the changes in risk associated with application of FUMS to existing safe life methodology. This to be done for service periods within and also service beyond the nominal design safe life.

1.3 Methodology

Original Approach

- Original approach to attempt quantitative calculations based on Sea King – use material and usage data from this application to obtain realistic specific probabilities of failure- not possible because of lack of usage data for Sea King
- Had decided to conduct experimental work on Sea King upper plate material 2S 97 high strength steel
- Other data taken from a variety of sources and helicopter types
- Calculated lives and probabilities only have significance in a relative not absolute sense
- Original intention to study effects of Westland calculation procedures in some detail- not done largely because of the above

Approach

Experimental

- Investigations of the accuracy of Miners law and the Goodman mean stress correction
- Measurement of material properties S- N data at a range of R values- assess accuracy & conservatisms of Goodman
- Calculation of lives under Rotorix spectrum using Miner and Goodman
- Validation tests under identical Rotorix spectrum
- Assess Errors
- Notched and smooth sample validations

Modelling and simulations

- Deterministic analysis of helicopter usage MDRE data
- Damage calculations using design authority S- N data
- Effects of loads analysis procedures

Monte Carlo simulations

- Effects of usage variability - MDRE data
- Effects of variability in manoeuvre damage content- Lynx OLM data, combined with DA S-N data
- Effects of S-N data variability combined with usage and OLM data
- Effects of Usage monitoring system error
- Failure probabilities interpreted as probability of damage sum becoming equal to one (1)

1.4 Thesis structure

An outline of the contents of each chapter is given below:

Chapter 1 provides background information to the project objectives and methodology.

Chapter 2 contains the outcome of a literature survey on the subjects of fatigue design of helicopter components, usage monitoring, statistical considerations and probabilistic approach to fatigue substantiation of helicopters.

Chapter 3 includes the experimental investigation regarding the accuracy of fatigue substantiation methodology tools as applied to helicopters.

Chapter 4 describes the results from the statistical analysis of available helicopter usage and loads data. The effect of variability was studied deterministically.

Chapter 5 demonstrates the application of a probabilistic fatigue life methodology, based on Monte Carlo simulation. The effect of variability from different sources is estimated taking into account the associated risk of failure.

Chapter 6 expresses the research conclusions and recommendations for future work.

2. Fatigue substantiation of helicopter components

2.1 Fatigue design principles

Fatigue failure investigations have led to the observation that the fatigue process embraces two domains of cyclic stressing or straining that are significantly different in character, and in each of which failure is probably produced by different physical mechanisms. One domain of cyclic loading is that for which significant plastic strain occurs during each cycle. This domain is associated with high loads and short lives, or low numbers of cycles to produce fatigue failure, and is commonly referred to as low-cycle fatigue. The other domain of cyclic loading is that for which the strain cycles are largely confined to the elastic range. This domain is associated with lower loads and long lives, or high numbers of cycles to produce fatigue failure, and is commonly referred to as high-cycle fatigue. Low cycle fatigue is typically associated with cycle lives from one up to 10^4 cycles, and high-cycle fatigue for lives greater than about 10^4 cycles. This project is dealing with high cycle fatigue.

2.1.1 Fatigue design criteria

Infinite-Life Design
Unlimited safety is the oldest criterion. It requires design stresses to be safely below the fatigue endurance limit. For parts subject to many millions of almost uniform cycles, like engine valve springs, this is still a good design criterion.

Safe-Life Design
The practice of designing for a finite life is known as "safe-life" design. It is used in many industries, such as automotive, railroad, pressure vessels, jet engines and helicopter dynamic components. The safe life must include a margin for the scatter of fatigue results and for other unknown factors. The calculations may be based on stress-life relations, strain-life relations, or crack growth. The margin for safety may be taken in terms of life, in terms of load, or by specifying that both margins must be satisfied.

Fail Safe Design

Fail-safe fatigue design criteria were developed by aircraft engineers. They could not tolerate the added weight required by large safety factors nor the danger to lives implied by small safety factors. Fail-safe design recognizes that fatigue cracks may occur and arranges the structure so that cracks will not lead to failure of the structure before they can be detected and repaired. Multiple load paths and crack stoppers built at intervals into the structure are some of the means used to achieve fail-safe design. This philosophy is applied mainly to airframes.

Damage Tolerant Design

This philosophy is a refinement of the fail-safe philosophy. It assumes that cracks will exist – caused either by processing or by fatigue – and uses fracture mechanics analysis and tests to check whether such cracks will grow large enough to produce failures before they are sure to be detected by periodic inspection. This philosophy is better applied to materials with slow crack growth and high fracture toughness.

2.1.2 Fatigue loading

When an engineer faces the design of a fatigue sensitive element in a structure, he is interested in the fatigue response of the available materials to various loadings that may occur during the life of the structure. That is, he is interested in the effect of various loading spectra and associated stress spectra, which will be in general a function of the design shape and the use of the structure.

The simplest fatigue stress spectrum is a zero-mean sinusoidal stress-time pattern of constant amplitude and fixed frequency. Such a stress-time pattern is shown in Fig.2.1a. Utilising the sketch of Fig.2.1, we can conveniently define several useful terms and symbols; these include:

S_{max} = maximum stress in the cycle

S_m = mean stress = $\frac{S_{max} + S_{min}}{2}$

S_{min} = minimum stress in the cycle

S_a = alternating stress amplitude = $\frac{S_{max} - S_{min}}{2}$

S_μ = range of stress = S_{max} - S_{min}

$$R = \text{stress ratio} = \frac{S_{min}}{S_{max}}$$

A spectrum with R=-1 is often referred as completely reversed cyclic stress spectrum.

A type of stress-time pattern often encountered is the nonzero mean spectrum shown in Fig. 2.1b. This pattern is very similar to the completely reversed case except that the mean stress is tensile or compressive.

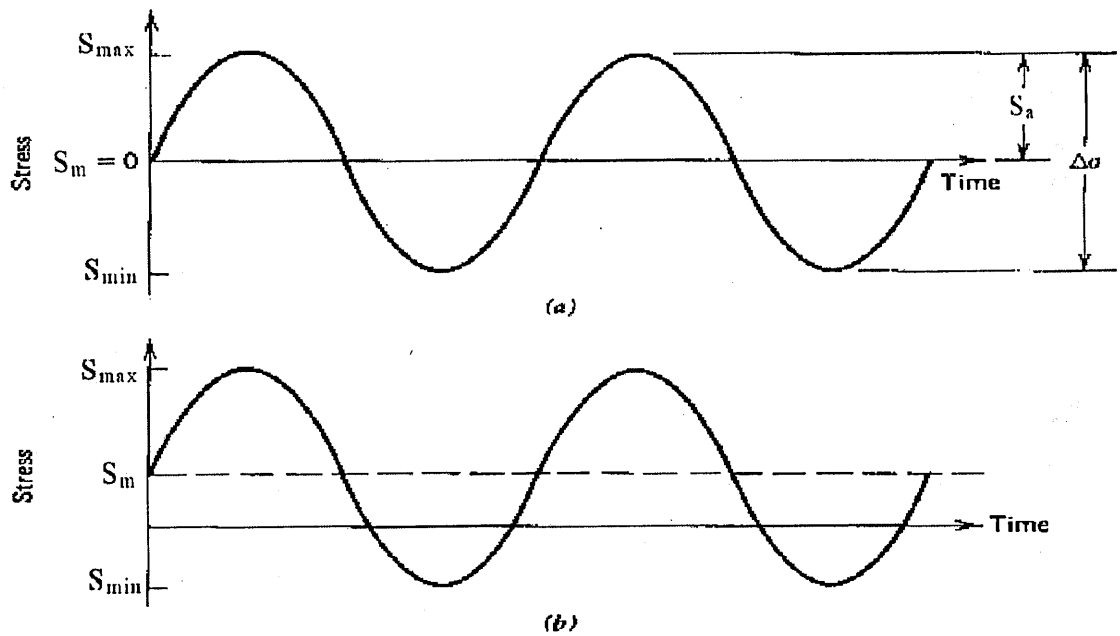

Fig. 2.1_ Constant-amplitude stress time patterns. (a) Completely reversed, R=-1, (b) Nonzero mean stress.

2.1.3 The mean S-N Curve

To calculate fatigue lives, some relationship must be obtained between cyclic loads and the corresponding fatigue damage produced for a particular component. In other words, an S-N curve (or curves) needs to be constructed for each component. An S-N curve is one which defines the relationship between the endurance, N, of a material as a function of the applied stress or load amplitude, S. N is given in terms of the number of load cycles endured prior to failure at a given value of S.

A commonly used equation [2] to represent the S-N curve from $N=1$ (static strength UTS), to $N=\infty$ (the endurance limit, S_{inf}) is that proposed by Weibull in 1961: $S = S_{inf} + (UTS - S_{inf})e^{-a(\log N)^{\beta}}$ where the values of the constants UTS, S_{inf}, a, and β are obtained from the test data by a least squares fit. This equation and its many variations can be found in the literature [3, 4, 5] along with the constants used to define the curve shapes. These constants vary widely from manufacturer to manufacturer. The several S-N curves which arise when the standard curve shapes are drawn through the test points are then consolidated into one curve which is the statistical mean of all the curves (Fig.2.2). This is the "Mean S-N Curve".

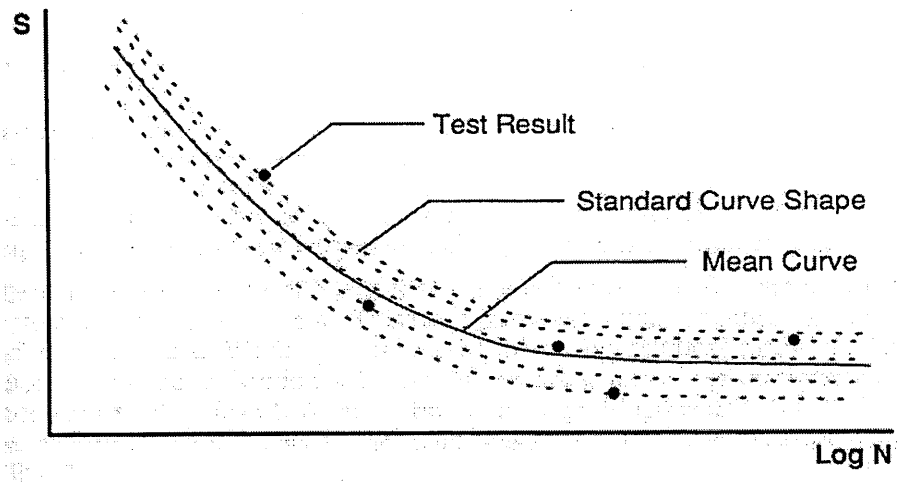

Fig. 2.2_ Derivation of the Mean S-N Curve from the test results

2.1.4 Cumulative damage theories

The first cumulative damage theory was proposed by Palmgren in 1924 and later developed by Miner in 1945 [6]. This linear theory, which is still widely used, is referred to as the Palmgren-Miner rule or the linear damage rule. The theory may be described using the S-N plot in Fig. 2.3.

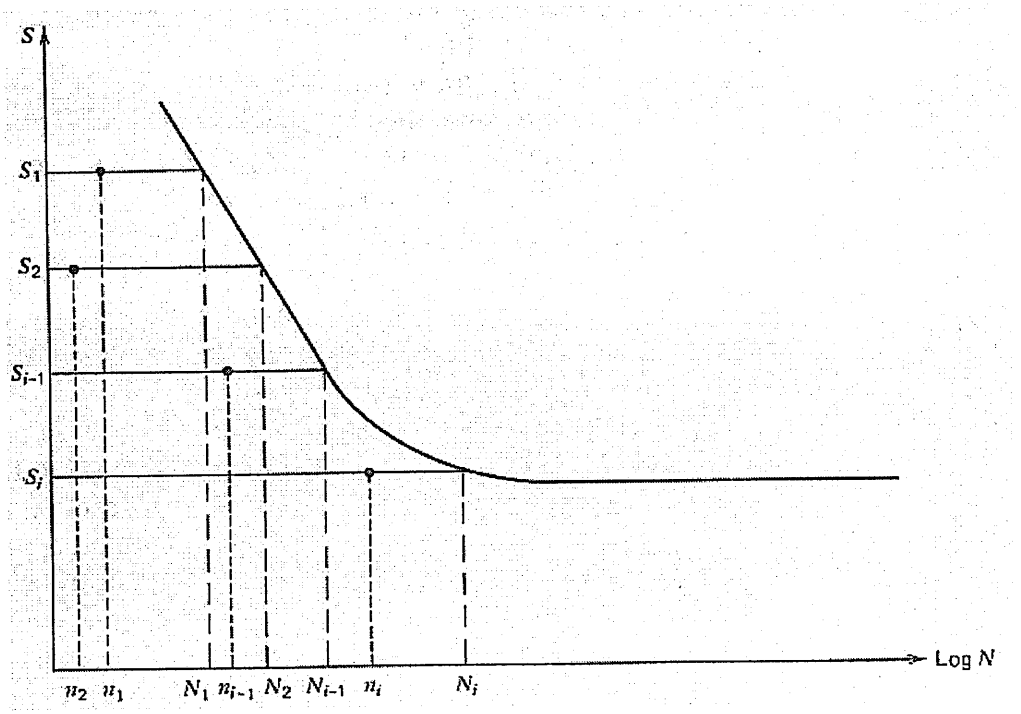

Fig. 2.3_ Illustration of spectrum loading where n_i cycles of operation are accrued at each of the different corresponding stress levels S_i , and the N_i are cycles to failure at each S_i.

By definition of the S-N curve, operation at a constant stress amplitude S_1 will produce complete damage, or failure, in N_1 cycles. Operation at stress amplitude S_1 for a number of cycles n_1 smaller than N_1 will produce a smaller fraction of damage, say D_1. D_1 is usually termed the damage fraction. Operation over a spectrum of different stress levels results in a damage fraction D_i for each of the different stress levels S_i in the spectrum. When these damage fractions sum to unity, failure is predicted;

$$D_1 + D_2 + \ldots + D_{k-1} + D_k = 1$$

The Palmgren-Miner rule asserts that the damage fraction at any stress level Si is linearly proportional to the ratio of number of cycles of operation to the total number of cycles that would produce failure at that stress level; that is

$$D_i = \frac{n_i}{N_i}$$

By the Palmgren-Miner rule, then, we may write that:

Failure is predicted to occur if:

$$\sum_{i=1}^{k} \frac{n_i}{N_i} \geq 1$$

This is a complete statement of the Palmgren-Miner rule, or the linear damage rule. It has one sterling virtue, namely, simplicity; and for this reason it is widely used.

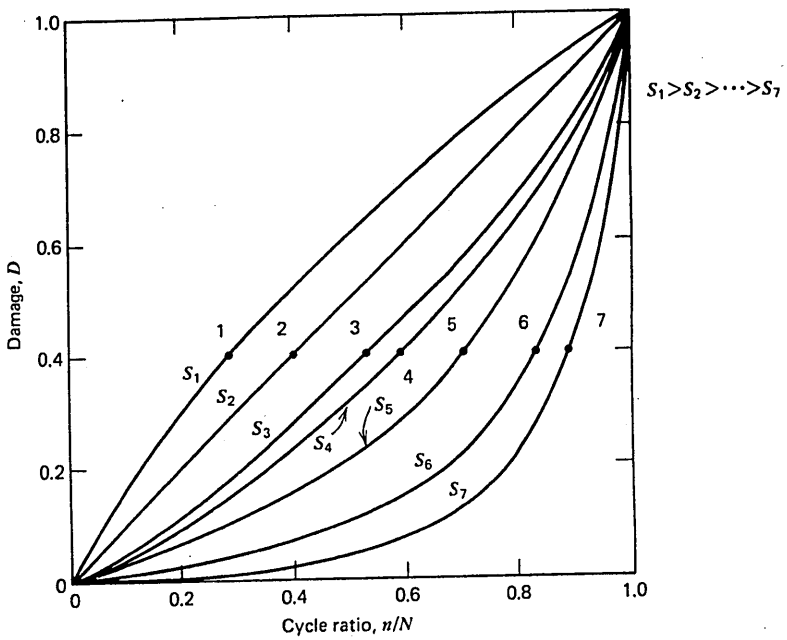

Fig. 2.4_ Damage VS Cycle ratio for various stress levels S

Unfortunately, it suffers from a number of drawbacks that make it often inaccurate. In many cases, the cumulative damage index $D = \sum_{i=1}^{k} \frac{n_i}{N_i}$ can vary from 0.8 to 1.2 and in some cases may be extremely un-conservative D=0.14 [7]. Hence in many industries, where the Palmgren-Miner rule approach is adopted, the life fractions are added together until $\sum_{i=1}^{k} \frac{n_i}{N_i} = 0.75$, at which time failure is assumed to occur. This uncertainty is unfortunate since under some conditions the reserve fatigue strength must be considerable. The method fails to account for R-ratio effects requiring an S-N curve for each R-ratio, load sequence effects (e.g. for stress-life based evaluation when large amplitude cycles precede smaller cycles the actual life is less than predicted), mean stress effects, notch effects, and the effect

of prior static loading. Also it does not account for any damage caused by small amplitude cycles beneath the S-N curve [8]. Despite its shortcomings, the Palmgren-Miner rule can provide a simple technique for obtaining an approximation of life under conditions of variable amplitude loading. When used with an appropriate cycle counting scheme (e.g., rain-flow counting), the method can be used to produce life estimates very quickly for extremely complex random loadings, which can be a considerable task when using other techniques.

In a survey for cumulative fatigue damage and life prediction theories by A. Fatemi and L. Yang [9] many of the models proposed since Palmgren-Miner rule are introduced. There exist six major categories in cumulative fatigue damage modelling:

(1) linear damage evolution and linear summation
(2) non-linear damage curve and two stage linearisation approaches
(3) life curve modifications to account for load interactions
(G.Schott, B.Donat and M.Schapter – [10])
(4) approaches based on crack growth concept
(5) models based on continuum damage mechanics and
(6) energy-based methods.

No clear boundaries exist among some of these approaches. Linear damage rules cannot account for load sequence and interaction effects due to their linear nature. The first non-linear load-dependent damage theory represented by the power relationship, $D = \sum \left(\frac{n_i}{N_i} \right)^{x_i}$, where x_i is a variable quantity related to the i^{th} loading level, was proposed by Macro and Starkey in 1954 (Fig. 2.4). In two stage linearisation approaches, the damage process is divided into two stages of crack initiation [11] and crack propagation and the linear damage rule is then applied to each stage [12], [13]. Life curve modification approaches are based on modifying the material S-N curve by reducing the S_{inf}. Also the approach is load-level dependent, and as a result can account for the load sequence effects [14], [15], [16]. Approaches based on the crack growth concept including macro crack growth retardation models have enjoyed some degree of acceptance since crack growth can directly be related to the physics of the damage process. Franke and Dierkes [17] presented in their work a model with a

new exponent, which is based on a crack growth boundary condition. The results are compared with experimental data from the literature –showing satisfactory agreement – and with other power law theories. Continuum damage mechanics approaches are relatively new approaches, modelling the material damage process at the continuum scale. These approaches were originally developed to model creep damage and later extended to include the fatigue damage process. Cheng and Plumtree [18] have presented a model based on continuum damage mechanics and ductility exhaustion that was capable of describing cumulative damage during variable cyclic loading. It showed good agreement with a few experimental results. Bhattacharya and Ellingwood have presented a model using continuum damage mechanics and focused in the crack initiation region. Cumulative damage theories based on energy have mainly been developed since the late 1970s [19] and have the potential to unify the damage caused by different types of loads such as thermal cycling, creep and fatigue.

Though many damage models have been developed, unfortunately, none of them enjoys universal acceptance. Each damage model can only account for one or at best a limited number of phenomenological factors, such as load dependence, multiple damage stages, non-linear damage evolution, load sequence and interaction effects, overload effects, small amplitude cycles below fatigue limit and mean stress. Due to the complexity of the problem, none of the existing predictive models can encompass all of these factors. The applicability of each model varies from case to case. Consequently, the Palmgren-Miner linear damage rule is still dominantly used in design, in spite of its major shortcomings. Also, the most common method for cumulative damage assessment using linear elastic fracture mechanics has been based on integration of a Paris Type crack growth rate equation, with modifications to account for load ratio and interaction effects.

More efforts in the study of cumulative fatigue damage are needed in order to provide design engineers with a general and reliable fatigue damage analysis and life prediction model (Chaudonneret and Robert [20] presented an analysis of the different approximations in life prediction algorithms and concluded that insufficiencies do exist, resulting from the laws ordinarily used).

2.1.5 Nonzero mean stress effect

Because normally only constant amplitude tests are carried out the design S-N curve is related to one mean load (the test load). However the actual loading of the component can be at various levels due to environmental and pilot technique variations. Therefore the cyclic loads of the actual load spectrum have to be adjusted to the mean load of the S-N curve (test load). Without this adjustment the actual loads will not cross the design curve (because it is based on conservative loading) and the life cannot be estimated.

Most commonly used is a reduction based on a diagram that gives the relation between mean load and endurance limit referred to as modified Goodman diagram or Soderberg diagram. It is assumed that one cyclic load S_1 at mean load S_{m1} gives the same damage as one cyclic load S_2 at mean load S_{m2} , S_2 being equal to:

$$S_2 = \frac{E(S_{m2})}{E(S_{m1})} S_1$$

The procedure is illustrated in Figure 2.5

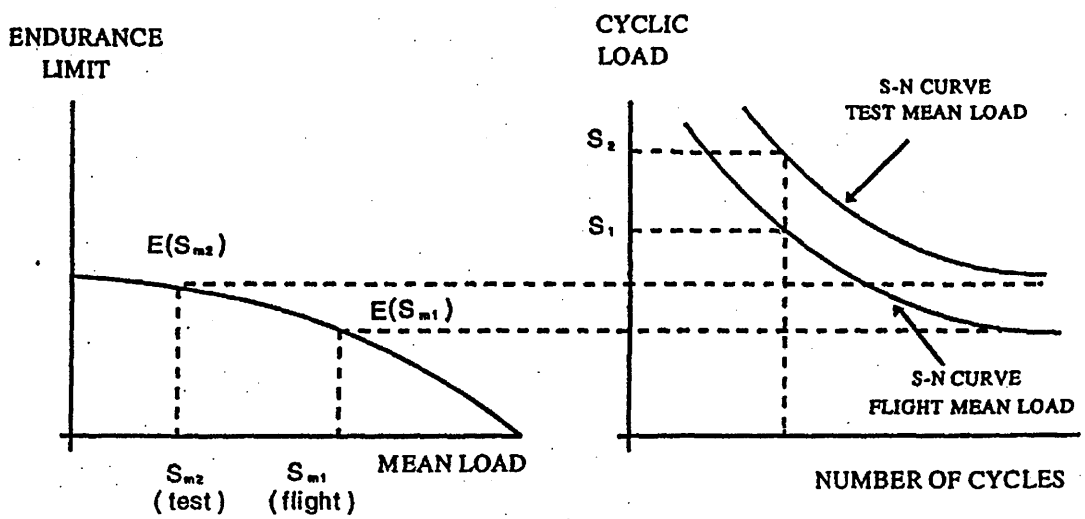

Fig. 2.5_ Mean stress correction [21]

In general the addition of non zero mean stress will result in diminished fatigue life. In the presence of a mean stress (σ_m), an approximation can be made by converting the stress amplitude to an equivalent completely

reversed stress amplitude that would result in the same cycles to failure. Three commonly used relations for making this conversion in stress-life calculations are presented in Fig. 2.6

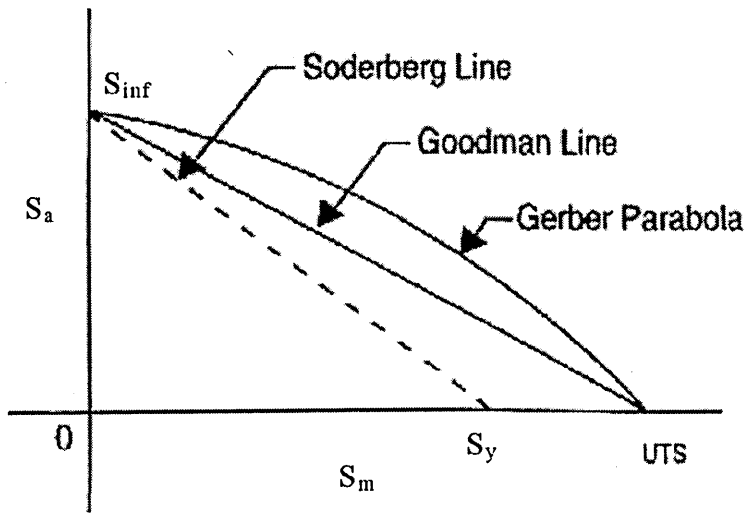

Fig. 2.6_4 A constant life diagram

the Goodman relation $$S_a = S_{\inf}\left[1 - \left(\frac{S_m}{UTS}\right)\right]$$

the Gerber relation $$S_a = S_{\inf}\left[1 - \left(\frac{S_m}{UTS}\right)\right]^2$$

and the Soderberg relation $$S_a = S_{\inf}\left[1 - \left(\frac{S_m}{S_y}\right)\right]$$

where S_{inf} is the endurance limit of the material, UTS is the ultimate tensile strength of the material, and S_y is the yield strength of the material. The Soderberg line is generally quite conservative. The Goodman line is fairly accurate for ductile materials; and the Gerber parabola generally describes the behaviour of ductile materials well. Master diagrams for alloy steel show dependency of the mean stress effect on the number of life cycles (high, low cycle fatigue, see Fig. 2.7 [22]). In fatigue design, the Goodman relationship tends to dominate, although conservative in most cases. Several ways to overcome this conservatism are suggested in the literature [23], [24].

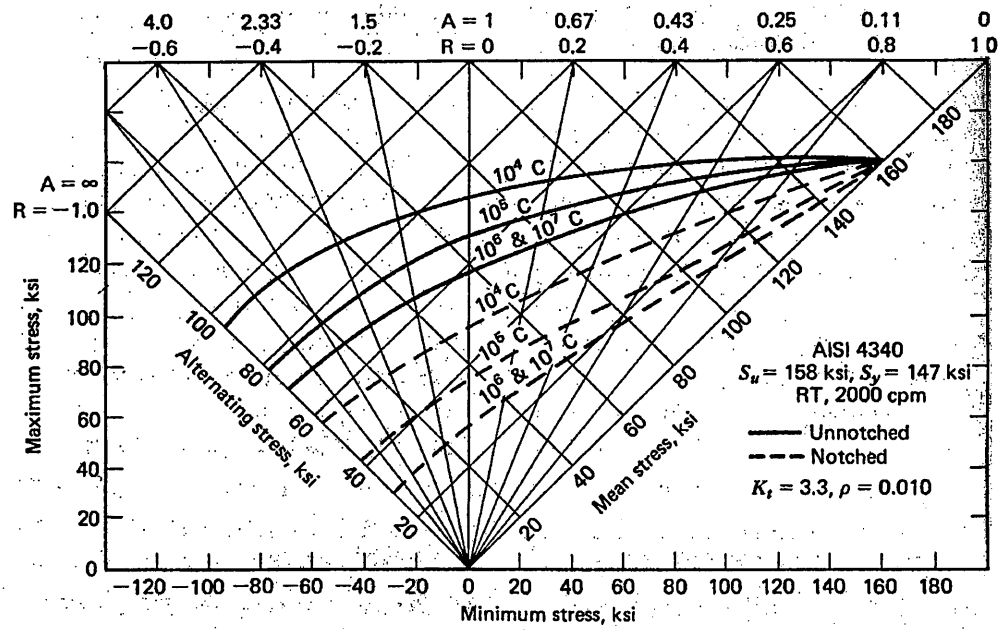

Fig. 2.7_Master diagram for alloy steel [22]

2.1.6 Cycle Counting - Rainflow counting

Cycle counting is referred to a mapping of real load time histories to cycle type loadings. This manipulation can be done in many ways, depending on the purpose of the analysis. For fatigue analysis the appropriate methods should be concerned with stress ranges since it is an important factor in the calculation of fatigue lives. Many range methods exist [25]: Range Pair, Hayes, Rainflow, Ordered Overall Range Counting, Racetrack Counting and Hysteresis Loop Counting. The Rainflow counting method is considered as the most accurate and it is also known as the Range Pair Range method.

The process of analysis takes into account the turning points in groups of three. The sequence is counted as a cycle if the stress range of the second and third turning points exceeds the stress range of the first 2 points. The cycle range is then defined as the range of the first 2 points, and the mean stress is defined as the mean of the first two points. If a cycle is counted it is removed from the history, if no cycle is counted, the process is moved ahead by one peak or valley. If the cycle includes the starting points in the history, it is counted as a half cycle, as are all cycles remaining at the end of the process. The method is best demonstrated by the example at Fig. 2.8 below, which also indicates which cycles are counted.

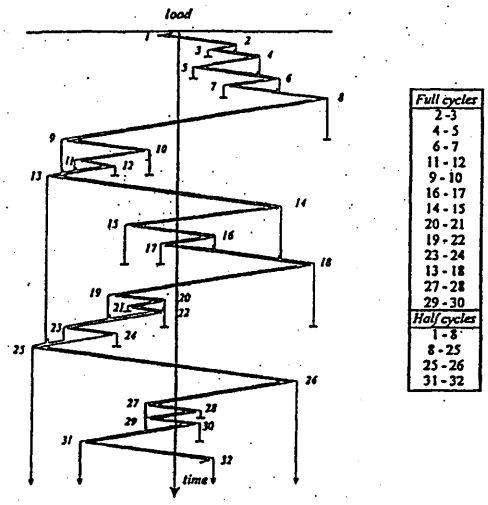

Figure 2.8_Rainflow Counting Example

2.1.7 The influence of stress concentration

Geometry effects, like notches, are influential to the stress distribution of a component under loading. The local stress at a stress concentration will be different to that at a point remote from the stress concentration, which is normally where strain gauges are located. It is necessary to define the stress at such points in terms of a function of the stress measured elsewhere on a component. This is done in the following 2 stages [26].

a. The local stress and strain histories at the tip of the notch must be known from knowledge of the imposed loads on a notched component.

b. The fatigue life that can be expected for the local stress and strain histories must be determined.

The fatigue strength is significantly reduced by the introduction of a stress raiser such as a notch or hole. Actual machines and components always have some stress raisers such as fillets, keyways, screw threads, press fits and holes. Fatigue cracks in structural parts usually initiate at such geometrical irregularities. The notch or hole introduces three effects in a stressed component [27].

Increase the concentration of stress at the root of the notch or hole. A stress gradient is set up from the root of the notch toward the centre of specimen. A triaxial state of stress is produced at the notch root.

The ratio of the maximum stress in the region of the notch to the corresponding nominal stress is the stress concentration factor K_t.

$$K_t = \frac{\text{actual maximum stress}}{\text{nominal stress}}$$

In some situations, the value of the stress concentration factor can be calculated using the theory of elasticity, or can be measured by using photoelastic methods or finite element methods. Fig.2.9 illustrates the general description of force line and stress concentration factor [28].

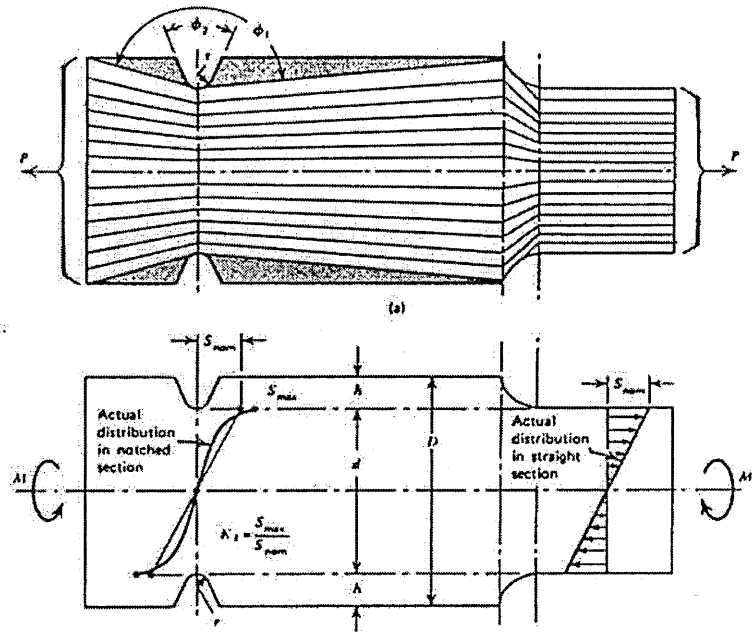

Fig. 2.9_Force Lines and the Stress Concentration Factor [28]

Adequately accurate values of K_t have been determined by experiment for a great variety of notch sizes, shapes, configurations and for many loading conditions as illustrated in Fig. 2.10 [29].

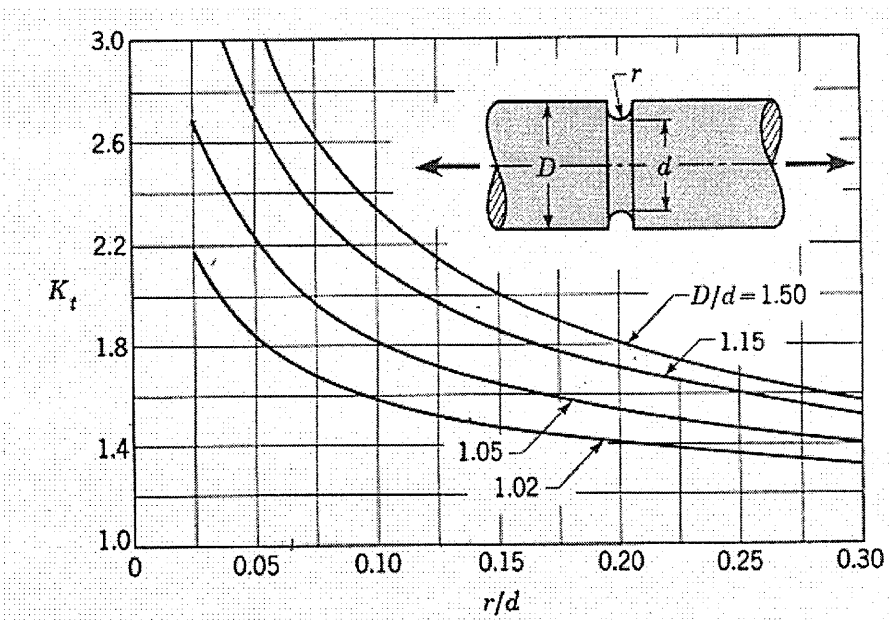

Fig. 2.10_Stress concentration factors for a shaft with a groove subjected to axial load [29]

The effects of notches on the fatigue strength is determined by comparing the (S-N) curves of notched and unnotched specimens. The effectiveness of the notch in decreasing the fatigue limit is expressed by the fatigue stress concentration factor K_f, which is defined to be the ratio of the effective fatigue stress that actually exists at the root of the notch to the nominal fatigue stress calculated as if the notch has no stress concentration effect.

$$K_f = \frac{\text{effective fatigue stress}}{\text{nominal fatigue stress}}$$

Unlike the theoretical stress concentration factor K_t, the fatigue stress concentration factor depends on the material as well as on the geometry and the loading type. To account for the influence of material characteristics, a notch sensitivity factor q has been defined to relate the actual effect of a notch on fatigue strength of a material to the effect that might be predicted solely on the bases of elastic theory. The definition of notch sensitivity factor is given by:

$$q = \frac{K_f - 1}{K_t - 1}$$

The reason for subtracting unity from the numerator and denominator in this definition is to provide a scale for q that ranges zero for no notch effect to unity for full notch effect. That is, for full notch effect K_f is equal to K_t. The notch sensitivity factor has been found to be a function of both material and notch radius (see Fig. 2.11) [30]

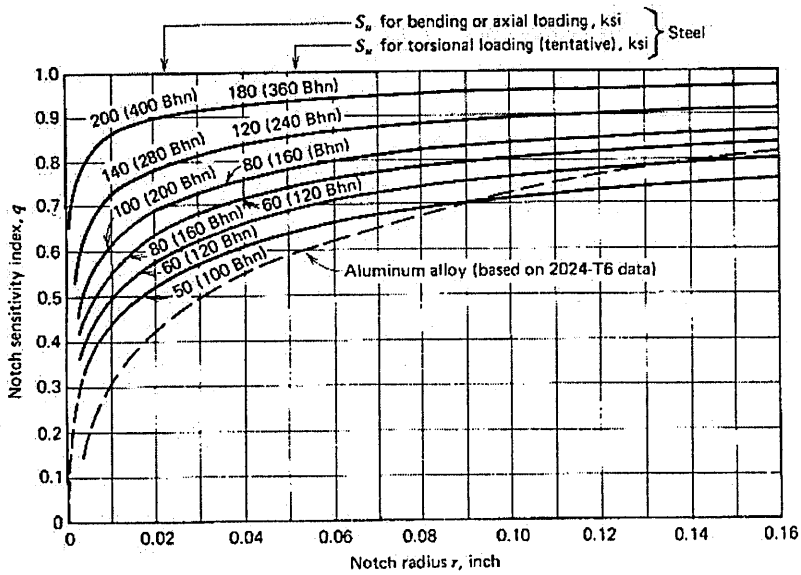

Fig. 2.11_Notch sensitivity factor (q) as a function of notch radius [30]

2.2 Fatigue design of helicopter components

The key points of the fatigue substantiation procedure of helicopter components are presented in Fig. 2.12. An analysis of every step has been made, based on available information [2], [3], [31] and issues concerning uncertainties arising from the methodology are noted. Statements are subject to change on the emergence of new and more accurate information.

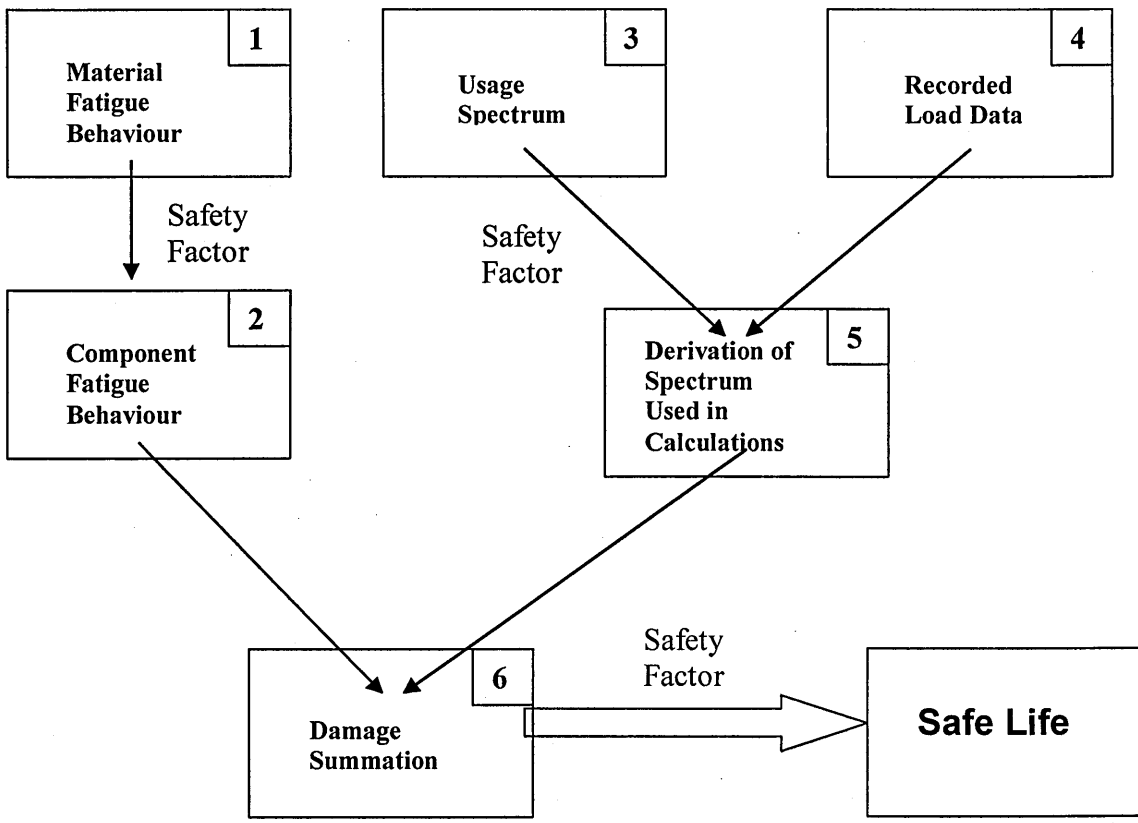

Fig. 2.12_Map of Fatigue Substantiation in Helicopter Design

In the following, each step of the fatigue substantiation procedure in helicopter design is briefly described.

1 Material Fatigue Behaviour

To establish the S-N curve shape and variability of a material, tests on coupons are carried out. Coupons are simple and inexpensive test specimens reproducing a single mode of fatigue failure.

2 Component Fatigue Behaviour

The endurance limit of an actual component is determined by testing a limited number of components under constant amplitude stress levels.

3 Usage Spectrum

Information on how the helicopter will be operated is provided by the customer to the design authority in the form of a mission spectrum.

4 Recorded Load Data

For the derivation of the actual flight loads, measurements are carried out on prototype helicopters that carry out manoeuvres as defined in the usage spectrum.

5 Derivation of Service Spectrum

During the production phase, recorded load data are processed and combined with the usage spectrum to generate the service spectrum used in the final calculations for a safe life.

6 Damage Summation

Miner's linear damage rule is employed for the damage calculation based on component data and the service spectrum.

Step (1) Material Fatigue Behaviour

Step (2) Component Fatigue Behaviour

The fatigue behaviour of the material has been established experimentally. Constant amplitude tests were carried out in the past, providing S-N curves for each material.

These tests concern smooth coupons and in order to apply the results on real components, the following procedure is followed.

The data are represented on a $\frac{S}{S_{inf}}$ vs. Life plot, so that the stress axis is dimensionless and an equation can be used to fit the experimental data:

$S = S_{inf}\left(1+\frac{A}{N^{\gamma}}\right)$, or $\frac{S}{S_{inf}} = 1+\frac{A}{N^{\gamma}}$, where S: stress amplitude, S_{inf}: fatigue endurance limit.

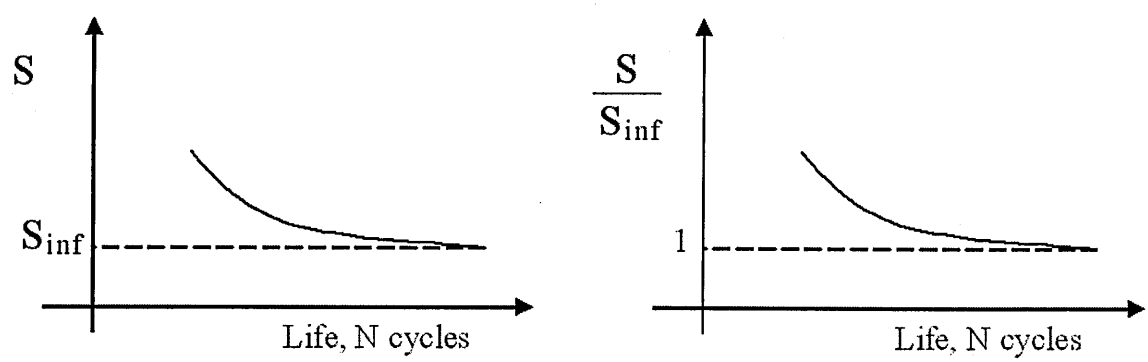

Constants A, γ are considered to be dependent only on the material (e.g. Steel, Titanium etc) and have been derived experimentally for coupons, several years ago [2].

The fatigue endurance limit (S_{inf}) calculation for the components is based on the results obtained from tests on coupons.

It should be noted that constants A, γ are assumed to be the same for the components as for coupons, although real components have different properties in fatigue, (e.g. stress concentration, non smooth surface, non uniaxial loading).

Three or four fatigue tests are carried out on components, and an S-N curve is fitted through each of the results on an $\frac{S}{S_{inf}}$ vs. Life diagram.

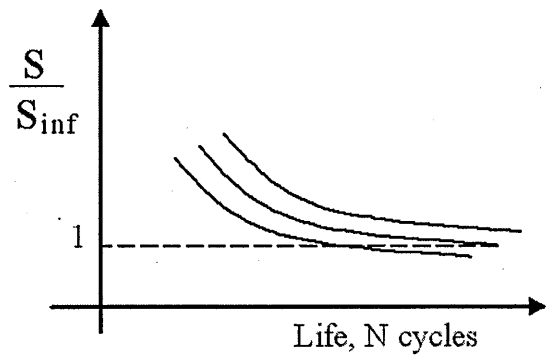

Knowing A, γ, S and N, the fatigue endurance limit S_0 is calculated from

$$S_{inf} = S \cdot \left(1 + \frac{A}{N^{\gamma}}\right)^{-1}.$$

The distribution of the data for the components is assumed to be the same as for the coupons. Hence, it is assumed that the same scatter and variability exists.

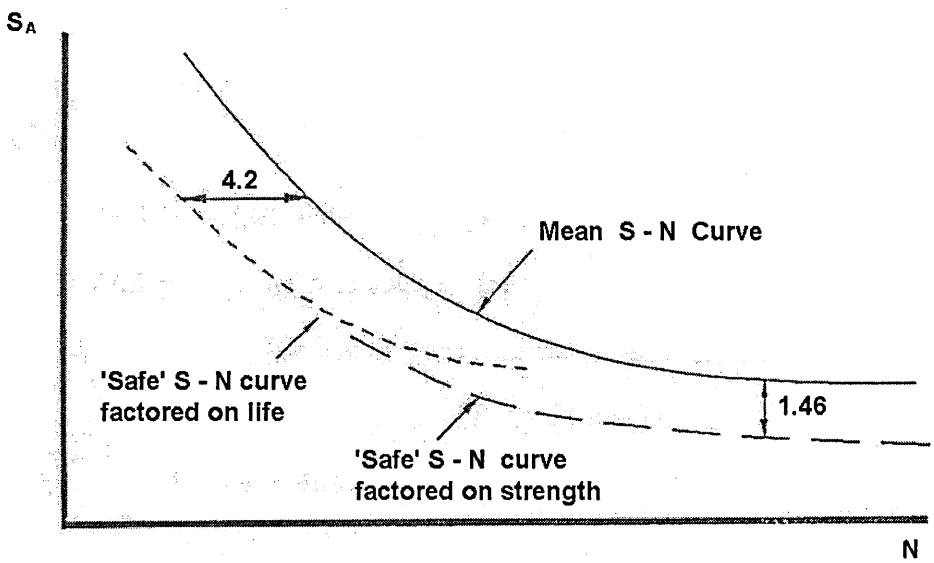

Fig. 2.13_S-N Curve Showing the Effect of Life and Strength Factors

As a safety measure, the S-N curve is reduced by three standard deviations (3σ) or equivalently safety factors are applied on strength and life, e.g. for Lynx Dogbone component 1.46 on strength and 4.2 on life is applied [32] (Fig 2.13).
It would be possible to apply a best fit instead of using the constants A, γ the scatter would be reduced leading to a reduction of the applied factors. More experimental results on the S-N curve exist in the literature. These extended data may be used to enhance our knowledge on the material's fatigue behaviour.

Step (3) Usage Spectrum

The usage spectrum is provided by the customer. The RAF, based on statistical data on the flight missions, specify helicopter usage rates. The usage is split into different manoeuvres and each manoeuvre is assigned a percentage of usage in 1 flight hour. RAF gives very strict definition of the manoeuvres, leaving possibly high damaging manoeuvres unattended (e.g. Level flight produces more damage than expected, when all the flight is used and not just the accurately executed manoeuvres [32]). As an alternative way, the use of sorties instead of individual manoeuvres could be considered.

Step (4) Recorded Load Data

Flight loads are acquired from instrumented (strain-gauged) prototype helicopters, that carry out several manoeuvres and the recorded data are analysed to give the actual stresses. There is an uncertainty on how accurately the recorded data are manipulated to provide the actual stresses experienced by the component.
In order to calculate the damage caused by each manoeuvre, the following procedure is adopted: Approximately 10 examples of each manoeuvre are split into LOW (ground-air-ground) and HIGH frequency and the damage summation is carried out separately for each frequency. It should be noted that with today's tools it is possible to calculate the complete load spectrum more accurately. After the separation, each manoeuvre is assumed to have a constant mean stress. The rainflow counting method is applied through the whole loading spectrum and the damage calculation is carried out. It should be noticed that in order to evaluate the reliability of the application of rainflow counting method, it is important that the gating

level used is known. Cycles less than the gate level are omitted. It is applied to stop large numbers of small, presumably non damaging cycles from complicating the calculation. It should be kept in mind that the higher the gating level, the less conservative the prediction will be. A safety factor of 1.2 is applied on top of the loading spectrum, when limited load data exist (less than 10 occurrences of the maximum load).

The following remarks point some issues on steps (3)-(4):

- Division of load spectrum in LOW-HIGH frequency.
- Gating level in cycle counting.
- Non-valid manoeuvres may contribute significantly more or less in damage. Also damage may arise from cycles in between the manoeuvres (transition, interaction). There may be significant differences depending on the component.
- Safety factors applied (1.0 to 1.2)
- Simplification of loading spectra

Step (6) Damage Summation

As a damage summation criterion Miner's rule summed to unity is used. When test loading fails to represent the actual service loading as closely as possible, an uncertainty factor of 0.75 instead of 1.0 is applied. It should be noted here that in order to take into account mean stress effects, the Goodman relationship is used. For both Miner's rule and Goodman's relationship an experimental investigation will be carried out aiming to quantify the uncertainty and conservatism involved in each one.

2.3 HELICOPTER HEALTH AND USAGE MONITORING

Many and varied techniques have been applied to the problem of monitoring the pattern of usage of a helicopter and the condition of critical components. As indicated by the heading of this Section, the majority of the methods used can be split into two categories: health monitoring (HM) and usage (or fatigue) monitoring (UM). Usage monitoring can be further subdivided into flight loads and flight condition monitoring (Fig 2.14).

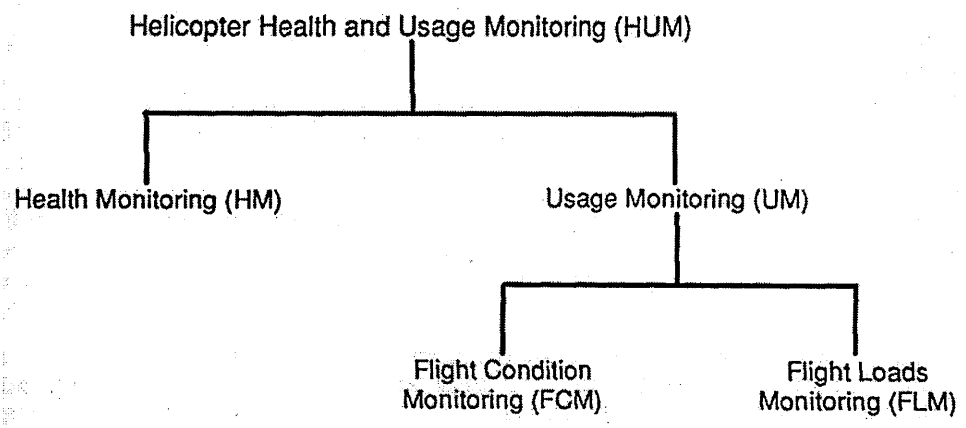

Fig. 2.14_The various categories of helicopter health and usage monitoring

Usage monitoring is necessary and is related to the uncertainty that exists over how helicopters are used. Helicopter design authorities can only make assumptions as to the type of missions and manoeuvres that the helicopter will carry out. However, the versatility of helicopters can lead to future usage beyond the originally envisaged design roles.
However, installation of a monitoring device on helicopters could establish the severity and type of missions flown or loads experienced which in turn would permit appropriate adjustment of the safe-life accordingly.

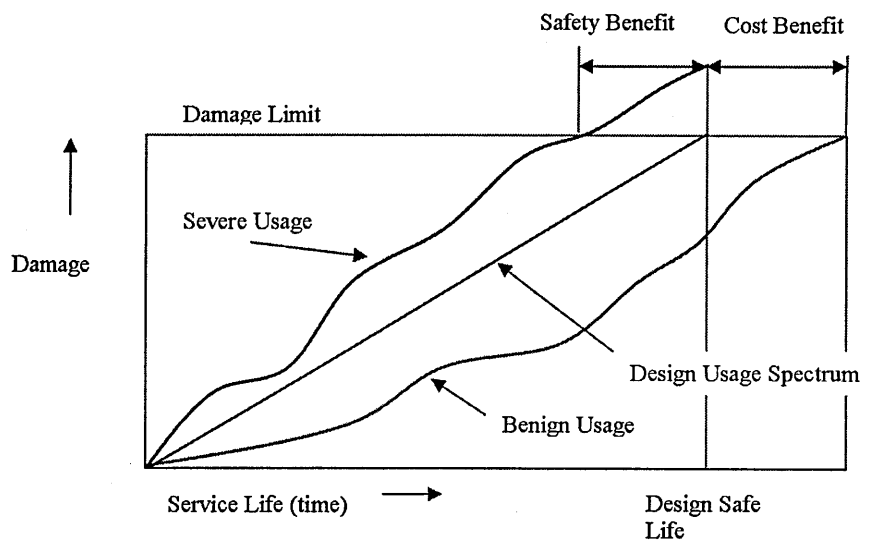

Fig. 2.15_ Benefits of Usage Monitoring

Health and usage monitoring can increase helicopter safety and has the potential to decrease operating costs by increasing the time between component replacements.

2.3.1 USAGE MONITORING

Usage monitoring (UM) examines the usage of a helicopter and then makes an estimate of how much safe-life remains in a component before it must be replaced. UM can be divided into two types as indicated in Fig. 2.14: flight condition and flight loads monitoring. Usage monitors can be exclusively of one type or the other, or can incorporate elements of both.

2.3.1.1 Flight Condition Monitoring

The aim of flight condition monitoring (FCM) is to identify how severely (or benignly) an individual helicopter is flown by determining the flight conditions which occur during flight. By establishing how the helicopter is used, an estimate can be made of the fatigue life expended in a particular component, provided that some link between flight condition and resultant fatigue damage can be found. This link is generally achieved by flight testing. Strain-gauging numerous components on a flight test helicopter that flies through a series of predetermined manoeuvres. Component loads are measured during different flight conditions.

The types of parameters which are measured on an FCM-equipped helicopter can include: control stick positions, altitude, outside air temperature etc. Since FCM relies on the measurement of several helicopter and environmental state parameters, it is sometimes referred to as parametric monitoring.

Once the flight test data are obtained, component loads, and hence fatigue damage, can be estimated. Fatigue damage will normally be estimated by using the safe-life technique. A diagrammatic representation of how a typical FCM system works is shown in Fig. 2.16.

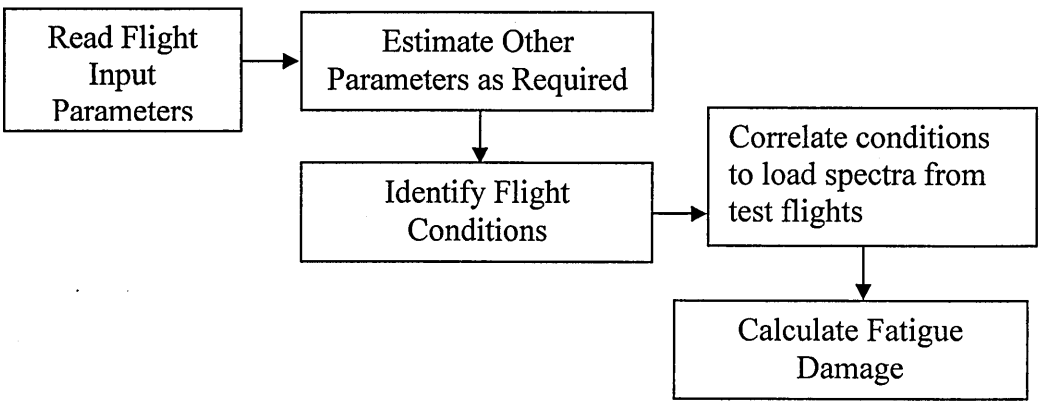

Fig. 2.16_ Sequence of events in a flight condition monitoring system.

2.3.1.2 Flight Loads Monitoring

Flight loads monitoring (FLM) is similar to FCM in that they both attempt to quantify in-flight fatigue damage. Unlike FCM, however, FLM rely on the output from strain gauges to determine loads on several key components. Indirect methods are still used, though, to estimate the loads on components that are impractical, inaccessible, or not necessary to strain gauge.

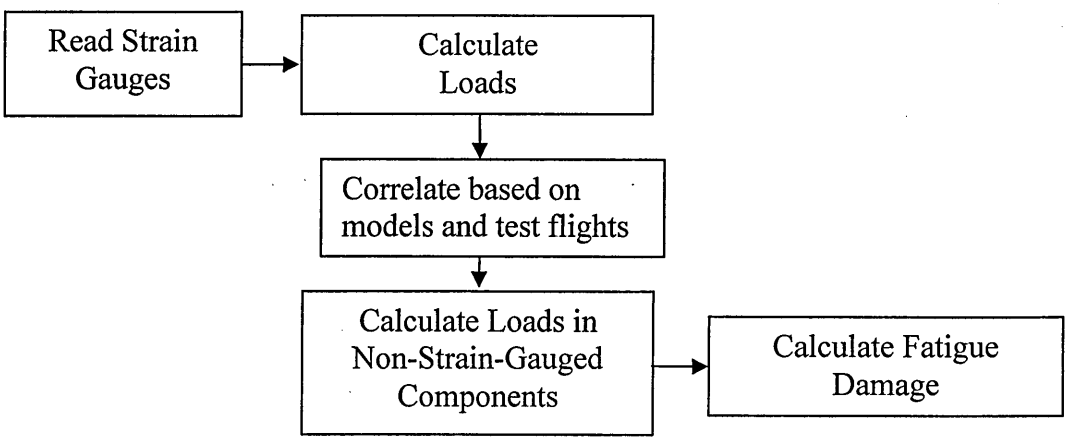

Fig. 2.17_Sequence of events in a flight loads monitoring system.

The components which are strain gauged are mainly those in the rotating system since these are the ones most prone to fatigue failures. The strain gauge signals must be transferred from the rotating system to the fixed system through the use of slip rings [33] or radio telemetry. These methods are likely to cause maintenance problems on in-service aircraft.

Strains are converted to loads that are then used to derive loads in non-strain-gauged components. After this, the fatigue damage is determined in the same way as is done in an FCM system.

2.3.1.3 Flight Condition versus Flight Loads Monitoring

The following list summarises some of the advantages and disadvantages of the two systems.

- FCM is compatible with the way that a helicopter is designed. A helicopter design is based on a usage spectrum which is defined in terms of the percentage time spent in various flight conditions and not in terms of component loads.

- The conservatism in FCM depends upon flight tests. If flight tests do not achieve the most damaging conditions for each flight condition it will be necessary to use safety factors in the safe-life calculations
- FLM systems eliminate the uncertainty of the FCM during indirect estimation of loads and it is possible to detect peak loads.

- A high-fidelity flight regime recognition algorithm is essential for FCM systems. The algorithm must be capable of recognising all the required flight conditions. However, the recognition of low speed manoeuvres in particular has always been difficult. This problem is yet to be adequately addressed.

- An FCM system should be easier and less expensive to install than an equivalent FLM system.

- Strain gauge signals can become corrupted by electrical noise as they are transferred across slip rings so this requires the addition of filters or error correction software to reduce the amount of bad data.

- Routine rotor head maintenance of helicopters equipped with an FLM system will become more complicated because of the presence of strain gauges and slip rings.

- FCM systems can provide a history of how the helicopter was used in a way that is easily understood, i.e. percentage times in various flight conditions and the resulting component loads. Such knowledge is useful in setting up mission spectra for new and derivative helicopter designs, but it

is especially useful for helicopter operators. By being able to correlate actual usage with fatigue damage, operators have the chance to alter their usage to minimise damage and hence operating costs.

- Some FLM systems that are currently being researched propose doing away with strain gauges in the rotating system and have them only in the fixed system. This reduces the expense of an FLM system, but introduces another level of calculation (and uncertainty) into the process by having to determine rotating system loads from fixed system loads.

There is no easy answer as to whether flight condition or flight loads monitoring is better, or whether a hybrid system, combining aspects of both FCM and FLM should be used. The decision on what to use depends on several parameters, such as: cost, reliability, maintainability, ease of use and application etc.

2.3 Statistical – Probabilistic

In the following a description of basic statistical tools is presented and a review of probabilistic approaches to fatigue substantiation of helicopters using Monte Carlo simulation.

2.3.1 Introduction to statistics - Statistical Representation of Fatigue Data

As many natural phenomena the precise fatigue life cannot be predicted with certainty due to the randomness of the process.
A continuous random variable, such as fatigue life, can be completely described by a cumulative distribution function (cdf). A cdf will have a probability density function associated with it, as indicated by the definition below:

$$F(x) = \Pr(X < x) = \int_{-\infty}^{x} f(\theta)d\theta$$

which can be represented graphically as in Fig. 2.18

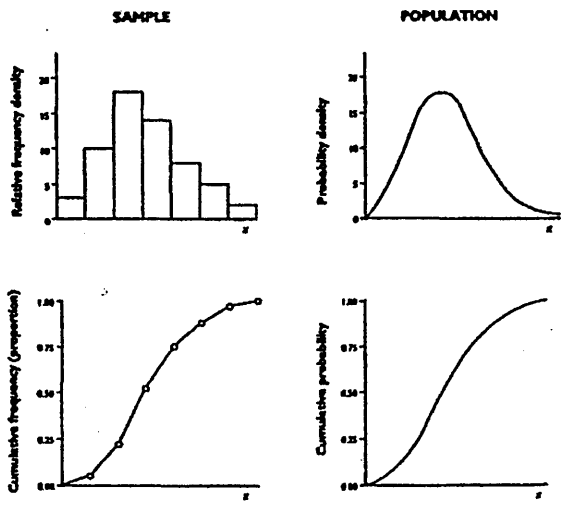

Fig. 2.18_Distribution Functions

2.3.2 Types of Distributions

The distributions generally used with fatigue analysis are: normal, lognormal and Weibull distributions. These distributions are shown at Fig. 2.19

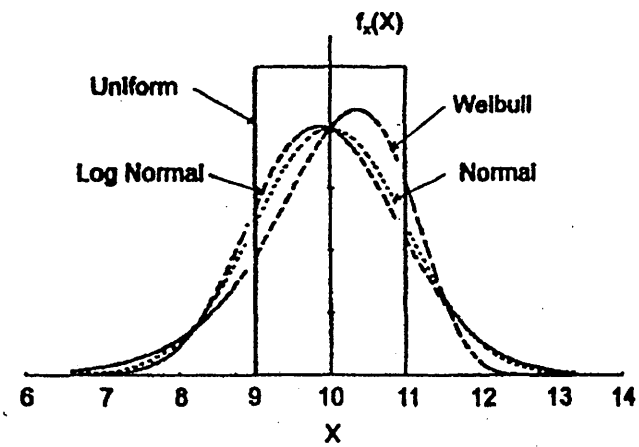

Fig. 2.19_Common Distributions

2.3.2.1 Normal Distribution.

A Normal (or Gaussian) distribution has the following pdf:

$$f(x) = \frac{1}{\sigma\sqrt{2\pi}} e^{-((x-\mu)/\sigma)^2/2} \quad \text{for } -\infty < x < \infty$$

It is characterised by a symmetric bell-shape. The curve falls off at both sides and large deviations from the measured value are extremely rare [34]. Accuracy improves with population size. The normal distribution is generated by additive co-operation of many random quantities, such as peoples' height.

2.3.2.2 Log-Normal Distribution.

A log normal distribution has the following pdf:

$$f(x)=\frac{1}{\zeta\sqrt{2\pi}}e^{-((\ln x-\lambda)/\zeta)^2/2}$$

where the mean, λ, and the standard deviation, ζ, are transformed into the logarithmic domain:

$$\zeta^2=\ln(1+\frac{\sigma_x^2}{\mu_x^2}) \qquad \text{and} \qquad \lambda=\ln(\mu_x)-\frac{1}{2}\zeta^2$$

A lognormal distribution is generated by multiplicative co-operation of many random quantities so that the effect of a random change is in every case proportional to the previous value of the quantity. A typical shape of log normal distribution is shown on Fig. 2.20.

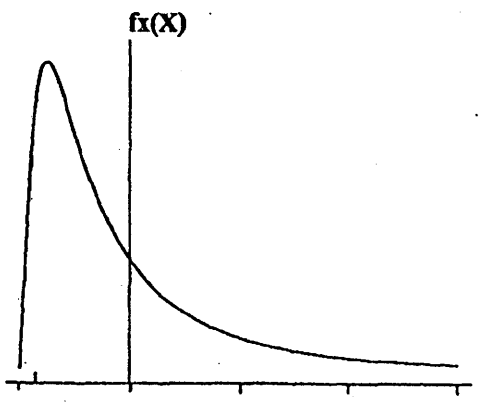

Fig. 2.20_Lognormal Distribution

2.3.2.3 Weibull Distribution.

Usually, the fatigue strength or the endurance limit values listed from experiments represent the arithmetic mean derived from multiple experiments.

Different sets of experiments conducted on the same material may not give the same arithmetic mean of the critical strength parameter. To address this issue, Weibull [35] proposed the concept of a probability of failure, P, at a given failure strength, σ_f normalised by an average value of a critical stress $\sigma_{cr,ave}$ (which may be identified with the average value of tensile fracture strength, σ_u for a brittle solid or with the fatigue limit σ_e for a metallic alloy). At low values of σ_f, P goes to zero, and at very high values of σ_f, P goes to one.
Weibull defined the failure probability as follows

$$P = 1\text{-}P_s = 1 - \exp\left[- \left(\frac{\sigma_f}{\sigma_{f,0}} \right)^{m_w} \right]$$

Where m_w is known as the Weibull modulus, and $\sigma_{f,0}$ is a reference strength.

A three parameter Weibull distribution has the following pdf:

$$f_z(Z) = \frac{k}{w-\varepsilon}\left(\frac{z-\varepsilon}{w-\varepsilon}\right)^{k-1} e^{\left[-\left(\frac{z-\varepsilon}{w-\varepsilon}\right)^k\right]}$$

$$\mu_z = \varepsilon + (w-\varepsilon)\Gamma\left(1+\frac{1}{k}\right)$$

$$\sigma_z^2 = (w-\varepsilon)^2\left[\Gamma\left(1+\frac{1}{k}\right)^2 \Gamma^2\left(1+\frac{2}{k}\right)\right]$$

where Γ is the gamma function. A full explanation of the parameters is given at Reference [34]. It is normally composed of 3 parameters which are: a characteristic value, w, Weibull slope, k, and a characteristic minimum life, ε. These terms are related to the mean and standard deviation in a complex manner. When ε is taken as zero, the formulation becomes a 2 parameter Weibull distribution

2.3.3 Definitions of Statistical Terms

The basic concept of statistical theory is to extract trends of the behaviour of the system under consideration by evaluating average values of the quantities of interest. These ensample averages are defined as follows:

2.3.3.1 Measures of Centrality

(1) Mean — The mean (μ) refers to the arithmetic mean unless stated otherwise. It is the average value of an element, obtained by adding all the data (x_i) and dividing by their number (N).

$$\mu = \sum_{i=1}^{N} \frac{x_i}{N}$$

(2) Geometric Mean - The geometric mean (μ_G) is the average value of an element, obtained by multiplying all the data from x_i to x_n and taking the n^{th} root.

$$\mu_G = \sqrt[n]{x_1 . x_2 ... x_n}$$

(where $x_i > 0$)

A non-typically large sample element has less influence on the geometric mean than it has on the arithmetic mean.

(3) Median — The median is simply the value of the middle element when all elements have been put in ascending order.

(4) Mode — The mode is the value of the element which occurs most frequently within the sample or population.

2.3.3.2 Measures of spread

Range – The value between the largest and smallest element

Variance – The variance is a measure of the dispersion or spread of a random variable. It is defined as the average of the squared deviations from the mean:

$$\sigma^2 = \frac{\sum_{i=1}^{N} (x_i - \mu)^2}{N}$$

Standard Deviation – The positive square root of the variance(σ)

Coefficient of Variation (CoV) – For processes with non-zero mean the CoV is defined as: $COV = \frac{\sigma}{\mu}$

It is convenient to normalise the standard deviation with the mean, when comparing the dispersion of 2 or more random variables with different units and magnitude.

2.3.4 Statistical Considerations

There are a number of sources of uncertainty in the analysis of fatigue results, in general, and in the use of the stress-life approach. These arise from:

Uncertainties and/or errors in the estimation of material properties which include micro-structural variability from one specimen or batch to another as well as experimental errors in the measurement of properties in the same batch of materials.

Uncertainties in the modelling of applied stresses, for a given service condition and environment. This variability stems from two sources: (i) the variability in the stress amplitudes during a known service cycle as a consequence of such factors as vibrations, and (ii) lack of knowledge about the exact distribution of stress cycles which occur over the design.

Uncertainties in the a priori estimation of the `environment` and in the ensuing variation in loading intensity. For example, in wind turbine and high speed transportation applications the `environment` and `loading intensity` refer to the wind speed. In the fatigue analysis of automobiles, they generally refer to the `driver profile` or the road condition. In offshore structural design, they refer to the `sea state`[37].

Uncertainties in modelling, predictions and life estimates for fatigue processes. Such uncertainties are analysed using known statistical approaches to derive the level of reliability or probability of failure.

2.3.5 Monte Carlo simulation

A popular and powerful tool among others [38] for analysing fatigue in probabilistic terms is Monte Carlo simulation, which is considered in this project. Monte Carlo simulation provides approximate solutions to

mathematical problems by performing statistical sampling experiments by computer [39].

2.3.5.1 The Application of Monte Carlo Simulation to Fatigue Analysis

The safe life substantiation process is assumed to depend on some distinct material or process parameters. Each of these parameters is associated with a probability density function. In order to estimate the overall probability of failure Monte Carlo simulation is used.
In Monte Carlo simulation, a computer random number generator selects a value between 0 and 1 each time a value for an input variable is needed. The random number is converted into a specific value of the input variable from the appropriate pre-defined cumulative distribution function (cdf).

2.3.5.1.1 Cumulative Distribution Function

For specific cases it is appropriate to analyse the implication of the variables on the expected cdfs. The cdf can be considered as a failure rate diagram as shown by Fig. 2.21 below. [40]

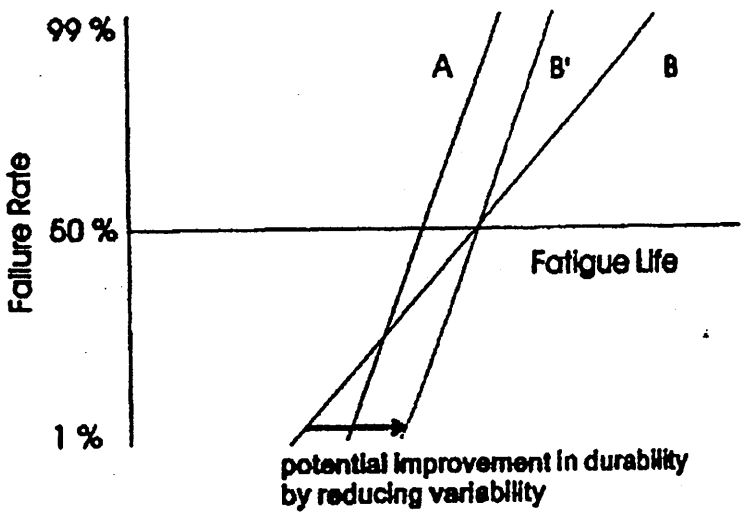

Fig. 2.21_Failure Rate Diagram

The effects of varying the mean strength, and of the variability in that strength, are shown in Fig. 2.21. Design A has a lower mean strength than design B but also has a lower CoV, as indicated by the gradient of the cdfs (failure rate diagram). This means that if a large number of components A and B were subjected to the same service conditions, the scatter in service

life would be greater for design B. Furthermore, the earliest failures of design B (e.g. the first 1%) would occur before the same percentage failures had occurred with design A. Even though design B displays greater fatigue resistance on average, the early failures could lead to a perception that it was a poorer design. Benefits in minimum fatigue lives are best achieved by increasing the mean strength without increasing the overall variability, as in design B'.

2.3.5.2 Probabilistic investigations

Probabilistic methods have been applied to fatigue life substantiation by a number of researchers. A Monte Carlo analysis was carried out by Irving et al [41] in the context of methods for realising the potential benefits of FUMS and included an investigation of the damage law and of loading and usage variability. A statistical analysis of the overall reliability of a helicopter was carried out by Viswanathan et al [38] who discussed models for strength and load spectrum variabilities. Zhang at Reference [42] investigated fatigue life prediction under random loading using a probabilistic damage rule and a probabilistic stress-life relationship.

Moon, Menon and Brandt [43] used the US Navy SDRS fitted to a fleet of 50 US Navy rotorcraft to explore the variation in usage distribution in the helicopter population. They found that usage variability in each manoeuvre was better modelled using a Weibull distribution. However, the fit was far from perfect. Variability in usage was large, with coefficients of variation ranging from 33% to 273%. These workers also present limited data on the variability of loads in each manoeuvre, with coefficients of variation ranging from 15% to 57%. They use this in conjunction with material fatigue data to perform Monte Carlo Simulations to derive the cumulative distribution of probability of failure of selected components.

Thompson and Adams [44] also performed a Monte Carlo simulation concerning three UH-60 main rotor components. They note that component strength was the overwhelming factor in the determination of component life and that the effects of spectrum and flight loads tended to average out over a lengthy period of simulation. Boorla and Rotenberger [45] performed a flight loads variability analysis using a Bell OH-58C helicopter. Load variability appears to be normally distributed with a median coefficient of variability of approximately 13%. It was also noted

that use of peak loads to characterise load variability may result in more scatter than is truly representative of inherent load variability.

Zion [46] carried out a variability study on two BH Model 234 dynamic components indicating that current deterministic methods are conservative enough to exceed six nines reliability. The study was based on loads and strength variability but it is also noted that operational variability in the fleet would be beneficial for component reliability when load severity of the flight test aircraft is high relative to the fleet. Harris et al [47] applied a probabilistic methodology to calculate the retirement life of a critical helicopter dynamic component, demonstrating a potential gain of 30% in life compared to the conservative deterministic approach.

Neal et al [48] used the Bootstrap method to carry out a sensitivity analysis on component reliability. Variability is introduced for the following factors: spectrum load, mean S/N curve and Miner's rule. Factors varied in combination as well as individually with CoV ranging from 1% to 5%. Strength variability for steel was assumed around 7%. Results show that small amounts of variability in load or strength result in substantial reduction in reliability. In contrast Miner's rule variability had little effect.

2.3.5.3 Robust estimation of total probability of failure

To realise the full potential of the probabilistic approach it is necessary to consider all uncertainties collectively. It was recognised that for the probabilistic approach to succeed it would be necessary to attain better models for the following categories of the substantiation process:

a. Variability in loading and usage
b. Variability in material properties.
c. Geometry effects.
d. Variability and uncertainties in analytical methods (Miner summation, Goodman).

3. Experimental study of fatigue substantiation tools

A considerable amount of research time was devoted to experimental work. This was necessary in order to validate analytical approaches employed in helicopter design. Areas of focus were damage summation rule and mean stress effect under both constant and variable amplitude loading. Therefore fatigue tests were carried out to validate Miner's rule and Goodman equation under typical helicopter loading spectra, using specimen material and geometry based on actual component.

3.1 Real case study

The selection of specimen properties and loading spectra were subjected to certain restrictions.

In order for the experiments to represent a realistic situation the specimen was based on an existing helicopter component. The helicopter type was required to be a non-current model for which appropriate loading data would be available in order to use for variable amplitude testing. The Sea-King helicopter and its main-rotor upper plate was initially selected (Fig. 3.1).

Based on that, appropriate specimens and grips were designed and manufactured. After the commencement and partial completion of testing under constant amplitude loading it was realised that appropriate dynamic loading data from the Sea-King could not be provided. This was due to the old age of the storage media and the low quality of the data acquisition system that was used at the time. It was unsuccessfully attempted to reconstruct a loading sequence based on some limited, written on paper, data regarding the Sea-King helicopter.

Hence, it was decided and approved to use the loading sequence of a current helicopter type. The Lynx helicopter and its main rotorhead was selected. The following paragraphs describe in more detail the various steps of the methodology.

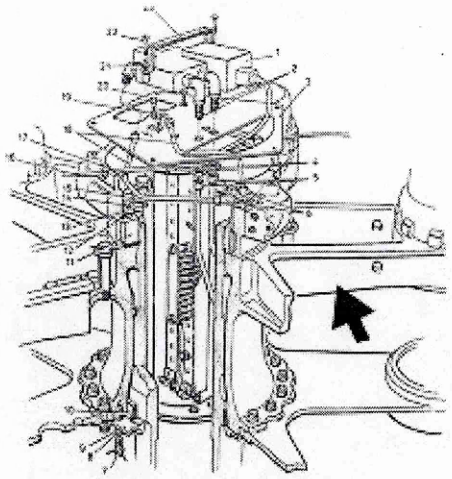

Fig. 3.1_ Sea–King Helicopter and its main rotor upper plate

3.2 Material properties

The material selected for the experiments was a quenched and tempered high strength steel (BS 2S97) as used on Sea King helicopter main rotor upper plate. The material was hardened (850°C Oil), tempered (600°C), stress relieved (570°C) and was supplied in bars of 19.05mm diameter. The chemical composition of the material is shown in table 3.1 and the mechanical properties in table 3.2.

BS 2S 97 – 2.5% Nickel-Chromium-Molybdenum Steel					
Chemical Composition					
C	Si	Mn	P	S	Cr
0.32%	0.24%	0.53%	0.004%	0.008%	0.68%
Mo	Ni	Cu	Al	Sn	
0.51%%	2.5%	0.14%	0.026%	0.012%	

Table 3.1_ Chemical composition of 2S97 steel (2.5% NiCrMo)

	Hardness (Vickers)	Tensile strength (MPa)	0.2% Proof Strength (MPa)	Elongation on 50 mm
Min	310	1000	540	12%
measured	351	1124	1025	21%

Table 3.2_ Mechanical properties of 2S97 steel

The material's hardness was tested three times on three different specimens, giving results within the above specified limits (351HV average, max. 364HV, min. 342HV).

Also, three tension tests were carried out to determine the Ultimate Tensile Strength of the material. The results were within the limits presented in the above table (UTS: 1124MPa average, max. 1133MPa, min. 1115MPa). The result of a test is presented on Fig. 3.2.
It should be noted that for steel materials it is generally accepted that up to a point, the ultimate tensile strength is in direct relation with the fatigue endurance limit [3].

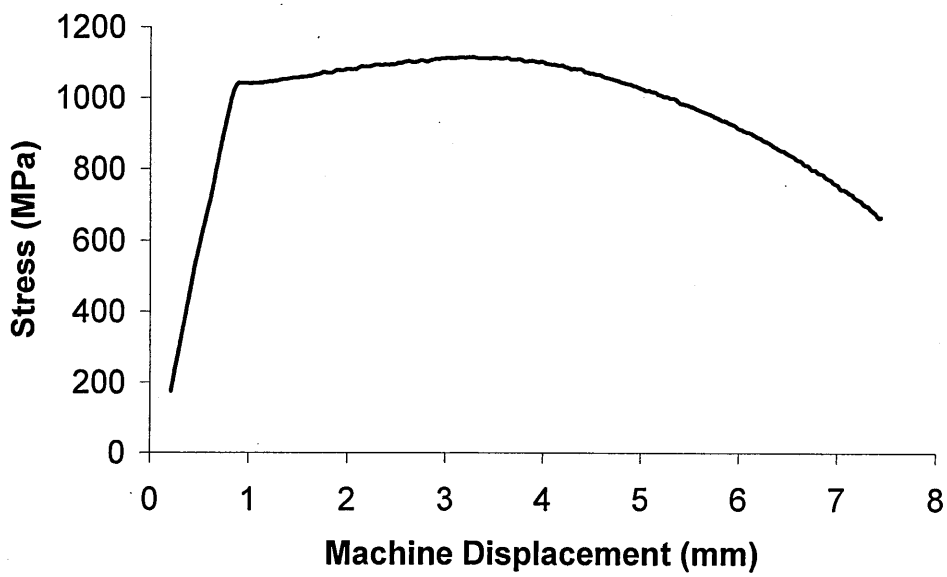

Fig. 3.2_ Data plot of tensile test results

3.3 Design of grips and specimens

In order to carry out the necessary fatigue tests the appropriate gripping fixture was designed and manufactured. The grips were employed to hold securely and in proper alignment the specimens during the test. Initially it was planed to use a modified version of existing grips (Appendix A, Fig.A1) due to easiness of manufacture and low cost. Further study on the subject led to the decision of designing and manufacturing new grips that would be more robust under fully reversed loading (R=-1) and able to ensure proper alignment during testing. These grips were modelled

(Fig.A2) and analysed using finite element methods (Fig.A3) on I-Deas CAD/CAE software package. In the following the grips were manufactured according to the mechanical drawings shown on Figs.A4, A5, A6.

Two types of cylindrical samples were machined from round bars to ASTM E466 standard. Manufacturing drawings are in appendix A. Smooth samples have a gauge diameter of 8mm and a gauge length of 30mm. Notched samples simulate the main rotor upper plate at a point of high stress concentration (Fig. 3.3). Theoretical stress concentration factor at that point is K_t=2.3 [49] and the same applies for the notched specimen according to finite element analysis and information based on graphs for the specific geometry [50, 51].

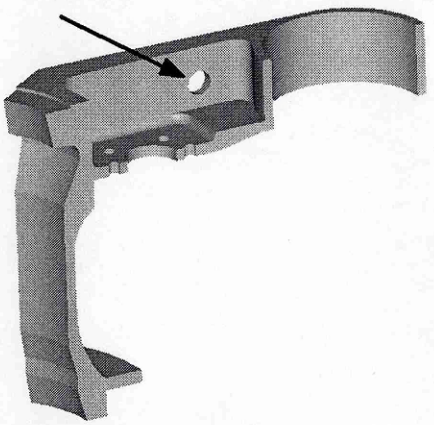

Fig. 3.3_ Point of high stress concentration on Sea King main rotor upper plate

3.4 Testing equipment

All fatigue tests were performed on a servo hydraulic, digitally controlled test machine comprising a Mayes frame and an Instron 8500 digital control unit (Fig. 3.4). The capacity of the machine was 100 kN. Loads were measured to an accuracy of 0.1%. Testing frequency ranged up to 24Hz depending on load level. For variable amplitude fatigue tests, a computer was used to input the sequence of peak and trough commands to the testing machine.

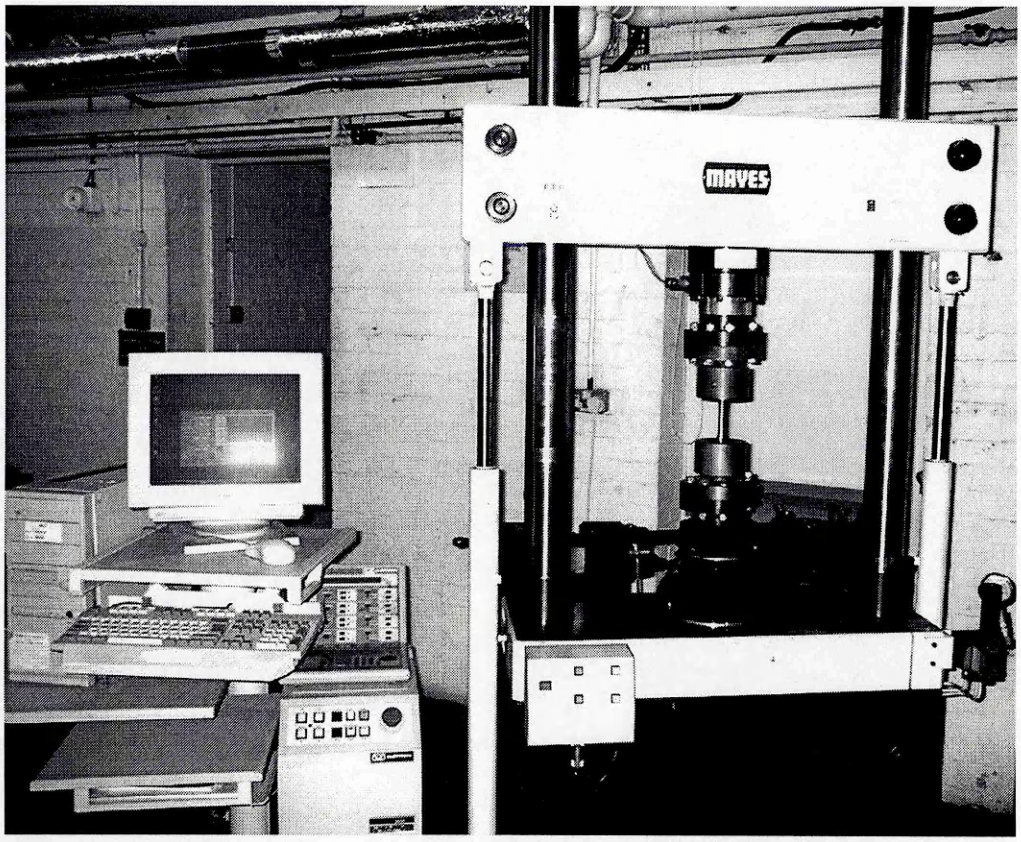

Fig. 3.4_ Hydraulic, digitally controlled test machine

3.5 Experimental results under constant amplitude loading

Experiments were performed using constant amplitude loading with smooth and notched specimens. All fatigue lives were to specimen separation. The aim of tests under constant amplitude is to develop the S-N curve of the material and to examine the effect of non zero mean stress.

3.5.1 Development of S-N curve

Fatigue data in the high cycle fatigue range can be displayed on a plot of cyclic stress level versus the logarithm of life. These plots called S-N curves constitute information of great importance in the safe life approach of fatigue design. The concept of Miner's rule for cumulative damage is entirely based on the S-N curve as seen in chapter 2.

The steps to develop the S-N curve begins with a selection of a group of well-prepared specimens of the material. Then a number of stress levels that span the stress range is selected and tests are run at each level. For each run, the specimen is carefully mounted so that no spurious stresses appear. The machine is set at the appropriate stress level and the cycle counter is restarted. The test is run until the specimen fails or runs out (approaches 10^6 to 10^7 cycles). The stress level and the cycles to failure (or run out) is recorded. After that another stress level is selected and the preceding procedure is repeated. The procedure is repeat until tests have been run at all stress levels. Finally the obtained data are plotted on a stress-life diagram.

For the development of S-N curve, uni-axial loading with ratio R = -1 (fully reversed tension – compression) was used. This way the mean stress would be zero, and no need for correction would be necessary. The frequency of loading varied considerably depending on the stress level. For example at high stress level (>780 MPa) the used frequency was limited to 0.5 Hz to avoid high temperature because of limited heat dissipation. On the other hand at lower stress levels (~550 MPa) the maximum achieved frequency was 25Hz.

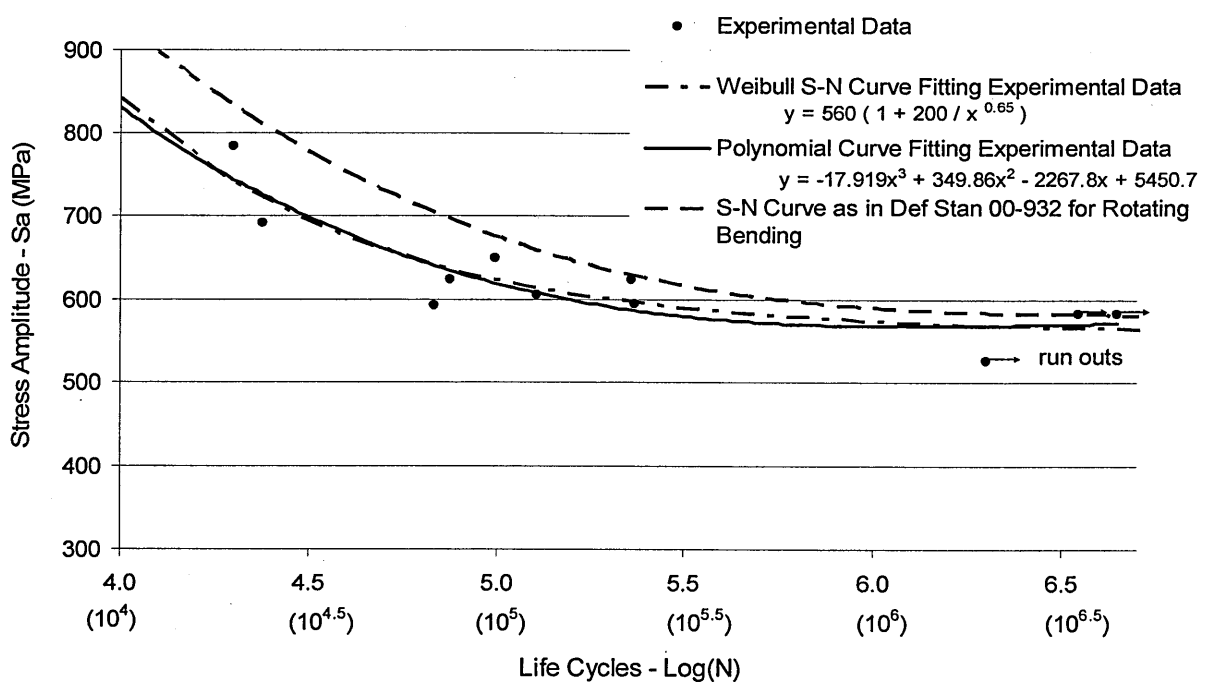

Fig. 3.5_ Plot of stress VS cycles (S-N) data.

The experimental results are shown in Table B1 – Appendix B. The plot of experimental data, together with published data [52] for the same material under rotating bending is shown on Fig 3.5.

As expected the S-N curve for uni-axial loading lies below the one for rotating bending. This is due to the limited volume of material that is subjected to maximum stress in rotating bending compared to the case of uni-axial loading, where the cross-sectional area is uniformly loaded [3]. The same experimental data in a broader range of life cycles are also shown on Fig. 3.6 with a four parameter Weibull curve fitting the data (Eq.3.1).

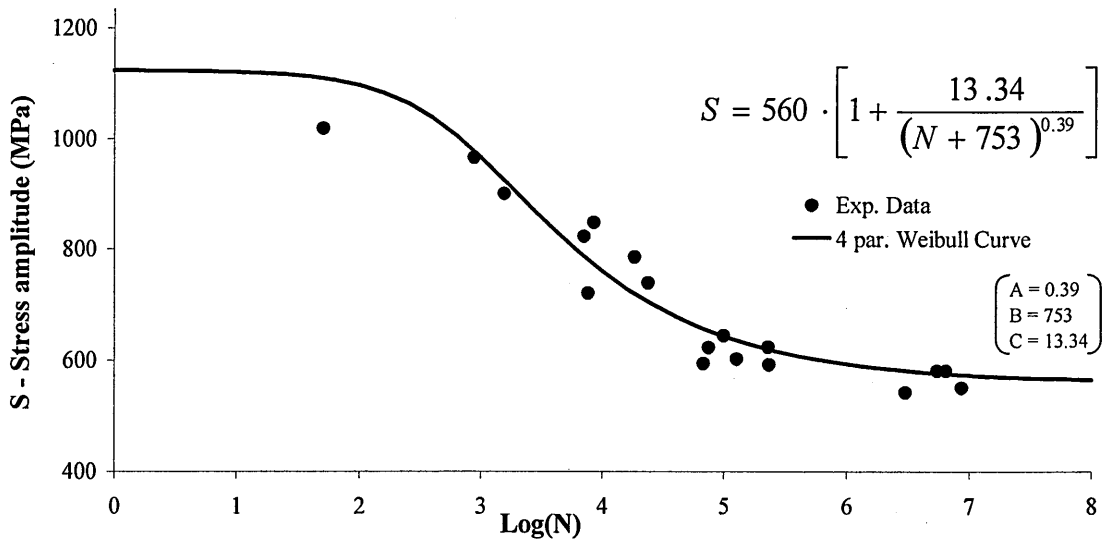

Fig. 3.6_ Stress Amplitude VS Life Cycles plot at ratio R = -1 with fitted S-N curve

Tests were also carried out on notched specimens at stress ratio R= -1. This was done to investigate the influence of geometry to the fatigue behaviour of the selected material. Specimens were designed and manufactured according to ASTM E466 (Fig. A8). Results are shown in Fig. 3.7 together with results for smooth specimens

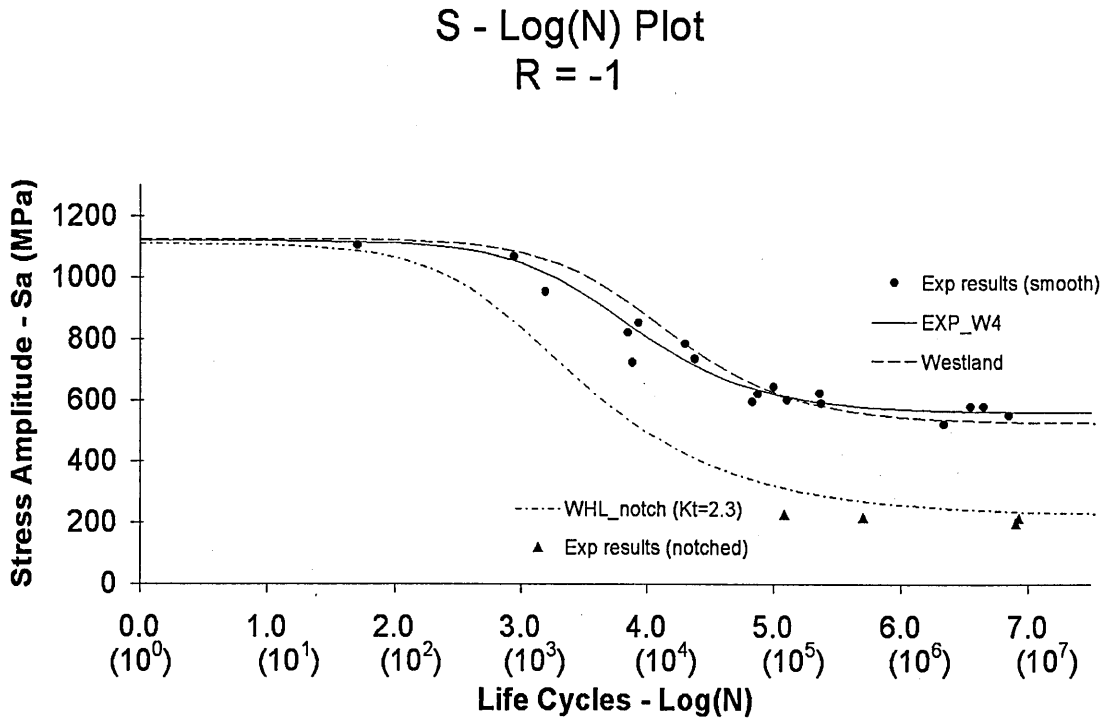

Fig. 3.7_ Stress Amplitude VS Life Cycles plot at ratio R = -1

A curve is fitted through the experimental results described by a four parameter Weibull equation (EXP_W4). On the plot is also presented a curve (Westland) as employed by Westland Helicopters for similar material. The parameters of the Weibull equation (Eq. 3.1) as used for both curves are presented in Table 3.3.

The fitting method is similar to that used by Westland. It involves manual adjustment of A, B parameters in a Microsoft Excel spreadsheet to achieve minimum values of the square of the Pearson product moment correlation coefficient (R-squared).

$$\frac{S}{S_{inf}} = 1 + \frac{C}{(N+B)^A}$$

Eq. 3.1_ Four Parameter Weibull Equation

	Weibull Equation Parameter Values			
Curve	**A**	**B**	**C**	**S_{inf} (MPa)**
EXP-W4	**0.7**	**4500**	**360.8**	**560**
Westland (smooth)	**0.7**	**8640**	**651.7**	**525**
Westland (notched Kt=2.3)	**0.453**	**800**	**82.2**	**223**

Table 3.3_ Weibull equation parameters

It is apparent that Westland curve has a lower endurance limit (S_{inf}) at high number of cycles but at stresses above 600MPa gives a larger number of life cycles, because of the S-N curve mid-section shape. The influence of the S-N curve shape in terms of damage is discussed in paragraph 3.6.2 Damage calculation.

In Fig. 3.7 it is seen that the presence of notch has a detrimental effect to the fatigue performance of the material. The theoretical stress concentration factor K_t for the specific geometry of notch is K_t=2.3 as seen in paragraph 3.3.

In view of the experimental results the fatigue notch factor K_f (Eq. 3.2) at high number of life cycles, is almost equal to Kt, with S_{inf} of un-notched specimen 560MPa and S_{inf} of notched Specimens 214MPa. This indicates a high value of notch sensitivity (q - Eq. 3.3). A further experimental investigation would be required to develop a better view of the material behaviour at stresses near its endurance limit (S_{inf}) for both smooth and notched specimens.

$$K_f = \frac{Endurance\_(S_{inf})\_of\_un-notched\_specimens}{Endurance\_(S_{inf})\_of\_notched\_specimens}$$

Eq. 3.2_ Fatigue notch factor

$$q = \frac{K_f - 1}{K_t - 1}$$

Eq. 3.3_ Notch sensitivity factor

3.5.2 Mean stress effect

Constant amplitude tests were performed at stress ratios, R, of -1 to 0.9. High stress ratios, (R values of 0.8 and 0.9) were investigated because a typical dynamic rotor component experiences a large number of cycles at these ratios. Cycles of high ratio and small range are usually omitted during the traditional fatigue substantiation process, but were included in this investigation in order to establish whether they are damaging or not.

Figure 3.8 shows the constant amplitude fatigue tests plotted as stress amplitude versus life, for a range of R values.

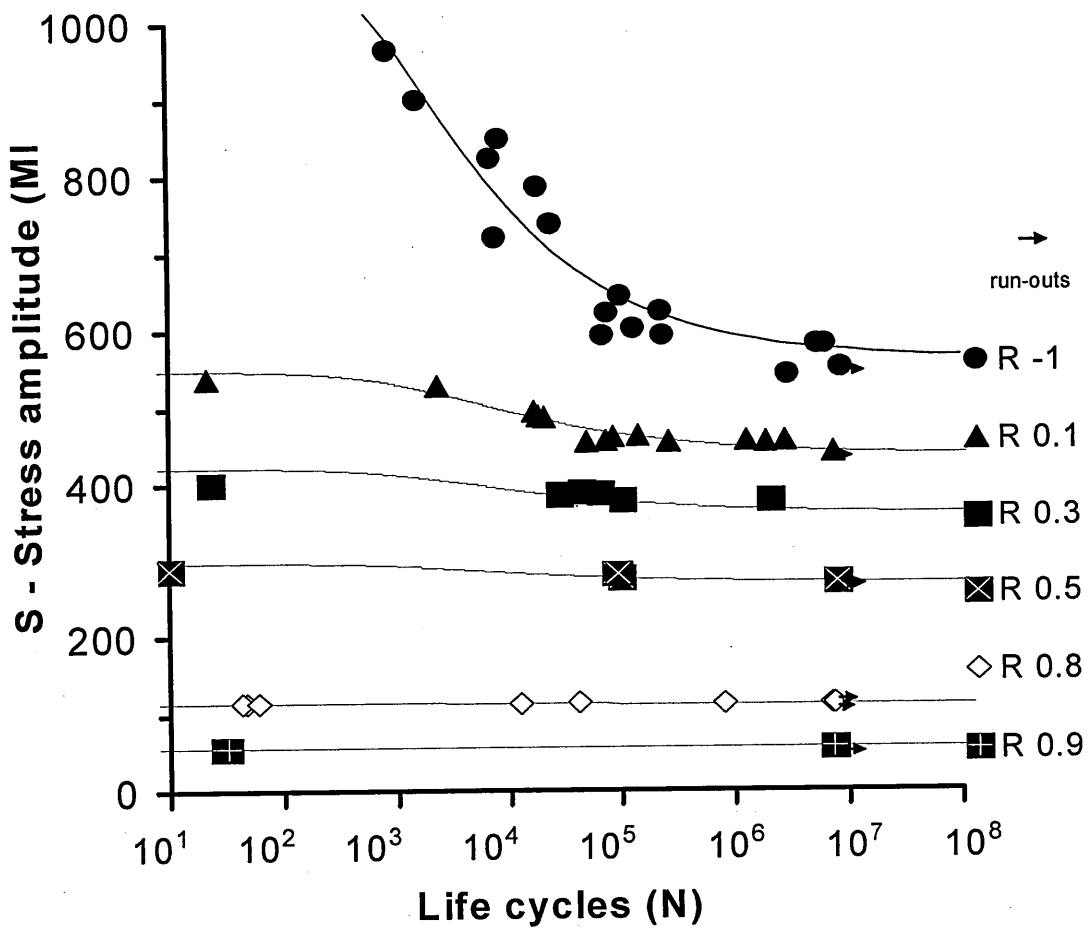

Fig. 3.8_ Stress Amplitude Vs life at stress ratios, R, -1, 0.1, 0.3, 0.5, 0.8, 0.9.

The endurance limit at R -1 for these tests was 560 MPa, decreasing to less than 60 MPa for tests at R = 0.9. It is noticeable that the S-N curve shape at high R ratios (0.8 and 0.9) approaches a horizontal line in which life is a highly sensitive function of stress amplitude. The stress level that will cause an almost instant failure is very close to the stress level that will lead to infinite life (non-damaging). In fatigue safe life design, this area is avoided and high R ratios stress amplitudes are designed to be well below the endurance limit. However, the effect of small cycles at high R ratio should be considered in association with large cycles at lower R ratios, when both are present in a variable amplitude load spectrum as will be seen in paragraph 3.6. Under these circumstances, small high R ratio cycles may be damaging even though they are of range less than the endurance limit.

Equation 3.4 is a modified Goodman equation using exponent parameter m. When parameter m equals unity the equation becomes Goodman's linear relation and when m equals two equation 3.4 represents Gerber's parabola.

$$S_a = S_{\text{inf}}\left[1-\left(\frac{S_m}{UTS}\right)^m\right]$$

Eq. 3.4_ Parametric version of Goodman's equation

Where S_a - stress amplitude
UTS – material ultimate tensile strength
S_{inf} – stress amplitude at fatigue endurance limit
S_m – mean stress
m – exponent – parameter

Figures 3.9 and 3.10 show the experimental results at various R ratios on a 3D (Stress Amplitude - Mean Stress – Life) plot, together with a graphical representation of linear Goodman equation and modified Goodman equation (Eq. 3.4) for parameter m equal to 1.5 and 2. The R ratio planes at which experiments were carried out are also shown.

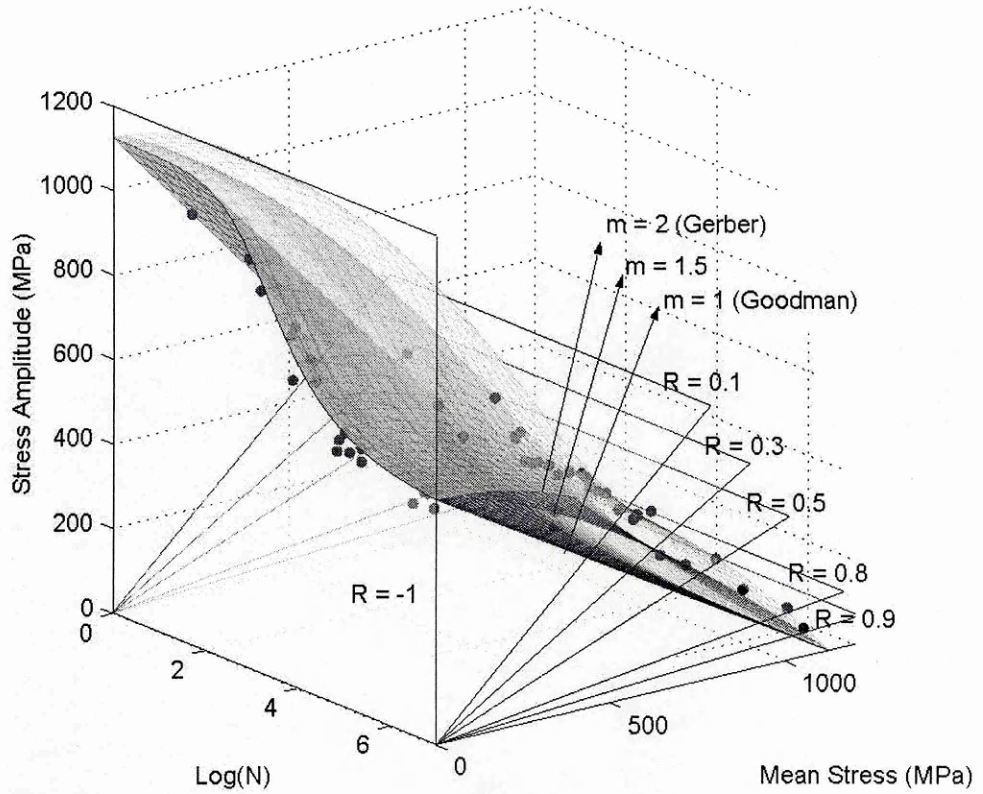

Fig. 3.9_ 3D plot of Stress Amplitude VS Mean Stress VS Life (view 1 – high cycle)

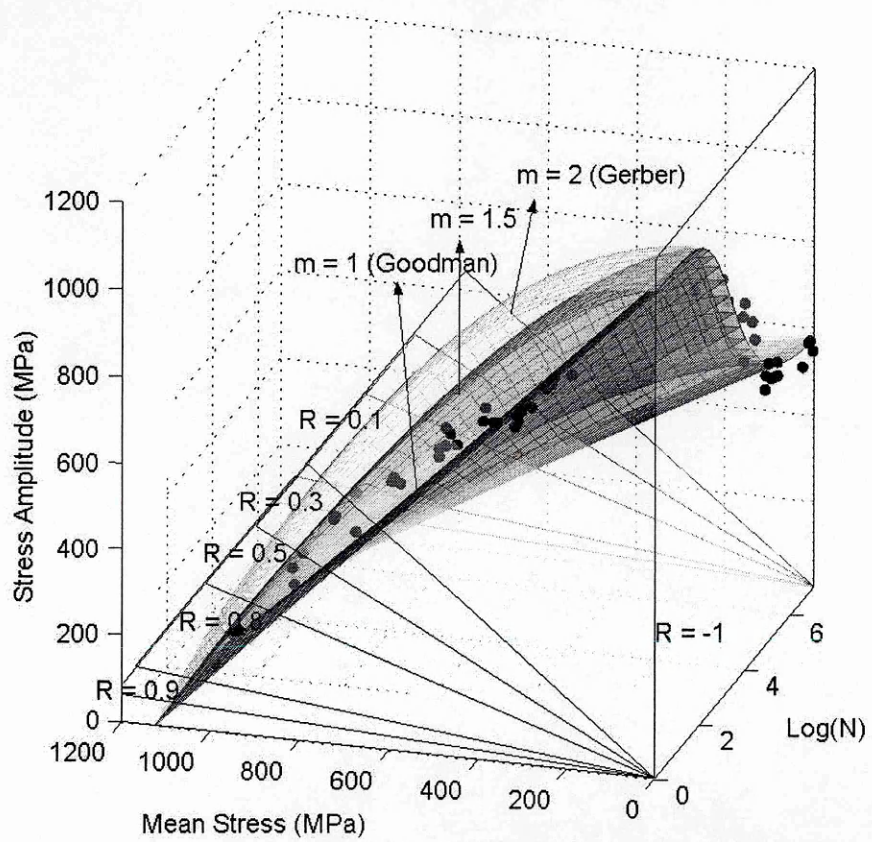

Fig. 3.10_ 3D plot of Stress Amplitude VS Mean Stress VS Life (view 2 – low cycle)

In an attempt to accurately describe the experimental data at various R ratios (mean stress effect) an analytical equation was developed based on Goodman equation and the four parameter Weibull equation describing the S-N curve at R = -1 (Fig 3.6).

$$N = \left(\frac{C \cdot S_{inf} \cdot \left[1 - \left(\frac{S_m}{UTS} \right)^m \right]}{S - S_{inf} \cdot \left[1 - \left(\frac{S_m}{UTS} \right)^m \right]} \right)^{\frac{1}{A}} - B$$

Eq. 3.5_Life Cycles (N) as a function of Stress Amplitude and Mean Stress

Where	A, B, C	parameters from fitted S-N curve at R = -1
	UTS	material ultimate tensile strength
	S_{inf}	stress amplitude at fatigue endurance limit
	S_m	mean stress
	S	stress amplitude
	m	exponent – parameter (Eq.A2)

$$m = \frac{1}{(UTS - S_{inf})} \cdot \left(\frac{S \cdot (k - l)}{1 - \left(\frac{S_m}{UTS} \right)^q} + l \cdot UTS - k \cdot S_{inf} \right)$$

Eq. 3.6_ parameter m as a function of Stress Amplitude and Mean Stress

Where k, l, q are parameters from fitted S-N curves at various stress ratios R.

Given stress amplitude and mean stress, equation 3.5 calculates the number of cycles to failure as required in fatigue substantiation procedure.
Figures 3.11 to 3.15 show the plots of stress amplitude VS life cycle at stress ratios 0.1, 0.3, 0.5, 0.8 and 0.9 with the fitted curve using equation 3.5 and 3.6 with parameter values: k = 1.1, l = 2.2, q = 1.5.

It can be seen that linear Goodman (m = 1) is always conservative and that the parametric equation is capable of describing the data well. It is noticeable that the S-N curve shape at high R ratios (0.8 and 0.9) approaches a horizontal line. Components at that high R ratio will most probably experience a quick failure or infinite life. The effect though of

cycles at high R ratio should be seen in association with cycles at lower R ratios (load interaction effect) as indicated by the experimental results under variable amplitude loading. Equation 3.5 can accurately describe the experimental results and thus allow for Miner's rule inaccuracy to be estimated alone and independent to mean stress effect when comparing calculated and experimentally measured damage under variable amplitude loading (see paragraph 3.6).

Equation 3.6 is able to describe the behaviour under various stress ratios R of other materials as well, for example titanium, where linear Goodman equation is non-conservative [23].

In figures 3.11 to 3.15 Mod. Goodman curve is based on equation 3.5.

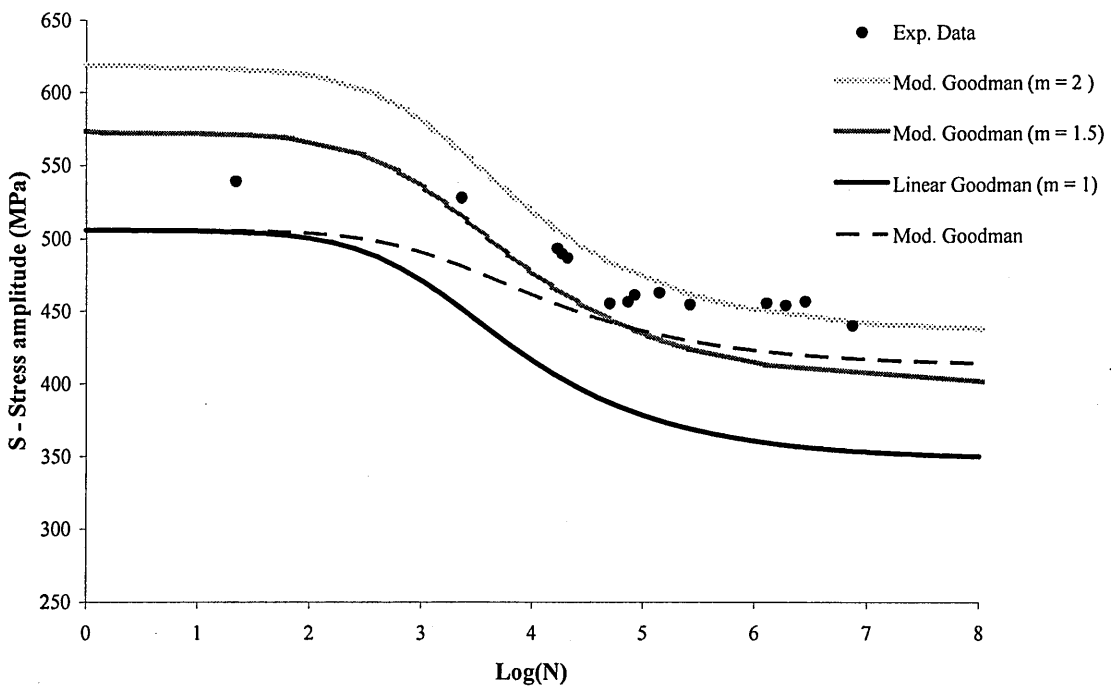

Fig. 3.11_ Stress Amplitude VS Life Cycles plot at ratio R = 0.1

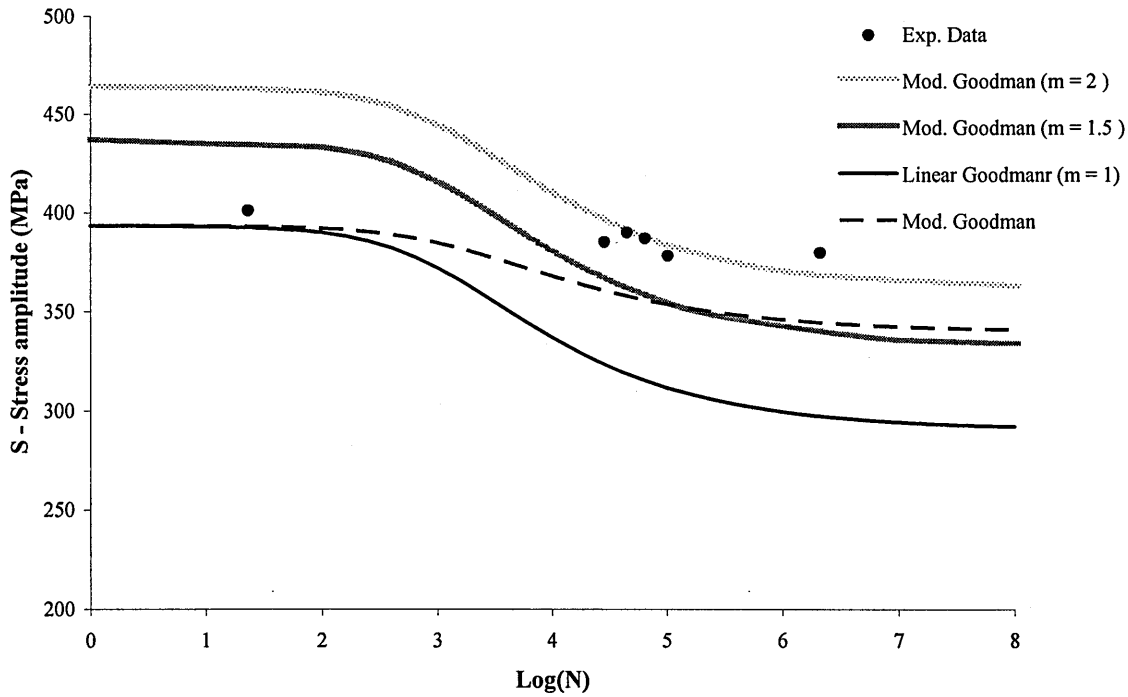

Fig.3.12_ Stress Amplitude VS Life Cycles plot at ratio R = 0.3

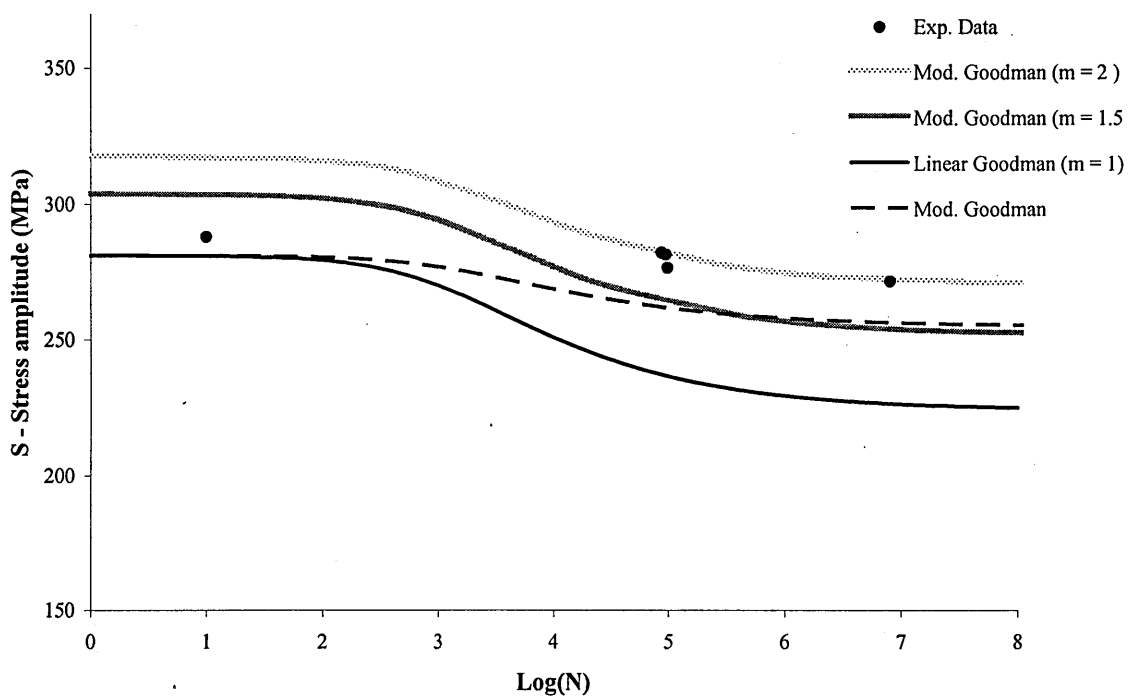

Fig.3.13_ Stress Amplitude VS Life Cycles plot at ratio R = 0.5

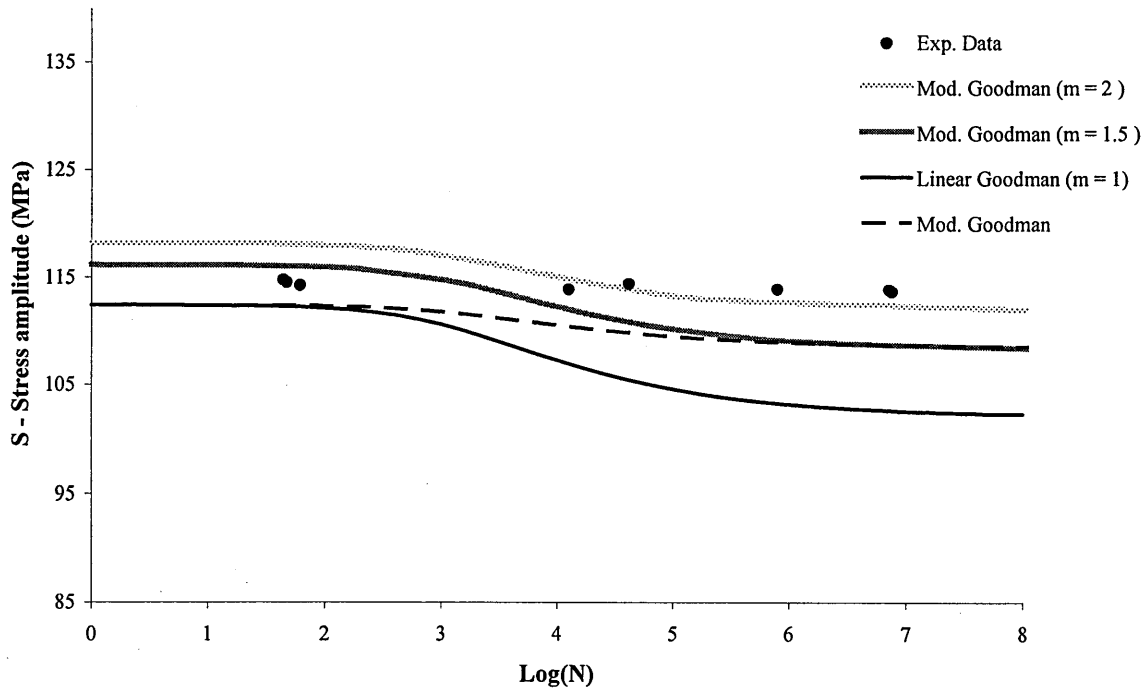

Fig.3.14_ Stress Amplitude VS Life Cycles plot at ratio R = 0.8

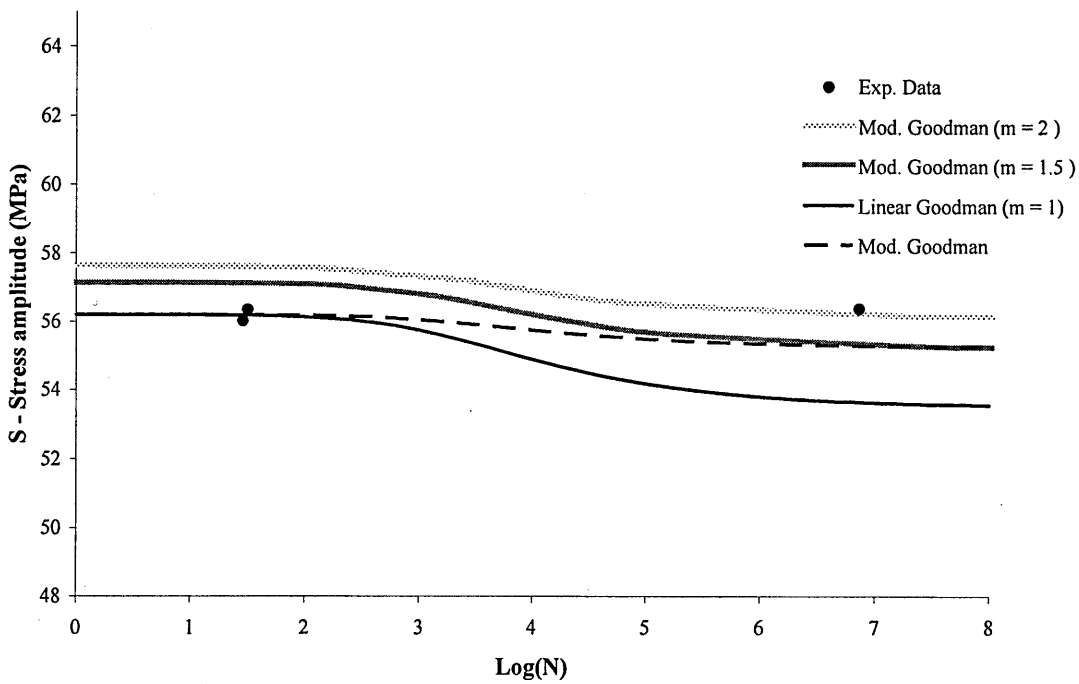

Fig.3.15_ Stress Amplitude VS Life Cycles plot at ratio R = 0.9

3.6 Experimental results under variable amplitude loading

Experiments were performed using variable amplitude loading with smooth and notched specimens. All fatigue lives were to specimen separation. Experimental life was compared to analytically calculated life under the same variable amplitude loading.

3.6.1 Variable amplitude loading spectrum

The loading spectrum chosen for the variable amplitude tests was a fatigue loading sequence developed for the Lynx helicopter main rotorhead mast. The loading sequence, called Rotorix [53], was compiled using an adaptation of the procedure used in the development of the standardised helicopter blade loading sequence, Felix and Helix [54, 55]. Like Helix and Felix, there are 25 levels in the sequence, numbered at intervals of 4 with the largest peak at level 100. Four versions of Rotorix called Rotorix 16, 20, 28, and 34 were developed for these tests, all representing 190.5 flight hours and 140 sorties. Rotorix 16 contains cycles of range 16 units (16% of max) and above (Fig 3.16). Ranges smaller than 16 units are gated out. Similarly the other three sequences have cycles of ranges less than 20, 28 and 34 units, removed. The sequence of remaining manoeuvres was retained after the gating process. The process is shown in figure 3.15. The level 16 cycles represented in Rotorix 16 are from the rotor motion, and occupy over 90% of the entire spectrum. The remaining cycles arise from manoeuvre loads. Level 16 cycles are removed in Rotorix 20 and the other gated spectra. The numbers of cycles in each sequence are shown in table 3.4 and examples of the spectra in Figure 3.17. In the process of gating small range cycles, every manoeuvre retained at least one cycle to maintain its identity. The maximum stress in the spectrum was set to 1020 MPa for the major part of the investigation with selected tests conducted at 980 and 950 MPa.

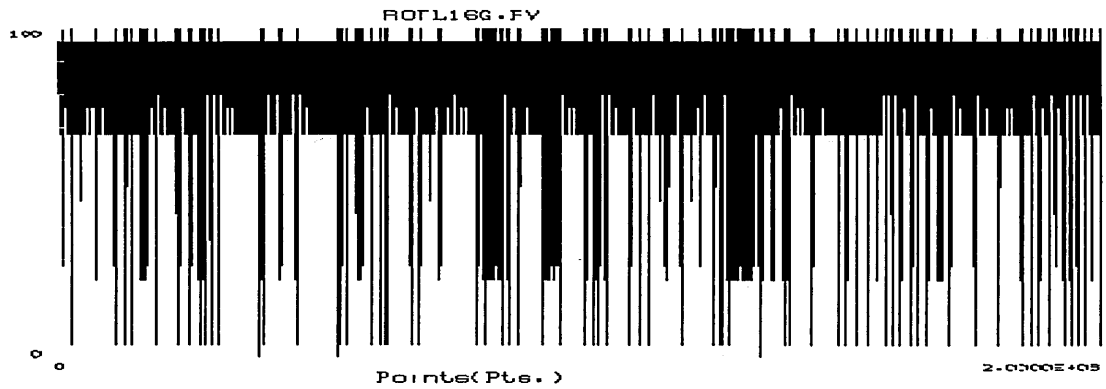

Fig.3.16_ The first 2 million cycles of Rotorix 16 sequence.

Load Cycles per pass	
Spectrum level	**Number of Load Cycles**
R16	1,978,110
R20	113,065
R28	53,435
R34	10,170

Table 3.4_ Number of load cycles of Rotorix sequence per spectrum level

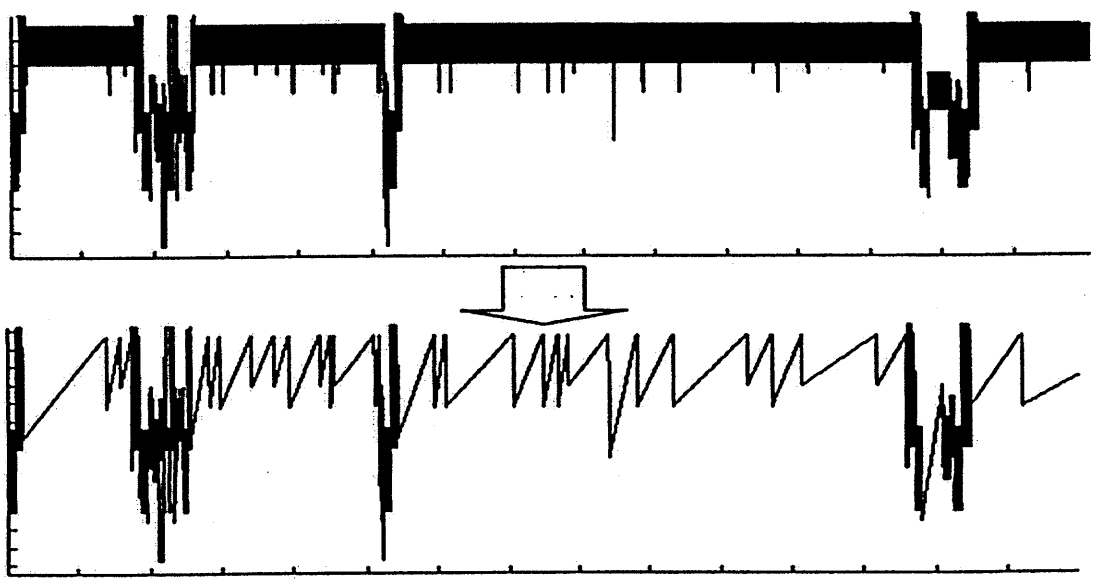

Fig.3.17_ Rotorix 16 and 28 load sequences showing the effect of cycle omissions

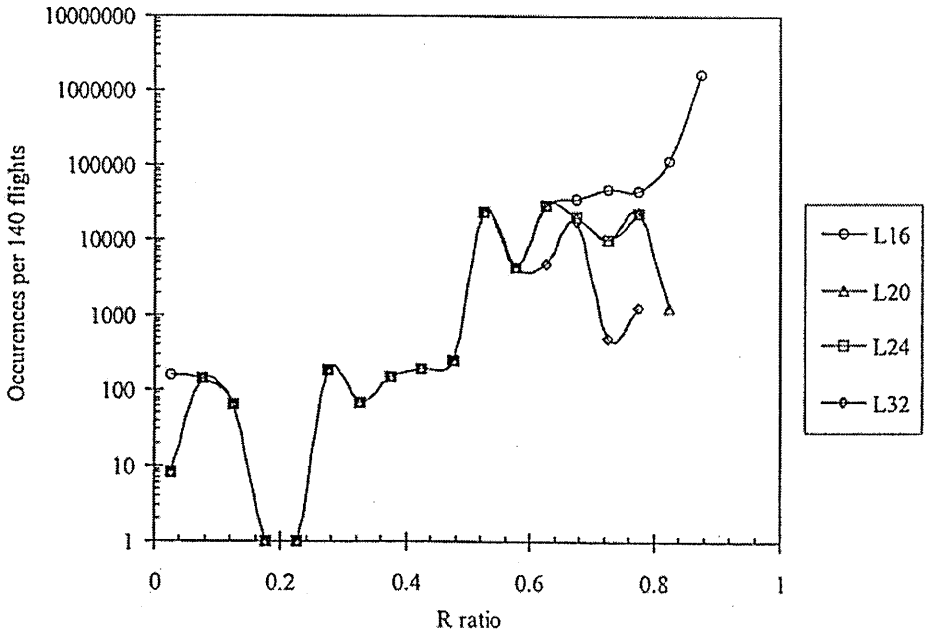

Fig.3.18_ Effect of different level of omission on stress ratio R distribution for Rotorix rotorhead loading sequence.

The distribution of the stress ratio R for different Rotorix levels is shown on Figure 3.18. Level 16 is selected for being more accurate. It is clear that a large number of small range cycles that dominate the loading sequence have very high mean stress values of between R=0.8 and 0.9, which makes more important the evaluation of Goodman relationship at these high ratios. To validate Miner rule under typical helicopter loading spectrum, Rotorix 16, 20, 28 and 34 were used.

3.6.2 Damage calculation

Damage calculations were performed using Rotorix loading spectrum, Miner's rule and modified Goodman's equation (Eq. 3.4). Three different versions of the spectrum were used depending on the level of omission of small range cycles, Rotorix Level 16, Level 20, Level 28 and Level 34.

Damage calculations were carried out using a modified version of a program written in C language originally by Mr. R.Hudson at Cranfield. The program counts the cycles of the spectrum using the rainflow method and uses Miner's rule to estimate the accumulated damage on a cycle by

cycle basis. The S-N curve is defined as a four parameter Weibull equation (Eq. 3.1) and correction for the mean stress effect is carried out using a parametric version of Goodman's equation (Eq. 3.4).

Damage calculations are performed for various values of spectrum maximum stress level. The maximum stress level has an immediate effect to the damage caused by the spectrum. At high stress levels damage is accumulated faster leading to shorter fatigue lives. Calculations are carried out varying three independent parameters. These are: the Rotorix version (Levels 16, 20, 28 and 34), the S-N parameters (two sets are used EXP: curve fitted through the experimental data and WHL: curve as employed by Westland Helicopters for similar material, see table 3.3) and the value of the parameter m in Eq.3.4, concerning the mean stress effect correction. For the parameter m, three cases were investigated, m=1 – Linear Goodman, m=2 - Gerber Parabola and m=1.5 – intermediate condition.

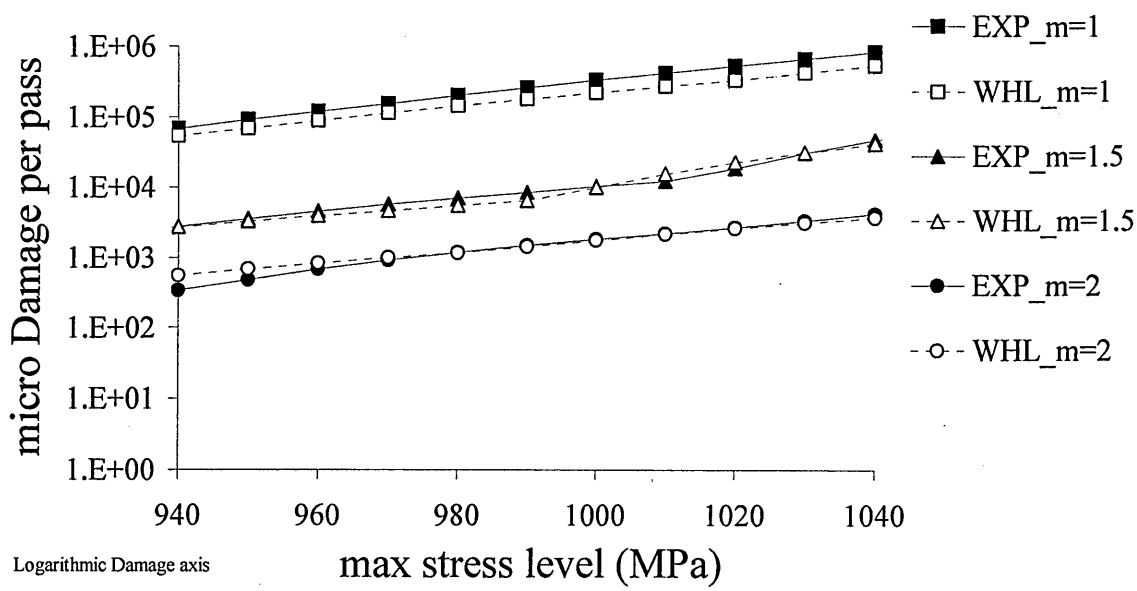

Fig. 3.19_ Micro-Damage per pass of the spectrum Vs spectrum max stress level (logarithmic damage axis)

Figure 3.19 shows the effect of Goodman parameter m and the effect of S-N curve fitting parameters. It is evident that the effect of S-N curve fitting is non-important. Calculations have shown that there is no difference in the predicted lives to failure for any of the 4 spectra,. This is believed to be because none of the gated cycles removed from the spectra would be damaging in a linear damage summation. To illustrate this, Figures 3.20 a and b show the rainflow cycle content of Rotorix 28 and Rotorix 16

together with a histogram showing the damage allocation to each of the cycle groups. Cycles removed from this and the other histograms by gating all fall on the other side of this line and are non damaging. Clearly this is at variance with the variable amplitude test results, which predict that cycles down to level 16 are all damaging in the presence of the larger range cycles (see paragraph 3.6.3).

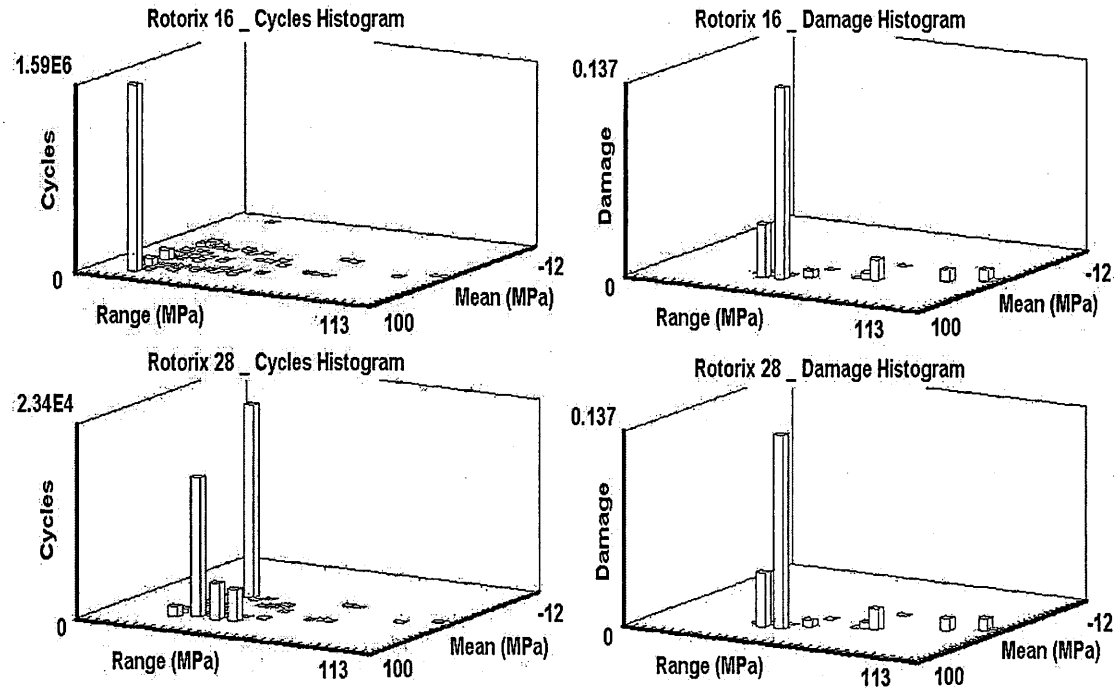

Fig. 3.20_ Rainflow counted cycles (a) and damage (b) histograms for Rotorix 16 and 28 spectra.

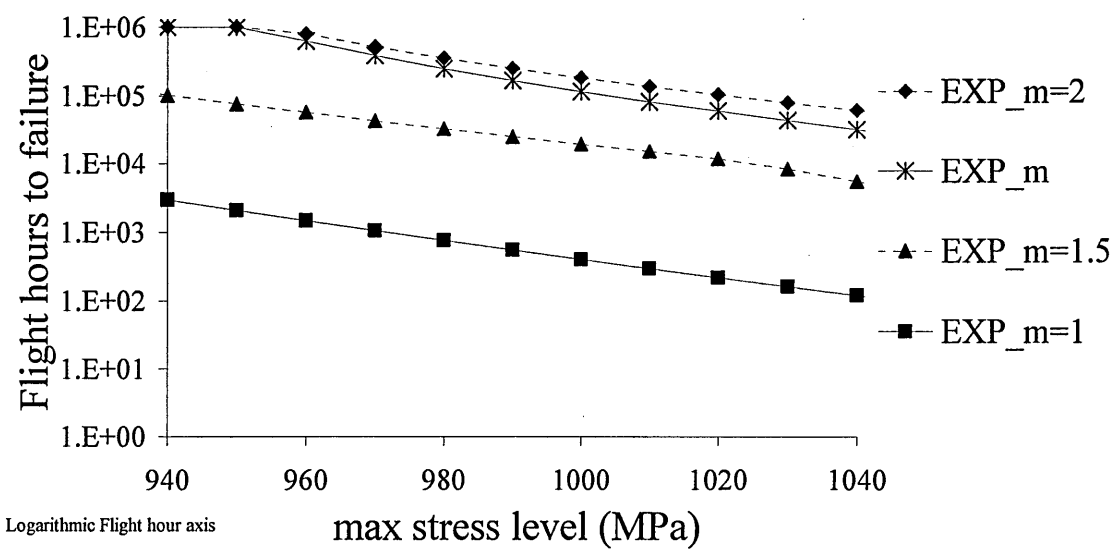

Fig. 3.21_ Damage calculations and experimental results under Rotorix loading spectrum, varying max. stress level

The lines on figure 3.21 are calculated lives for the tested spectra for a range of peak stress values, calculated from the measured constant amplitude data and the load spectrum, assuming Miners linear damage law, and the Goodman mean stress correction. In this case parameter m is based on equation 3.6 and represents in a better way the behaviour of the material under constant amplitude loading at various stress ratios R. The results show similar behaviour in terms of calculated damage to the Gerber parabola.

3.6.3 Experimental results

The results of the variable amplitude tests under Rotorix 16, 20 28 and 34, at the three maximum stress values are shown in table 3.5 and figure 3.22. It can be seen that all experimental results fall above the life curve using linear Goodman (m=1) (continuous line) and below the life curve using m=1.5 (dotted line) and of course well below the life curves that used Gerber parabola (m=2) or the modified Goodman where parameter m was modified to accurately describe the material behaviour under constant amplitude loading (see Fig. 3.21 for comparison of EXP_m and EXP_m=1.5). Hence, accurate description of mean stress effect, using Eq.3.5 and S-N parameters from fitted experimental data at R = -1 yield significantly non-conservative lives.

Damage calculations using Miner could not differentiate between different version of Rotorix spectrum, although experiments show the opposite. The results show that for 1020MPa maximum stress, life to failure expressed as flight hours, decreases from about 5,000 hours for Rotorix 34 to around 1,000 hours for Rotorix 16. Therefore, all cycles down to level 16 are damaging, as their addition to the spectrum decreases flight hours to failure. The other point to note in figure 3.22 is the conservatism of the Goodman correction, which will go some way to removing the non conservatism found in the Miner summation.

The more sparse results at lower maximum stress levels confirm the broad trends although data from Rotorix 16 spectra are not incluted, since a complete test using Rotorix 16 at that low stress level would require approximately an uninterrupted testing period of three months.

Experimental Results for Un-notched Specimens		
Rotorix Level	Max. Stress (MPa)	Flight Hours
R16	1020	1,241
R16	1020	909
R20	1020	2,148
R20	1020	3,178
R28	1020	1,700
R28	1020	3,014
R34	1020	4,614
R16	980	2,239
R28	980	10,508
R34	980	37,336
R28	950	15,318

Experimental Results for Notched Specimens		
Rotorix Level	Max. Stress (MPa)	Flight Hours
R16	1020	1,692
R28	1020	2,475
R28	1020	2,874
R28	980	9,461
R16	980	2,856

Table 3.5_ Experimental results under Rotorix loading spectrum

Test results on notched specimens using Rotorix 16 and 28 show similarities to the test results from smooth specimens. Hence the effect of small range cycle omission is independent of component geometry.

It can be seen that use of Rotorix 28 instead of Rotorix 16 would lead to 40 times faster execution of testing, due to fewer loading cycles (Table 3.4). On the other hand there is a non-conservative average difference of 60% for high stress level (1020 MPa) and 75% for lower stress level (980MPa) between the two spectra. The differences in lives are non-conservative since Rotorix 16 gives smaller lives in every case, hence the omission of small range cycles (non damaging according to Miner and Goodman rules) in favour of a simpler loading spectrum should be avoided.

Differences between R16 and R28 tests are significant at 98.7% confidence level using Student's t-test for all tests (notched and smooth specimens) at 1020MPa max stress level. Differences between R16 v R20 and R16 v R28 are significant at 90% and 95% confidence level respectively for tests on smooth specimens at 1020MPa max stress level. Smaller confidence levels are due to limited number of experimental results (two examples for each spectrum)

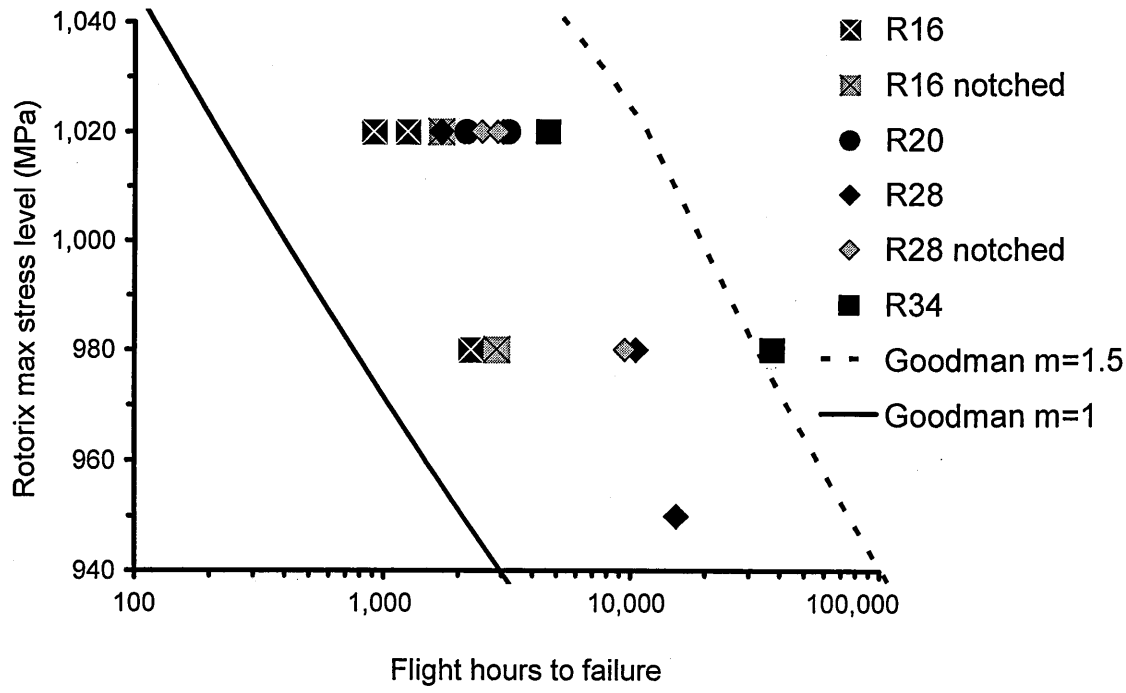

Fig. 3.22_ Experimental results under VA loading and calculated life curves.

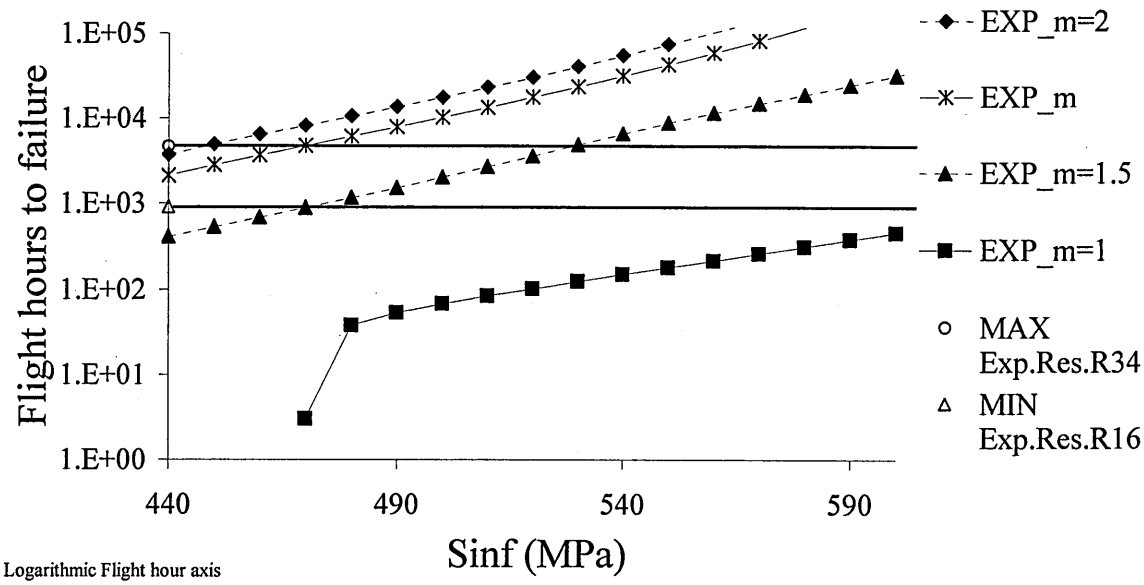

Fig. 3.23_ Damage calculations and experimental results under Rotorix loading spectrum (at 1020MPa), varying S_{inf}

Figure 3.23 shows that the non-conservatism of EXP_m curve can not be attributed to inaccuracy in S_{inf} estimation. From figure 3.23 and experimental results at 1020MPa we have maximum life with Rotorix 34 equal to 4614 flight hours and minimum life with Rotorix 16 equal to 909 flight hours. Assuming correct estimation of Goodman with EXP_m curve

the error for S_{inf} would be of 18% in estimation of mean, equal to two standard deviations, assuming material S_{inf} COV 10% (see Chapter 2).

This raises the question of how realistic is the assumption of Goodman being independent of Miner and invites new theories to be applied. The most popular alternative theories to Miner also use mean stress correction. It would be beneficial for a theory beyond S-N curve and load ratio effect [11, 17] to be evaluated and compared against the experimental results. These theories though require totally different testing equipment and methodology from that used for the project and in general the helicopter industry.

3.7 Discussion

Significant scatter is evident from experimental results under constant and variable amplitude loading. Figures 3.5 and 3.6 show that scatter increases when stress amplitude approaches the endurance limit. Fatigue is a stochastic phenomenon with inherent variability and the fatigue limit is an artefact of constant amplitude fatigue tests in order to describe the material behaviour for component design purposes. The effect of variability is depicted on figure 3.24 where S-N curves are shown for probability of failure from 1% to 99% assuming S_{inf} normally distributed with COV=10%.

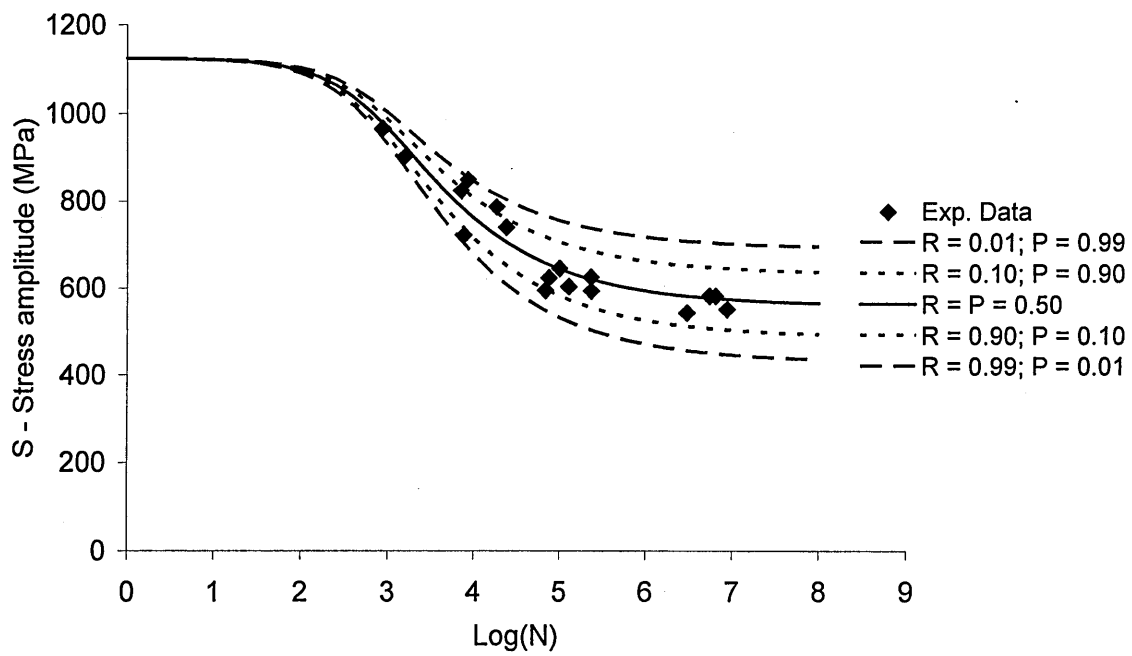

Fig. 3.24_ S-N-P curves or R-S-N curves for tested material assuming S_{inf} COV=10%. Note: P = probability of failure; R = reliability = 1 – P.

The observed scatter is associated with the inherent variability of fatigue failure. To identify the source of variability it is necessary to examine the mechanism leading to crack initiation, since the initiation stage covers most of the specimen's life for the selected material (2S97 high strength steel). Fatigue crack initiation is a consequence of cyclic slip in slip bands. It implies cyclic plastic deformation as a result of moving dislocations at low stress levels (below yield stress) limited to a small number of grains usually at the surface of the material (Fig. 3.25) [56]. Macroscopic parameters influencing the phenomenon (surface quality, residual stress, environmental condition etc) remain constant from sample to sample during testing. Inherent variability exists mainly due to scatter of the local conditions for micro-crack nucleation which are non-controllable (variation of the shape, size and orientation of grains and/or inclusions contributing to an inhomogeneous stress distribution on a micro level). Test results under variable amplitude loading (table 3.5) also show the effect of inherent variability. The experimental results at 1020MPa for Rotorix 16, 20 and 28 vary form 36% to 43% difference in total life.

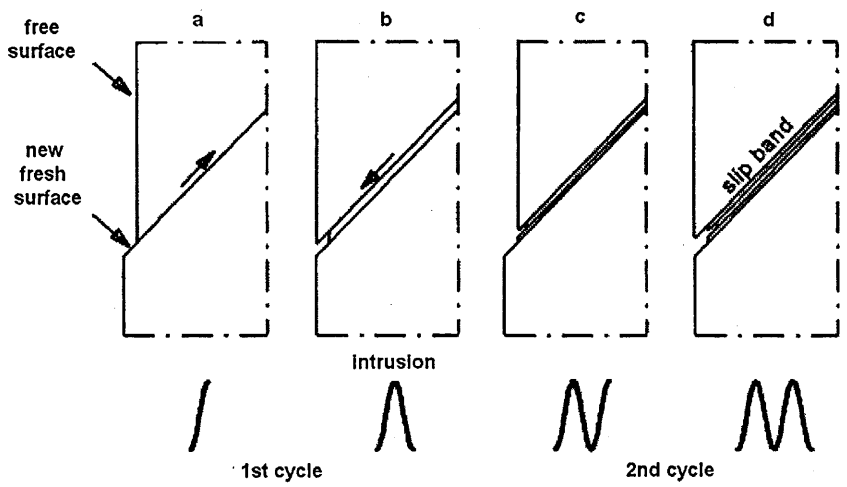

Fig. 3.25_ Cyclic slip leading to crack nucleation.

It was attempted to draw conclusions regarding material behaviour under Rotorix spectrum by observing the fractured surface of samples. For this reason several tested specimens were examined under a Scanning Electron Microscope. Pictures taken from several samples show similar results. Appendix C includes pictures from sample No. 77 tested under variable amplitude loading Rotorix28. Figure C1 shows dimples from the final overload fracture region. Unfortunately, fractography has shown little clear

indication of fatigue striations (Fig. C2-C4) and this is characteristic of all high strength steels [57].

Gating of small range, high R cycles as non damaging when performing design calculations, on the basis of the present results is a non conservative procedure. To a great extent, on the load spectra studied in this work, the error is offset by the conservatism of the Goodman law in accounting for mean stress effects.

In general, specimen fatigue tests under both constant and variable amplitude loading have demonstrated conservative and non conservative errors in damage calculation techniques for rotorcraft.

In extensions of this work it is hoped to investigate the real errors in Miner's rule more comprehensively than has been done so far. This may require a different approach to the fatigue problem from the safe life approach. Perhaps a crack growth or energy-based approach. There is also the possibility of a more sophisticated methodology that would describe the stochastic behaviour of the material, based on theory of chaos.

In damage calculations, the accuracy of Goodman and Miner is frequently not considered. Only direct experimental measurements, as has been done in this work, can estimate the true extent of the errors. An extensive work on the issue could investigate the real errors in Miner more comprehensively. Once the errors are known, they may be represented in simulations and permit accurate estimates to be made of the probability of failure (see Chapter 5).

4. Deterministic approach to fatigue substantiation of helicopter components

The effect of variability in usage, loads, damage and life calculation techniques was initially studied using the deterministic methodology. Statistical analysis was carried out on data sets of usage and loads to estimate distribution type and parameters that could describe the data. Also the effect of errors in damage calculation techniques was studied in terms of their effect on calculated component life.

4.1 Source of data

Fig. 4.1_ Westland Lynx helicopter

As explained in paragraph 3.1 main source of real data was the Westland Lynx helicopter (Fig. 4.1). All data were provided by UK Royal Air Force. Load data came from three Lynx components: the dogbone rotor linkage, the spider rotor component and a lift frame component (station 420A). Appendix D shows pictures of the three components and the approximate position of the strain gauges that measured the load data.

4.1.1 Usage data

Usage data were gathered during a Manual Data Recording Exercise (MDRE) carried out by UK RAF. Service measurement of manoeuvre occurrence was performed on a lap top computer by observers flying with the helicopter. The measurement records what manoeuvre the aircraft is carrying out and for how long. A total of 22 helicopters flying 72 hours (49 missions) was observed to produce the data analysed in this work. Data were supplied in Access data base format containing more than 23,000 events in total. The manoeuvre usage spectra were analysed in terms of operation type and also were compared with the design spectrum. Four types of operation, namely training, anti- tank, personnel carrying (CT Trooping) and utility missions were investigated (Table 4.1).

Lynx Helicopter Mk 7 (Army)	
Mission Type	**No. of recorded missions**
Anti tank	12
CT Trooping	16
Training	18
Utility	3
TOTAL	**49**

Table 4.1_ Lynx helicopter recorded missions from MDRE

The original design usage spectrum of the Lynx Mk 7 helicopter is shown in Table 4.2, together with a modified spectrum which reflects the more limited range of manoeuvres recognized by the usage measurement technique. A few manoeuvres, notably cruise turns and control reversals either were not recognised or did not occur in the service measurement of manoeuvre usage. The percent time which these manoeuvres represented were reallocated proportionately among the remaining manoeuvres so that the total manoeuvre time still totalled 100% of a flight hour. It is seen that large usage percentage manoeuvres generally have less variability (CoV) than the manoeuvres of smaller usage percentage. The statistical analysis of data was performed on a sortie by sortie basis and the coefficient of variation is calculated assuming a normal distribution for every manoeuvre.

Manoeuvre		Design		Measured Usage	
		A	B	Mean	COV
1	0 - 0.2 VNE	10.05	10.49	6.18	68%
2	0.2 - 0.4 VNE	5.43	5.67	3.34	68%
3	0.4 - 0.6 VNE	6.33	6.61	3.89	68%
4	0.6 - 0.8 VNE	12.66	13.21	37.53	51%
5	0.8 - 0.9 VNE	19.40	20.23	8.65	170%
6	0.9 - 1.0 VNE	0.90	0.95	3.06	336%
7	*VNO - 50kts (60deg)*	0.80			
8	*VNO - 20kts (45deg)*	0.64			
9	*VNO - 20kts (30deg)*	0.96			
10	0.9 VNE (30deg)	2.51	2.63	0.01	441%
11	1.0 VNE (20deg)	0.11	0.13	0.01	700%
12	*Control Reversal*	0.50			
13	Autorotation	0.50	0.53	0.26	315%
14	Hover	14.10	14.71	9.35	91%
15	Sideways	2.01	2.10	0.48	166%
16	Rearwards	1.01	1.06	0.01	320%
17	Spot Turns	1.86	1.95	1.75	98%
18	*Hover Control Reversals*	1.13			
19	Climb	5.53	5.77	0.84	180%
20	Descent	5.57	5.81	0.25	242%
21	*Take-off*	0.21			
22	Transition to Hover	0.70	0.74	0.49	135%
23	Transition from Hover	0.70	0.74	0.49	135%
24	Landing	0.35	0.38	0.06	259%
25	Rotor Turning on Ground	6.03	6.30	23.37	46%
	Total	100.0	100.0	100.0	

Table 4.2_ Lynx Mk7 – Usage percentage per manoeuvre

This is supported by the results at Table 4.3 for four significant manoeuvres: Hover, Sideways, Spot Turn and Climb (their contribution to damage is shown at figures 4.20, 4.21). Both a Normal and a three parameter Weibull distribution were fitted through the data. Figures 4.2 to 4.9 show the usage distribution and the cumulative usage distribution for the studied cases. It is observed that Normal distribution gives better results in more cases. Goodness of fit check was based on the chi square method and was preferred over the Kolmogorov - Smirnoff method for providing confidence levels for any case (chi-square is a continuous function). Weibull distribution was problematic when many sorties contained no example of the manoeuvre (Sideways, Climb). In some cases though [43, 44] it is regarded that usage variability is better described by a Weibull distribution. An investigation on the matter would require a larger

and more comprehensive set of data from an integrated usage monitoring system. For most of the other manoeuvres the limited amount of data did not allow a comprehensive study.

Lynx Mk7 manoeuvre	Normal distribution			3 parameter Weibull distribution			
	mean	CoV	Level of confidence	a	b	c	Level of confidence
HOVER	9.35	91%	92.90%	0.93	8.04	0.630	98.59%
SIDEWAYS	0.48	166%	91.13%	1.75	0.19	-0.003	0.00%
SPOT TURN	1.75	98%	68.10%	0.66	1.58	-0.090	36.99%
CLIMB	0.84	180%	87.30%	1.30	0.45	-0.012	0.41%

Table 4.3_ Data fitted distribution parameters

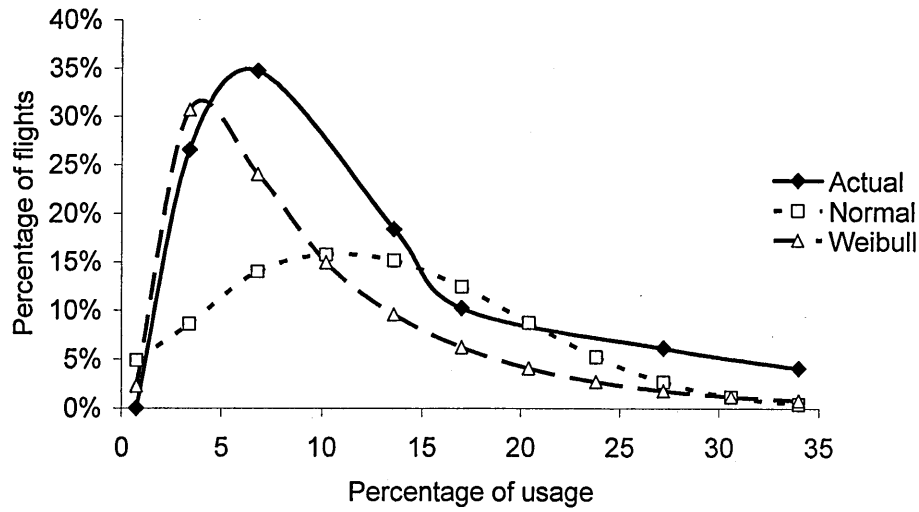

Fig. 4.2_ Usage Distribution for Lynx Mk7 Hover manoeuvre

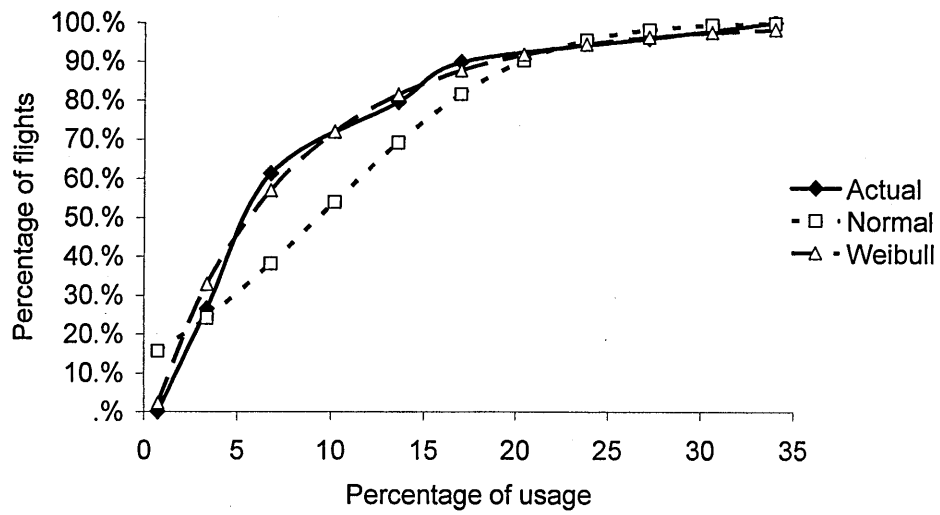

Fig. 4.3_ Cumulative Usage Distribution for Lynx Mk7 Hover manoeuvre

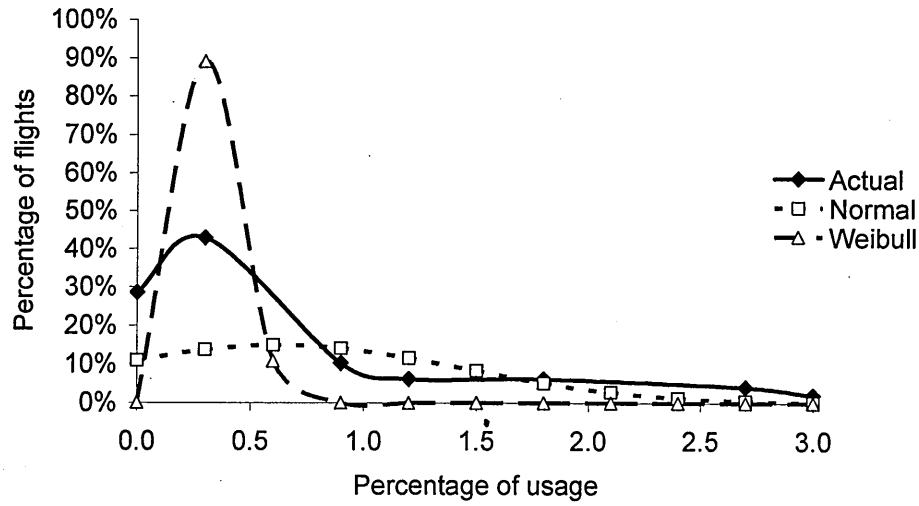

Fig. 4.4_ Usage Distribution for Lynx Mk7 Sideways manoeuvre

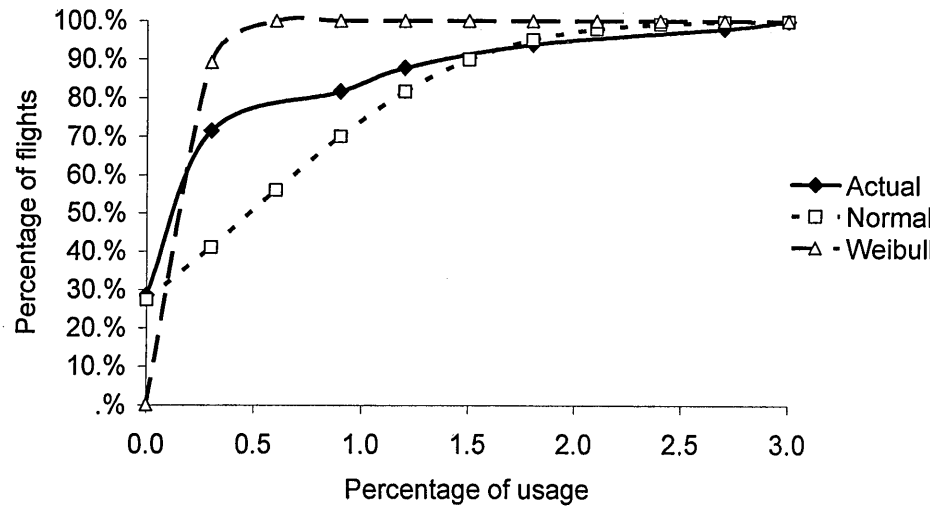

Fig. 4.5_ Cumulative Usage Distribution for Lynx Mk7 Sideways manoeuvre

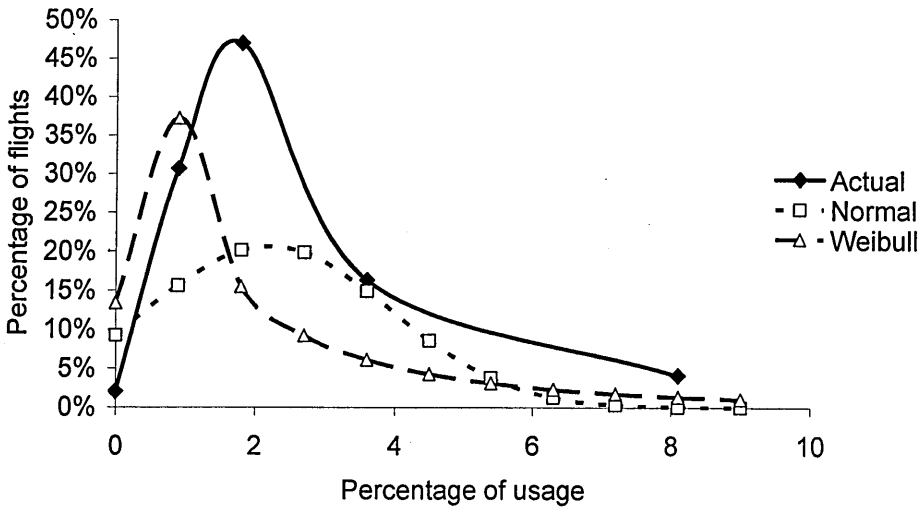

Fig. 4.6_ Usage Distribution for Lynx Mk7 Spot Turn manoeuvre

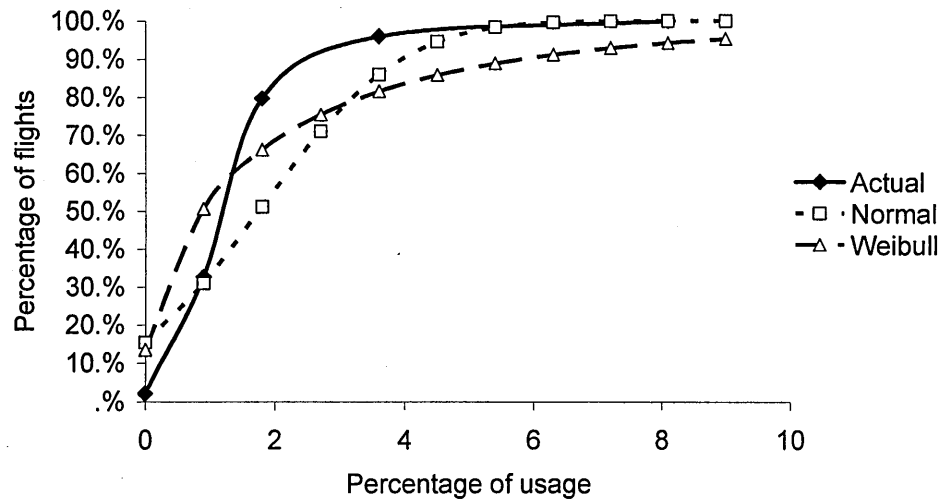

Fig. 4.7_ Cumulative Usage Distribution for Lynx Mk7 Spot Turn manoeuvre

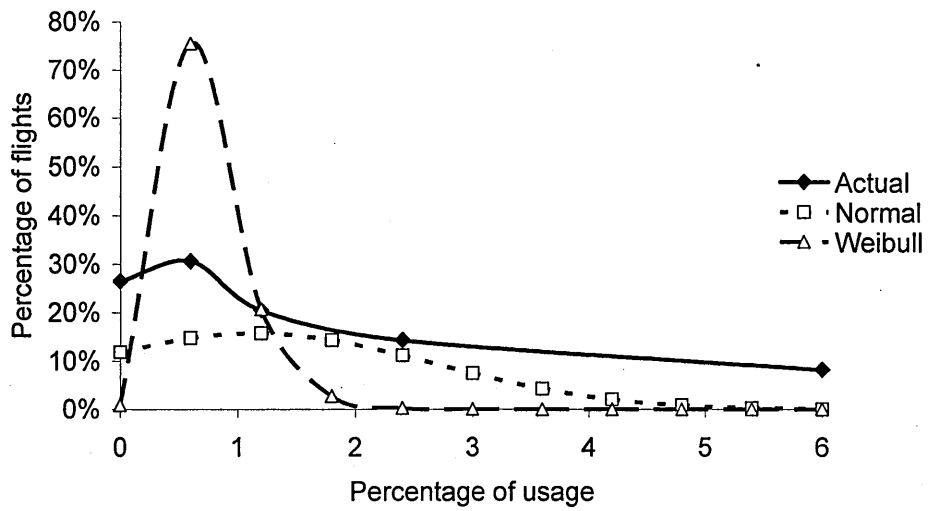

Fig. 4.8_ Usage Distribution for Lynx Mk7 Climb manoeuvre

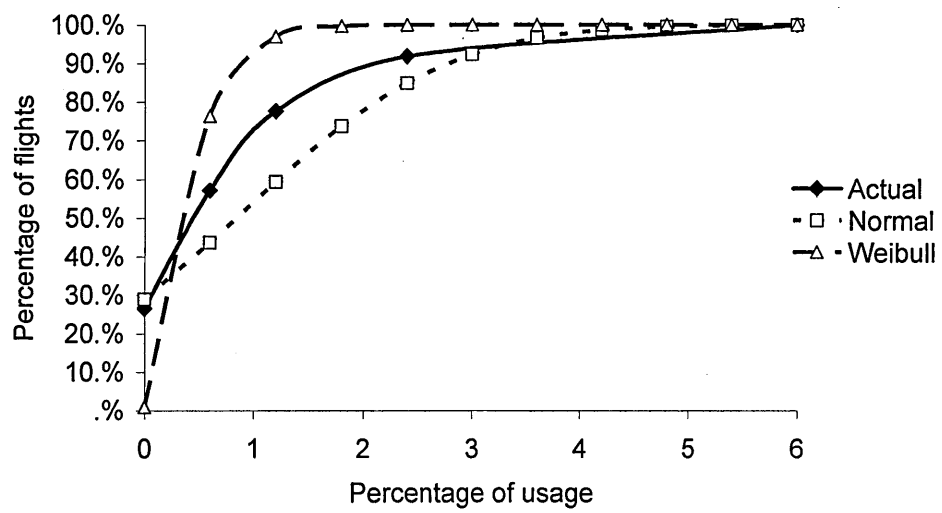

Fig. 4.9_ Cumulative Usage Distribution for Lynx Mk7 Climb manoeuvre

4.1.2 Load data

The investigation was performed using 10 hours of flight load data gathered on a Westland Lynx Mk 9 helicopter. Data were recorded as 55 channels of flight parameters, of which 7 were strain or bending moment data from specific components. In this research load data from the dogbone rotor linkage, the spider rotor component and a lift frame component (station 420A) were studied. Prior to supplying the data it was necessary to remove the many 'dropouts' that were found in the data due to random faults in the instrumentation equipment that caused full scale deflections of the recording trace. The dropouts caused spurious results when analysing the data. Analysis was performed using programs written in C and Fortran code. For graphical representation of data SOMAT SAFE package was used. Representative examples of stress versus time data for the first two components are shown in figures 4.10 4.11 and 4.12. There is an apparent difference in loading pattern. Dogbone experiences many cycles of small amplitude at high mean stress (similar to Rotorix) and spider arm has most cycles with mean stress around zero. It should be noted that all load data were provided for use with the appropriate S-N data.

The data had factors embedded that produced values of stress that are not representative of the material properties (dogbone – titanium, spider arm – steel S99, 420A lift frame – aluminium). This was probably done to take into account the component geometry and strain gauge type and position. It was not possible to acquire data in a 'virgin' format i.e. before the design authority applied any kind of factors. Since the aim of the project was to investigate the methodology and the extent of variability and its effect on total life, and since the factoring methodology remains constant (hence introduces no variability) the damage calculation method used the loading data as they were. This means that the stress values in figures 4.10, 4.11 and 4.4 should be received as indications of the loading form but not for the absolute values of stress. Actually for dogbone it is effective bending moment(lb-ins), for spider arm it is load (lbs) and for 420A lift frame it is micro strain.

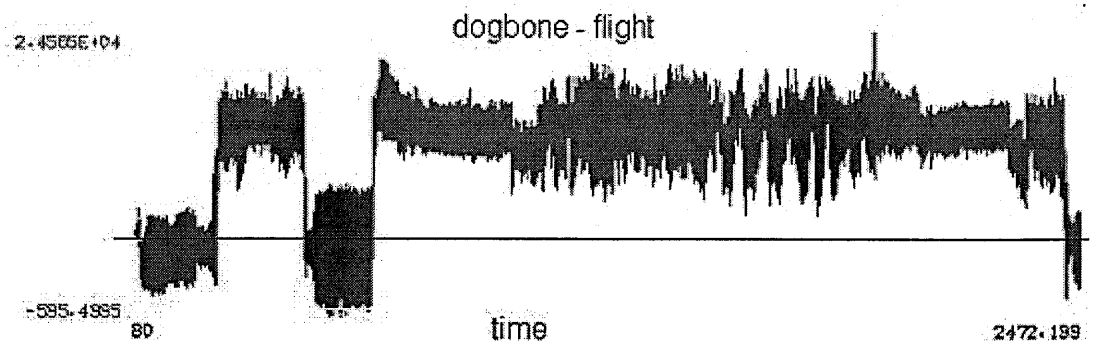

Fig. 4.10_ Effective bending moment VS time(sec) plot for dogbone (flight 1566b)

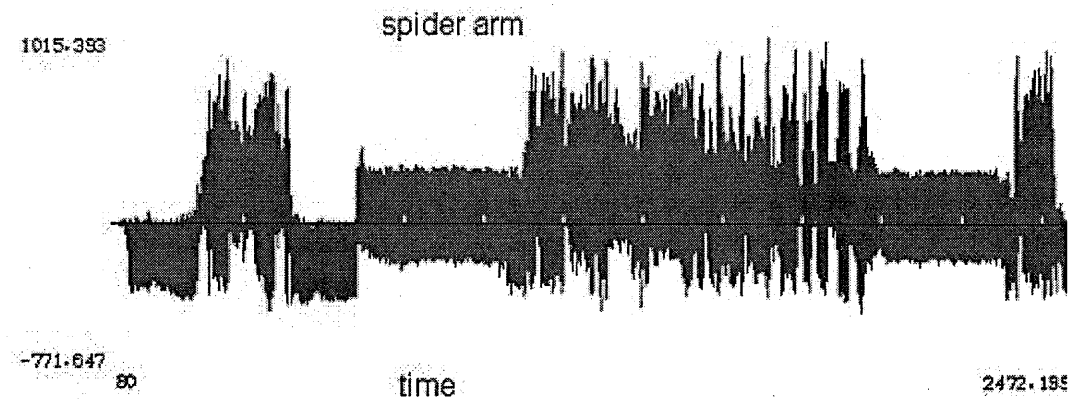

Fig. 4.11_ Load VS time(sec) plot for spider arm (flight 1566b)

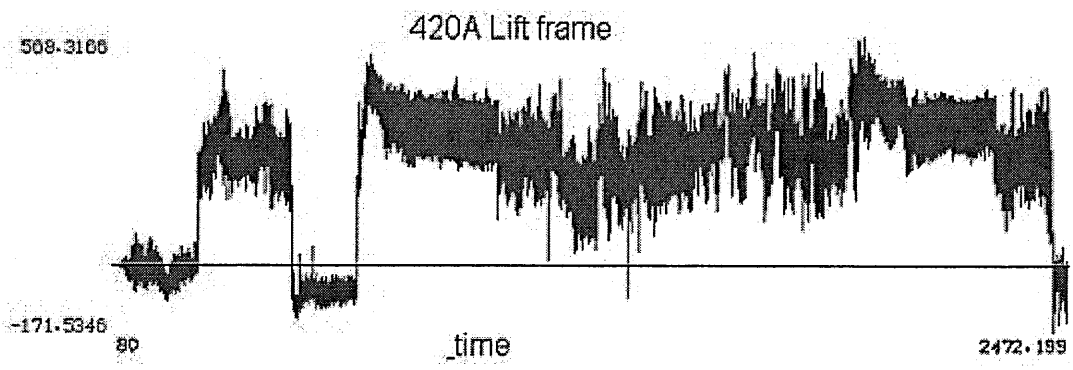

Fig. 4.12_ Micro strain VS time(sec) plot for lift frame 420A component (flight 1566b)

4.2 Damage calculation method

The damage calculation method could be described by the following steps:

1. Specify manoeuvre
2. Rainflow cycle count manoeuvre
3. Combine with WHL S_N data
4. Derive life

The strain or bending moment vs time data were converted to stress vs time data based on procedures provided by the design authority. The stress-time history between a start and stop point for each manoeuvre was then rainflow cycle counted. The rainflow spectrum was then used together with the component constant amplitude S-N curve, in a Miner summation calculation of the damage and damage rate for each occurrence of each manoeuvre type. Failure was defined as a damage sum of unity. The Goodman equation was used to account for mean stress effects using the UTS values.

4 parameter Weibull equation $\frac{S}{S_{inf}} = 1 + \frac{C}{(N+B)^A}$			
	Helicopter component		
Parameter	**Dogbone**	**Spider arm**	**Lift frame**
UTS	35200 lb-ins	6587 lbs	7866.01 micro strain
S_{inf}	16456 lb-ins	1135 lbs	149.47 micro strain
A	0.63	0.6667	0.55812
B	0	0	470.8
C	4886	5260	593.6
Strength factor	1.46	1.42	1
Life factor	4.2	3.75	1
Load factor	1.2	1.2	1.2

Table 4.4_ S-N fatigue data and factors

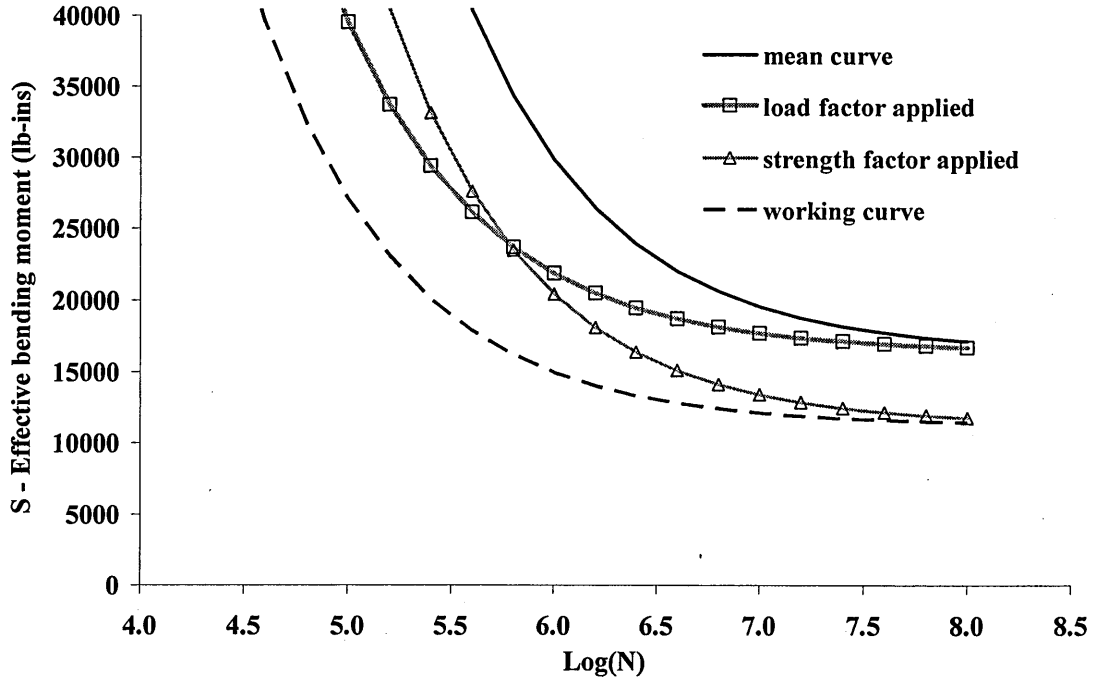

Fig. 4.13_ S-N curve at R=-1 for dogbone

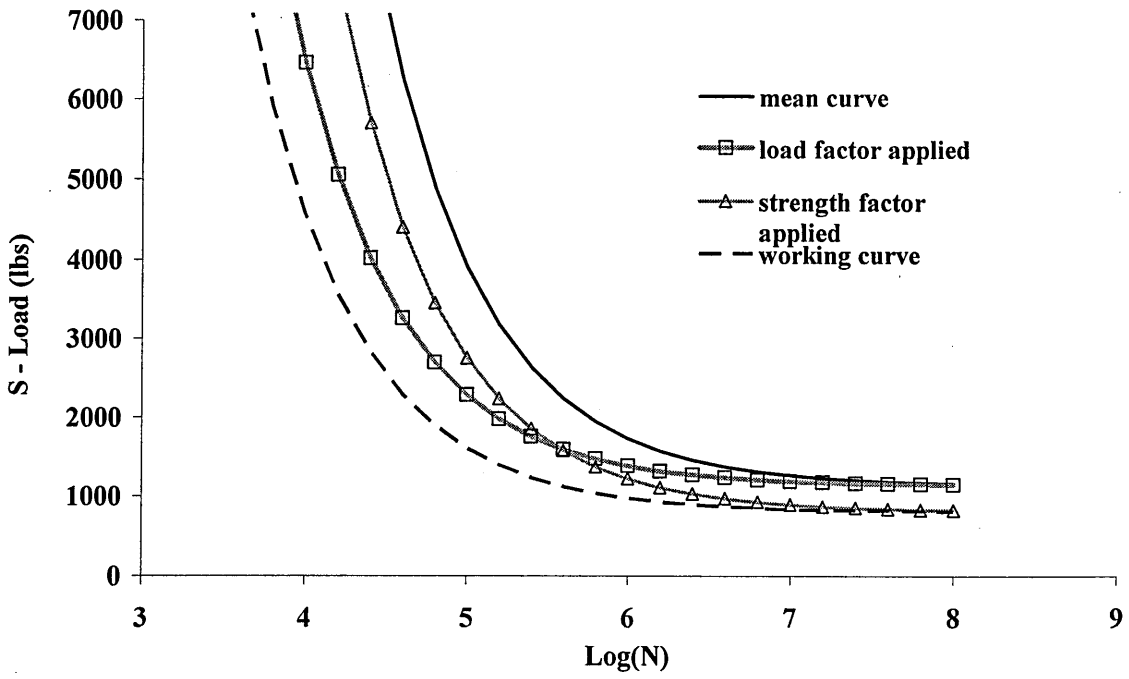

Fig. 4.14_ S-N curve at R=-1 for spider arm

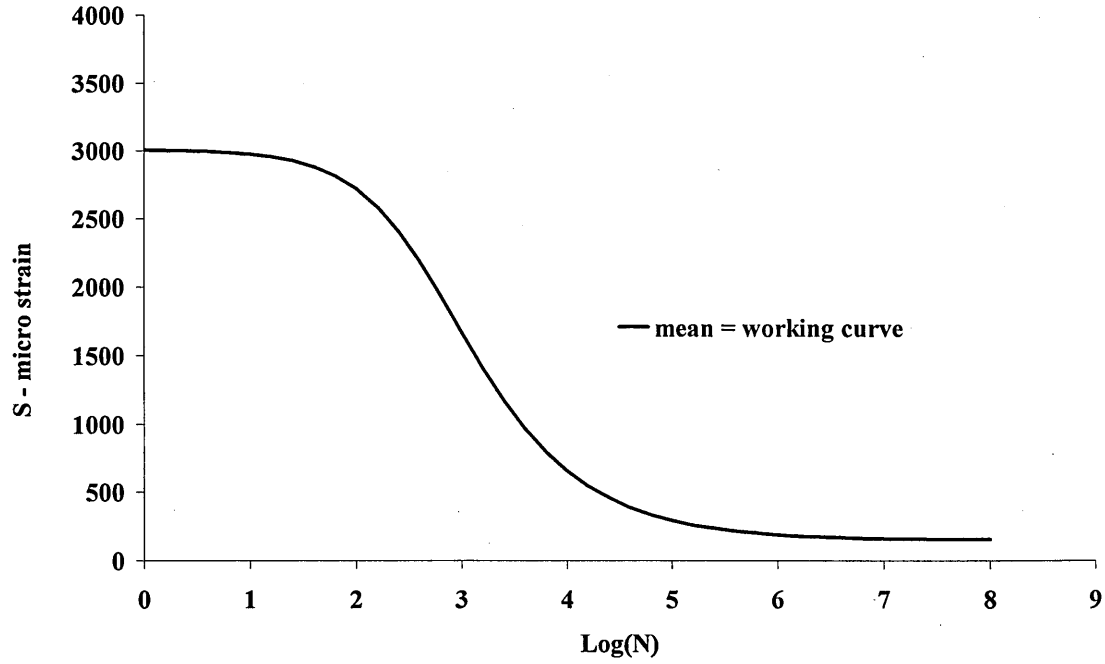

Fig. 4.15_ S-N curve at R=-1 for 420A lift frame

Constant amplitude (S-N) fatigue data for each component was supplied by the design authority (Table 4.4 and Figs 4.13, 4.14, 4.15). For deterministic analysis, as noted earlier, factors to reduce the S-N curve were applied to account for scatter in component properties.
Strength factor is applied to S_{inf}

$$S_{\text{inf\_Factored}} = \frac{S_{\text{inf}}}{Strength\_factor}$$

and life factor is applied to C parameter

$$C_{Factored} = \frac{C}{(Load\_factor)^{A}}$$

This procedure leads to the working S-N curve [58, 59]. For lift frame component no factors are applied. For investigation of the effect of usage and manoeuvre variability, these factors were applied to the S- N curve to ensure that a significant number of manoeuvres were damaging. Having calculated the damage content of each manoeuvre, the damage rate was derived by dividing by the manoeuvre duration.

4.3 Usage variability results

Next a study based on statistical analysis of MDRE data is presented. Results and comparisons are made in regards to damage (based on WHL procedures and data) and time in order to estimate the effect of usage variability. The statistical analysis of measured usage data was carried out on a manoeuvre per manoeuvre basis leading to a comparison of measured usage against the assumed design usage spectrum in terms of time and damage.

A comparison of the measured incidence of manoeuvres (or usage) compared with the original design usage spectrum is shown in figure 4.16, 4.9 for a selection of the most commonly occurring manoeuvres. Not surprisingly there are significant deviations from the original spectrum, with some manoeuvres having greater incidence than design, (e.g. forward flight at 0.6-0.8 VNE) and others less (e.g. hover and forward flight at 0.8-0.9 VNE). The coefficients of variation of the usage (std dev/mean values) were very large for all manoeuvres in all types of operation and frequently exceeded 100%. This is shown in figures 4.16, 4.17 as range bars around the mean levels. Table 4.2 shows a complete list of time spent in individual manoeuvres expressed as a percentage of the time allocation in the design spectrum.

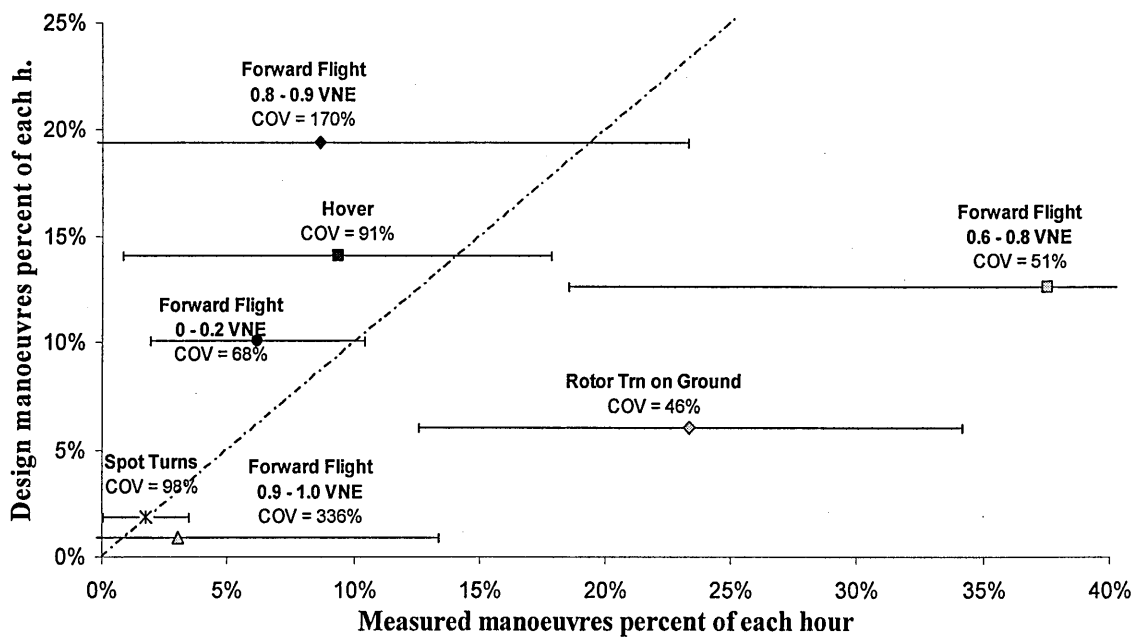

Fig. 4.16_ Measured usage Vs design usage spectrum on Lynx Mk 7. Data points are mean values, Bars represent one standard deviation.

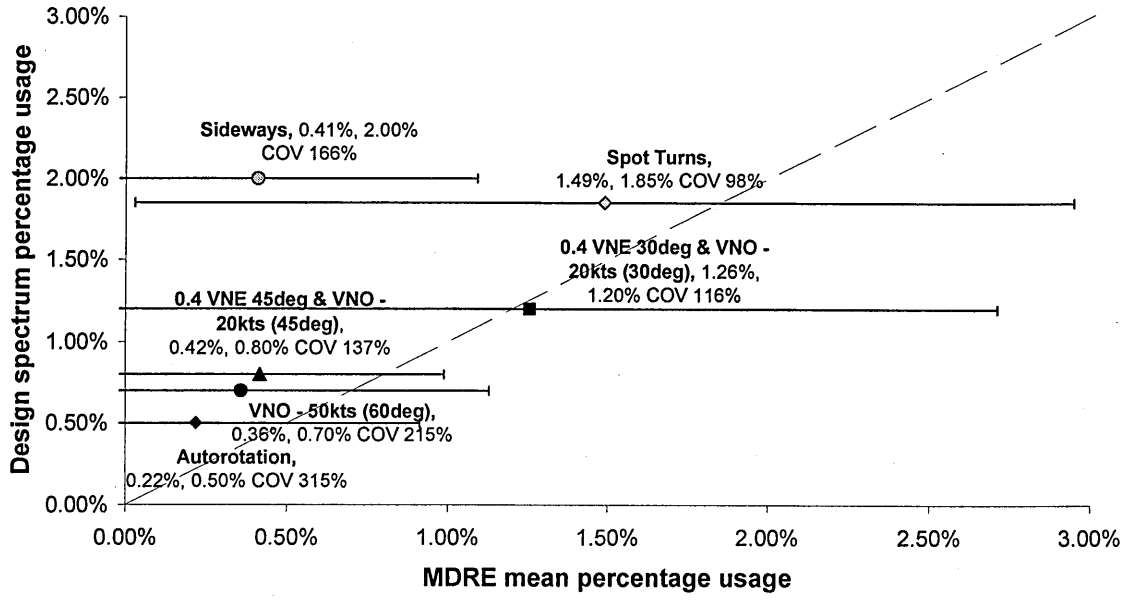

Fig. 4.17_ Measured usage Vs design usage spectrum on Lynx Mk 7. (up to 3%)

Figures 4.18 and 4.19 show the differences in measured and design usage mean values for the most significant manoeuvres, expressed as % time occupied by the manoeuvre in a flight hour. There are major changes in how the helicopter spends each flight hour, when design and measured usage values are compared. Forward flight, hover and rotor turning on the ground occupy almost 70% of the design spectrum and almost 90% of the measured spectrum. As these manoeuvres are largely undamaging these differences do not matter greatly from the viewpoint of component life.

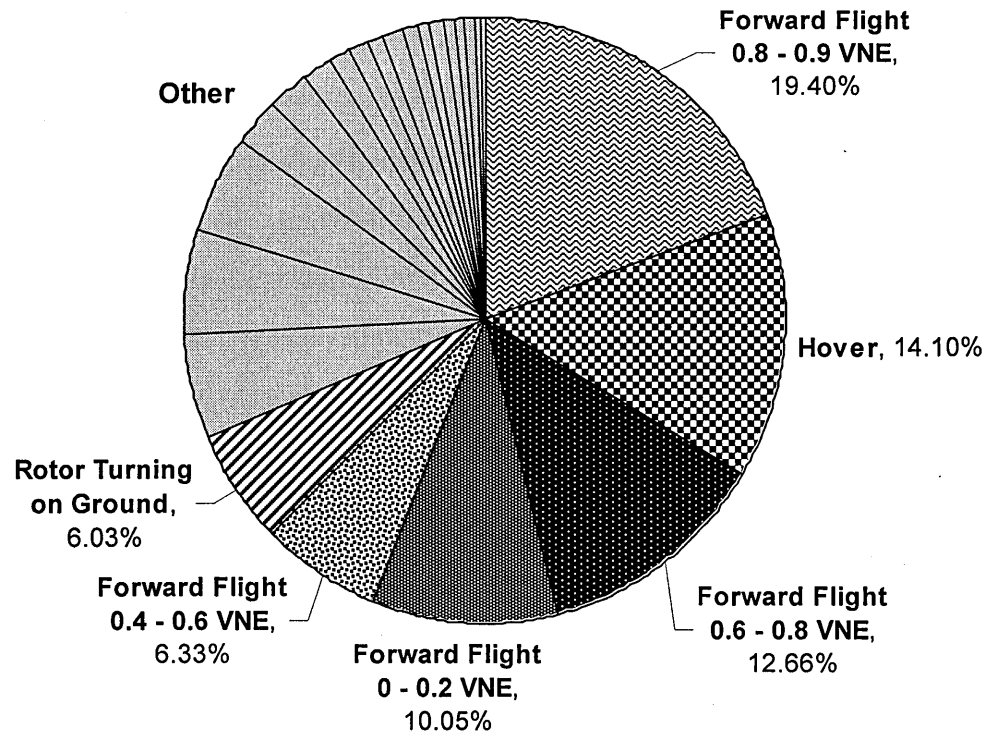

Fig. 4.18_ Design usage percentage - Lynx Mk7

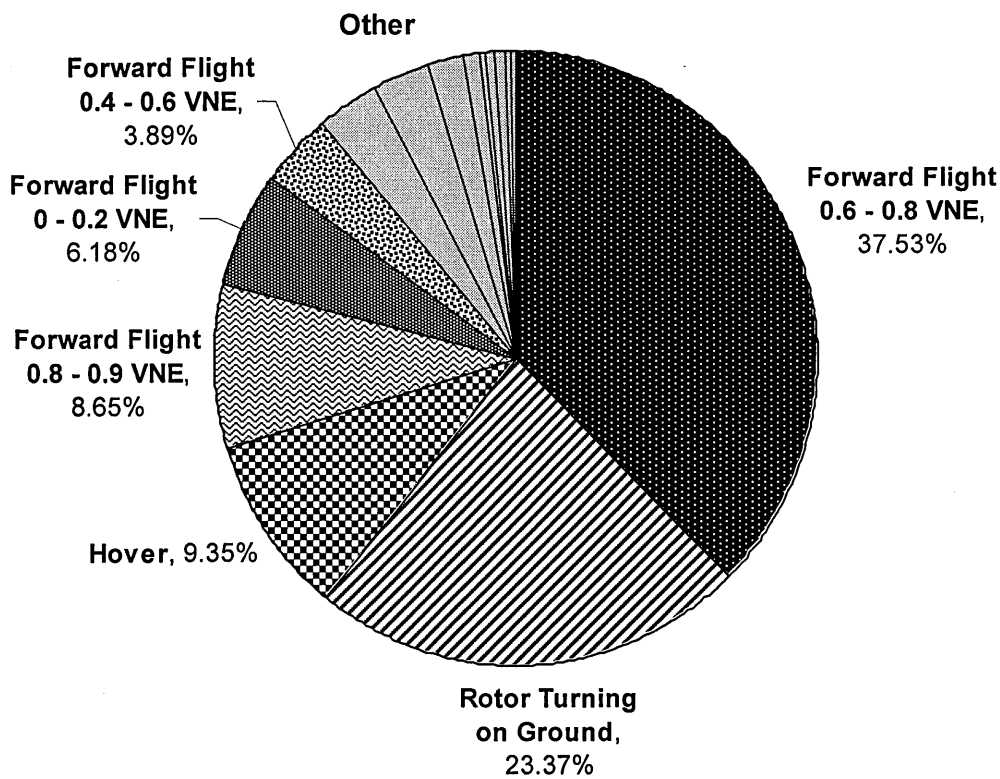

Fig. 4.19_ Measured mean usage percentage – all mission types - Lynx Mk7

Figures 4.20 and 4.21 show a similar plot but based on damage caused by the incidence of the manoeuvres shown in figures 4.18 and 4.19, rather than time. The damage figure used is that caused by a single instance of the manoeuvre, with 50% probability of occurrence. Because the overall average damage per hour is reduced from that of the design spectrum by a factor of about 2.5 for the dogbone component, it is possible for manoeuvres to have a reduced incidence from the design spectrum, but a greater measured percent damage contribution. An example of this is the hover manoeuvre.

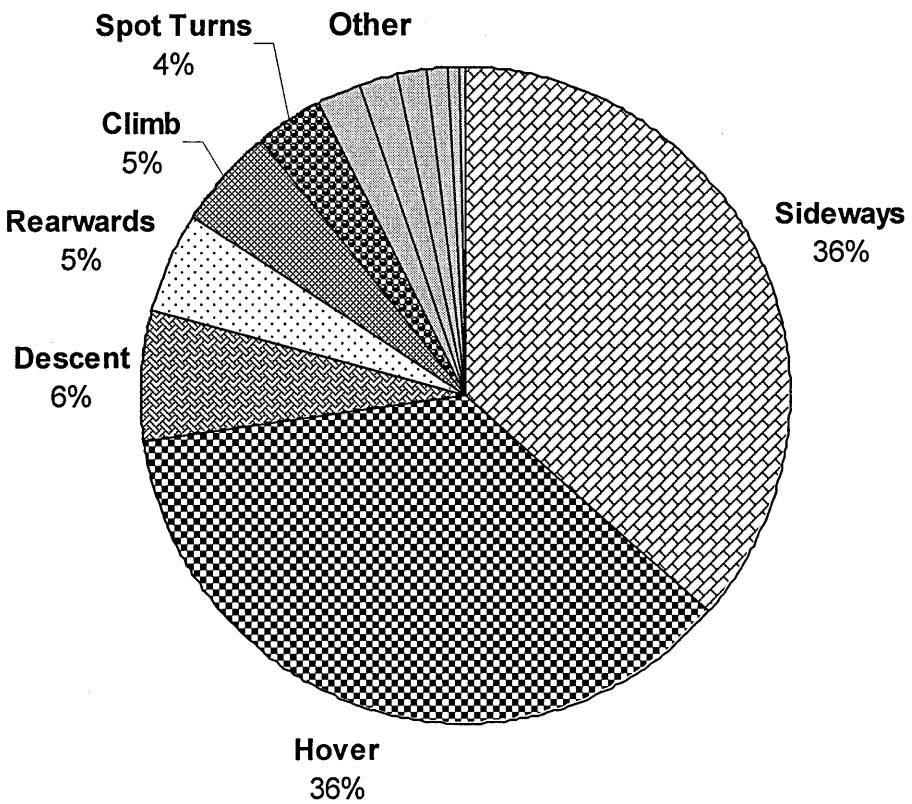

Fig. 4.20_ Damage per hour contribution of each manoeuvre using Design spectrum – Dogbone component.

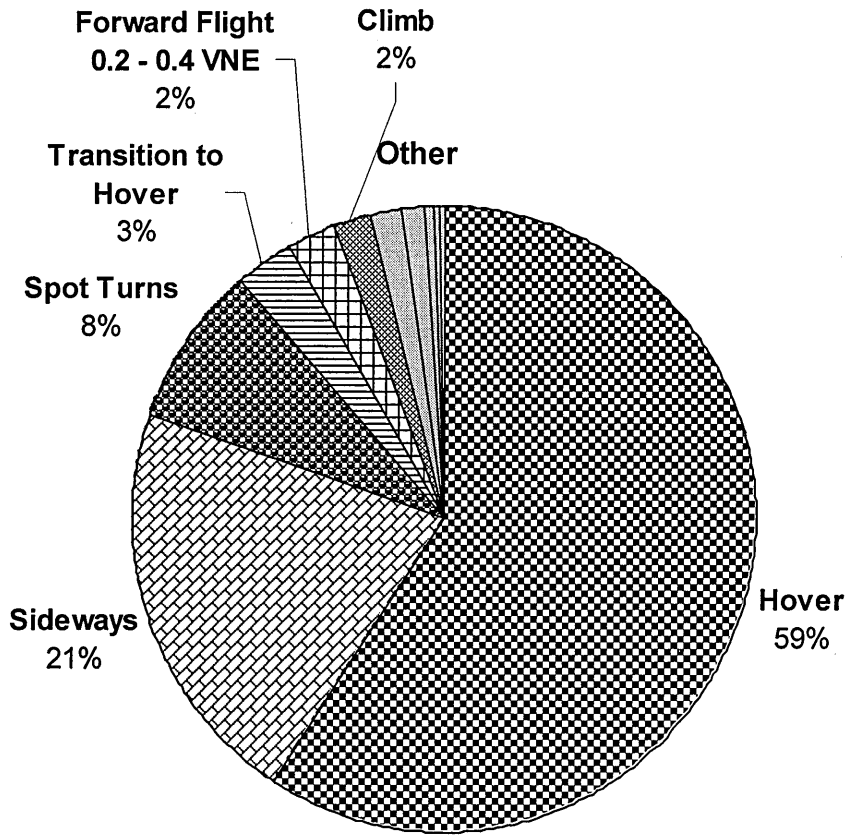

Fig. 4.21_ Damage per hour contribution of each manoeuvre using measured usage spectrum – Dogbone component.

In figures 4.20 and 4.21, the majority (70-80%) of the damage in the dogbone component is caused by hover and sideways flight, with other manoeuvres making little contribution. Monitoring helicopter usage for this type of operation therefore reduces largely to monitoring the incidence of hover and sideways flight and perhaps one or two other manoeuvres. The contribution of other manoeuvres to accumulated damage is negligible. This comparison is for the dogbone rotor component, other components have different results.

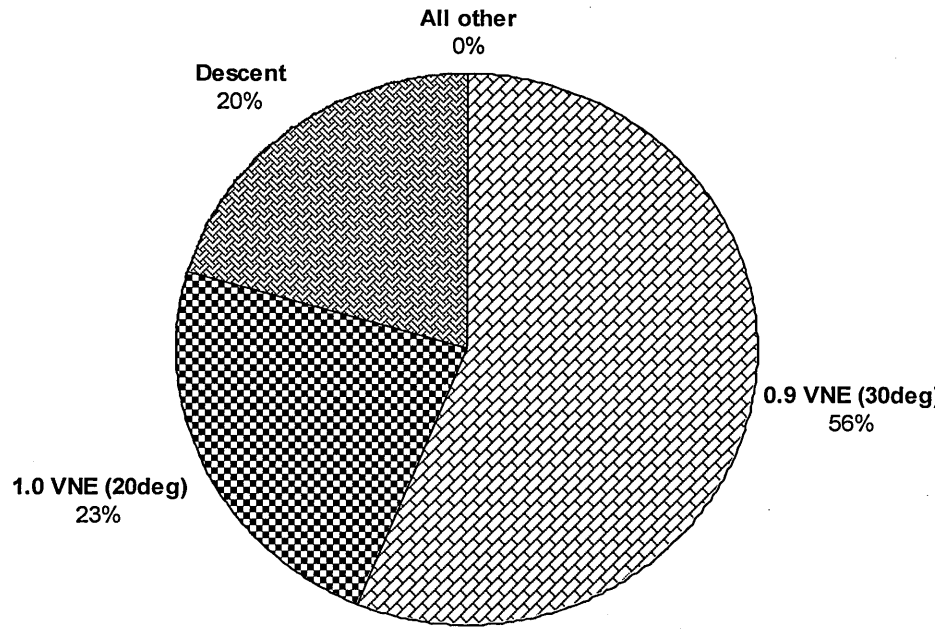

Fig. 4.22_ Damage per hour contribution of each manoeuvre using. Design spectrum – Spider.

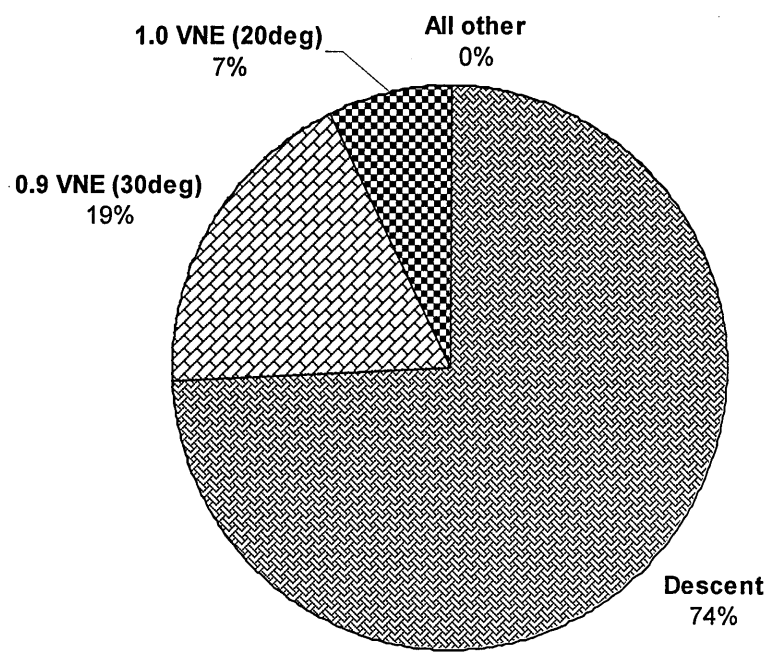

Fig. 4.23_ Damage per hour contribution of each manoeuvre using measured usage spectrum – Spider.

In figures 4.22 and 4.23, the majority (70-80%) of the damage in the spider arm component is caused by descent, 0.9 VNE (30deg) and 1.0 VNE (20deg) with other manoeuvres making no contribution. Monitoring helicopter usage for these manoeuvres would be adequate for the spider component alone. This analysis is for the spider arm rotor component, other components will have different manoeuvres which cause the most damage, and differing damage levels.

Figures 4.24, 4.25 show a comparison taken from the MDRE data for selected manoeuvres of the percent time spent in each manoeuvre for different types of service operation. Figures 4.26, 4.27 show the percent damage contribution for the figures 4.24, 4.25 data. Significant differences both in terms of percent time and percent damage were found between the different types of service. However the overall conclusions noted earlier still applied. For the dogbone in terms of time spent in manoeuvres, forward flight and hover manoeuvres were responsible for the majority of time in flight, but in terms of damage hover and sideways flight were responsible for the majority. For the spider arm descent, 0.9 VNE (30deg) and 1.0 VNE (20deg) manoeuvres have little contribution in terms of time, but in terms of damage these manoeuvres are responsible for the total. These conclusions were irrespective of the operation type, with one or two exceptions.

Figures 4.24, 4.25, 4.26 and 4.27 imply that different usage types will have different mean damage values and different times to achieve the limit of safe life. In theory, usage monitoring would allow extension of lives.

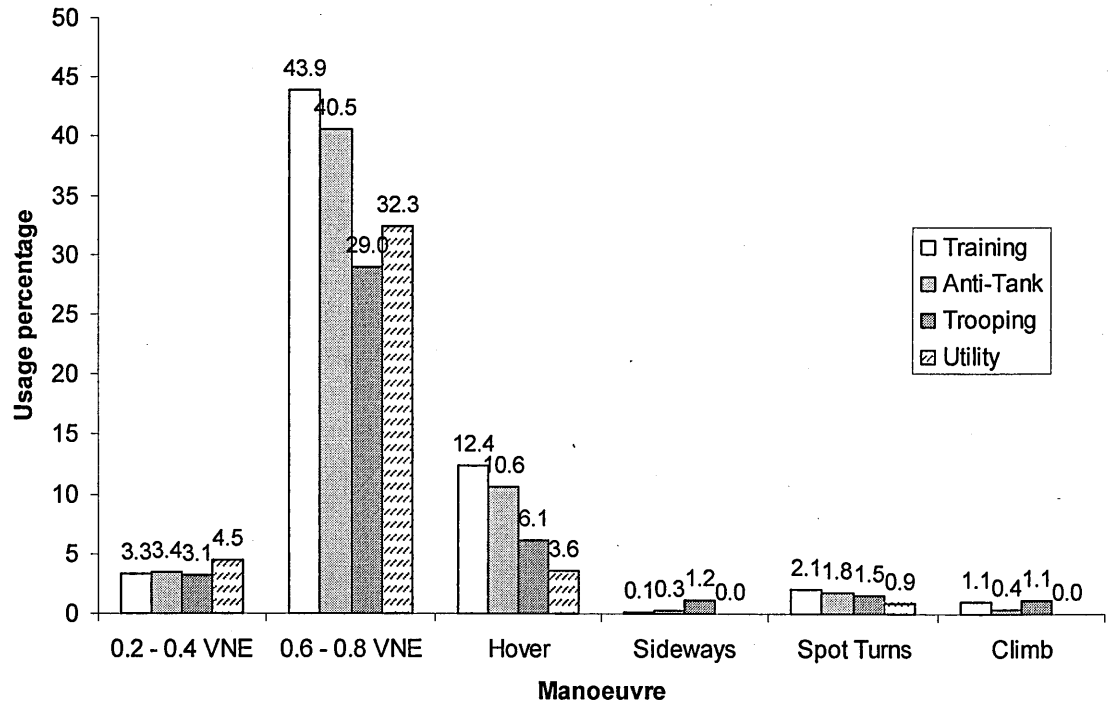

Fig. 4.24_ Measured usage percentage (time) per manoeuvre and mission type – major manoeuvres only.

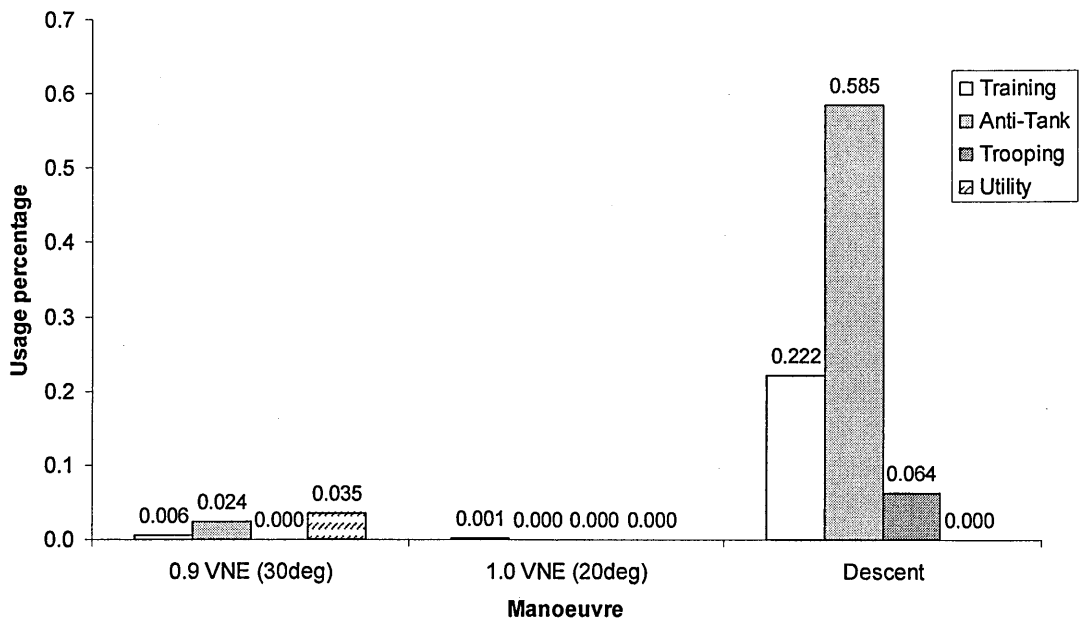

Fig. 4.25_ Measured usage percentage (time) per manoeuvre and mission type – major manoeuvres only (up to 0.7% usage)

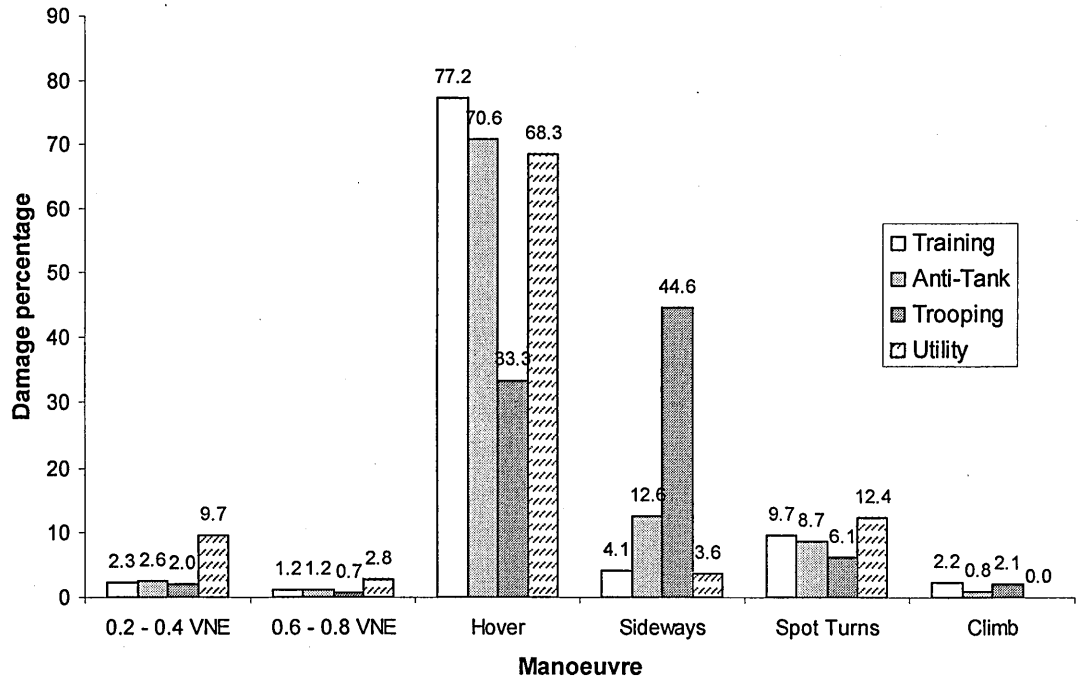

Fig. 4.26_ Damage contribution percentage per manoeuvre and mission type – Dogbone component.

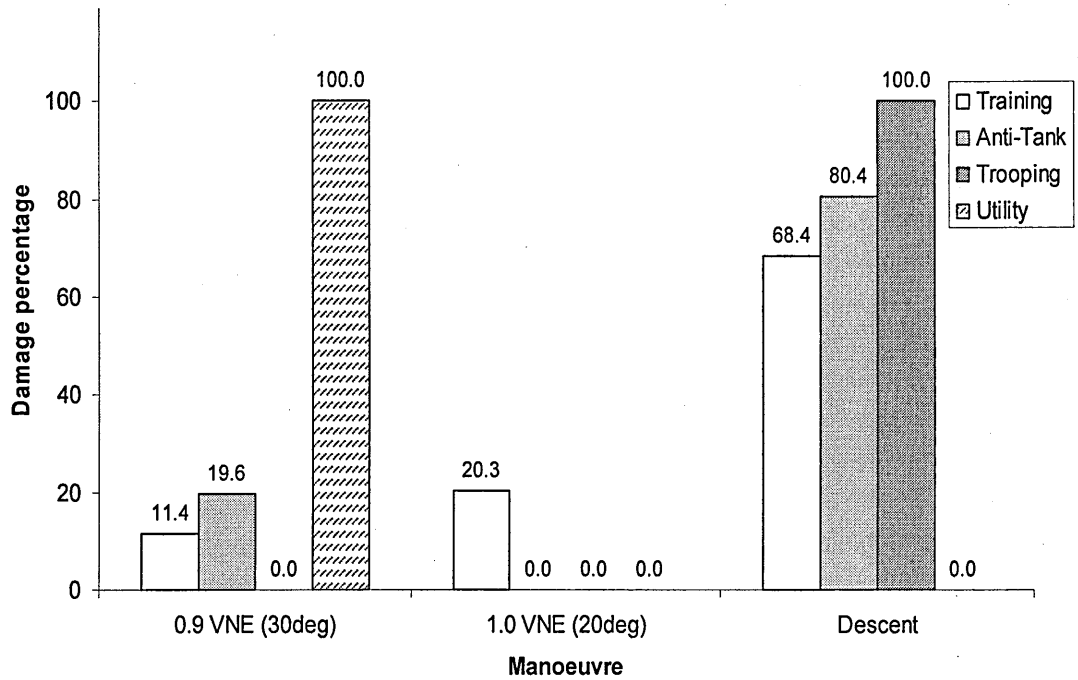

Fig. 4.27_ Damage contribution percentage per manoeuvre and mission type – Spider arm component.

Figure 4.28 compares the total damage content of the different usage types against that predicted by the design usage spectrum. The design spectrum by definition contributes 100% damage per flight hour. Three of the four types of usage, all result in significantly less damage 66-68% than predicted for the design spectrum. The fourth usage is more benign with only 55% of the design spectrum damage. These are deterministic calculations. To explore the effect of variability in damage caused by usage, Monte Carlo simulations were done in which different types of usage were systematically varied at different intervals.

Changes in mean damage levels caused by usage change have been demonstrated to be significant. In the example given, 66% increases in life could have been obtained by operation of a manoeuvre based usage monitoring system for rotorcraft operating the utility spectrum.

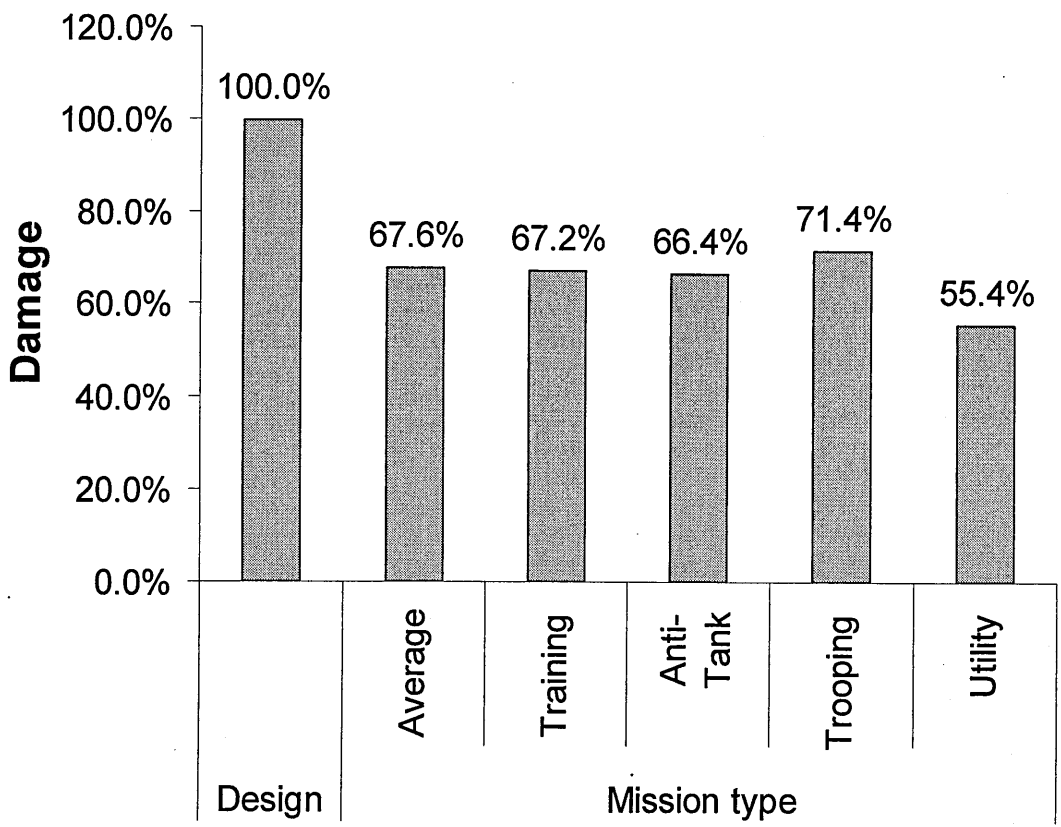

Fig. 4.28_ Damage for each mission type, compared to assumed design usage spectrum. Damage content of each manoeuvre fixed.

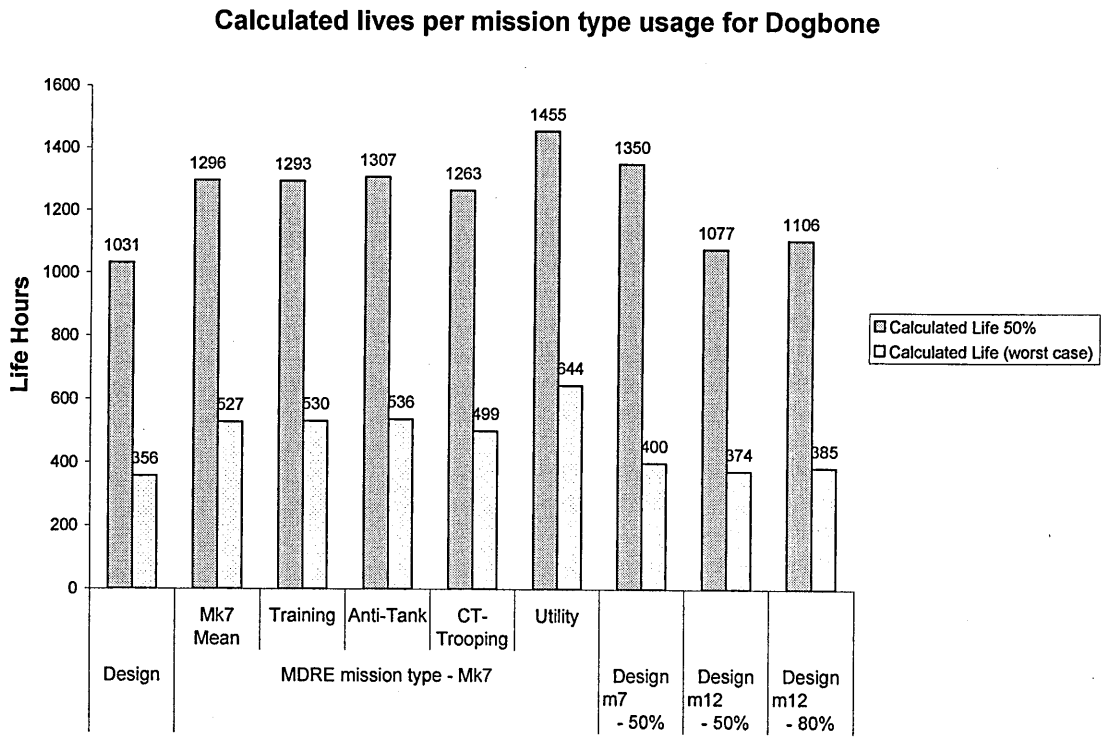

Fig.4.29_ Damage calculation results for dogbone component for various usage spectra

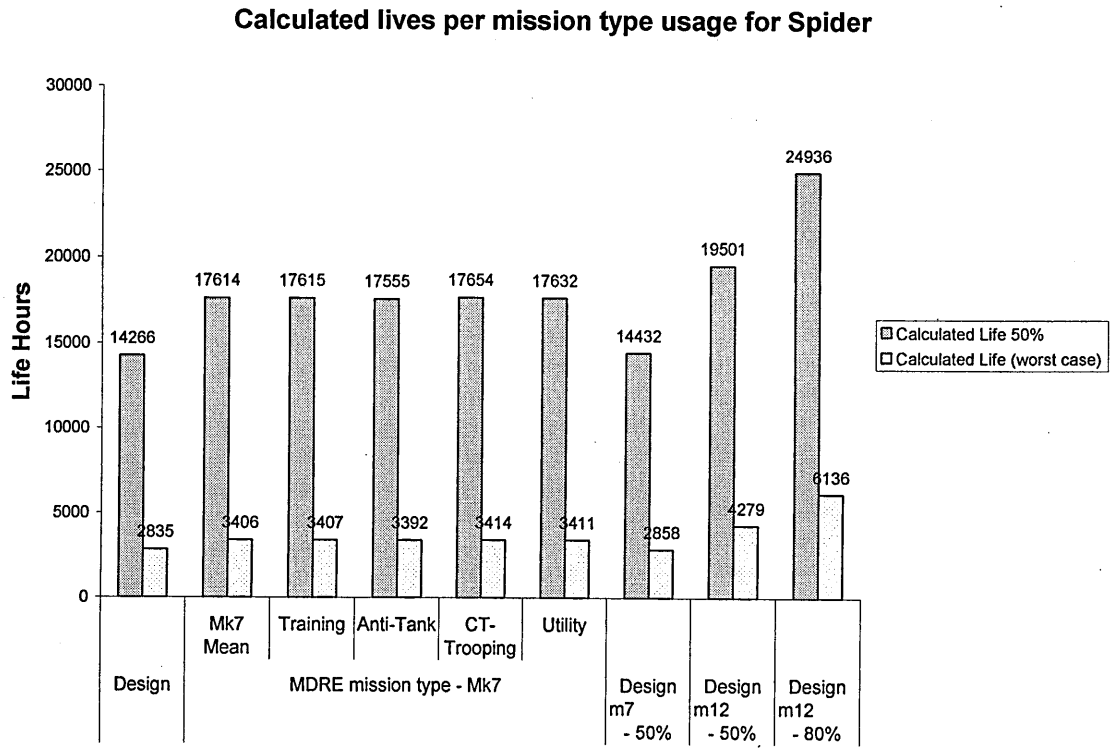

Fig.4.30_ Damage calculation results for spider component for various usage spectra

Damage calculations carried out for dogbone and spider components use the assumed design usage spectrum along with measured spectra. Calculation is based on WHL procedures (S-N curve, factors) and recorded loads. For each manoeuvre several examples exist, hence the variability in calculated life (mean 50% and min = worst case). Figures 4.29, 4.30 present the life calculation results for various usage spectra (based on MDRE data analysis) depending on aircraft mission type. Also three cases are identified where usage of damaging manoeuvres (Man.7 and 12) has been reduced by 50% and/or 80%. Usage monitoring of these two manoeuvres is necessary to be accurate and continuous. Actual usage (MDRE) is less damaging than assumed design usage, leading to an increase of life by a factor of 1.2 to 1.4.

Statistical analysis of mission data has shown that design usage spectrum is not always conservative for some components. Figures 4.31, 4.32 and 4.25 show the results for dogbone, spider arm and 420A lift frame respectively. Comparing the damage caused from the usage of each sortie (mission flight) against the damage from the design spectrum it is concluded that only for spider arm the design spectrum is in every case conservative. For the other two components there are some sorties that produce significant damage. The results of the comparison is shown in tables 4.5 and 4.6 analysed also per mission type. It is seen that different mission types contain extra damaging sorties for each component. For the dogbone it is the trooping and training missions, and for 420A lift frame it is anti-tank, trooping and utility mission types. It should be noted that for the spider component the most damaging manoeuvre is the control reversals at 0.9 VNE [59] which exist in the design spectrum but is a rare manoeuvre and was not recorded during the MDRE. This could explain why no actual sortie produced more damage than the design spectrum. It is seen that the range of lives is significant (most damaging vs least damaging sortie).

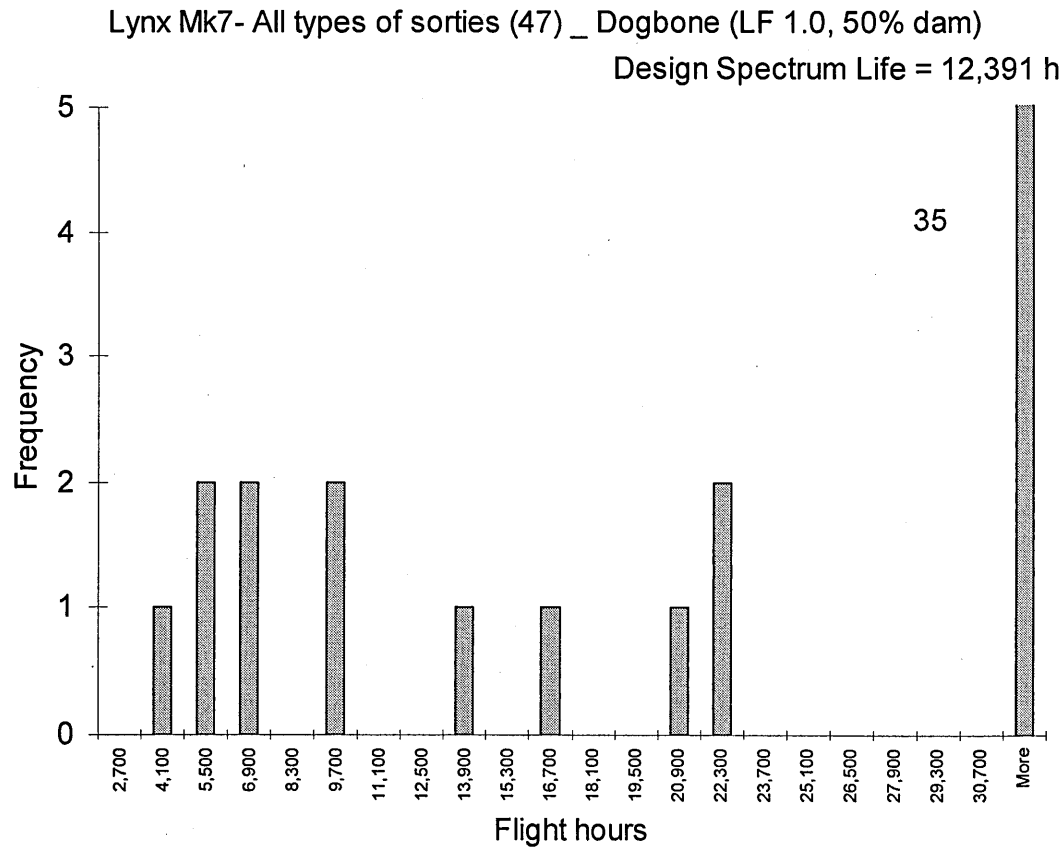

Fig.4.31_ Frequency occurrence plot of all sorties for dogbone

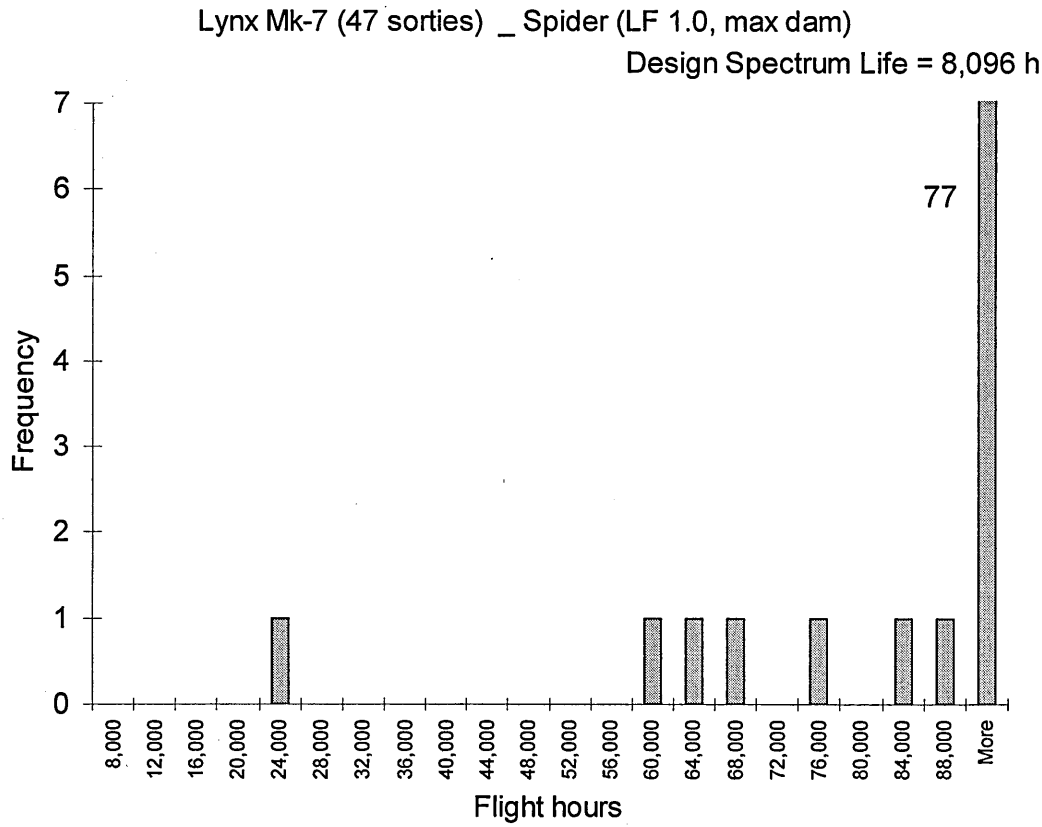

Fig.4.32_ Frequency occurrence plot of all sorties for spider arm

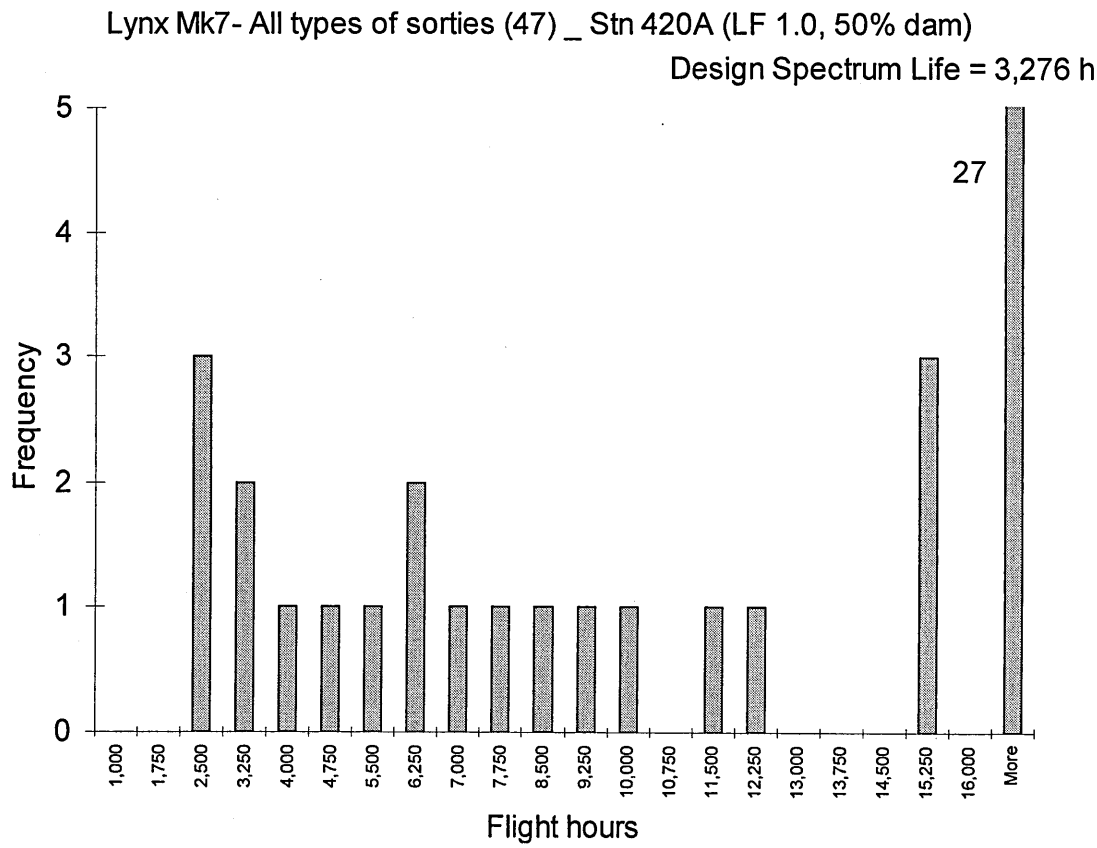

Fig.4.33_ Frequency occurrence plot of all sorties for 420A lift frame

Dogbone	No. of sorties more damaging than Design Spectrum
Utility	0 out of 3
Training	2 out of 18
Trooping	5 out of 14
Anti-Tank	0 out of 12
TOTAL	7 out of 47

Table 4.5_ Results per mission type for dogbone

Stn420A	No. of sorties more damaging than Design Spectrum
Utility	1 out of 3
Training	0 out of 18
Trooping	1 out of 14
Anti-Tank	3 out of 12
TOTAL	5 out of 47

Table 4.6_ Results per mission type for 420A lift frame

4.4 Loads variability results

Load variability investigations for dogbone and spider arm components have been already carried out [58, 59]. In the following the statistical analysis of loading data regarding the lift frame component (420A) is presented. Appendix E contains the results with plots of cumulative probability distribution of damage rate (Fig. 4.34) for all the manoeuvres in the design spectrum for 420A lift frame component

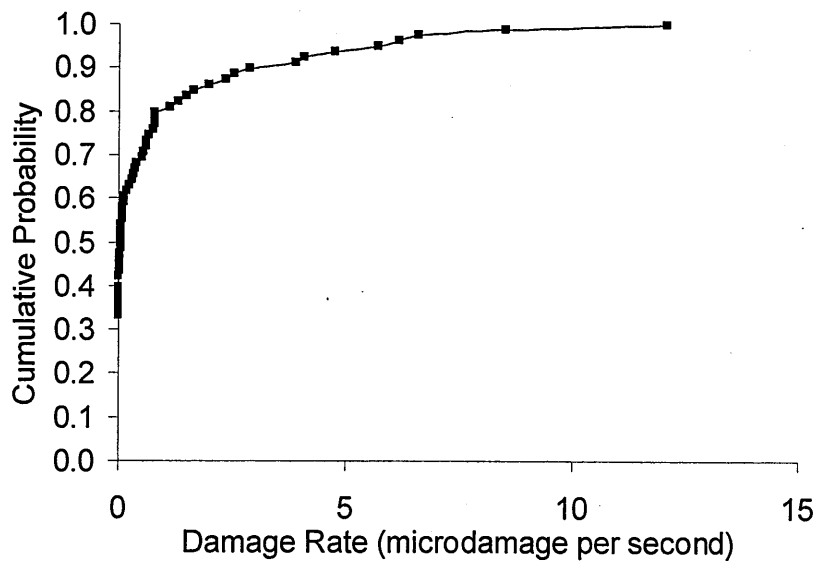

Fig. 4.34_ Cumulative probability distribution of damage rate for 78 examples of transition to hover manoeuvre for 420A lift frame component

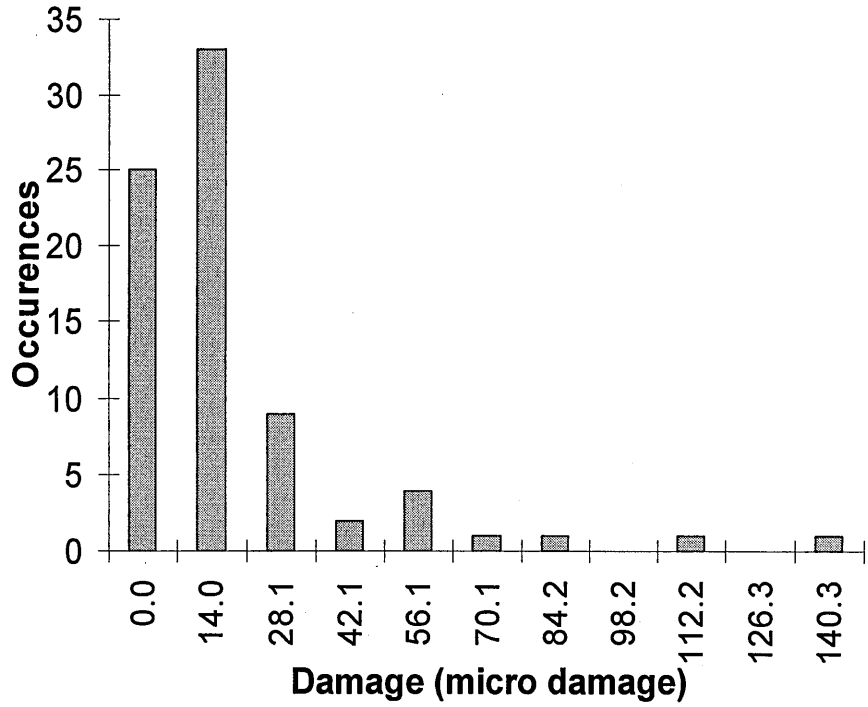

Fig. 4.35_ Frequency distribution of damage for 78 examples of transition to hover manoeuvre for 420A lift frame component

Calculations of fatigue damage for individual manoeuvres showed that as found in other recent work [41], [60] repeated occurrences of the same manoeuvre produced substantially different load spectra and fatigue damage values. A typical example of damage distribution for the 420A lift frame component is shown in figure 4.35 for the transition to hover manoeuvre. It can be seen that many occurrences of the manoeuvre resulted in zero damage with individual damage values approaching a largest value of 140 micro damage in a sample total of 78. The most common damage value was around 14 micro damage. The largest damage value was therefore about ten times greater than the most common. The general forms of the distributions were similar in all manoeuvres and all components, although the mean values of damage differed greatly. For instance forward flight was generally un-damaging, while control reversals almost without exception produced substantial damage.

4.5 Effect of safety factors

Deterministic calculations showing the effect of factors on loads and S-N curve were carried out. For the damage calculations the data and methods supplied by the design authority were applied.

Figure 4.36 presents the effect of the load factor. Calculated lives using various load factors from 0.9 to 1.3 are expressed relative to life with load factor 1. It is seen that a load factor of 1.2 as it is commonly used leads to 7.7 times reduction in life for the dogbone component.

Figure 4.37 shows the effect of Strength and Life factors applied to the mean S-N curve. Figure 4.38 presents the effect of the S-N factors to life for varying S_{inf} with a 20 to 30 times reduction in life when both factors are applied. It should be noted that in Monte Carlo simulations (see chapter 5) strength variability is simulated by varying S_{inf}. Figures 4.39 and 4.32 present the effect of Goodman (m) and Miner (D) on calculated life. Differences of 20% in Goodman parameter m lead to 50% influence on life. Miner's effect is as expected linear with life.

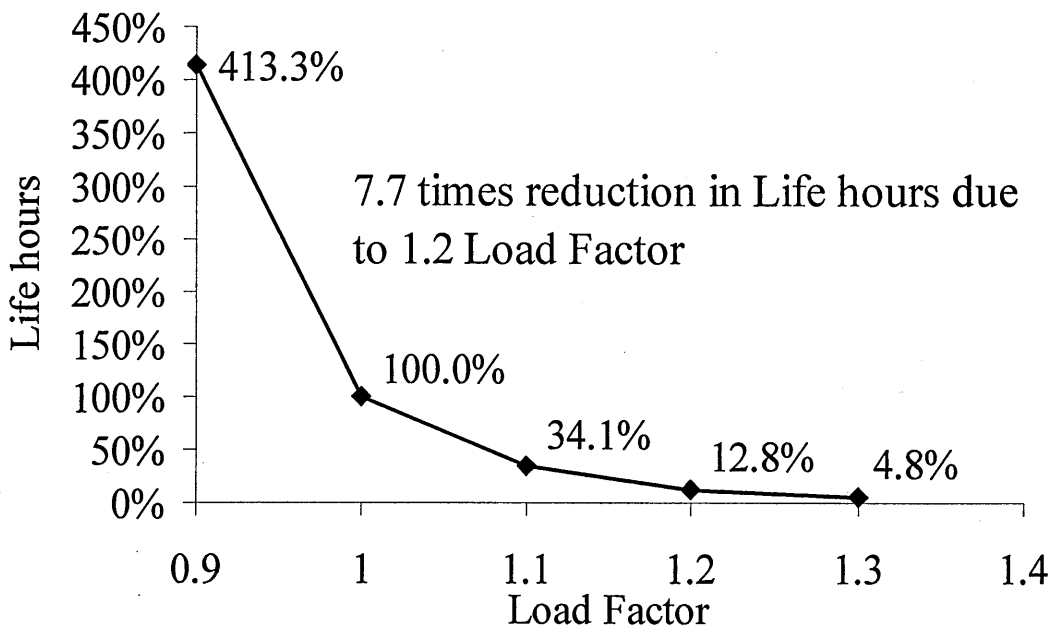

Fig. 4.36_ Life(h) VS Load factor (1.2 in design) for dogbone

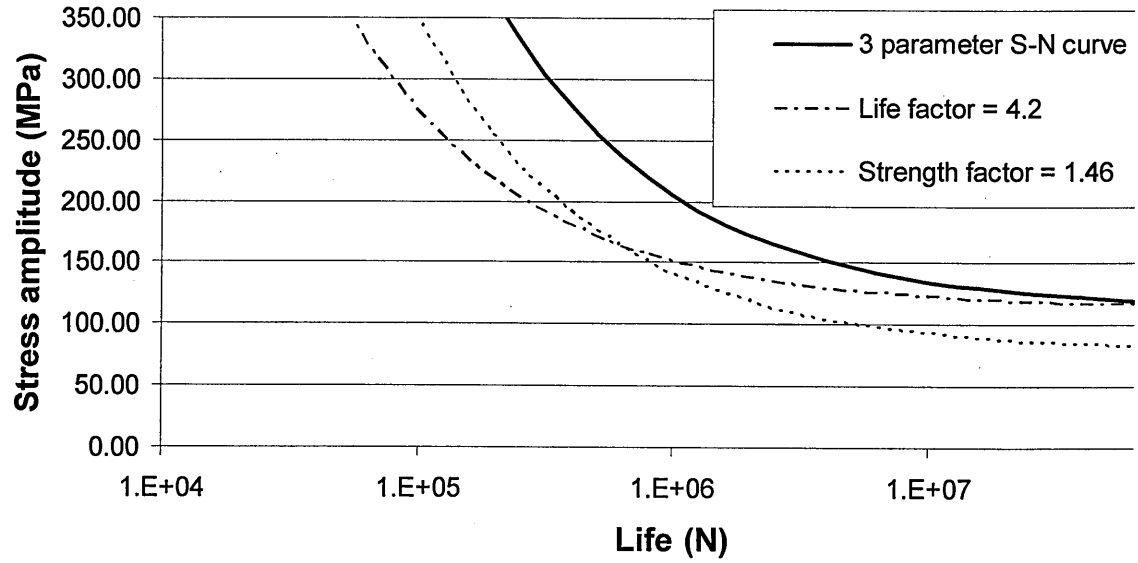

Fig. 4.37_ Effect of Strength and Life Factors on S-N curve for dogbone component

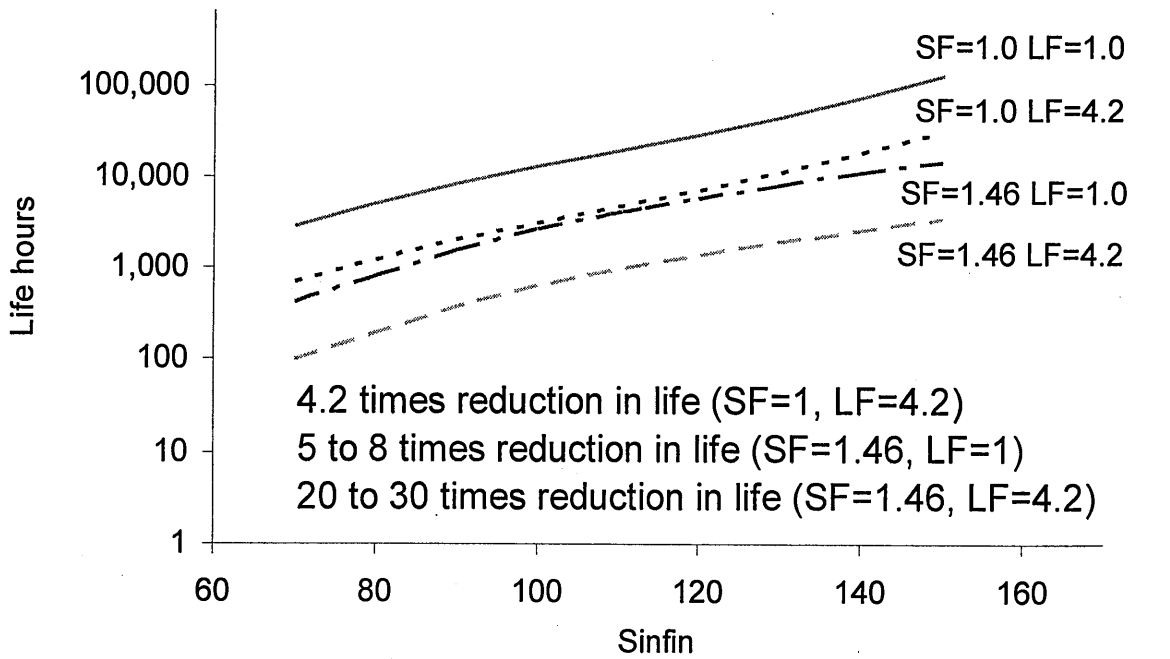

Fig. 4.38_ Life (h) VS S_{inf} for various S-N curve factors (SF: strength factor, LF: life factor) for dogbone component

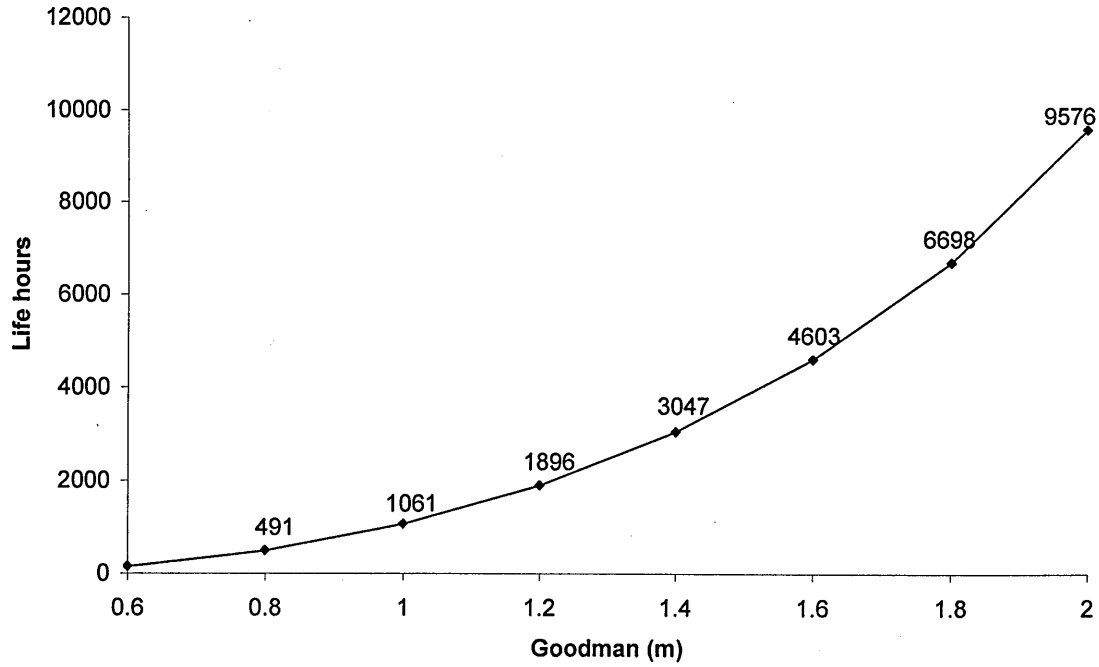

Fig. 4.39_ Life (h) VS Goodman parameter m for dogbone component

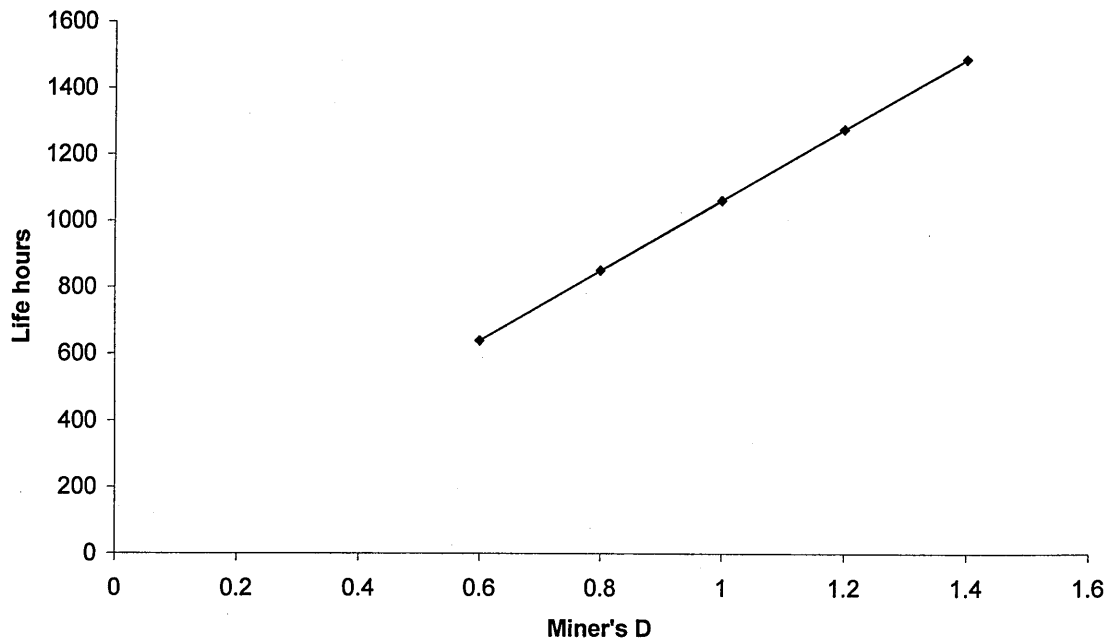

Fig. 4.40_ Life (h) VS Miner parameter D for dogbone component

4.6 High and low frequency analysis

Design Authority fatigue calculations are made using a concatenated spectrum made up from different flights or worst case manoeuvres from different flights. This causes fatigue cycles additional to those contained within individual manoeuvres – these are artificial and never really existed in the original flights. This extra damage is added in design authority fatigue substantiation. Calculations were carried out to determine the total damage in a flight compared with sum of manoeuvre damage from the same complete flight. Figure 4.41 depicts a typical helicopter flight pattern.

High frequency analysis is based on the application of the rainflow cycle counting method for each manoeuvre individually. A damage is associated with each manoeuvre using the damage calculation method as described in paragraph 4.2. The total damage of the flight is the summation of damage from all manoeuvres. It should be noted that for the particular investigation the total flight was attributed to manoeuvres, that means that the time length of the complete flight was exactly the same as the sum of the manoeuvre lengths.

Low frequency analysis is applied in order to take into account cycles that are omitted during high frequency analysis. These are the transition from one manoeuvre to another, especially when this is accompanied with significant change in the average stress of the manoeuvre. In practice for this investigation low frequency analysis is applied as follows:
The maximum and minimum stress values of every manoeuvre is identified.
Two lists are formed from these values. One in descending order of all maximum stress values and one in ascending order of all minimum stress values. A cycle is formed from the first value of each list i.e. max maximum with min minimum. This process continues until all cycles are exhausted. The damage of each cycle is calculated and their total is added to the damage from the high frequency analysis.

For this analysis three flights were used and damage calculations were performed for three components (dogbone, spider arm and lift frame component). Results are shown in figure 4.42. The calculated damage of the complete flight using the rainflow cycle counting method is expressed

as 100% and is regarded as the actual damage. All damage results from high and low frequency analysis are expressed as percentages of damage from total flight (100%). It is seen that high frequency analysis is non-conservative in every case. It should be noted that the closure option of the rainflow cycle counting technique is used, i.e. any incomplete cycle at the end of the counting process of the spectrum is automatically closed by the addition of an extra point. Errors of high frequency compared to total flight vary from 1% to 23% depending on component and flight. On the other hand low frequency analysis is conservative in every case. Additional damage varies from 7% to 91% compared to high frequency damage and from 6% to 68% compared to flight damage depending on component and flight. The reason of high frequency inaccuracy lies with the fact that the cycles from manoeuvre to manoeuvre is omitted. On the other hand, Low frequency analysis introduce non existing cycles that lead to overestimation of damage.

Until recently the design authority employed engineering judgment to overcome the over conservatism of low frequency analysis wherever necessary. Current design authority policy is to treat manoeuvres in groups, so that a realistic loading sequence would be formed when performing low frequency analysis. A proposed way would be to form a representative flight that would have its characteristics (length, manoeuvre sequence etc) determined from a statistical analysis of a large number of recorded representative actual flights. Application of rainflow cycle counting method to that flight would give realistic results of damage. As a measure of safety, that result would be compared with the most damaging recorded flight leading to any necessary modifications.

Although the materials studied are used for helicopter components and the loads and usage data are measured values, the calculated lives shown cannot be interpreted as bearing any relation to component safe lives substantiated by the Design Authority or which might occur in service. This is because the factors used will be different to those imposed by the Design Authority. Trends and comparisons may still be made; inferences on absolute lives cannot.

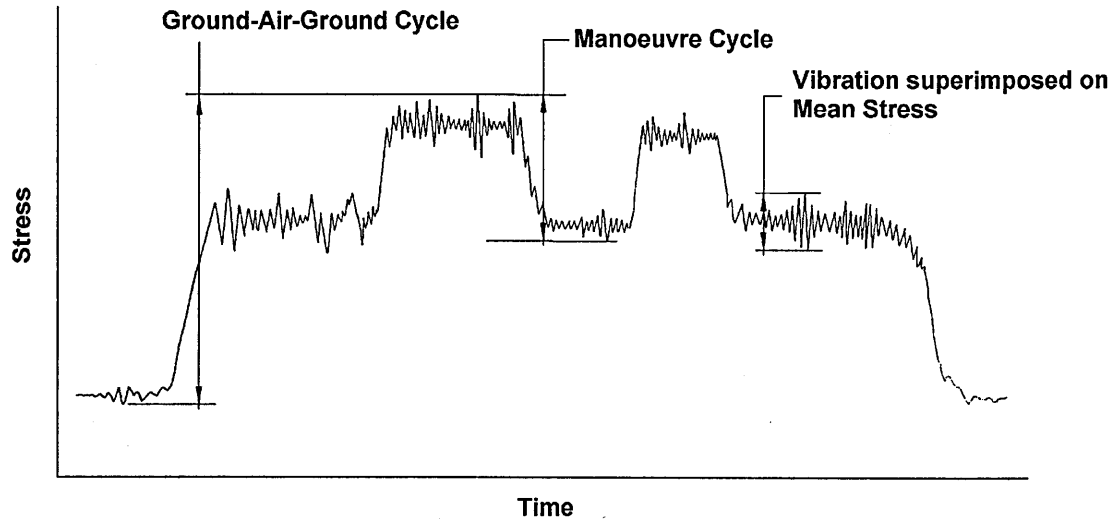

Fig. 4.41_ Representation of Stress - time data of a typical helicopter flight

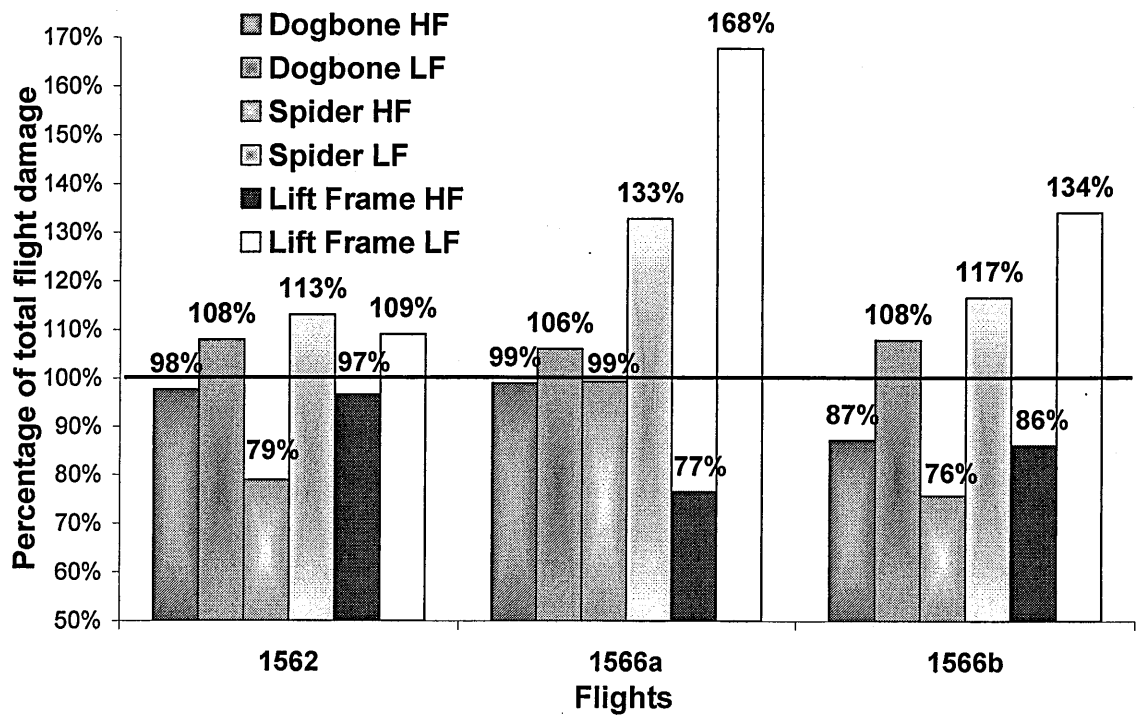

Fig. 4.42_ Damage sum of High Frequency analysis and damage sum of Low Frequency analysis against damage from entire flight (100%)

5. Probabilistic approach to fatigue substantiation of helicopter components

The Monte Carlo simulation method was employed to study the effect of variability in fatigue substantiation stages to calculated component life. The influence of usage and manoeuvre load variability on probability of component failure was modelled together with the influence of errors in Miners law and mean stress correction (Goodman). Material variability was taken into account through variability of endurance limit (S_{inf}).

5.1 Model description and parameters

For Monte Carlo simulations a program was written in C code. The program is capable to take into account the variability in four stages of the fatigue substantiation process using the results from the analysis of available data for usage and loads (see chapter 4). 26 input parameters are required before every run. Appendix F contains analytical description of all the parameters together with explanations. The four stages that are modelled in Monte Carlo simulations are: a) material properties, simulated via variability of the endurance limit following a normal distribution, b) damage calculation errors, simulated via variability of Miners damage sum (D) and Goodmans modified equation exponent (m) following normal distributions, c) usage spectrum, simulated via variability of the percentage of time associated with each manoeuvre following normal distribution, and d) loads, simulated via random pick of a manoeuvre example from the available data. Parameters that have a variability that follows a normal distribution are associated with a mean value and a coefficient of variation (CoV).

Important options in the program regarding usage and loads variability are two parameters a) intervals type and b) rate of change. These two options allow a better study of the effect of variability of usage and loads (see paragraph 5.2.1). Intervals type refers to usage and how its variability will be applied during simulation. There are three options for intervals type: 1)

fixed, here it is assumed that usage remains constant throughout the simulation, 2) per flight, here it is assumed that usage changes every flight, 3) per component, here it is assumed that usage changes every time a component reaches the failure criteria (total damage = D). The option of interval type 2 (per flight) combined with a rate of change define how often the usage is changing within the life time of a component. Rate of change for usage is effective only with option of interval type 2 (per flight). Rate of change for loads defines how often a new example of a manoeuvre loading spectrum is selected. This option leads to useful conclusions as seen in paragraph 5.2.1.

The program is explained with a flow chart in figure 5.1. Initially a usage spectrum is acquired from a text file containing the average usage as percentage time of every manoeuvre, with a COV for every manoeuvre if elected. Then the material properties, Miner and Goodman parameters are selected based on program input parameters i.e. mean values and associated COVs. Following that and based on the previous data a damage calculation is carried out for every example of every manoeuvre. This is the stage of the program where most of the running time is spent. There are several thousand cycles that need to be compared against the material S-N curve (based on input parameters, S_{inf}, and m). Depending on selected intervals type, a new set of manoeuvre intervals will be selected (usage spectrum). After that, one example from each manoeuvre will be randomly selected. Based on the previously selected parameters, the total damage will be calculated. All manoeuvres will proportionally contribute to the total damage based on the usage spectrum. If total damage is smaller than Miners criterion (D) the component will execute another flight loop (1 hour of flight) by selecting a new usage spectrum and new set of manoeuvre examples, based on interval type and rate of change parameters. If the total damage is equal or greater than Miners criterion, the component has failed and its life (hours of flight, or number of flight loops) is calculated. A new component loop will start, unless the number of failed components is adequate (for example 10,000 to 100,000 components). Results are statistically analysed and represented on a cumulative probability of failure versus life (hours of flight) plot.

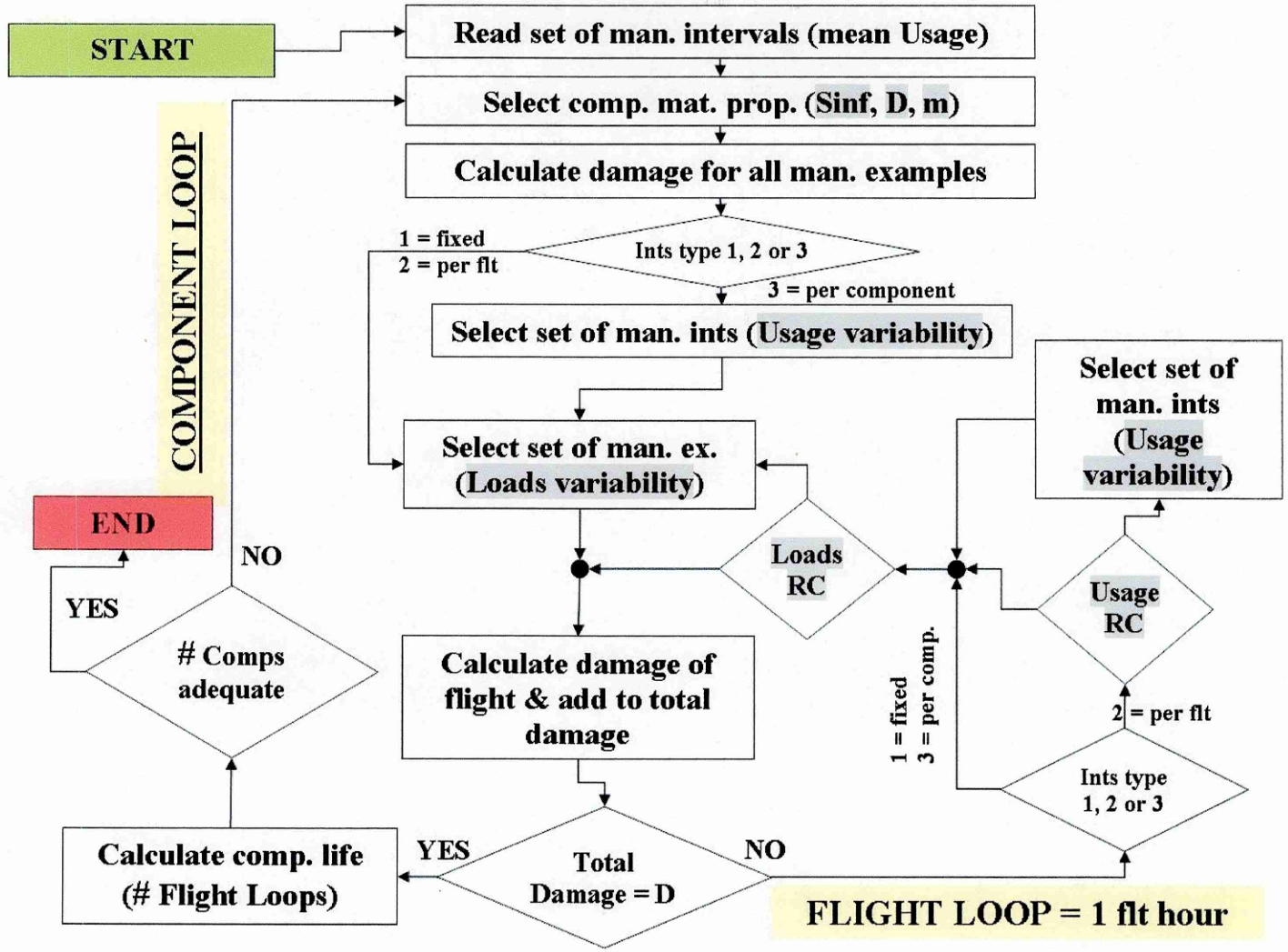

Fig. 5.1_ Flow chart of Monte Carlo program

5.2 Usage and Loads variability

Monte Carlo simulations were carried out using results from statistical analysis of data for usage and loads. Simulation results with variability of usage and loads lead to interesting conclusions regarding their averaging out effect. Also utilising the usage variability option of the Monte Carlo simulation program it was possible to study the influence of inaccuracies in a usage monitoring system applied on every aircraft. For these simulations no variability was assumed for material S_{inf}. Factored S- N curves were used to calculate a damage distribution for each manoeuvre. This was repeatedly sampled, together with the measured usage distributions found in the different service types. The damage was accumulated, until failure was predicted at a damage sum of unity. The process was repeated to yield a distribution of lives for the different usage types.

5.2.1 Averaging effect

Monte Carlo simulations have shown that when usage and loads vary frequently enough, the effect of their variability on component life is minimised. Especially when it is varied in parallel with material parameters like endurance limit, Miner criterion and Goodman parameter m.

Figure 5.2 shows the result of four Monte Carlo simulations in which usage is changed at different intervals from 1 hour to 500 hours. In this calculation the damage content for each manoeuvre was first calculated from fixed load and fixed S-N curves. The incidence of each individual manoeuvre was then allowed to vary randomly, independently of the other manoeuvres, assuming a normal distribution. Once the incidence of each manoeuvre had been fixed, damage was accumulated for defined period, and the total added to the distribution at the end of the period. Usage of each manoeuvre was then re selected and the process repeated.

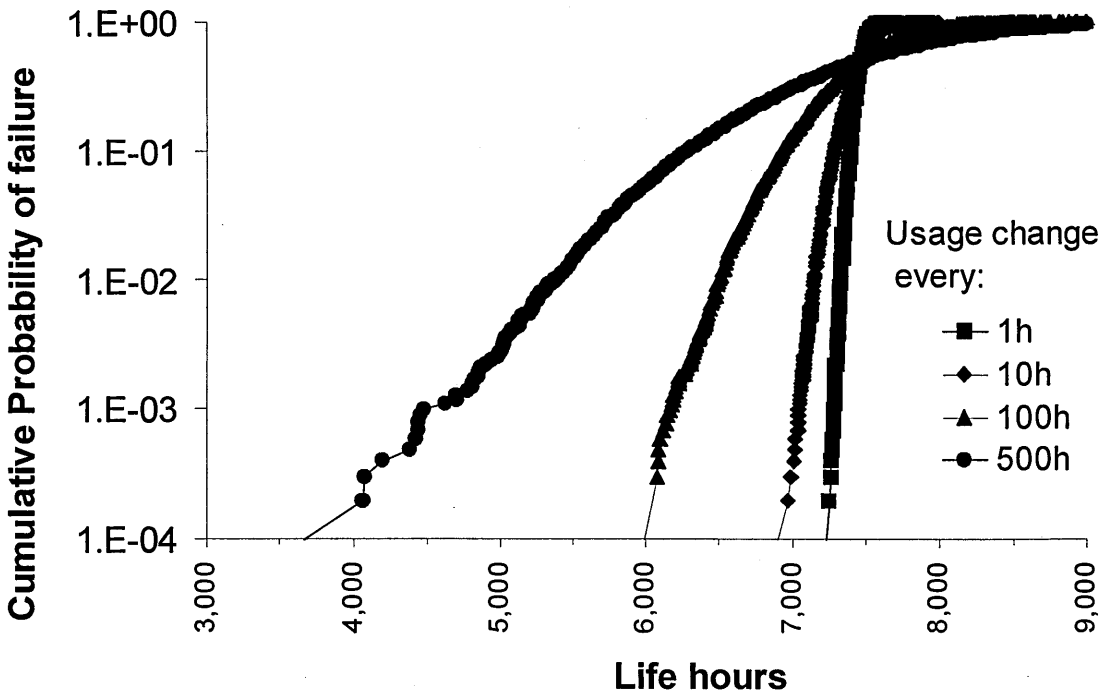

Fig. 5.2_ Effect of frequency of usage change on cumulative probability of failure. (Dogbone component fixed S/N curve with factors applied, measured usage CoV 80%)

The period of accumulation of fixed usage was varied from 1 flight hour up to 500 flight hours. This corresponds to changing helicopter usage after different periods of flight. Figure 5.2 shows that frequent changes of usage spectrum produce distributions of life with little or no variability. In contrast keeping usage fixed for extended periods result in distributions with large coefficients of variation, and a wide distribution. Figure 5.3 gives insight into the averaging effect by showing the damage against life hours for 100 components together with distribution parameters (CoV and standard deviation) of life hours. Each line in the top plots represent one component through its life from zero damage to damage equal one. The rate of change of usage is 100, 10 and 1 hour. It is seen that variability decreases with rate of change. Life curves with 100 hours rate of change have wider spread compared to 10 hours rate of change. The interpretation of the results is in close analogy with the random walk problem [61].

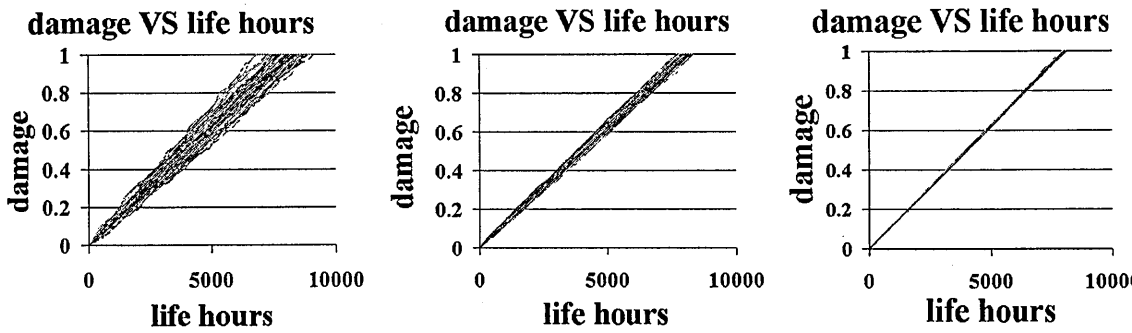

Fig. 5.3_ Effect of frequency of usage change on damage variability (Usage intervals (change) every 100h, 10h, 1h, Damage per manoeuvre held constant, Usage CoV 80%, Dogbone component)

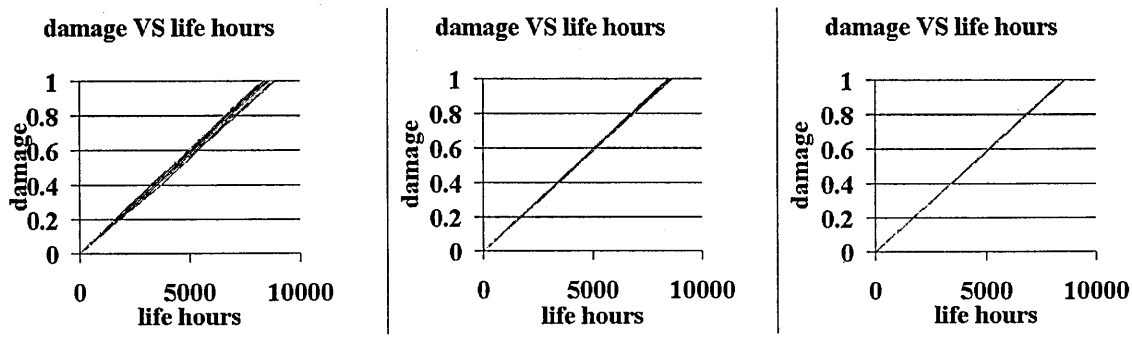

Fig. 5.4_ Effect of frequency of loads change on damage variability (Loads intervals (change) every 100h, 10h, 1h, Usage and material held constant, Dogbone component)

Figure 5.4 shows the results of similar analysis concerning loads variability. In this case variability stems from random pick of manoeuvre examples. Results show that loads variability tends towards a mean value faster that usage variability. Random pick of manoeuvre examples has little effect on life. It is not possible though to assume a mean value of manoeuvre loading for each manoeuvre when material variability is taken into account. This is because different values of S_{inf} and Goodman parameter m will lead to different damage content of each manoeuvre example. Hence loads variability should be incorporated in every Monte Carlo Simulation, except in cases were the most damaging manoeuvre example is used per manoeuvre which leads to conservative results (reduced lives).

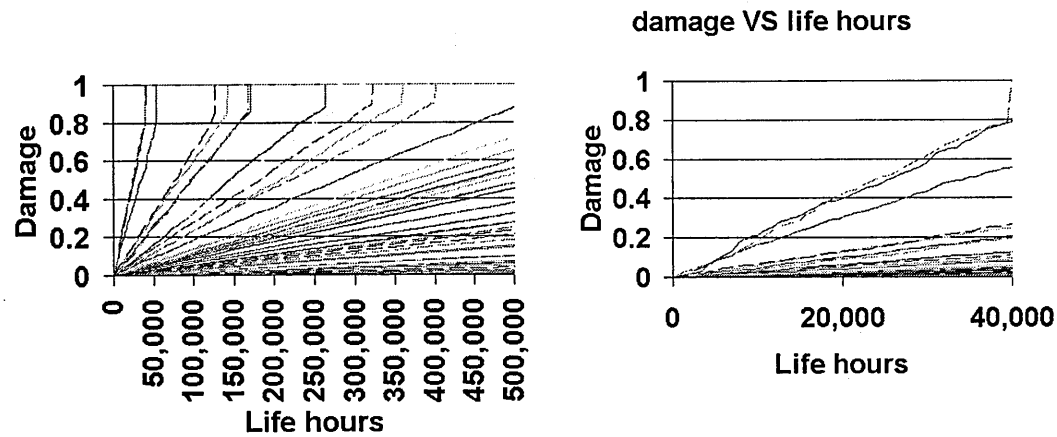

Fig. 5.5_ Varying all parameters: Strength, Miner, Goodman, Usage, Loads. (Right plot focuses in the region of up to 40,000 hours life)

Figure 5.5 shows the results of Monte Carlo simulation with all parameters varying (Material strength, Miner, Goodman, Usage and Loads). It is evident that life curves present significant variability. Most of them lead to high number of life hours, with only few leading to lives less than 50,000 hours. It should be noted that this simulation concerns only 100 components and hence the minimum life is not comparable to safe life. Actually it is associated with a one in a hundred probability of failure. Comparing this result with results in figures 5.3 and 5.4 it is evident that variability of damage curves is greater in the last case. It should be noted that this simulation was run with rate of change 100, 10 and 1 hour for usage and loads variability giving very similar results. This leads to the conclusion that usage and loads variability is not particularly significant in the presence of variability in material properties (S_{inf}), Miner and Goodman, as is also seen in figure 5.6.

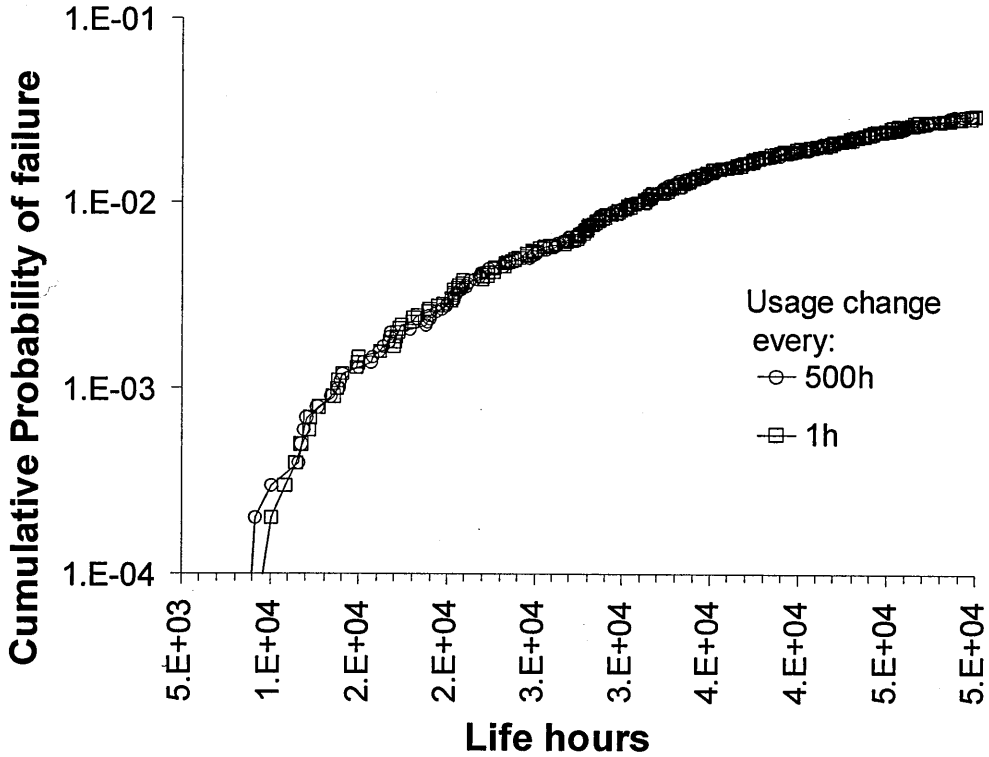

Fig. 5.6_ Effect of usage change frequency in the presence of modelling errors and variation of S-N curve for dogbone component, (endurance limit CoV 10%, Miner CoV 8.5%, Goodman CoV 5%, Measured Usage CoV 80%).

Figure 5.6 shows the results of Monte Carlo calculations where simulation of the variation of S- N curve and model errors , shown in figure 5.6, are combined with the influence of usage change at 1 hour and 500 hour intervals. The resultant curves are very similar to the curve with errors in figure 5.13, demonstrating the importance of material and modelling variability over and above variation caused by usage and loads changes.

5.2.1.1 Discussion

Monte Carlo experiments showed that there was almost no variation in component accumulated damage arising from manoeuvre damage variations. Although the scatter in damage content for each manoeuvre in the design spectrum is large (see chapter 4, paragraph 4.4), when damage is accumulated during flight, with random occurrences of individual manoeuvre damage levels, it was found that the variability in accumulated damage decreased so that within a few tens of flight hours, the variation in

accumulated damage on a component became very small. Under these conditions an almost constant mean damage value can be used to represent damage in each manoeuvre type.

This conclusion is true for random variation in manoeuvre damage alone. If an individual helicopter experiences loads which are systematically greater or smaller than a random mean, then there will result a systematic increase or decrease in the accumulated damage values. This could arise for instance from poorly maintained rotor track and balance.

The observation that manoeuvre damage variation is unimportant in determining variability in accumulated damage is largely a consequence of the relatively small damage levels associated with each manoeuvre occurrence. Damage levels for individual manoeuvres are most commonly between zero and 30 microdamage, although the larger values can attain several hundred microdamage. Even at this level, 100-1000 repeats are required to produce failure, and more typically 10^{4} -10^{5} repeats are required. This is easily sufficient for the average accumulated damage to approach a virtually constant mean level. However, persistent changes in mean load or damage level, caused by changes in rotorcraft mass, pilot technique, malfunction or misalignment of components could cause non conservative changes in accumulated damage. The extent to which this occurs is unknown and suggests that unless flight loads can be monitored using flight parameters, that some form of Operations Data Recording during the service life of the rotorcraft is desirable.

The great variability in incidence of individual manoeuvres is also under many circumstances unimportant in determining probability of failure. This is due to the same reasons as was the case for manoeuvre damage variation. The circumstances where it is important are where the usage change is infrequent, or where the period of the change is comparable to the mean life of the component. Figure 5.2 illustrated that changes in life of up to a factor of 2 were possible at a cumulative failure probability of 10^{-4} for lives between 4,000 and 8,000 hours. However, in figure 5.6 the usage changes are combined with S-N variation and model errors in a simulation where safety factors have been removed. The latter results in longer overall lives and the usage change interval of 500 hours becomes a smaller fraction of the mean life. This will have the effect of reducing the influence of usage change on overall variability.

5.2.2 Accuracy of Usage monitoring system

An investigation was carried out regarding the effect on predicted life of the accuracy of a usage monitoring system. Monte Carlo simulations were conducted to estimate this effect for three helicopter components (dogbone, spider arm, 420A lift frame). During the simulation it is assumed that inaccuracies are due to wrong recognition of manoeuvres i.e. a manoeuvre flown by the helicopter is associated with a different one by the usage monitoring system. The simulation results are presented as percentages of the life that would be calculated with the actual usage of the helicopter (average life -100%). The accuracy is expressed as percentage of manoeuvres that are correctly recognised. For example an 80% accurate system would associate 80% of the time to the correct manoeuvres the remaining 20% is randomly associated to other manoeuvres. Three levels of accuracy were assumed 90%, 80% and 70%. The results are shown in figures 5.7, 5.8 and 5.9 for dogbone, spider arm and 420A lift frame components respectively.

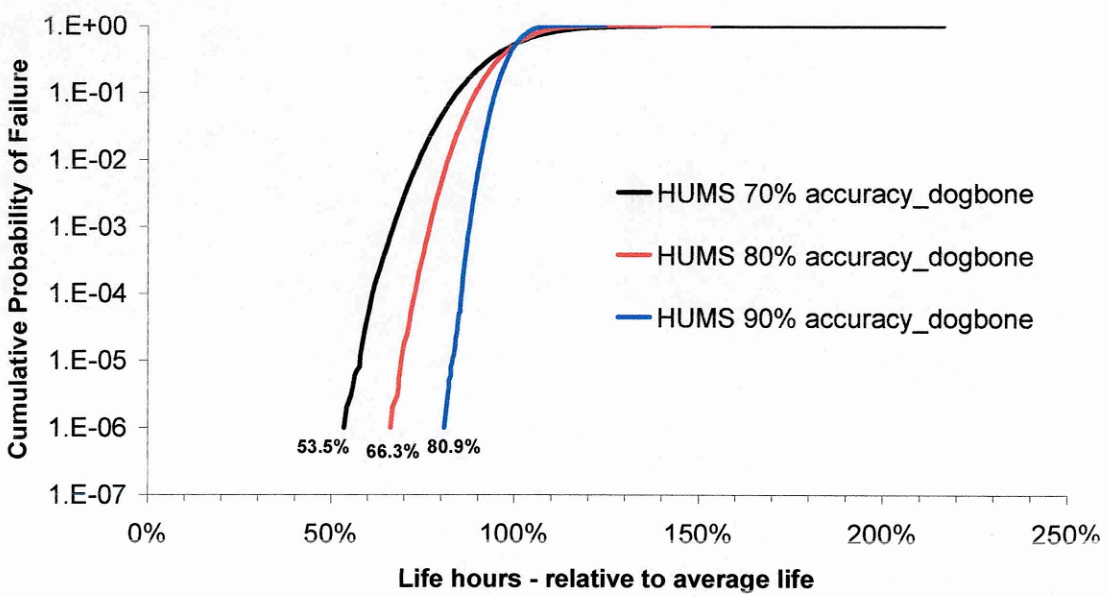

Fig. 5.7_ Effect of usage monitoring system accuracy for dogbone component

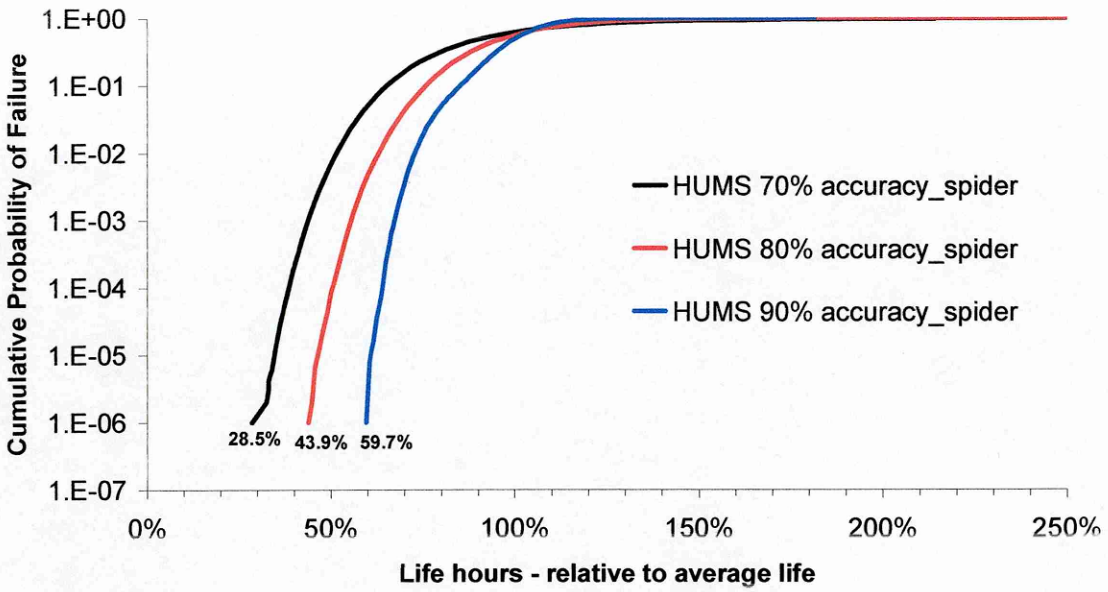

Fig. 5.8_ Effect of usage monitoring system accuracy for spider arm component

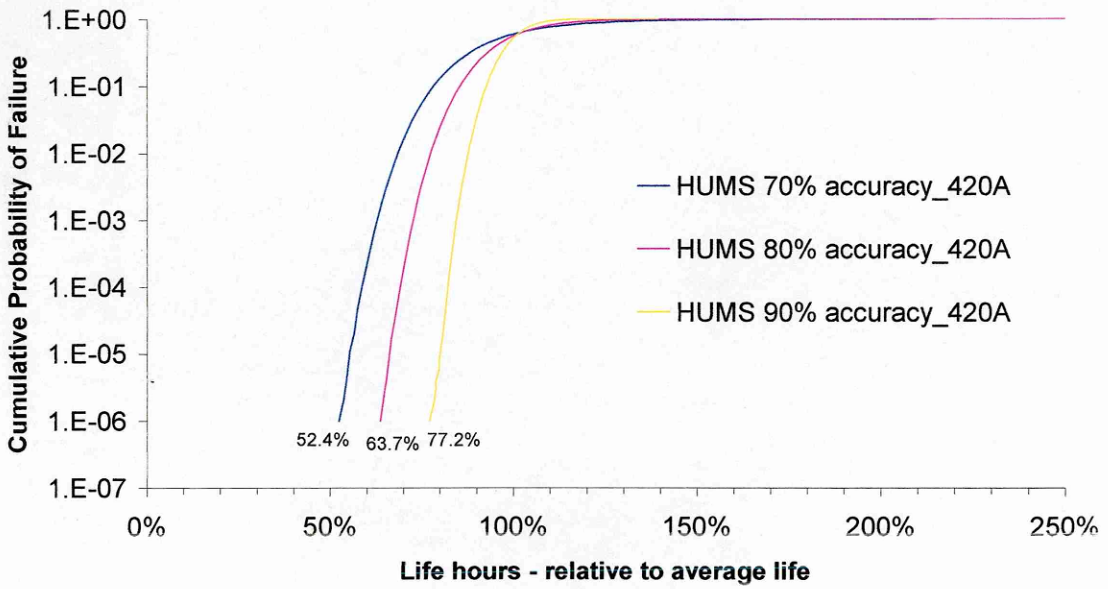

Fig. 5.9_ Effect of usage monitoring system accuracy for 420A lift frame component

It is evident that the effect of Usage Monitoring System inaccuracies is important and highly depends on the degree of inaccuracy and the component under investigation. Results show that spider arm appears most sensitive due to high variability in damage content of manoeuvres (only few are damaging [59]). Dogbone and 420A show similar behaviour. In general it is seen that 10% inaccuracy can lead to more than 20% loss in reliable fatigue life.

The fact that the non recognised manoeuvres are randomly associated with other manoeuvres may not be true for an actual usage monitoring system. In reality there will be a number of manoeuvres that are similar in terms of input parameters (speed, altitude, control positions etc). Inaccuracies would be among these manoeuvres and if the damage content of these manoeuvres is similar, then the influence on calculated life would be less important. Further analysis would require an investigation of specific usage monitoring systems to estimate their accuracy, the sources of inaccuracies and their effect to estimated component life.

5.3 Material properties variability

Monte Carlo simulations were carried out to simulate the effect of variability in material properties to calculated component life. Simulations were performed for dogbone and spider arm components made of titanium and high strength steel respectively. The 420A lift frame component had no safety factors applied to the S-N curve according to information from the design authority. It was not clear how the design authority took into account the material variability for the 420A component. Supposedly the component is subjected to periodic inspections and a combination of safe life and fail safe design is incorporated.

Variability in the S-N curve was simulated by assuming that the endurance limit (S_{inf}) varied about a normal distribution (Fig. 5.10) with a coefficient of variation of 10%. This value of COV is quoted in references [44, 46, 48] as being appropriate for these materials.

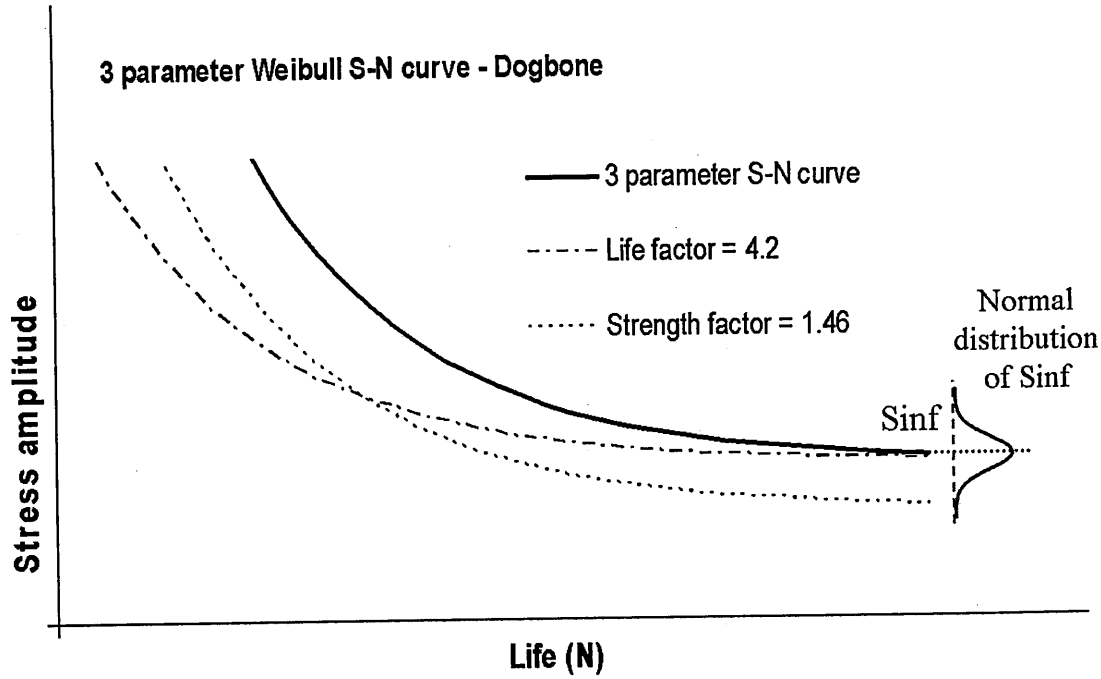

Fig. 5.10_ Representation of endurance limit variability (S_{inf}) on an S-N curve plot

Figures 5.11 and 5.12 show the results of Monte Carlo simulations with all parameters varying. Two cases were studied for each component. One case with S_{inf} CoV of 10% and one case with CoV of 8%. The second case represent the implementation of more sophisticated and expensive manufacturing methods that would lead to improved control over the component material properties (reduced strength variability). The comparison of the two cases may lead to useful conclusions regarding the investment into improved manufacturing methods. For the dogbone component there is a potential gain of 1.7 times increase in calculated life due to a decrease in S_{inf} variability from 10% CoV to 8% at the same probability of failure. For the spider arm component the potential gain is 1.3 times in calculated life. Apparently the potential gain depend on the component type and this should be taken into account during the consideration of manufacturing improvements.

It should be noted that for Spider arm the Design usage spectrum is used because the MDRE spectrum gives very little damage leading to erroneous results (damaging manoeuvres for spider arm were not recorded adequately i.e. Ctrl reversals at 0.9 VNE_ velocity)

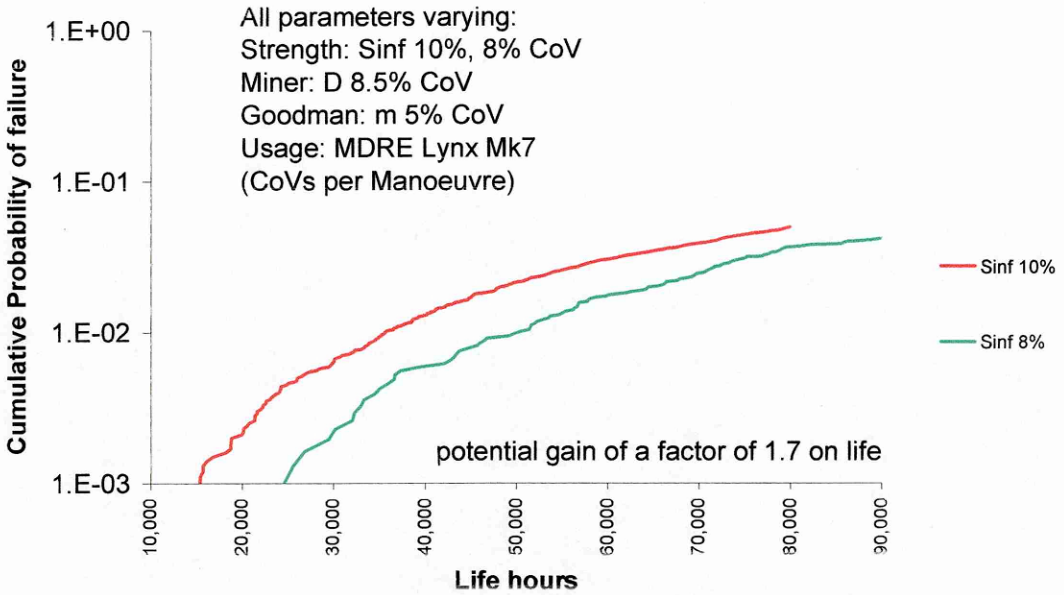

Fig. 5.11_ Effect of material endurance limit (S_{inf}) variability on cumulative probability of failure (Dogbone component)

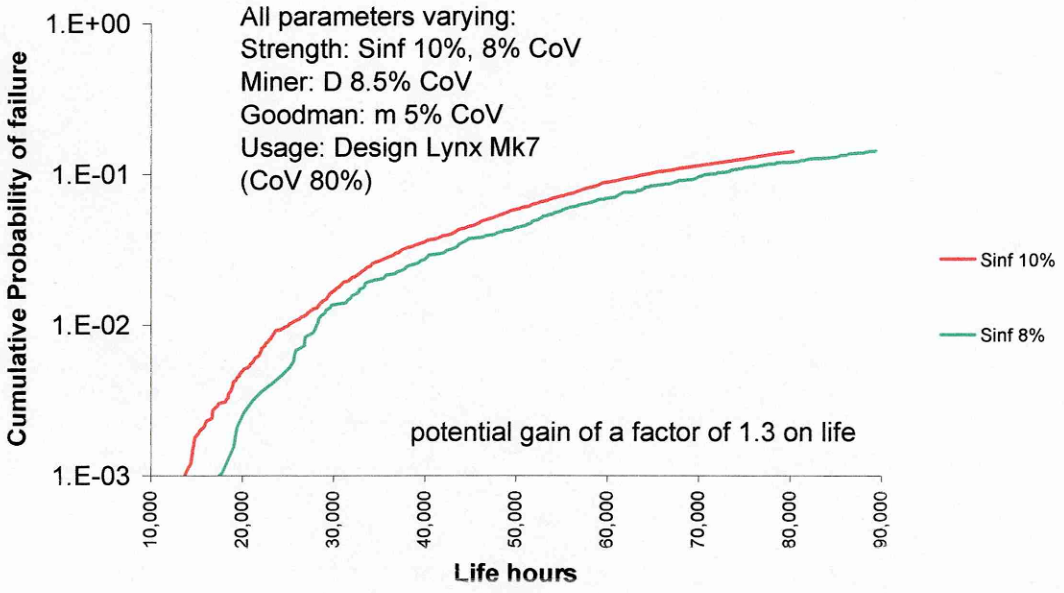

Fig. 5.12_ Effect of material endurance limit (S_{inf}) variability on cumulative probability of failure (Spider arm component)

5.4 Damage calculation tools inaccuracies

In damage calculations, the accuracy of Goodman and Miner is frequently not considered. Monte Carlo simulations were performed to study the influence of inaccuracies on the probability of failure. Error in Miner damage summation was modelled by assuming that failure could occur at a normally distributed value of damage (D), with a mean of 1 and a coefficient of variation of 8.5%. this value was selected because safety factors applied to Miners rule often assume that failure occurs at a damage sum of 0.75. Assuming that this represents 3 standard deviations on a normal distribution with a mean of unity, implies a COV of about 8.5%. Experimental evidence [7] of accuracy of Miners rule predictions tends to suggest much larger values of CoV. However, these are for widely different component materials and loading types, rather than the individual ones considered here. Goodman rule accuracy was similarly modelled, with a COV of 5% corresponding to the scatter in mean stress effects found experimentally.

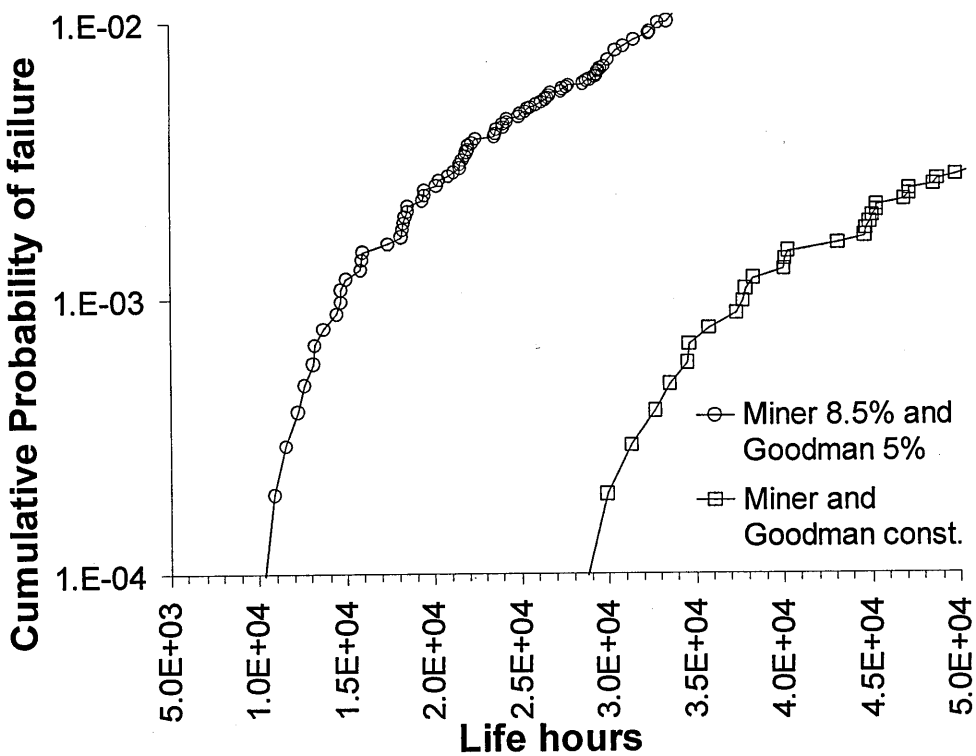

Fig. 5.13_ Effect of modelling errors on cumulative probability of failure for dogbone component. S_{inf} CoV 10%, fixed component damage and usage

Figure 5.13 shows the effect of errors in Goodman and Miner on cumulative probability of failure. In these simulations the S-N material data was allowed to vary, assuming a normal distribution of S_{inf}. Usage is fixed and load spectrum for each manoeuvre type is fixed. As noted earlier, damage variations arising from manoeuvre loads rapidly converge to an almost constant value, and similarly virtually constant values of accumulated damage are produced by rapid changes in usage type. The changes in cumulative probability of failure caused by S- N curve variation alone, are compared with the effect of adding in random errors arising from the Miner and Goodman calculation models. At a low cumulative probability of failure of 10^{-4} the addition of modelling errors reduces life by a factor of almost three.

The simulation results suggest that material S-N data together with modelling errors are the major factors influencing variability and probability of failure of rotorcraft components. In chapter four the large scatter in manoeuvre loads together with usage variability were identified. However the large scatter appears to be relatively unimportant when combined with material properties variability. Combining the experimental observations of significant errors in both Miner and Goodman seen in chapter three with simulation results, it is suggested that increased emphasis should be placed on defining the component S-N curve and its associated scatter with high confidence.

5.5 Safe life and risk of failure with application of usage monitoring system and probabilistic methodology

Usage variability has been evaluated in chapter four. Comparisons of calculated lives based on measured usage against life predicted using the design usage spectrum so that significant increases in life could have been obtained by operation of a manoeuvre based usage monitoring system.

Monte Carlo simulations allow the verification of the capability of increases in life at low probability of failure while taking into account the variability of material properties. It has been seen that measured usage gives larger lives than the design spectrum, when applying deterministic safe life calculation techniques. It is important though to estimate the risk associated with the maintenance credit claimed by the application of usage

monitoring systems. It is necessary to investigate whether or not the use of the claimed extended life would lead to an increase of the probability of failure. On the other hand, if there is a decrease of the probability of failure, it is useful to estimate the over-conservatism in the safe life calculation technique. In this case a reduction of safety factors could be suggested, which leads to concerns on persuading the Aviation Authorities about the associated risk.

Monte Carlo simulations can provide useful information for the above questions. Simulations with usage variability alone (based on measured data) could approximate the behaviour of a fleet of helicopters with usage monitoring, that experience variable usage and component life is estimated using current safe life calculation methodology. Also, simulations with variability associated to all model parameters can represent an approximation of reality or the results of the adaptation of a probabilistic methodology for calculation of component lives.

Usage monitoring on every helicopter can be simulated with usage variability per component (every helicopter is associated with a usage based on recorded usage data) with different CoV per manoeuvre based on analysis of measured data (table 4.2). Loads variability will average out as seen in paragraph 5.2.1 and is simulated via random pick of manoeuvre load spectrum example. Variability of model parameters is described in table 5.1.

Model parameter	**Variability**
Strength (S_{inf})	10% CoV
Miner (D)	8.5% CoV
Goodman (m)	5% CoV
Loads	Rate of change per 1h
Usage	Rate of change per component

Table 5.1_ Description of model parameters in Monte Carlo simulations regarding application of usage monitoring.

Figures 5.14, 5.15 and 5.16 present three cases of possible outcomes and conclusions from Monte Carlo simulations regarding application of usage monitoring and probabilistic methodology. The green line represents the application of usage monitoring on every aircraft and use of safe life calculation for damage calculation. The vertical dashed blue line represents the deterministic safe life of the component with all safety factors applied. The red line represents a probabilistic approach to life calculation where all model parameters are taken into account with their respective variability.

In case one (Fig. 5.14) the application of usage monitoring leads to non-conservative results. The apparent gain in life is associated with increased risk of failure, that can be quantitatively identified as shown on the plot.

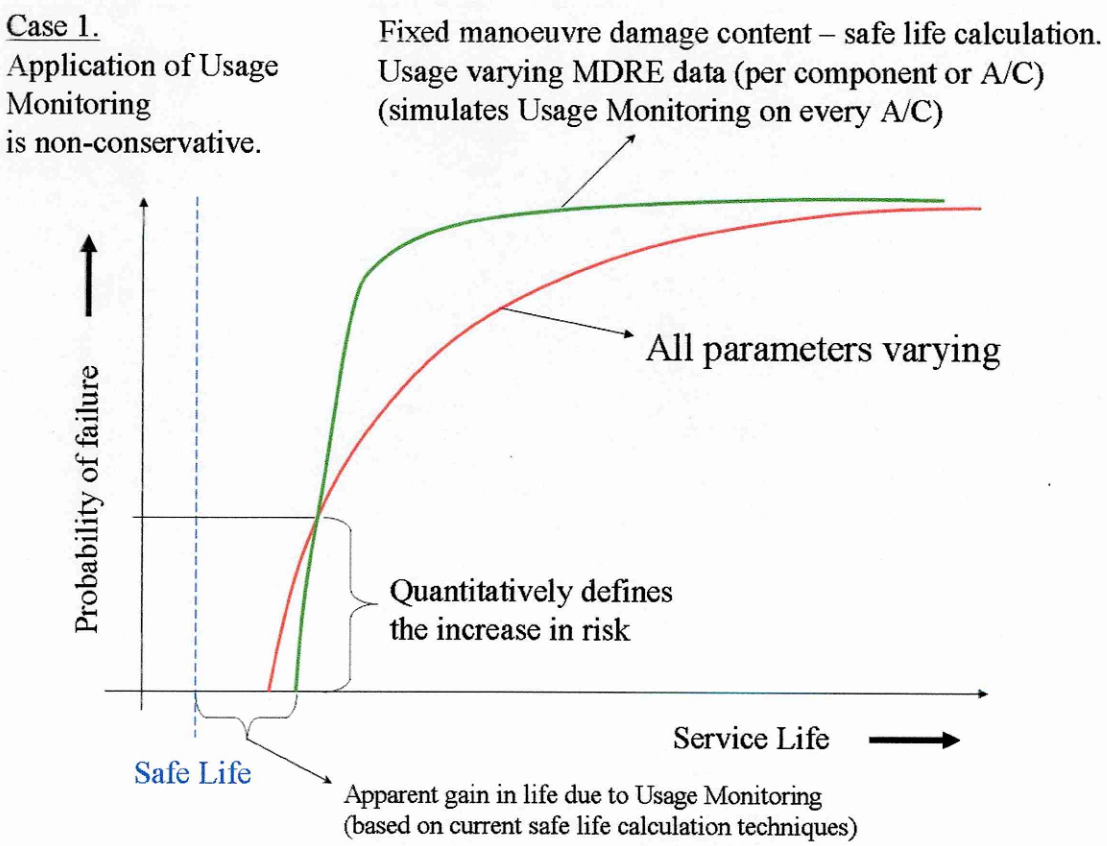

Fig. 5.14_ Case1 of possible simulation results

In second case (Fig. 5.15) the application of usage monitoring leads to maintenance credit by maintaining an acceptable probability of failure. Also it is useful to notice that there could be an additional benefit by moving towards a probabilistic fatigue substantiation methodology combined with usage monitoring. Case three (Fig. 5.16) is presenting the unlikely situation where safe life was not adequately conservative due to unexpected deviation from the design usage spectrum. In this case usage monitoring leads to safety credit that can be identified in terms of risk and in terms of service life.

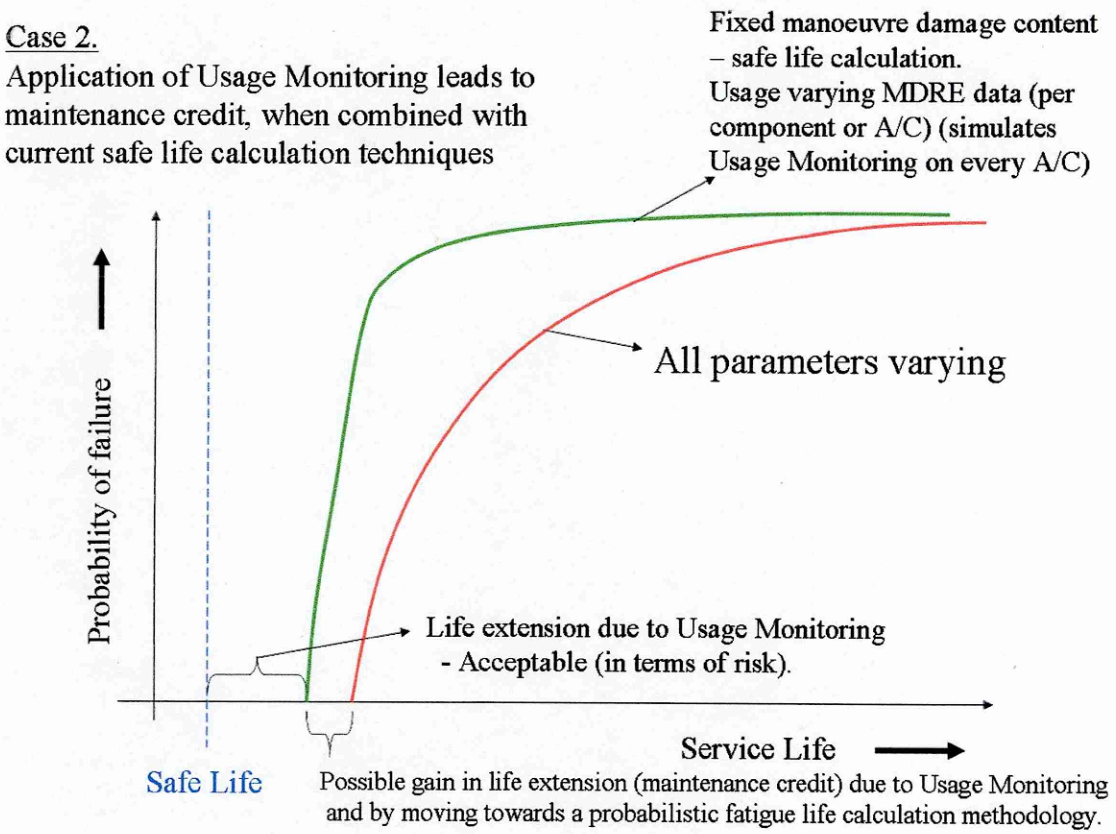

Fig. 5.15_ Case2 of possible simulation results

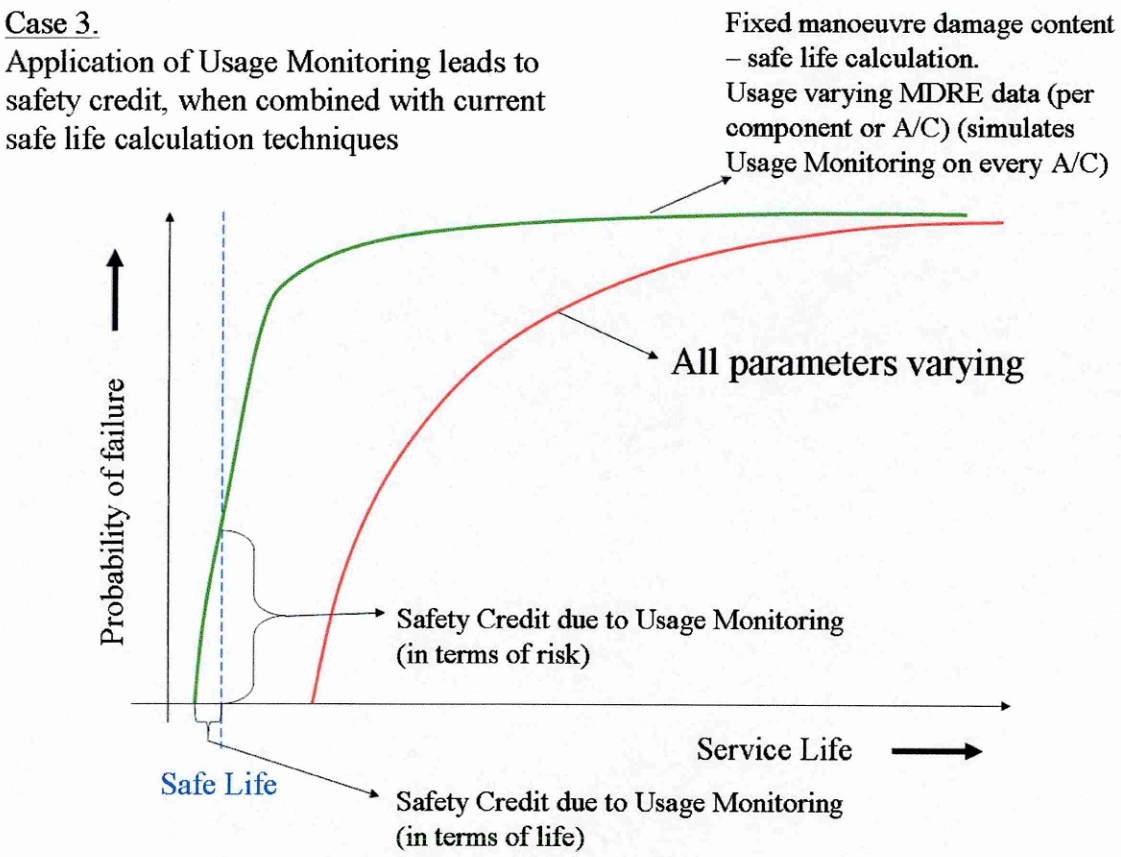

Fig. 5.16_ Case3 of possible simulation results

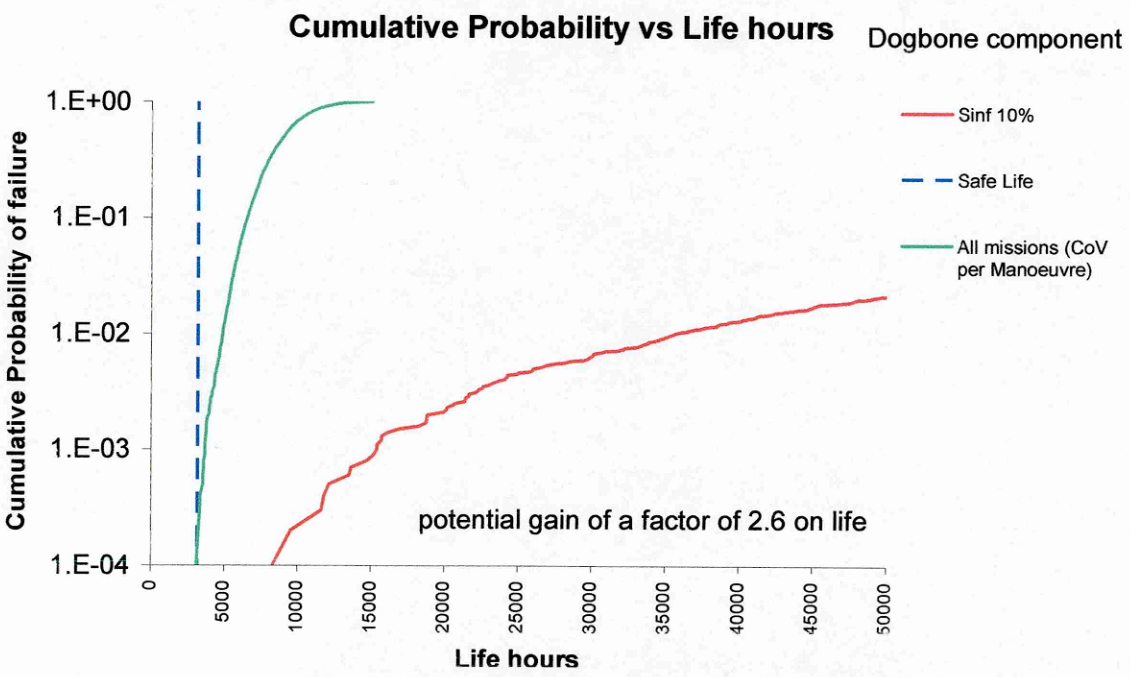

Fig. 5.17_ Simulation results for dogbone component

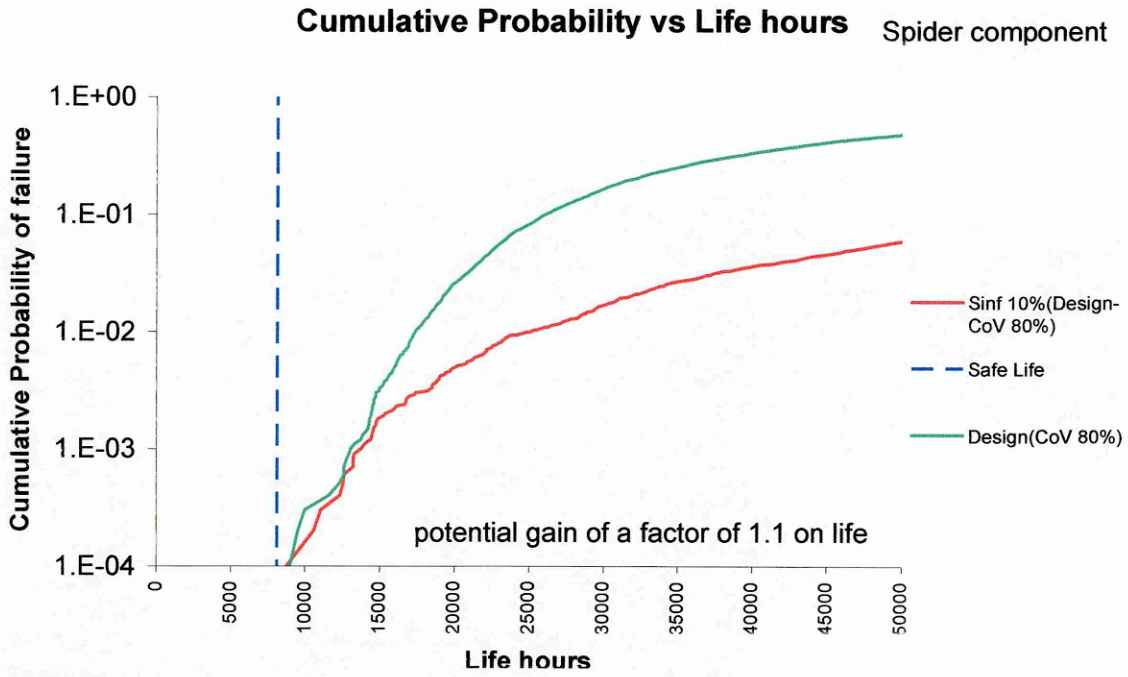

Fig. 5.18_ Simulation results for spider arm component

Figures 5.17 and 5.18 show the simulation results for the dogbone and spider arm components. Results for dogbone component (Fig. 5.17) appear to belong between cases two and three. The application of usage monitoring combined with safe calculation methodology lead to same result as the safe life methodology using design usage spectrum at a probability of failure equal to 10^{-4}. At the same probability of failure a probabilistic methodology would yield an increased life by a factor of 2.6. The design usage spectrum appears to be adequately defined for the case of the dogbone component. On the other hand the safe life methodology appears to create over conservatism when compared to the probabilistic approach.

Results for the spider arm component belong to case two where application of usage monitoring with safe life methodology leads to some life extension which is acceptable in terms of risk at 10^{-4} probability of failure. The potential benefit though appears to be limited to an increase of a factor 1.1 on life. The same potential benefit appears for the application of a probabilistic methodology. For the spider component it appears that the safe life methodology gives similar results to probabilistic methodology in contrast to the results for the dogbone component. Also the design usage

spectrum is adequately conservative to compensate for the variability of in service usage.

Both simulation results are evaluated at probability of failure of 10^{-4}. This was elected due to the extended time required to acquire results at a lower probability of failure. The simulation program needs almost a month running time for each curve. The simulation stage that consumes most of the time is the damage calculation from the manoeuvre loading spectra. This is required to be performed for every component, for all manoeuvre examples, since material properties vary per component. Several suggestions have been made about an acceptable probability of failure. The suggested values range from 10^{-9} [62] to 10^{-4} [63]. The US army requires demonstration of six nines reliability (10^{-6} probability of failure). The selection of the appropriate value as an acceptable probability of failure could be part of investigation. For the purposes of this project though, where assumptions had to be made for various stages of the model a value of 10^{-4} would be adequate. Also it should be noted that one of the main goals was to compare the contribution of usage monitoring together with methods and techniques employed for fatigue design. This comparison was performed against life hours under the same probability of failure (10^{-4}).

Among the assumptions that were made was the confidence regarding the description of the variability of the simulation parameters. The amount of data (usage and loads) was not large enough for every manoeuvre to analyse and fit confidently a Weibull distribution (see Table 4.3) with associated parameters as performed in other similar work [43]. Also the fact that the simulations were performed for different components than the one that was initially selected and had experiments performed (see section 3.1), does not add confidence to the parameters regarding the material behaviour.

Nevertheless all results presented give valuable information about the influence of every significant step in the fatigue substantiation process. It should be noted that for better simulations it is important to obtain more real data from operational helicopters.

5.6 Discussion

Monte Carlo method was used for probabilistic analysis during this project. Some limitations of the technique exist and are discussed in the literature [64], [65].Most significantly; the fact that in order to simulate very small probabilities of failure it is necessary to carry out a large number of simulations which is time consuming. It is suggested [66] that the number of simulations (runs) for a 95% confidence level in the failure probability must be three times greater than the inverse of the cumulative failure probability, whilst some authors suggest an even greater number of runs [67]. An additional disadvantage of the Monte Carlo method is its inefficient integration within the design process. For example the use of finite element analysis models would increase the necessary hardware capacity and small changes in design concept stage would require the simulations to be performed repeatedly. Alternative techniques to Monte Carlo exist (direct analytical integration, propagation of errors, g-function methods etc), but a study of them was not feasible within the scope of this research.

In Monte Carlo simulations there are two options regarding usage variability. First, usage variability per component means that the usage spectrum is selected only once at the beginning of the component life, and remains the same until failure. Secondly, usage variability per hour or multiple of hours means that a new usage spectrum is selected many times within the life period. The first case is representing a fleet and the second case is representing one aircraft. In the second case the aircraft will vary its usage many times within its life span, which will lead to the averaging out effect as has been seen in section 5.2.1. It is necessary to note here that an aircraft by aircraft analysis of the usage data is appropriate for fleet simulation and a sortie by sortie analysis is appropriate for single aircraft simulation. An analysis of the data on an aircraft by aircraft basis would reduce the variability (averaging out effect), since the average length of a period recording aircraft usage would be a lot longer than the length of one flight (average 1-2 hours). For the current investigation it was not possible to perform this type of analysis because the available usage data came from very few aircraft.

In Monte Carlo simulations every variable is supposed to be independent from each other. This is a matter of discussion for material properties (endurance limit S_{inf}, Miner sum D and Goodman parameter m). On the other hand usage and loads variability are independent, since they are two different procedures that are combined only during the life calculation process. It should be noted though that in the case of a monitoring system that extrapolates loads based on usage monitoring this would not be the case. During this project it is supposed that loads are measured accurately and independently from usage. The three material parameters used in the simulations are part of the methodology that attempts to describe and predict the material behaviour under various loading conditions. The S-N curve is the main tool which is expanded to a three dimension plot (Stress amplitude-N life cycles – Stress mean) with the introduction of Goodman equation. The approach adopted for the project and the current methodology of the helicopter industry is based on macroscopic observations (life cycles at failure) and attempts to fit equations to the observed data and methods to combine the available data. Hence, it is not possible to understand the material mechanisms that lead to the observation and consequently acquire a better knowledge of the interactions and dependencies of the parameters that are currently used. This would involve a more sophisticated approach to the fatigue problem with models based on micro- or nano- scale observations that use advanced theories to describe and predict the stochastic behaviour of the material.

Uncertainty in the variability of different parameters impacts the Monte Carlo simulations. For example, the tail sensitivity problem is a well-known problem in reliability analysis since the very beginning. As indicated by Mathew and Neal [48] the estimates of the extreme tail quartiles and their corresponding reliabilities can be unstable unless large data sets are used. This is the justification for accurately fitting the tail of the data sample by appropriately using a Normal or Weibull distribution. Using data from Table 4.3 in a Monte Carlo simulation for dogbone component where the only parameters varying were the usage of manoeuvres fitted using Normal and Weibull distributions (see section 4.1.1). Figure 5.19 show the influence of distribution type to component life. Variability of usage is per component. At low probability of failure (10^{-4}) there is a 30% difference on life, Fitted Normal distribution with wider tail characteristics (see figures 4.2 - 4.9), contributes to more variability, hence lower life.

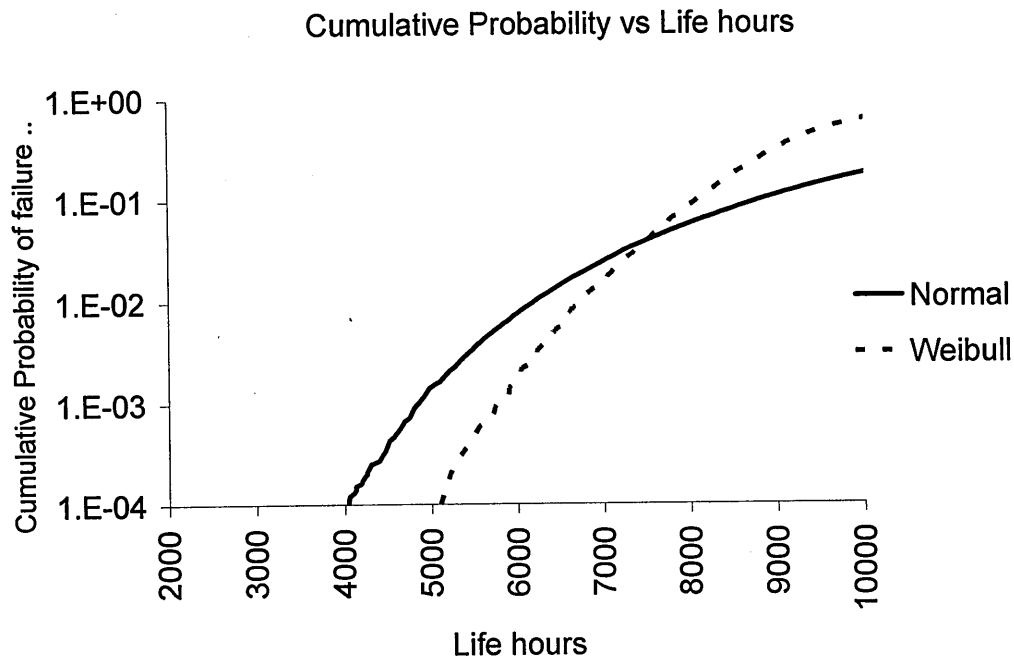

Fig. 5.19_ Simulation results (dogbone component) using different distribution types for usage variability

The reliability of input data is one important aspect of structural risk and reliability analysis. The collection of representative data and accumulation of practical data is a valuable asset for risk and reliability assessment. The fact that reliability assessment deals with relatively rare events and working with such small probabilities, a large number of data or the accurate estimation of the population is highly necessary for accurate prediction. The exact reliability would require the true population to be known, which it could require some sampling of a million specimens or by pooling tens of thousands groups of data. Of course, this is impossible in term of practicality, cost and availability of data. However, it should be keep in mind that statistical and probabilistic theories are implemented and employed for approximating the true population in the best suitable manner using limited amount of data and small sampling, rather than for determining the exact distribution of the population. This indicates that uncertainty exists even in reliability analysis such as performed here, and it is the analysts' duty to approximate the population in the best possible manner.

6. Conclusions and recommendations for future work

6.1 Conclusions

This research has investigated factors contributing to safe life and fatigue usage damage calculations. Comprehensive investigations have been made into errors and uncertainties in the safe fatigue life calculation process, particularly those associated with Miners summation and mean stress corrections. This has been supplemented by extensive studies of loads and usage (manoeuvre) variability throughout service operation on three components in a military helicopter.

It has been identified through experiments and damage calculations that omission of small range cycles during experimental fatigue testing is non-conservative due to Miners rule inadequacy. At the same time Goodmans mean stress correction appears conservative enough to lead to reasonable results when combined with Miners rule for the specific material under investigation.

Extensive statistical analysis of available usage and loads data was performed. The calculated distributions of service lives were compared with lives from an average usage for all mission types, and also with the distribution predicted for the design usage spectrum. Variability is significant and application of usage monitoring systems may lead to maintenance credit of a factor of two on life depending on component and usage profile.

Monte Carlo simulations demonstrate that damage population variability is dominated by the coefficient of variation of the S- N curve and by errors in damage calculation models (Miner, Goodman). Effects of loads and usage variability is of a different order to that of S-N data scatter due to cumulative averaging effect of usage variation- S-N data effects are not subject to this effect. Measured variability in manoeuvre load spectra and in manoeuvre usage contribute little under most circumstances.

The risk associated with the application of Usage Monitoring and possible credits (safety or maintenance) can be predicted by Monte Carlo simulations.

Reduction of material properties variability may lead to life benefits, that are component dependant.

Errors in usage monitoring system has a large effect on failure probabilities, working within a constant S-N curve.

The risk associated with the application of usage monitoring systems has been identified and is in principle calculable.

6.2 Recommendations for future work

Use of Crack Growth life calculation method and compare with Stress-Life technique under helicopter variable spectrum loading.

Use of Bayesian updating method to improve initial assumptions during design (assumed usage and associated variability) by analysing HUMS data as they arrive.

Experimental study using actual components experiencing realistic multi axial loading conditions.

Investigation of the increasing failure probability associated with increasing incidence of corrosion and mechanical damage.

REFERENCES

1. Arden R. W., *"Hypothetical fatigue life problems"*, Midwest region, Helicopter fatigue methodology specialists meeting, American Helicopter Society, St Louis, MO, Mar 1980

2. AGARD, *"Helicopter fatigue design guide"*, NATO, Advisory group for aerospace research and development, AGARDograph AGARD-AG-292, Nov 1983

3. Och F., *"Fatigue strength"*, Helicopter fatigue design guide, AGARD-AG-292, NATO, AGARD, pp 109-131, 1983

4. Liard F, *"Fatigue of helicopters - service life evaluation methods"*, Advisory group for aerospace research and development, NATO, AGARD report No. 674, pp 54-69, Feb 1978

5. Wolfe R. A., Arden R. W., *"U.S. army helicopter fatigue requirements and substantiation procedures"*, Advisory group for aerospace research and development, NATO, AGARD report No. 674, pp 1-12, Feb 1978

6. Miner M. A., *"Cumulative damage in fatigue"*, Journal of Applied Mechanics, 67, A159-A164, 1945

7. Shütz W. and Heuler P., *"Miner's rule revisited"*, AGARD meeting, 1993

8. Vormwald M. and Seeger T., *"Consideration of fatigue damage below the endurance limit in life predictions for variable amplitude loading"*, Fatigue 90; Proc 4th Intl Conf on Fatigue and Fatigue Thresholds, Materials & Component Eng Pub, Honolulu, Vol. 1, p. 517-522, Jul 1990

9. Fatemi A., Yang L., *"Cumulative fatigue damage and life prediction theories: asurvey of the state of the art for homogeneous materials"*, Int. J. Fatigue, 20, pp. 9-34, 1998

10. Schott G., Donat B. and Schapter M., *"The consecutive Wöhler curve approach to damage accumulation"*, Fatigue & Fracture of Engineering Materials & Structures, 19, pp. 373 385, 1996

11. Halford Gary R., *"Cumulative fatigue damage modeling-crack nucleation and early growth"*, Int. J. of Fatigue, 19, pp. S253 S260, 1997

12. Manson S. S. and Halford G. R., *"Re-examination of cumulative damage analysis an engineering perspective"*, Engineering fracture Mechanics, 25(5/6), p 539-571, 1986

13. Manson S. S. and Halford G. R., *"Practical implementation of the double linear damage rule and damage curve approach for treating cumulative fatigue damage"*, International Journal of Fracture, 17(2), p 169-192, 1981

14. Haibach E., *"Betriebfestichkeit"*, VDI-Verlag, Düsseldorf, 1989

15. Henry D. L., *"Theory of fatigue damage accumulation in steel"*, ASME Transactions, 77, 913, 1955

16. Corten H. T. and Dolan T. J., *"Cumulative fatigue damage"*, Proceedings of International Conference on fatigue of Metals, ASME and IME, 235ff, 1956

17. Franke L., Dierkes G., *"A non-linear fatigue damage rule with an exponent based on a crack growth boundary condition"*, Int. J. of Fatigue, 21, pp. 761 767, 1999

18. Cheng G. and Plumtree A., *"A fatigue damage accumulation model based on continuum damage mechanics and ductility exhaustion"*, Int. J. Fatigue, 20, pp. 495 501, 1998

19. Tchankov D. S., Vesselinov K. V., *"Fatigue life prediction under random loading using total hysteresis energy"*, Int. J. Pres. Vess. & Piping, 75, pp. 955 960, 1998

20. Chaudonneret M. and Robert M., *"Fatigue lifetime prediction methods: an analysis of the different approximations involved in local approaches"*, Int. J. Pres. Ves. & Piping, 66, pp. 113 123, 1996

21. Noback R., *"State of the art and statistical aspects of helicopter fatigue substantiation procedures"*, 51st meeting of the AGARD structures and materials panel, Aix-en-Provence, AGARD-CP-297:Helicopter fatigue life assessment, Sep 1980

22. Grover H. J., *"Fatigue of aircraft structures"*, Government printing office, Washington, D.C., 1966

23. ESDU, *"Fatigue limit of un-notched steels (Related to tensile strength)"*, 88008, pp 6-41, Jul 1988

24. Hung-Kuk Oh, *"A note on the effect of the mean stress in a new fatigue theory"*, Journal of Materials Processing Technology , 54, p 362-364, 1995

25. ASTM, *"Standard Practices for Cycle Counting in Fatigue Analysis"*, Metals, Mechanical Testing, Annual Book of ASTM Standards, Sect 3 Vol 03-01, E1049-85, 2001

26. Suresh S., *"Fatigue of materials"*, second edition, Cambridge University Press, 1998

27. Fuchs H. O. Stephens R. I., *"Metal Fatigue in Engineering"*, Wiley Interscience, 1980

28. Osgood C. C., *"Fatigue design"*, Pergamon Press, Oxford, 1982

29. Neuber H., *"Kerbspannungslehre"*, Springer Verlag, Berlin, 1958

30. Junivall R. C., *"Stress strain and strength"*, McGraw Hill, New York, 1967

31. Cavallini G., Lanciotti A., Aldinio G., and Rovellotti R. *"Fatigue behaviour of helicopter dynamic components under constant amplitude and spectrum loading"*, Helicopter fatigue life assessment, AGARD CP 297, 1981

32. Hill K., Hudson R.A., Irving P.E., and Vella A.D, *"Loading spectra, usage monitoring and prediction of fatigue damage in helicopters"*, Estimation, enhancement and control of aircraft fatigue performance, p 531-551, May 1995

33. Holford D. M., *"Operational load measurements on service helicopters"*, 69th Symposium of the AGARD flight mechanics panel, AGARD, NATO, Amsterdam, Netherlands, Oct 1986

34. Kennedy J. B., Neville A. M., *"Statistical methods for engineers and scientists"*, 1986

35. Weibull W., *"A statistical theory of the strength of materials"*, Proceedings 151, Royal Swedish Academy of Engineering Sciences, Stockholm, 1939

36. Metcalf A. V., *"Statistics in engineering"*, Chapman and Hall, London, 1994

37. Veers P. S., *"Statistical considerations in fatigue and fracture"*, ASM Handbook, Materials Park, Vol. 19, pp. 295-302, 1996

38. Viswanathan S.P., Tata V., Boorla R., McLeod G., and Slack J., *"A statistical analysis to assess the reliability of a rotorcraft component in fatigue"*, 43rd annual national forum and technology display of the American Helicopter Society, St. Louis, MO, USA, May 1987

39. Fishman G.S., *"Monte Carlo: Concepts, algorithms and applications"*, Springer, 1995

40. Carter A. D., *"Mechanical reliability and design"*, Macmillan, 1997

41. Irving P.E., Hudson R.A., *"The contribution of health and usage monitoring systems to calculations of damage state and future life of helicopter components under safe life and damage tolerant designs"*, RTO AVT specialists' meeting on "Exploitation of structural loads/health data for reduced life cycle costs", RTO MP-7, Brussels, Belgium, p 7-1 7-11, May 1998

42. Zhang J., Kececioglou D., *"Fatigue life prediction under random loading using distributional stress life relationship"*, American institute of aeronautics and astronautics, St Louis, Apr 1999

43. Moon Suresh, Menon Dinesh, and Barndt Gene, *"Fatigue life reliability based on measured usage, flight loads and fatigue strength variations"*, 52nd annual forum of the American Helicopter Society, Washington, p 366-389, Jun 1996

44. Thompson A.E. and Adams D.O., *"A computational method for the determination of structural reliability of helicopter dynamic components"*, 46th annual forum of the American Helicopter Society, Washington, D.C., USA, p 859-873, May 1990

45. Boorla Raghupati and Rotenberger Kevin, *"Load variability of a two-bladed helicopter"*, Journal of the American Helicopter Society, p 15-26, Jan 1997

46. Zion Lewis H., *"Safe life reliability: Evaluation of new statistical methods"*, 47th annual forum of the American Helicopter Society, Phoenix, AZ, USA, p 257-272, May 1991

47. Harris W.D., Larchuck T., Zanoni E., and Zion L., *"Application of probabilistic methodology in the development of retirement lives of critical dynamic components in rotorcraft"*, 55th annual forum of the American Helicopter Society, Montreal, Canada, p 1254-1267, May 1999

48. Neal D.M., Matthews W.T., Vangel M.G., and Rudalevige T., *"A sensitivity analysis on component reliability from fatigue life computations"*, U.S. army materials technology laboratory, Technical Report MTL TR 92-5, Feb 1992

49. Sikorsky engineering report, *"Fatigue substantiation of the S-61L/N main rotor head, design report"*, SER-611464, Unpublished, 1980

50. Sikorsky Aircraft, *"Fatigue substantiation of the CH/HH-3C/E main rotor hub plates"*, Report No. SER-611625, Unpublished, 1980

51. Juvinall Robert C., *"Fundamentals of machine component design"*, 3rd ed., New York: Wiley, 2000

52. Prieur P., *"Reliability of underwater inspection: a computer simulation"*, Cranfield University, MSc Thesis, Sep 1986

53. Buller R.G., *"A standardised fatigue loading sequence for helicopter main rotorhead structures (Rotorix)"*, Cranfield University, DTI link project, CU/927N/27, Aug 1996

54. Edwards, P. R. and Darts, J., *"Standardised fatigue loading sequences for helicopter rotors (Helix and Felix), Part 1: Background and fatigue evaluation"*, Royal Aircraft Establishment, Technical report 84084, Aug 1984

55. Edwards, P. R. and Darts, J., *"Standardised fatigue loading sequences for helicopter rotors (Helix and Felix), Part 2: Final definition of Helix and Felix"*, Royal Aircraft Establishment, Technical report 84085, Aug 1984

56. Schijve J., *"Fatigue of structures and materials"*, Kluwer Academic Publishers, Dordrecht, 2001

57. Fitzwilliams O. and Hill D., *"Strength and fatigue substantiation of helicopters"*, Loading actions sub-committee, Aeronautical Research Council, Nov 1963

58. Irving P.E. and Hudson R.A., *"Cost-benefit analysis of Fatigue Usage Monitoring Systems (FUMS) fatigue analysis of Lynx dogbone and spider components."*, Report No. MoD/WQ9610V/38, Apr 1998

59. Irving P.E. and Hudson R.A., *"Fatigue analysis of Westland Lynx hellicopter spider component."*, Report No. MoD/WQ9620N/50, Mar 2001

60. Irving P.E., Strutt J.E., Hudson R.A., Allsop K., and Strathern M., *"The contribution of fatigue usage monitoring systems to life extension in safe life and damage tolerant designs"*, CEAS forum on life extension, Royal Aeronautical Society, Cambridge, UK, Mar 1999

61. Papoulis A., *"Probability, random variables and stochastic processes"*, McGraw Hill international editions, second edition, p.212, 1984

62. Lunberg, *"Notes on the level of safety and the repair rates with regard to fatigue"*, The Aeronautical Research Institute of Sweden, Stockholm, FAA/M/PE-15, 1962

63. Osgood, C. C., *"Fatigue design"*, Pergamon Press, Oxford, p.131, example.3, 1982

64. Ebbeler D. H. et al, *"Alternative computational approaches for probabilistic fatigue analysis"*, American Institute of Aeronautics and Astronautics, New Orleans, Apr 1995

65. Chee Tong Yu, *"Literature review on aircraft structural risk and reliability analysis"*, DSTO Aeronautical and Maritime Research Laboratory group for aerospace research and development, Melbourne, Australia, DSTO-TR-1110, Feb 2001

66. Melchers R.E., *"Structural reliability analysis and prediction"*, second edition, John Wiley and Sons Ltd, Chichester, 1999

67. Provan J.W., *"Probabilistic fracture mechanics and reliability"*, Martinus Nijhoff Publishers, Dordrecht, 1987

APPENDICES

Appendix A _ Specimens and test grip assembly drawings

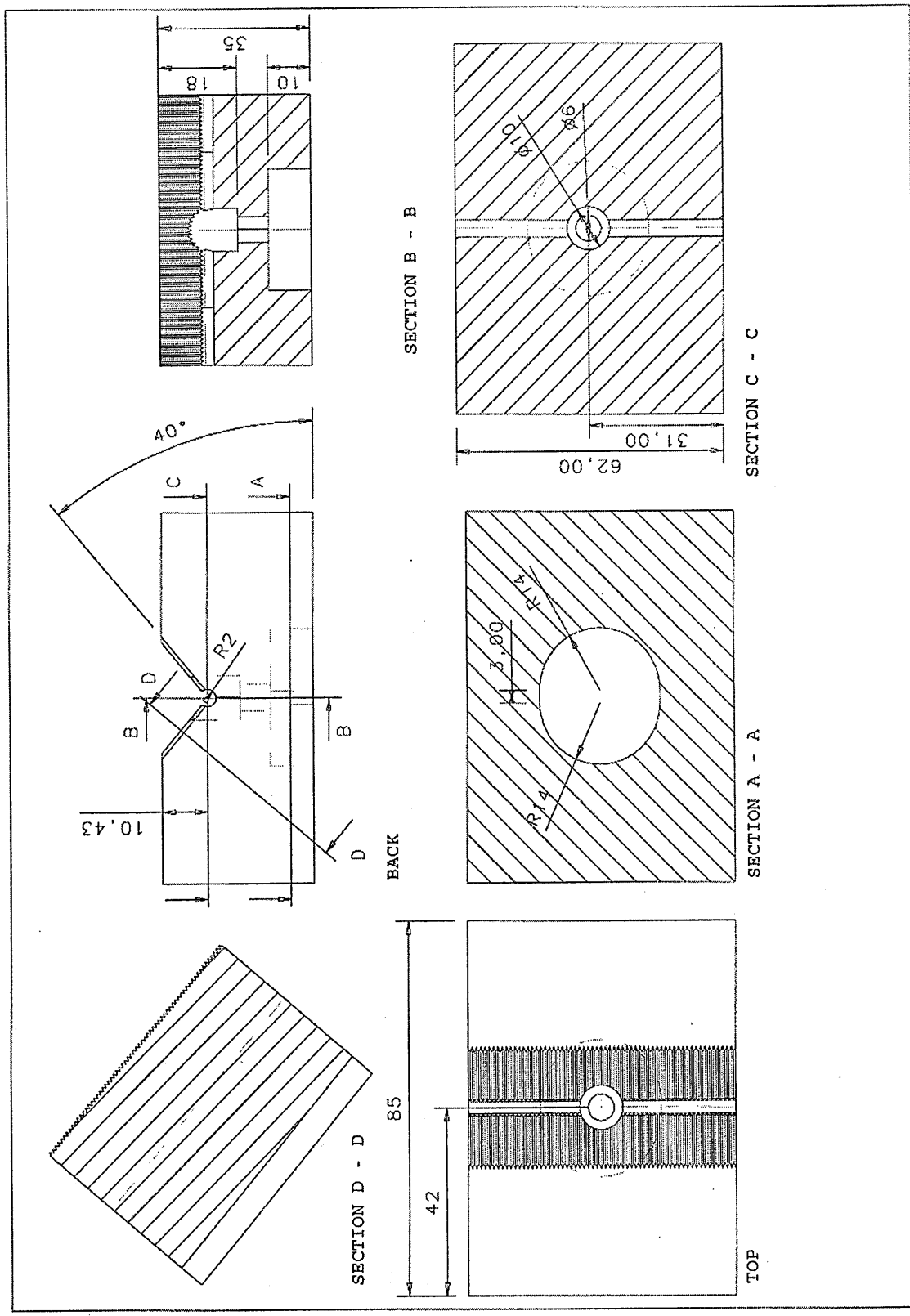

Fig.A1 Modified version of existing grips (V notch)

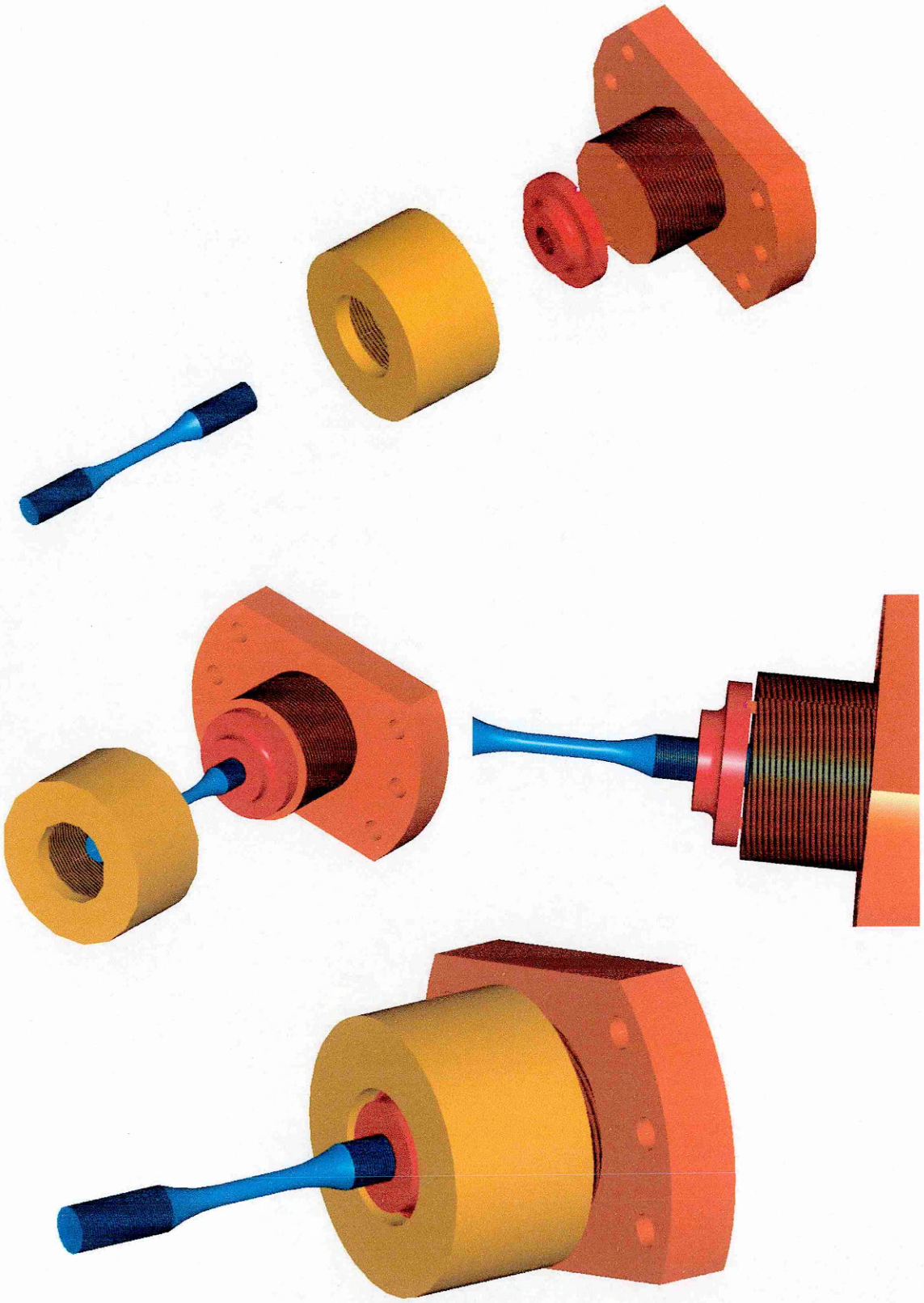

Fig.A2 3D model of designed grips assembly

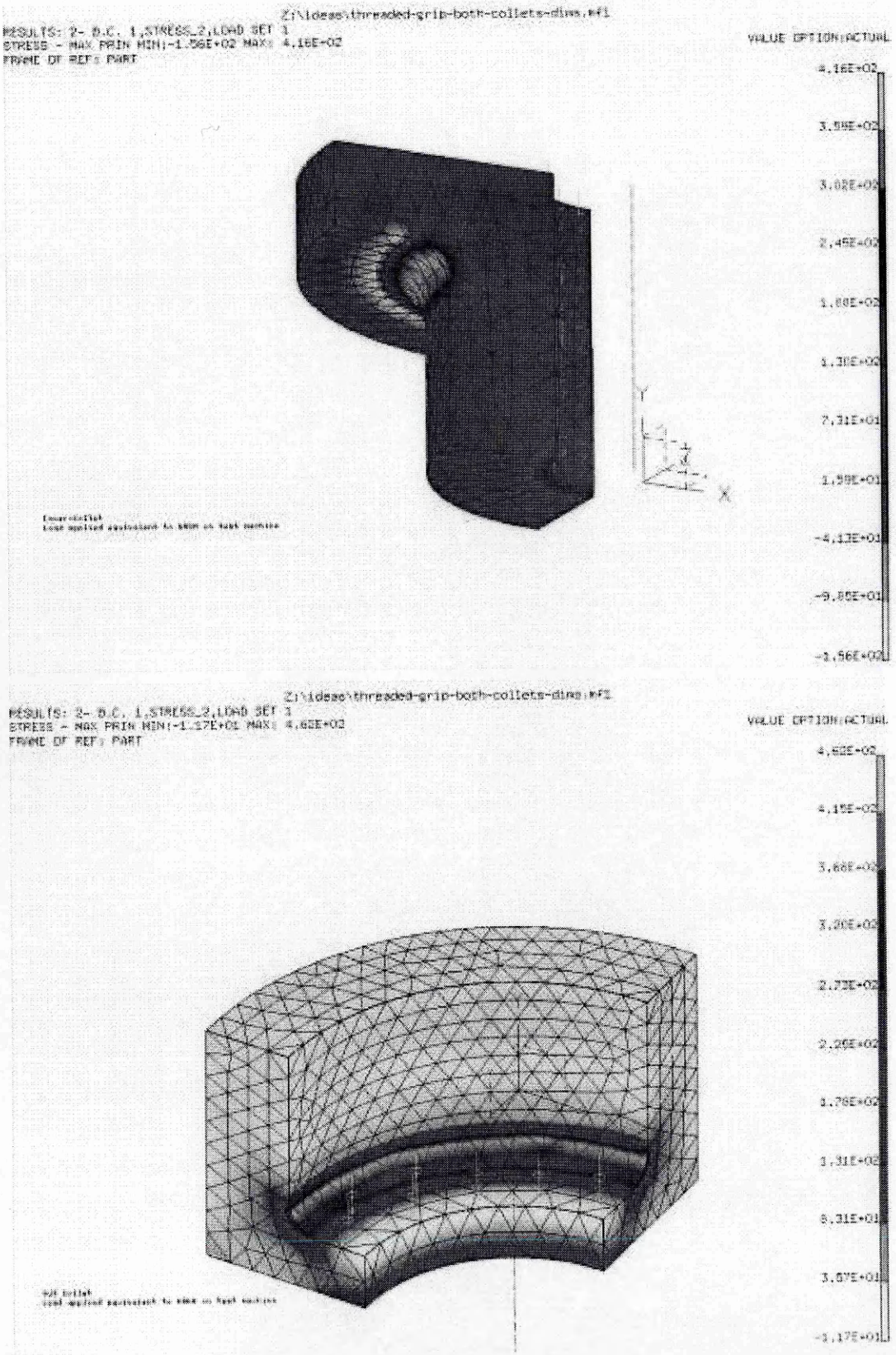

Fig.A3 Finite Element Analysis of inner and outer collet

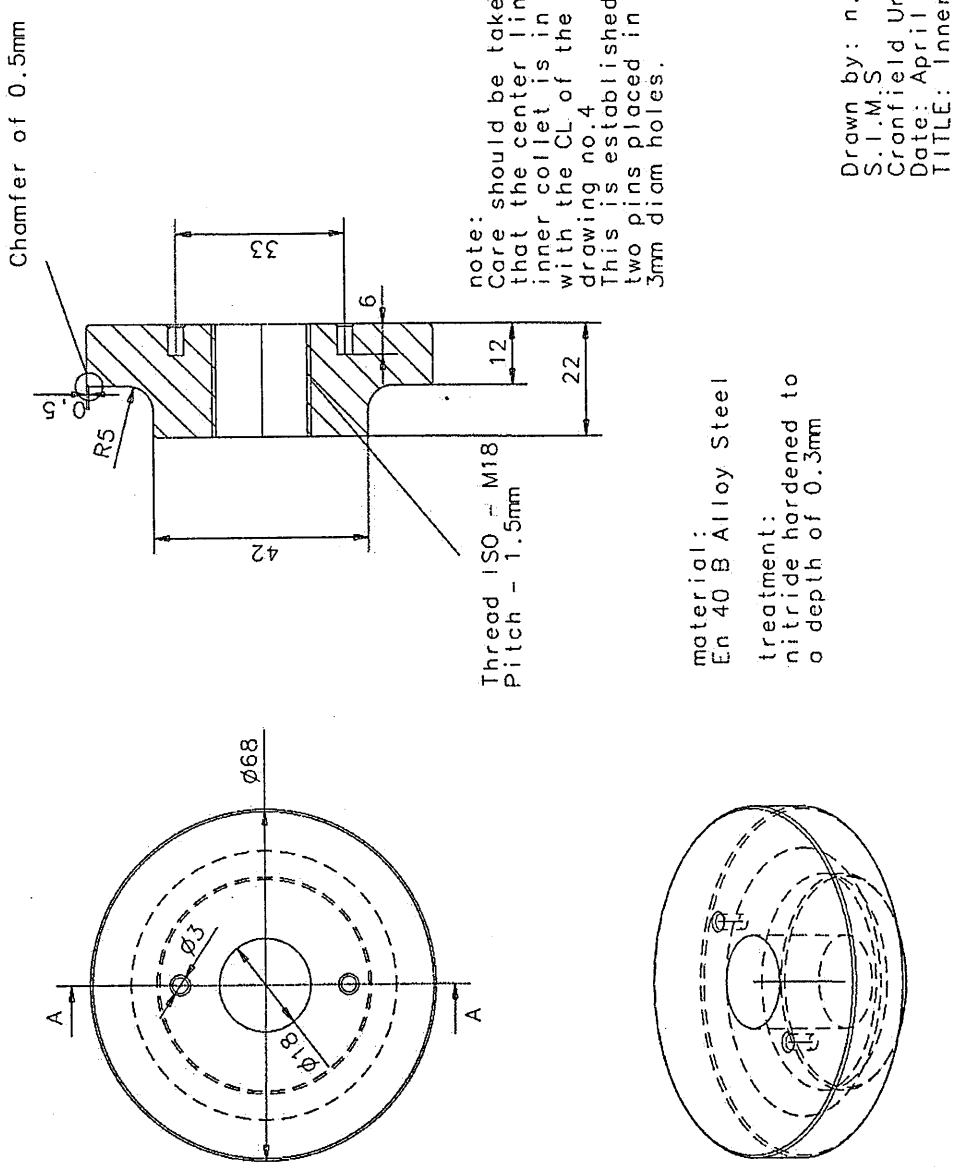

Fig.A4 Mechanical drawing of inner collet

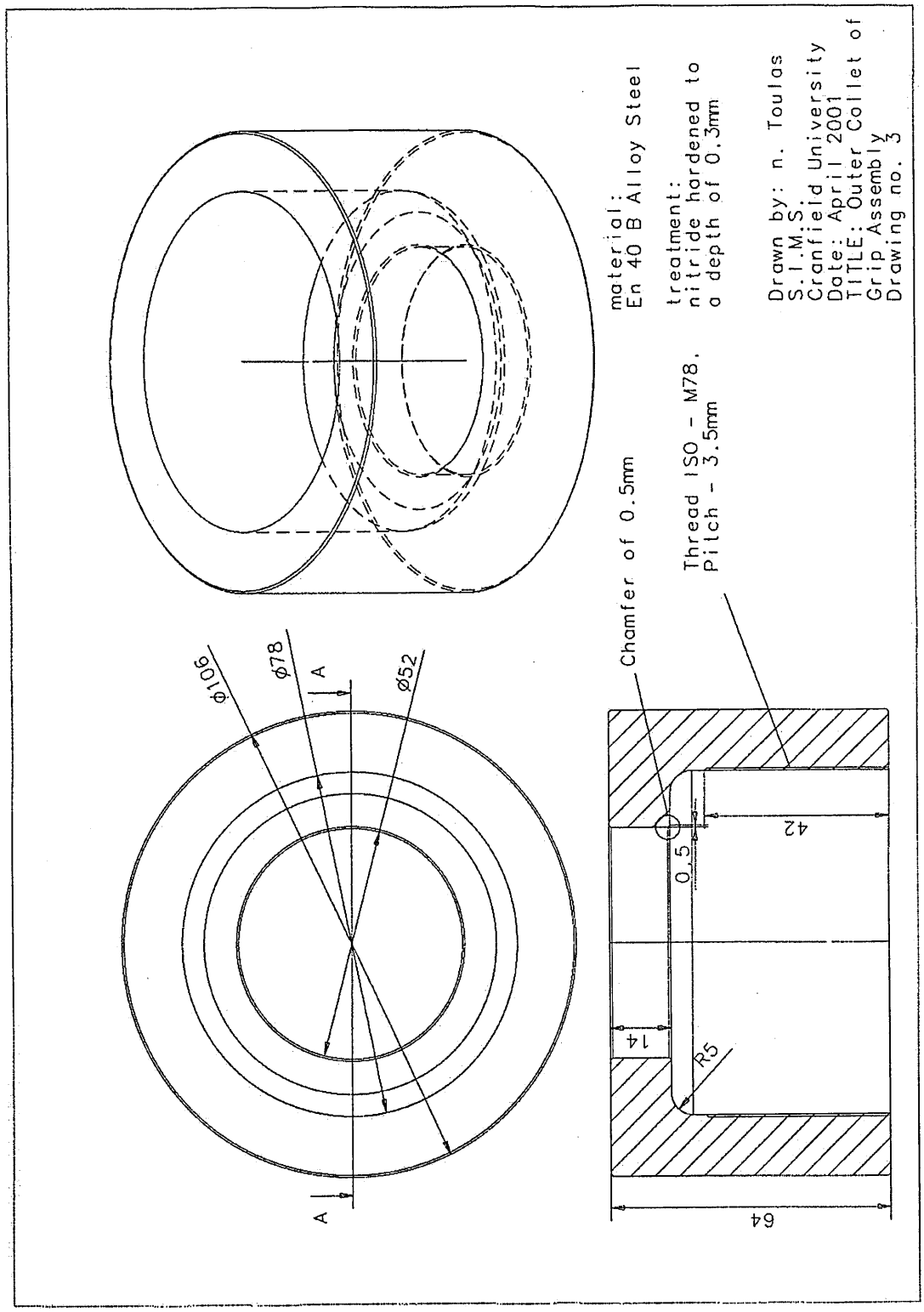

Fig.A5 Mechanical drawing of outer collet

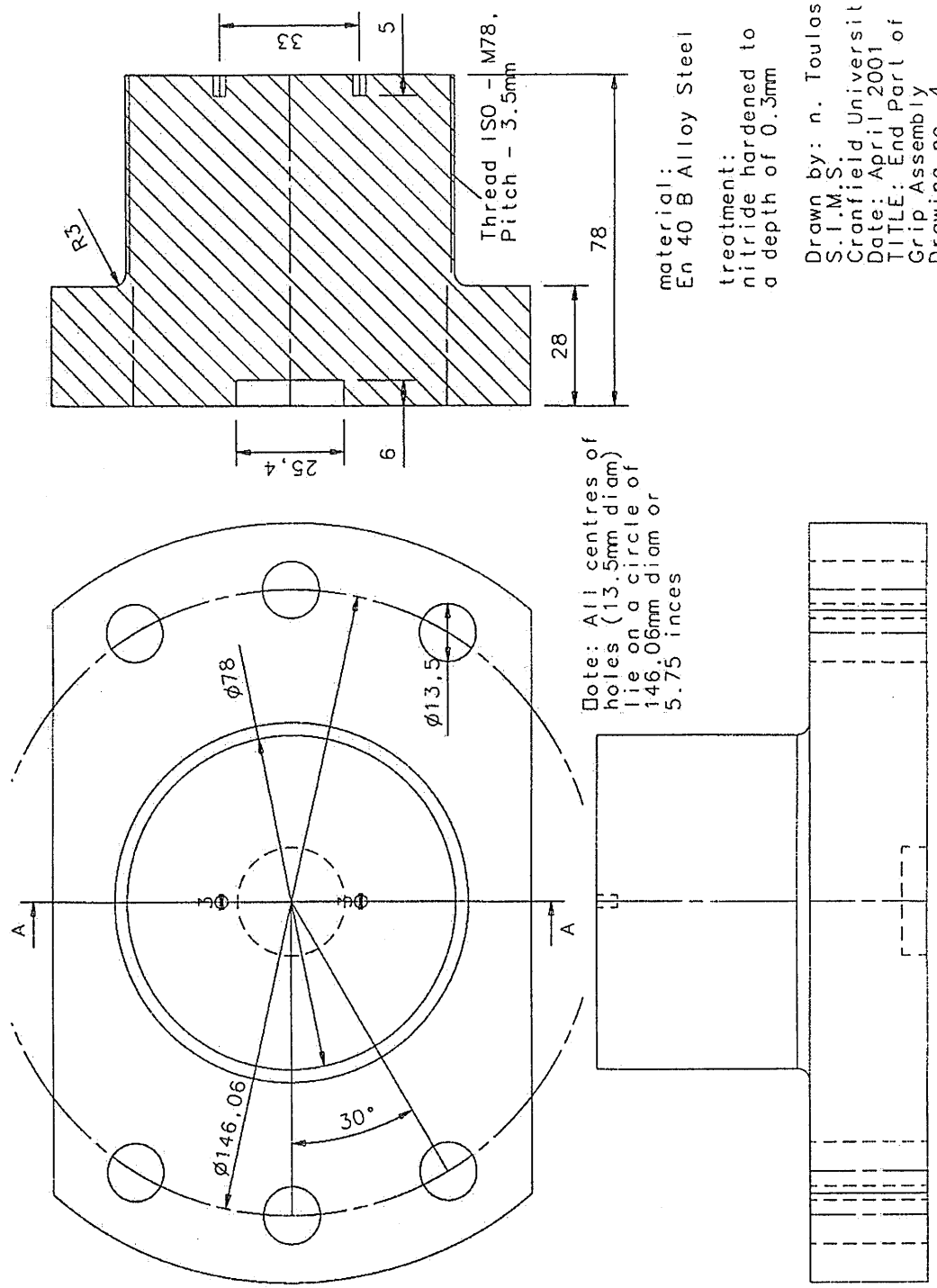

Fig.A6 Mechanical drawing of top part

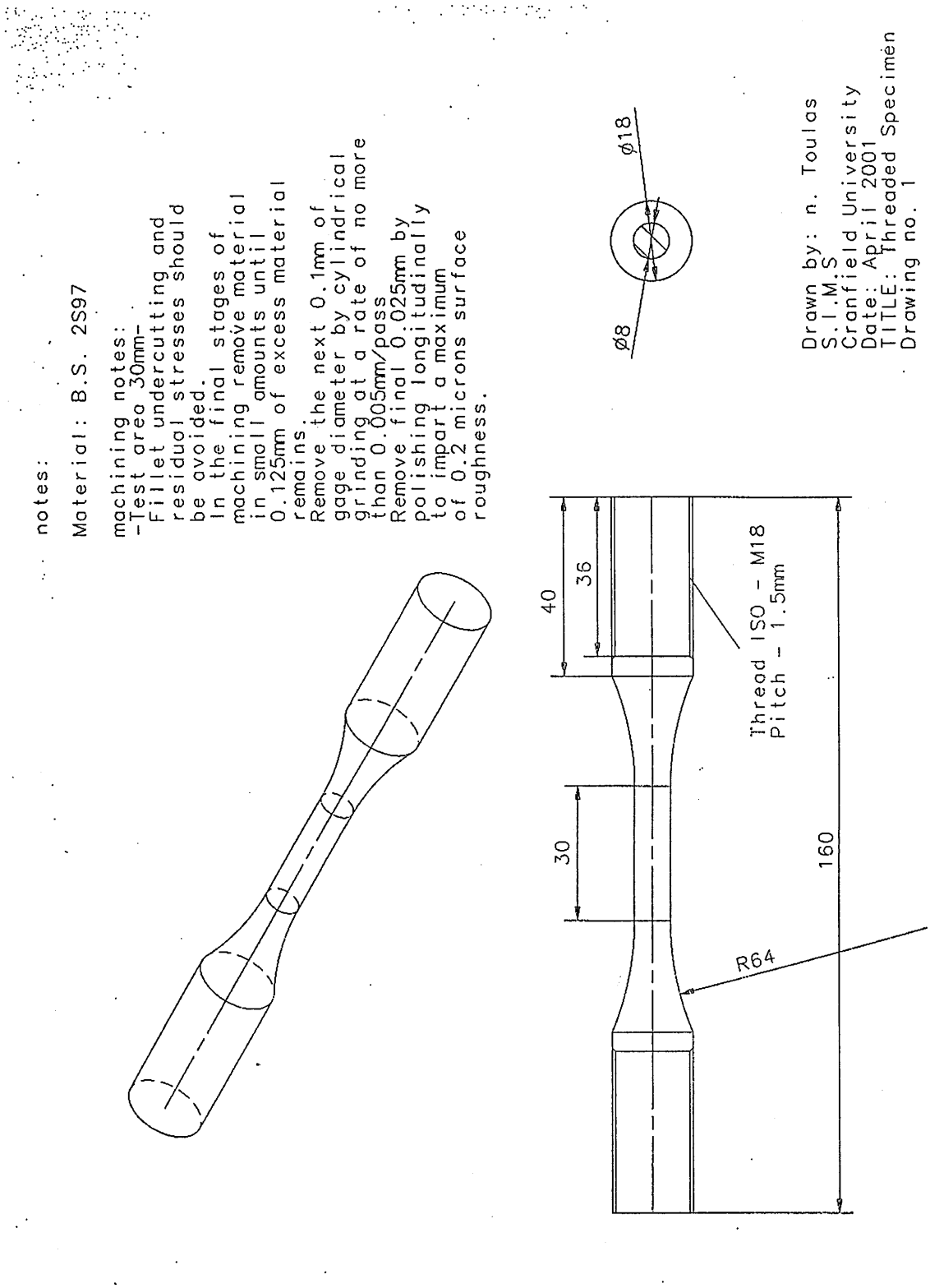

Fig.A7 Designed coupon specimens (un-notched)

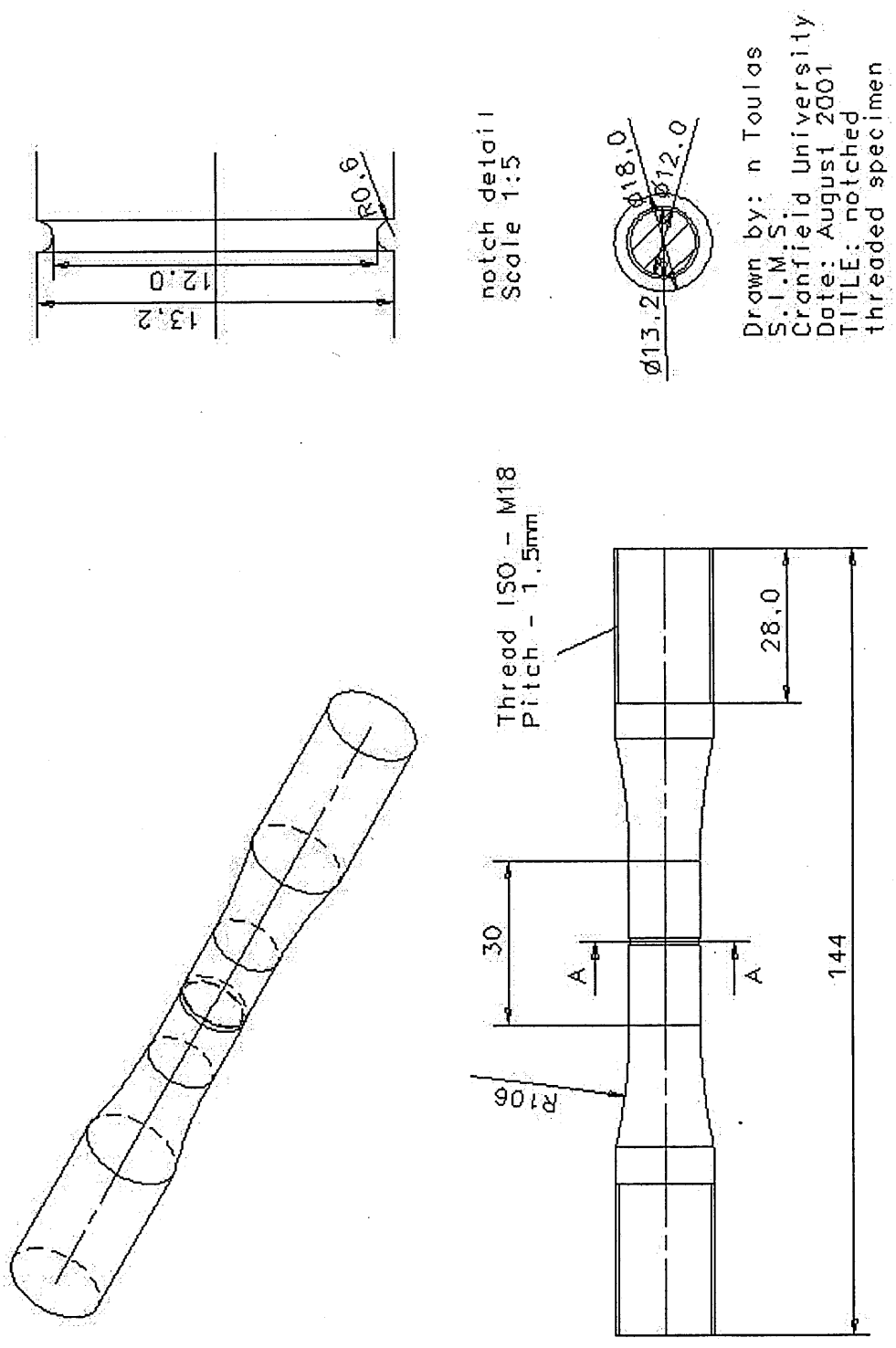

Fig.A8 Designed coupon specimens (notched)

Appendix B _ Experimental results table

Specimen No.	Diameter (mm)	R ratio	P_a (kN)	P_m (kN)	S_a (MPa)	S_m (MPa)	Smax (MPa)	S_G (MPa)	Test Frequency (Hz)	Life Cycles at failure (N)	Life Cycles at failure Log(N)
1	7.981	Tension test, displacement controled, to determine material UTS									
2	7.948	Tension test, displacement controled, to determine material UTS									
3	7.977	Tension test, displacement controled, to determine material UTS									
16	7.978	0.9	2.80	53.20	56.0	1064.2	1120.2	1053.2	5	29	1.462
33	7.953	0.9	2.80	53.20	56.4	1070.9	1127.3	1193.7	15	7382000	6.868
34	7.955	0.9	2.80	53.20	56.3	1070.4	1126.7	1181.1	5	32	1.505
14	7.961	0.8	5.70	51.30	114.5	1030.6	1145.1	1378.1	5	47	1.672
15	7.985	0.8	5.70	51.30	113.8	1024.4	1138.2	1284.8	15	7155000	6.855
26	7.953	0.8	5.70	51.30	114.7	1032.7	1147.4	1412.3	5	44	1.643
27	7.984	0.8	5.70	51.30	113.9	1024.7	1138.5	1288.4	10	12567	4.099
28	7.966	0.8	5.70	51.30	114.4	1029.3	1143.7	1357.6	10	41522	4.618
29	7.991	0.8	5.70	51.30	113.7	1022.9	1136.5	1263.3	15	7538000	6.877
30	7.971	0.8	5.70	51.30	114.2	1028.0	1142.2	1337.7	5	61	1.785
35	7.983	0.8	5.70	51.30	113.9	1024.9	1138.8	1292.1	15	796687	5.901
36	7.957	0.5	13.50	40.50	271.5	814.5	1085.9	985.8	20	8012000	6.904
37	7.973	0.5	13.80	41.40	276.4	829.2	1105.6	1053.9	15	97547	4.989
38	7.951	0.5	14.00	42.00	282.0	845.9	1127.9	1139.6	8	86460	4.937
39	7.961	0.5	14.00	42.00	281.3	843.8	1125.0	1128.1	17	94125	4.974
40	7.980	0.5	14.40	43.20	287.9	863.8	1151.7	1243.5	5	10	1.000
32	7.955	0.3	18.80	34.91	378.3	702.5	1080.7	1008.6	15	101355	5.006
45	7.981	0.3	19.00	35.29	379.8	705.3	1085.1	1019.6	20	2112284	6.325
44	7.966	0.3	19.20	35.66	385.2	715.4	1100.7	1059.9	8	28307	4.452
42	7.968	0.3	19.30	35.84	387.1	718.8	1105.9	1073.7	8	64074	4.807
43	7.978	0.3	19.50	36.21	390.1	724.4	1114.5	1097.3	8	44480	4.648
31	7.968	0.3	20.00	37.14	401.1	744.9	1146.0	1189.1	5	23	1.362
56	7.978	0.1	22.00	26.89	440.1	537.9	978.0	844.0	23	7501000	6.875
19	7.989	0.1	22.75	27.81	453.8	554.7	1008.5	896.0	22	1908096	6.281
22	7.975	0.1	22.75	27.81	455.4	556.6	1012.1	902.3	22	1279558	6.107
21	7.972	0.1	22.78	27.84	456.4	557.8	1014.2	906.0	22	72956	4.863
23	7.970	0.1	22.78	27.84	456.6	558.1	1014.7	906.9	22	2852220	6.455
25	7.988	0.1	22.78	27.84	454.6	555.6	1010.1	898.8	22	264014	5.422
20	7.990	0.1	22.83	27.90	455.3	556.5	1011.8	901.8	22	50045	4.699
18	7.969	0.1	23.00	28.11	461.1	563.6	1024.7	924.9	20	84072	4.925
24	7.956	0.1	23.00	28.11	462.6	565.5	1028.1	931.0	20	139869	5.146
51	7.958	0.1	24.35	29.00	489.6	583.0	1072.6	1017.2	7	18464	4.266
53	7.989	0.1	24.40	29.00	486.8	578.5	1065.3	1003.0	7	20653	4.315
52	7.953	0.1	24.50	30.00	493.2	603.9	1097.1	1065.9	7	16786	4.225
55	7.950	0.1	26.20	32.00	527.8	644.7	1172.5	1237.6	7	2301	3.362
54	7.986	0.1	27.00	33.00	539.0	658.8	1197.9	1302.4	5	22	1.342
13	7.959	-1	27.00	0.00	542.7	0.0	542.7	542.7	5	3018053	6.480
7	7.972	-1	27.50	0.00	550.9	0.0	550.9	550.9	24	8732877	6.941
4	7.970	-1	29.00	0.00	581.3	0.0	581.3	581.3	20	6442000	6.809
10	7.970	-1	29.00	0.00	581.3	0.0	581.3	581.3	15	5504000	6.741
11	7.952	-1	29.50	0.00	594.0	0.0	594.0	594.0	24	68119	4.833
12	7.959	-1	29.50	0.00	592.9	0.0	592.9	592.9	20	234330	5.370
8	7.960	-1	30.00	0.00	602.8	0.0	602.8	602.8	16	127661	5.106
5	7.960	-1	31.00	0.00	622.9	0.0	622.9	622.9	17	75124	4.876
9	7.951	-1	31.00	0.00	624.4	0.0	624.4	624.4	10	230523	5.363
6	7.953	-1	32.00	0.00	644.2	0.0	644.2	644.2	15	99492	4.998
17	7.978	-1	36.00	0.00	720.2	0.0	720.2	720.2	5	7654	3.884
50	7.988	-1	37.00	0.00	738.3	0.0	738.3	738.3	15	23903	4.378
46	7.950	-1	39.00	0.00	785.7	0.0	785.7	785.7	5	18455	4.266
49	7.965	-1	41.00	0.00	822.9	0.0	822.9	822.9	0.4	7102	3.851
48	7.976	-1	45.00	0.00	900.6	0.0	900.6	900.6	0.3	1561	3.193
41	7.955	-1	48.00	0.00	965.8	0.0	965.8	965.8	0.4	876	2.943
57	7.985	-1	51.00	0.00	1018.4	0.0	1018.4	1018.4	0.2	51	1.708

Table B1_ Constant Amplitude experimental results

Appendix C _ Fractography – SEM pictures

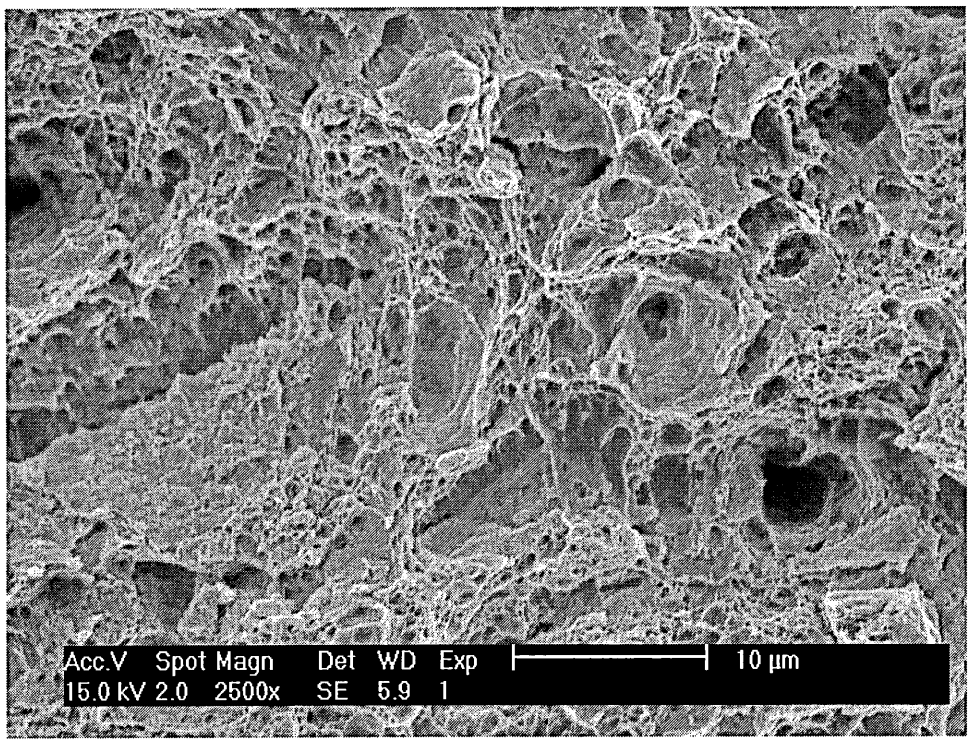

Fig. C1_ SEM picture from sampleNo.77 tested under R28

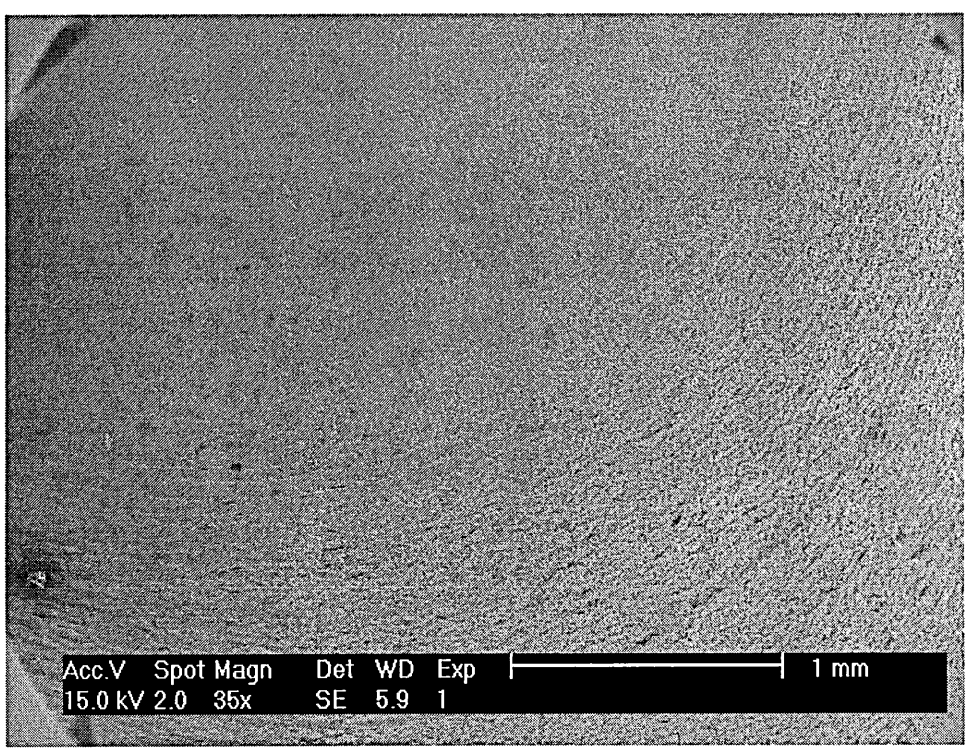

Fig. C2_ SEM picture from sampleNo.77 tested under R28

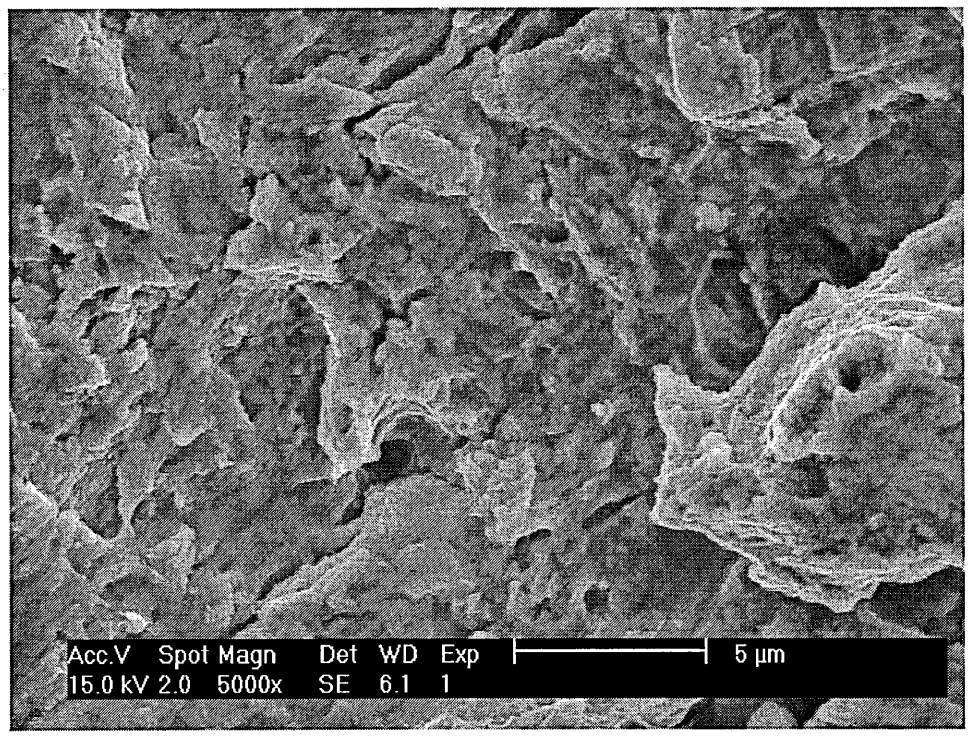

Fig. C3_ SEM picture from sampleNo.77 tested under R28

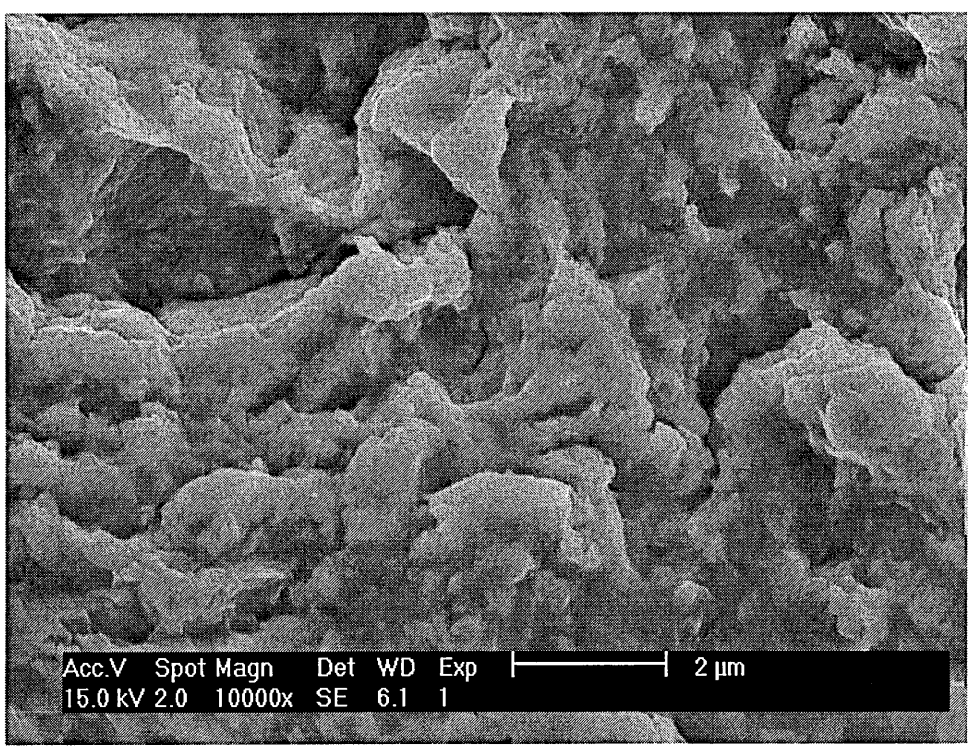

Fig. C4_ SEM picture from sampleNo.77 tested under R28

Appendix D _ Helicopter components

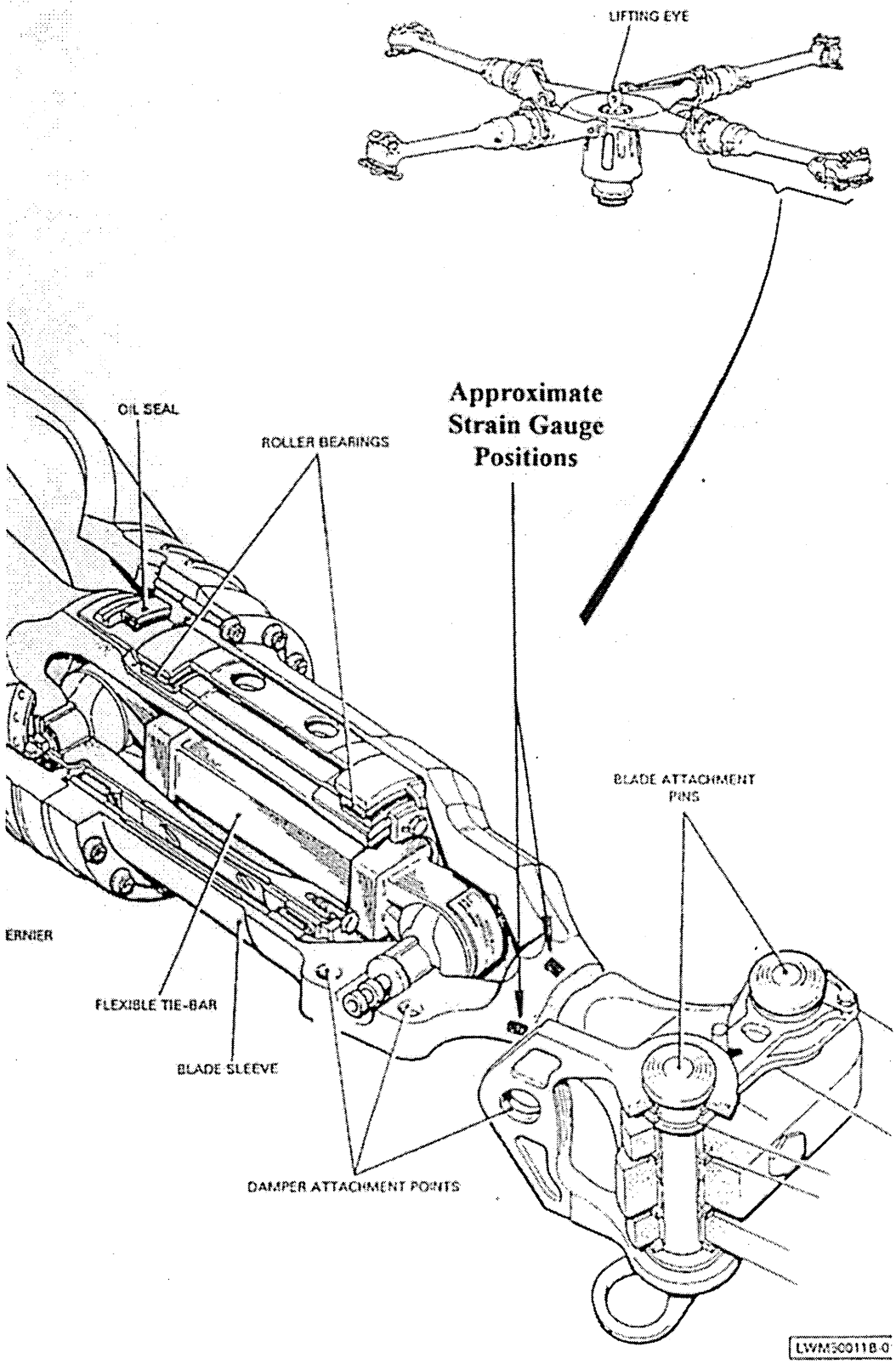

Fig. D1_ Westland Lynx helicopter main rotor head feathering sleeve (Dogbone)

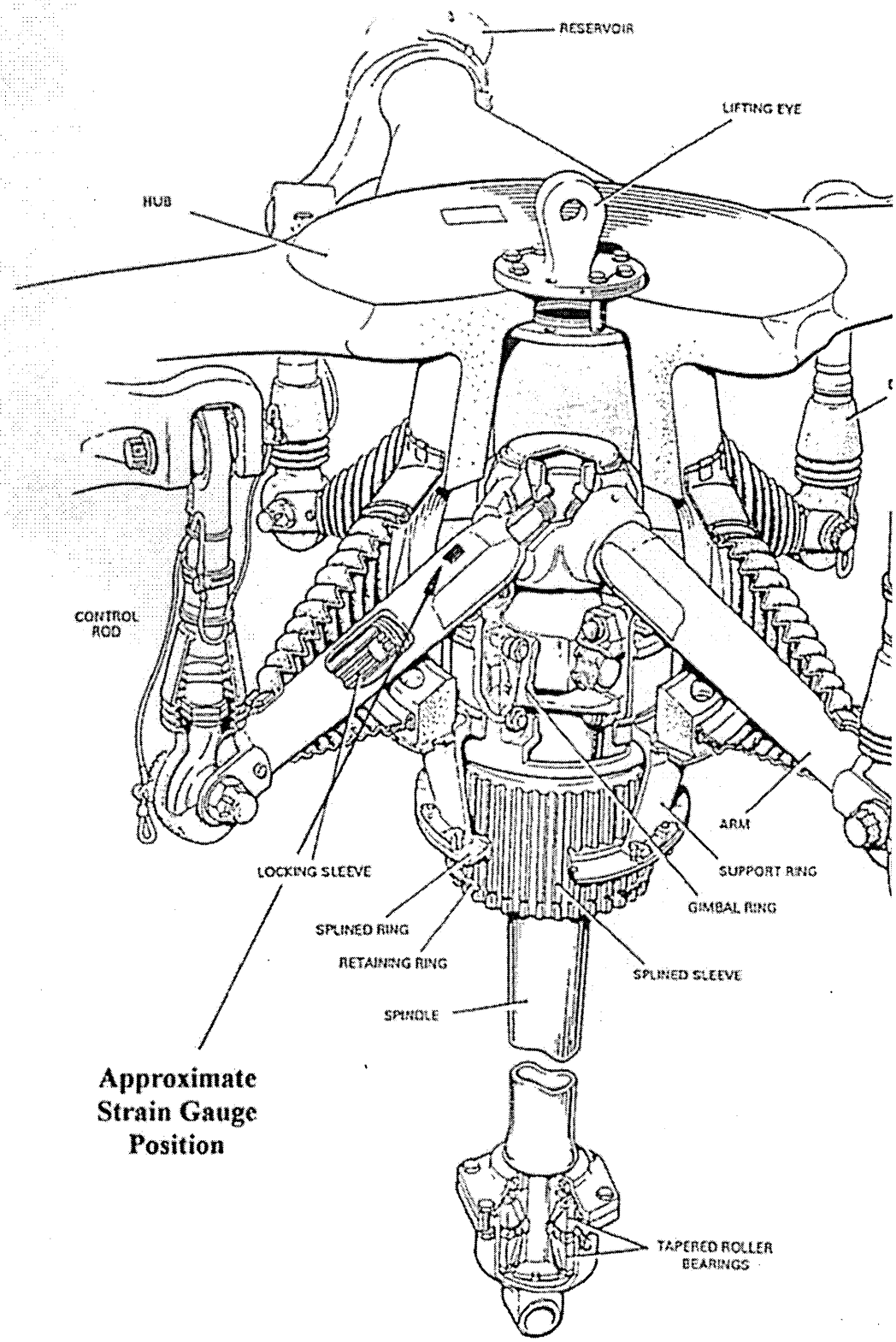

Fig. D2_ Westland Lynx helicopter main rotor head pitch change arm (Spider arm)

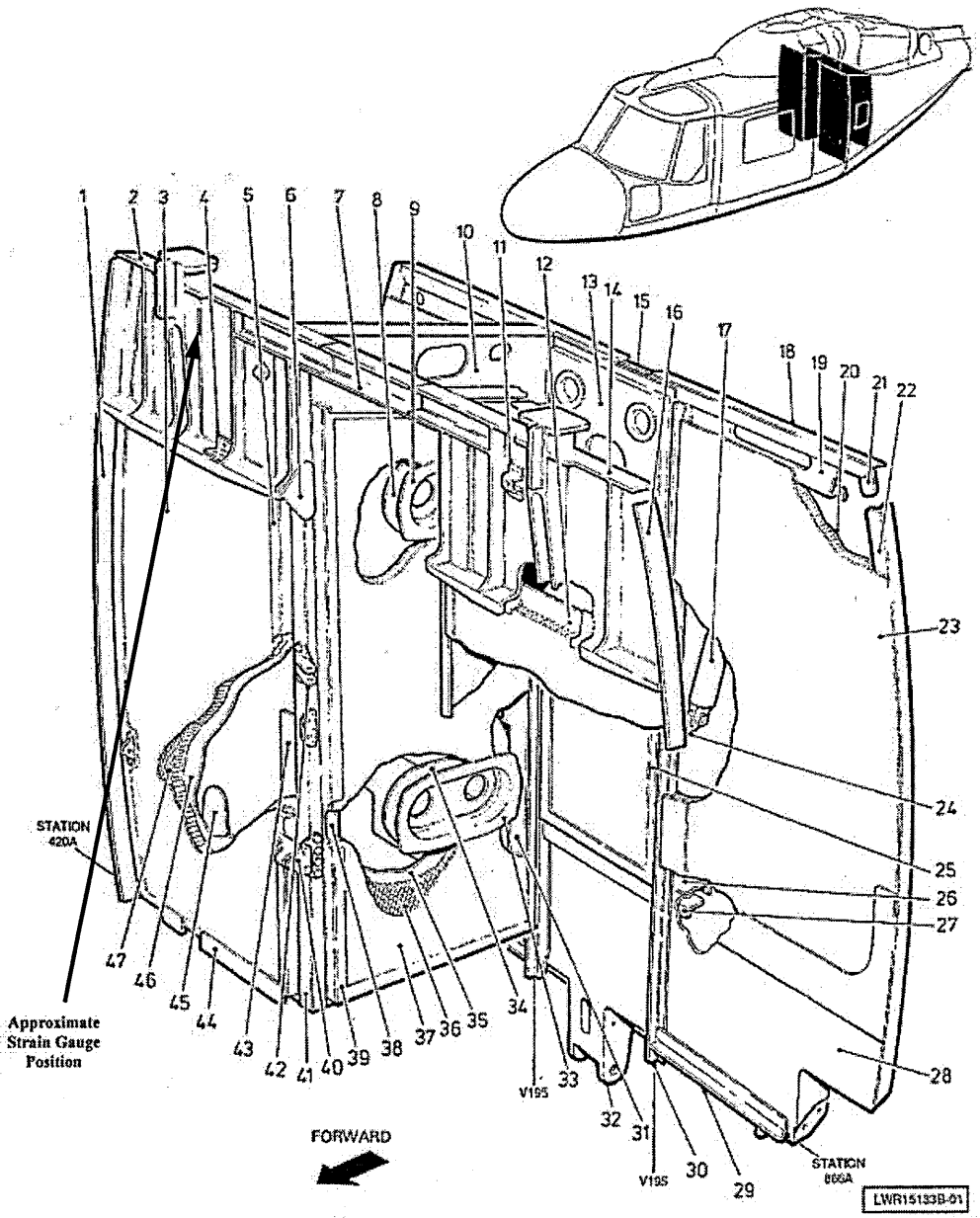

Fig. D3_ Westland Lynx helicopter Station 420A Starboard rear Main Rotor gearbox attachment fuselage fitting.

Appendix E_ Loads data analysis results

In the following the results from the statistical analysis of loads data is presented. The analysis was carried out for the 420A lift frame component for all the manoeuvres in the design spectrum. No example existed for manoeuvre 7. The following table shows the manoeuvres and the results of statistical analysis.

420 A lift frame - Damage rate per manoeuvre				
Manoeuvres	No. of examples	Damage rate (microdamage per sec)		
		50% cum prob	average	max
Manoeuvre 1 - Level Flight 0.1 to 0.2 VNE	44	0	0.0324	0.7311
Manoeuvre 2 - Level Flight 0.2 to 0.4 VNE	46	0	0.0297	0.5555
Manoeuvre 3 - Level Flight 0.4 to 0.6 VNE	26	0	0.0342	0.4632
Manoeuvre 4 - Level Flight 0.6 to 0.8 VNE	88	0	4.5722	82.2996
Manoeuvre 5 - Level Flight 0.8 to 0.9 VNE	72	0	3.2172	69.0574
Manoeuvre 6 - Level Flight 0.9 to 1.0 VNE	39	0	0.0001	0.0037
Manoeuvre 7 - VNE-50 kts @ 60 degrees - Nil	-	-	-	-
Manoeuvre 8 - VNO-20 kts @ 40 degrees	7	0	0.0030	0.0208
Manoeuvre 9 - VNO-20 kts @ 30 degrees	8	0	0.0000	0.0000
Manoeuvre 10 - 0.9 VNE @ 30 degrees	13	0	0.0010	0.0098
Manoeuvre 11 - 1.0 VNE @ 20 degrees	0	0	0.0000	0.0000
Manoeuvre 12 - Control Reversals @ 0.9 VNE	38	0	0.2965	8.4601
Manoeuvre 13 - Autorotations	5	0	0.0417	0.1691
Manoeuvre 14 - Hover	174	0	0.1959	3.9996
Manoeuvre 15 - Sideways Flight	22	0	0.0018	0.0184
Manoeuvre 16 - Rearwards Flight	13	0	0.0100	0.0462
Manoeuvre 17 - Spot Turns	17	0	0.0071	0.0807
Manoeuvre 18 - Hover Control Reversals	17	0	0.0800	1.3467
Manoeuvre 19 - Climb	77	0	0.0217	0.6617
Manoeuvre 20 - Descent	53	0	0.0179	0.2178
Manoeuvre 21 - Take Off	29	0	0.0000	0.0000
Manoeuvre 22 - Transition to Hover	78	0.0593	0.9866	12.0995
Manoeuvre 23 - Transition from Hover	72	0	0.0041	0.2961
Manoeuvre 24 - Landing	24	0	0.0167	0.2747
Manoeuvre 25 - Rotors Running on Ground	47	0	0.0349	0.2551
Total	1009			

Table E.1_ Damage rates per manoeuvre for 420A lift frame component

The following 24 plots show the cumulative probability distribution of damage rate for all manoeuvres.

Manoeuvre 1 - Level Flight 0.1 to 0.2 VNE (44)

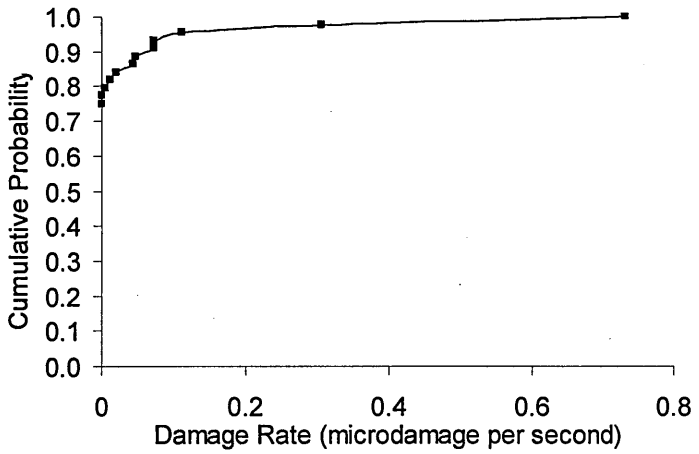

Manoeuvre 2 - Level Flight 0.2 to 0.4 VNE (46)

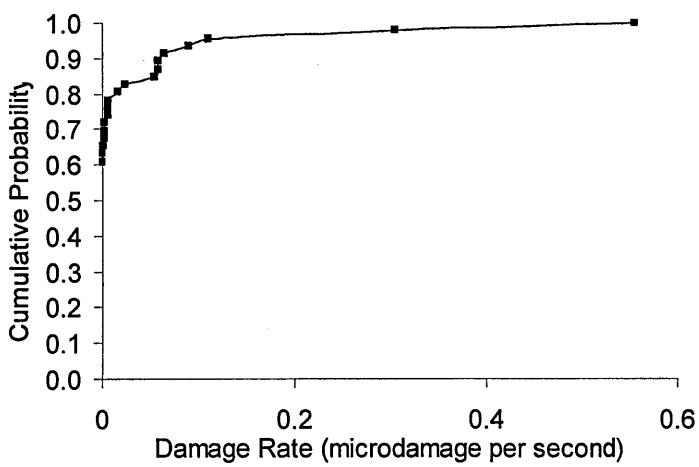

Manoeuvre 3 - Level Flight 0.4 to 0.6 VNE (26)

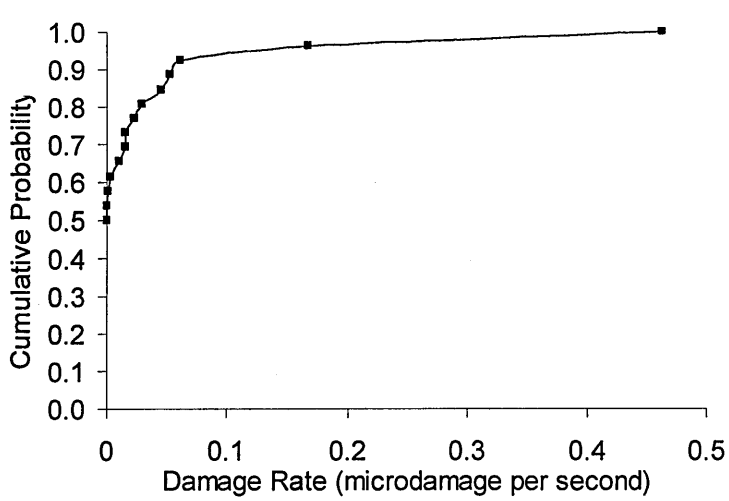

Manoeuvre 4 - Level Flight 0.6 to 0.8 VNE (88)

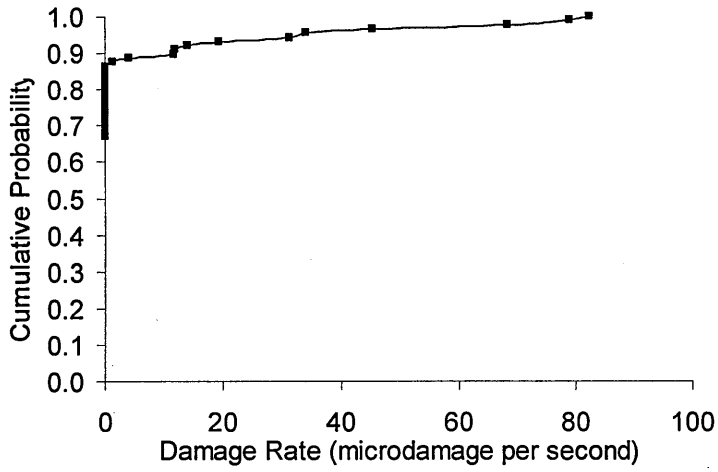

Manoeuvre 5 - Level Flight 0.8 to 0.9 VNE (72)

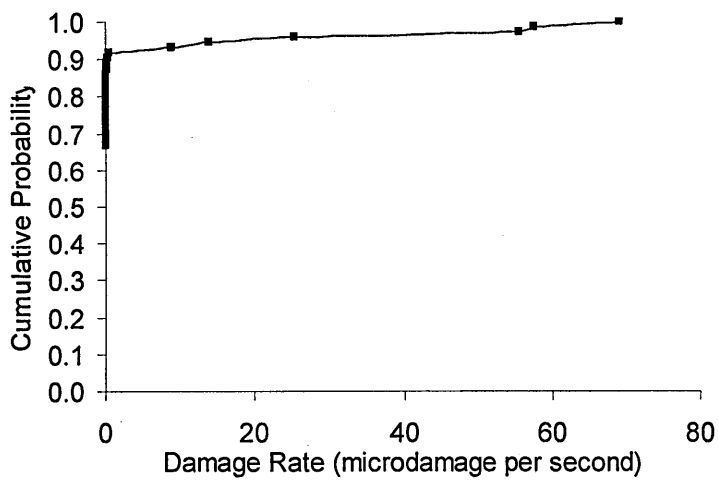

Manoeuvre 6 - Level Flight 0.9 to 1.0 VNE (39)

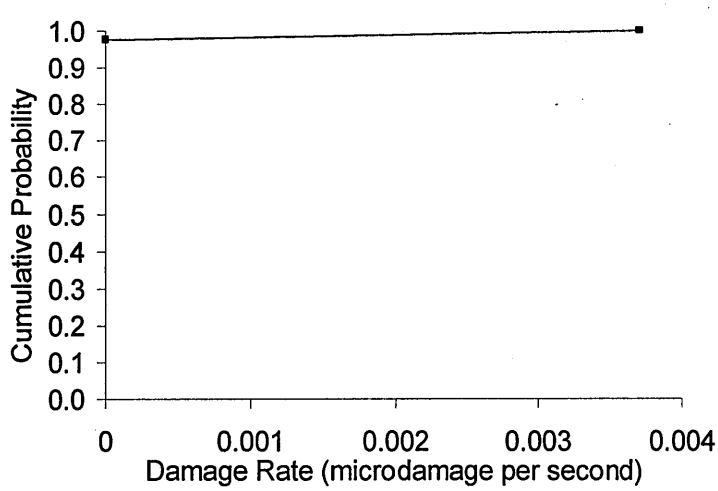

Manoeuvre 8 - VNO-20 kts @ 40 degrees (7)

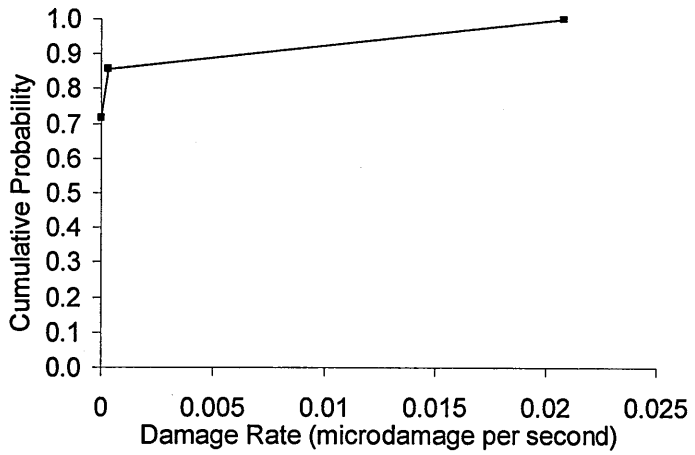

Manoeuvre 9 - VNO-20 kts @ 30 degrees (8)

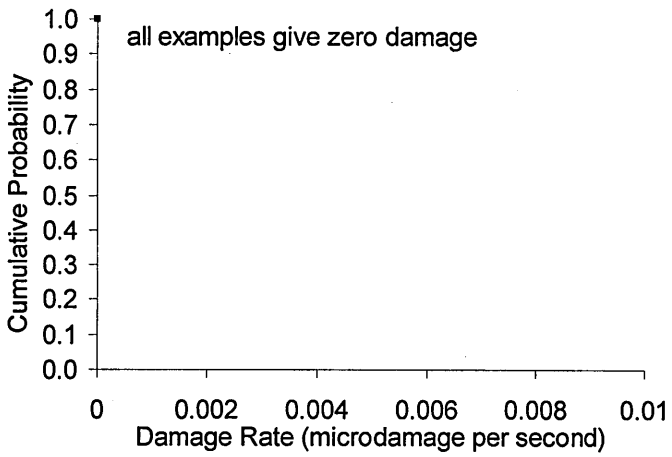

Manoeuvre 10 - 0.9 VNE @ 30 degrees (13)

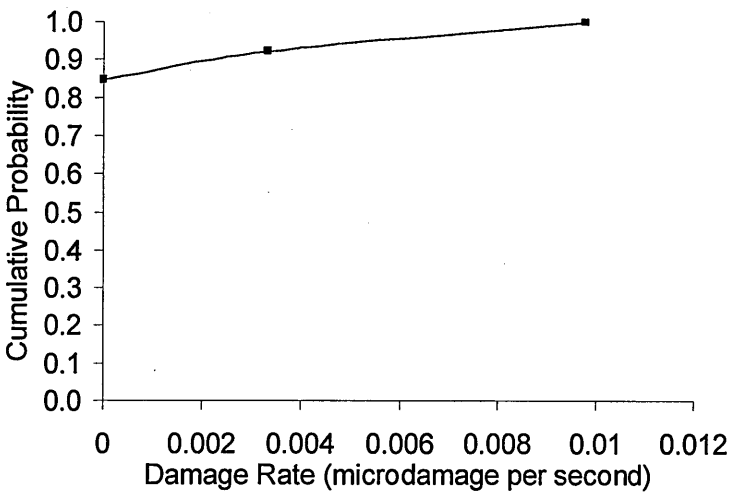

Manoeuvre 11 - 1.0 VNE @ 20 degrees (8)

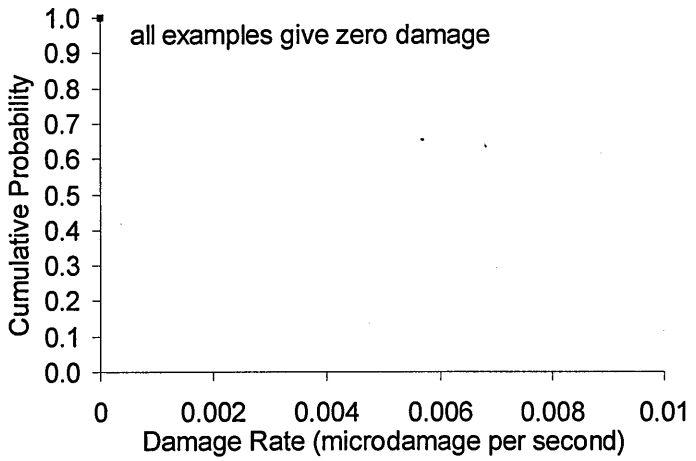

Manoeuvre 12 - Control Reversals @ 0.9 VNE (38)

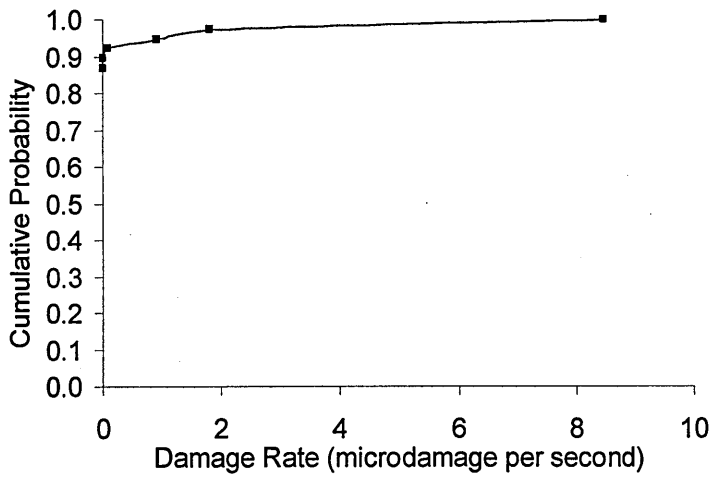

Manoeuvre 13 - Autorotations (5)

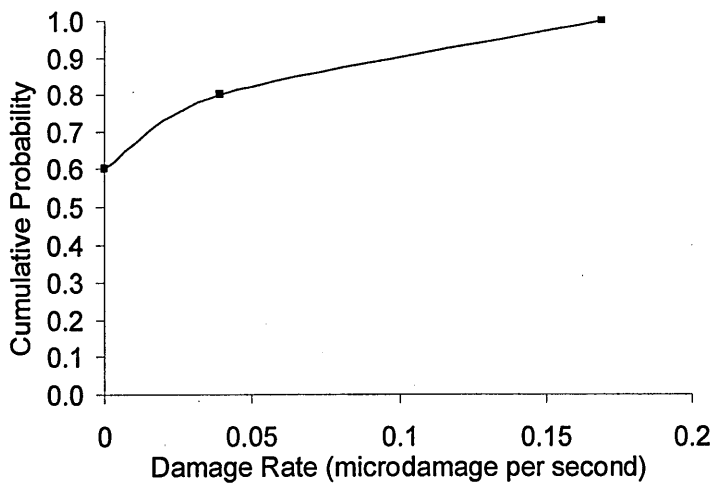

Manoeuvre 14 - Hover (174)

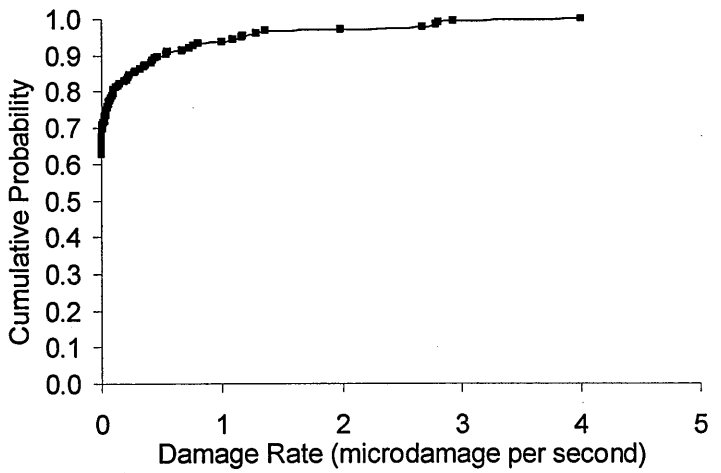

Manoeuvre 15 - Sideways Flight (22)

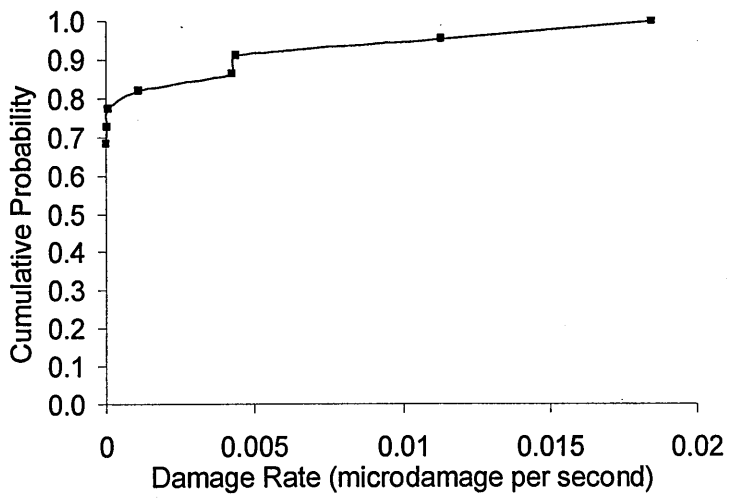

Manoeuvre 16 - Rearwards Flight (13)

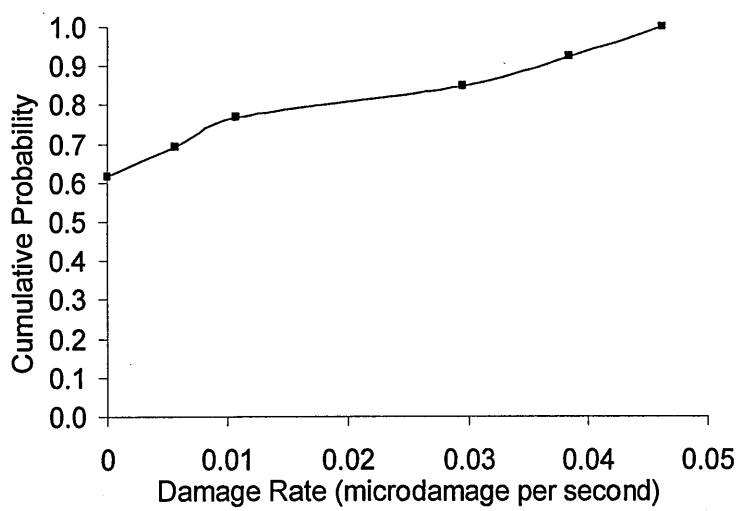

Manoeuvre 17 - Spot Turns (17)

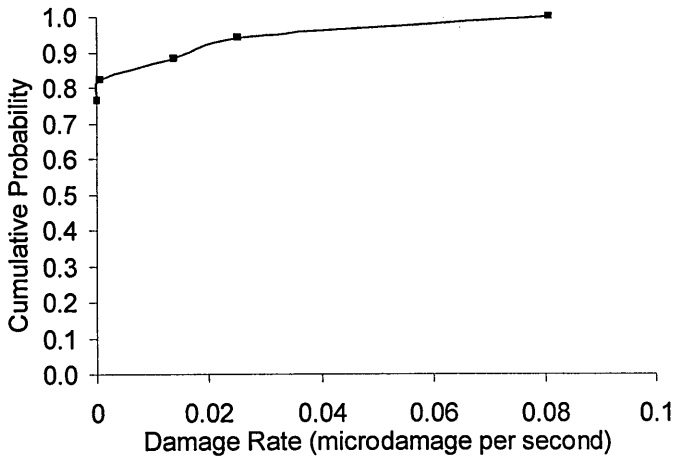

Manoeuvre 18 - Hover Control Reversals (17)

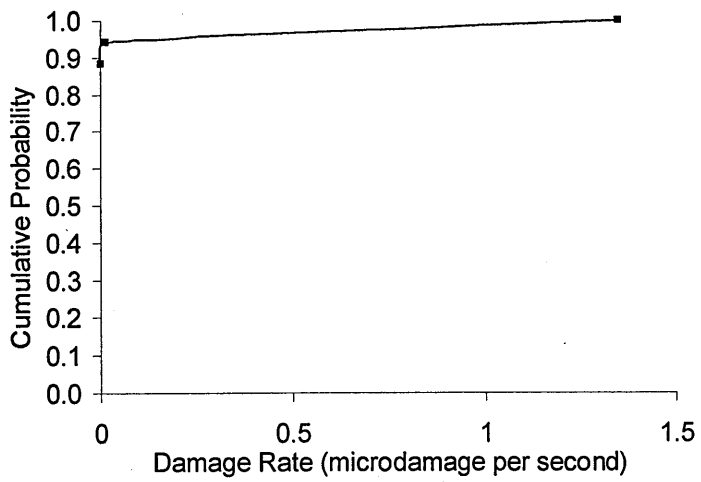

Manoeuvre 19 - Climb (77)

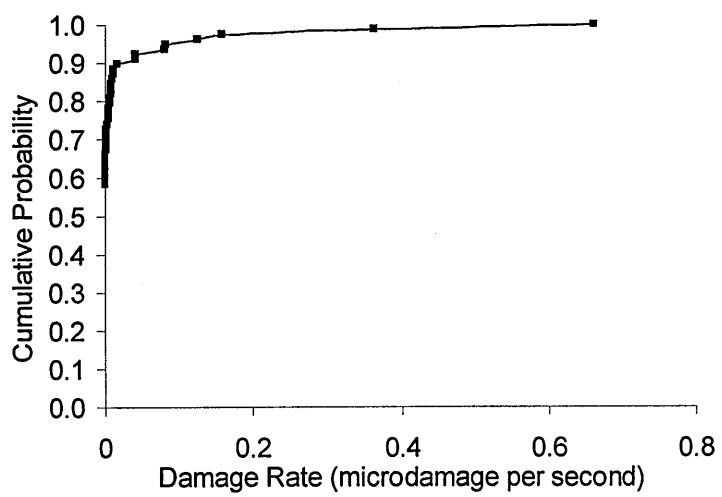

Manoeuvre 20 - Descent (53)

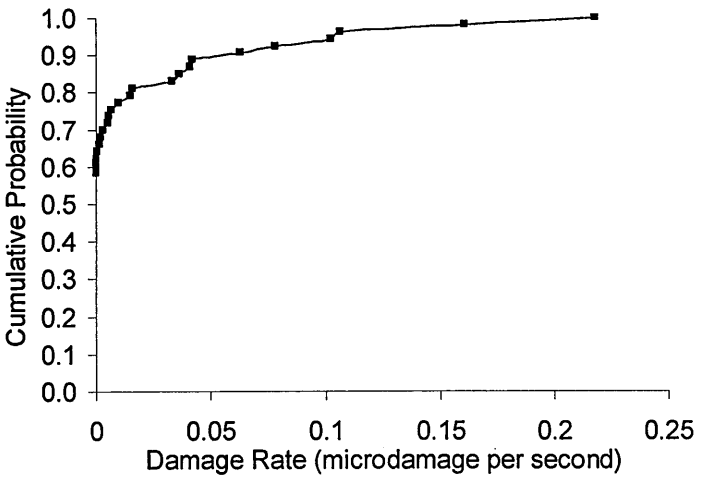

Manoeuvre 21 - Take Off (29)

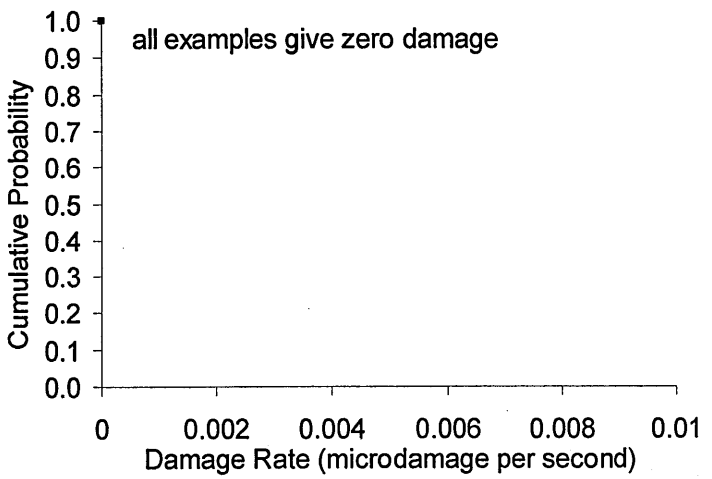

Manoeuvre 22 - Transition to Hover (78)

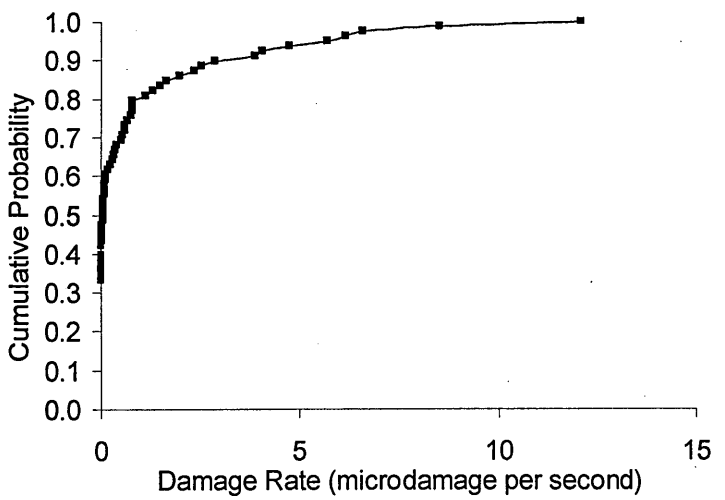

Manoeuvre 23 - Transition from Hover (72)

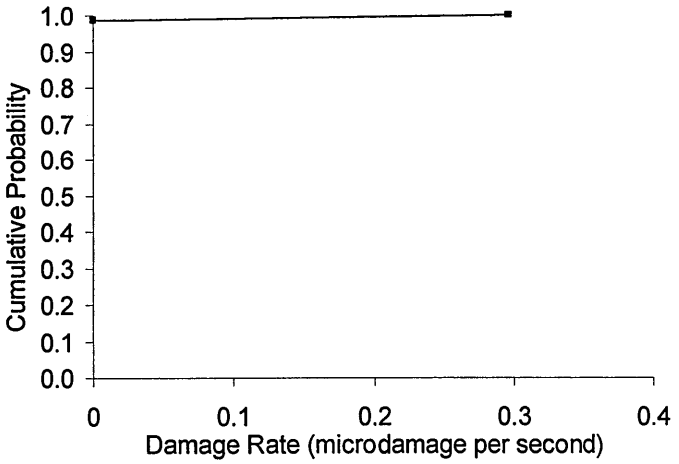

Manoeuvre 24 - Landing (24)

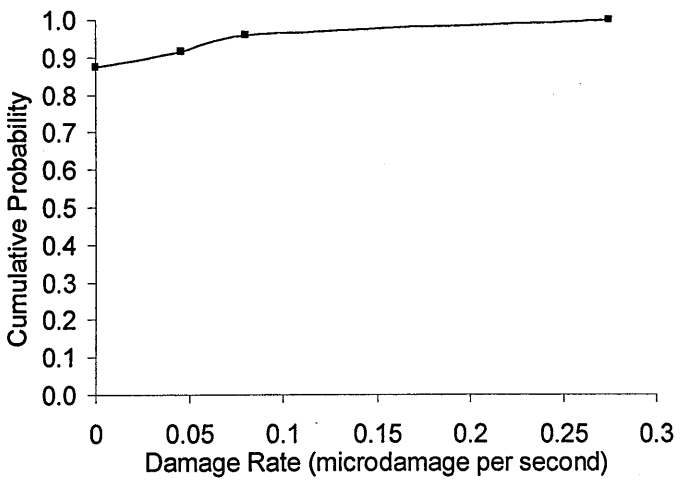

Manoeuvre 25 - Rotors Running on Ground (47)

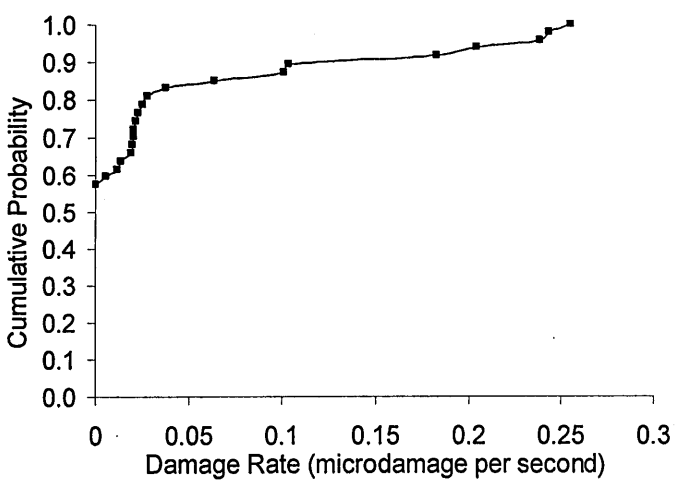

Appendix F _ Monte Carlo simulation program

A program was written in C language to perform the Monte Carlo simulations. 26 input parameters were specified before each run.

Input parameters:

1. <number of component lives N>
2. <COV of sinfin>
3. <lives output file>
4. <A>
5. <sinfin input file>
6. <B>
7. <C>
8. <mean of m>
9. <UTS>
10. <load factor input file>
11. <strength factor>
12. <life factor>
13. <life_limit>
14. <location of cycle files>
15. <random no. file>
16. <interval type(1,2,or3)>
17. <constant damages (y/n)?>
18. <manoeuvre lengths etc. input file name >
19. <cov of m>
20. <mean of miner>
21. <cov of miner>
22. <check dump of miners, sinfs and ms(y/n)?>
23. <check dump of intes and manexs (y/n)?>
24. <arg24> (loads rate of change per 1h, 10h ...)
25. <arg25> (usage rate of change per 1h, 10h ...) works with interval type 2.
26. <arg26> - damage recording rate (hours)

In the following the parameters and their role in simulation are described with a flow chart of the program's functions.

- S-N parameters **A, B, C** $\frac{S_a}{S_{\inf}} = 1 + \frac{C}{(N+B)^A}$
- Material
  - Strength
    - **UTS**
    - Endurance: **Sinf** – mean and CoV (normal distribution)
- Calculation
  - Miner: **D** – mean and CoV (normal distribution)
  - Goodman: **m** - mean and CoV (normal distribution)

$$S_a = S_{\inf}\left[1 - \left(\frac{S_m}{UTS}\right)^m\right]$$

- Factors
  - Applied on S-N curve
    - Life factor: **LF**
    - Strength Factor: **SF**
  - Applied on loads
    - Loads Factor: **LdF**
- Loading Spectra
  - **Manoeuvre examples**
- Usage Spectrum
  - Percentage of time spent in each manoeuvre: **Usage** - mean and CoV (normal distribution)
- Loads rate of change
- Usage rate of change

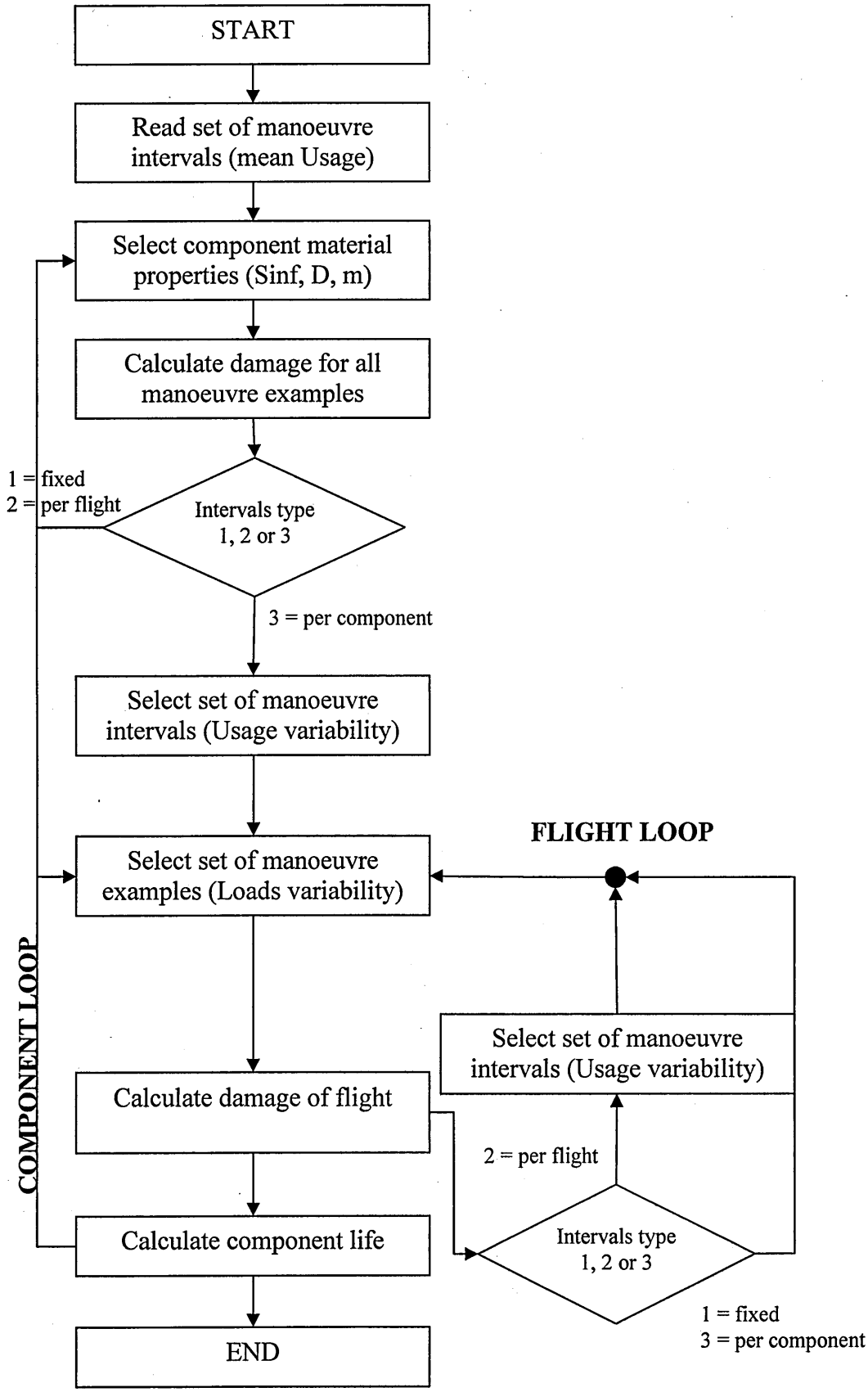
START
Read set of manoeuvre intervals (mean Usage)
Select component material properties (Sinf, D, m)
Calculate damage for all manoeuvre examples
1 = fixed
2 = per flight
Intervals type 1, 2 or 3
3 = per component
Select set of manoeuvre intervals (Usage variability)
FLIGHT LOOP
Select set of manoeuvre examples (Loads variability)
COMPONENT LOOP
Select set of manoeuvre intervals (Usage variability)
Calculate damage of flight
2 = per flight
Intervals type 1, 2 or 3
1 = fixed
3 = per component
Calculate component life
END